Multi-responsive copolymers : effect of composition and-or structure on their properties in water

Fang Yin

Université Fédérale
Toulouse Midi-Pyrénées

THÈSE

En vue de l'obtention du
DOCTORAT DE L'UNIVERSITÉ DE TOULOUSE

Délivré par l'Université Toulouse 3 - Paul Sabatier

Présentée et soutenue par

Fang YIN

Le 2 décembre 2021

Copolymères multi-stimulables: effet de la composition et de la structure sur leur propriétés en solution aqueuse

Ecole doctorale : **SDM - SCIENCES DE LA MATIERE - Toulouse**

Spécialité : **Chimie Macromoléculaire et Supramoléculaire**

Unité de recherche :
IMRCP - Laboratoire des Interactions Moléculaires et Réactivité Chimique et Photochimique

Thèse dirigée par
Nancy LAUTH-de VIGUERIE et Jean-Daniel MARTY

Jury

M. Patrice WOISEL, Rapporteur
M. Didier GIGMES, Rapporteur
M. Simon HARRISSON, Examinateur
M. Rinaldo POLI, Examinateur
Mme Nancy LAUTH-de VIGUERIE, Directrice de thèse
M. Jean-Daniel MARTY, Co-directeur de thèse

Acknowledgements

I would like to thank all jury members: Prof. Patrice Woisel, Dr. Didier Gigmes, Dr. Simon Harrisson and Prof. Rinaldo Poli for their time and energy to read and to participate in the defense of the thesis. The discussion and comments are quite inspiring and valuable, deepening my understanding of the research project and making me keep thinking from different angles.

I would like to express my sincere appreciation to my supervisors: Prof. Nancy Lauth-de Viguerie and Dr. Jean-Daniel Marty, who provided me this Ph.D. position and supervised the project in the past three years. I am really grateful that they are always available, patient and passionate to discuss the thesis project process and to help me find the solutions to problems that I came across in the research. Their enthusiasm, sense of responsibility, rigorous academic attitude, profound knowledge and innovative thinking have left me a deep impression, which inspires and motivates me on how to do scientific research. I am very lucky and happy to work under their guidance.

Special thanks are extended to Caroline Toppan, Pierre Lavedan and Yannick Coppel for NMR measurements, Bruno Payré for microscopy analysis, Stéphanie Balor for cryo-TEM experiments, Annie Brûlet for SANS analysis, Charles-Louis Serpentini for his warm-hearted help and useful suggestions on using UV-visible spectroscopy, Juliette Fitremann for rheological study of sol and gel, Stéphane Gineste for Multi-angle DLS analysis, Pascale Saint-Aguet for SEC measurements, Lucie Perquis for DSC experiments, Mathias Destarac for his kind help in the synthesis of (co)polymers, Stéphanie Cassel for teaching me how to operate freeze dryer, and many other people for their great help in the instrument operation and data analyses.

Many thanks go to IMRCP members, D. Ciuculescu-Pradines, Clément, B. Lonetti, C. Mingotaud, Anne-Françoise, C. Coudret, B. Farias-Mancilla, Mingxi, Baptiste, Alexis, Marjorie, Liming and Faniry for their encouragement, kindness and fruitful

discussions, which broadens my research horizons and deepens understanding of French culture. I really enjoyed the time in lab.

Meanwhile, I would like to express my thanks to my Chinese friends in Toulouse and elsewhere, Hui, Huan, Meiling, Qilin and Jieli for their accompanying and encouragement during these years, I am very happy to travel and to share the foods and happiness with them, which makes my life more colorful and enjoyable. I hope we can keep this friendship wherever we are in future.

I would like to thank China Scholarship Council (CSC) and Centre National de la Recherche Scientifique (CNRS) for the financial support of my Ph.D. project.

Last but not least, my deepest gratitude is dedicated to my family: grandmother, parents, brother, sister-in-law and little nephew, their unwavering support and encouragement are my biggest motivation to overcome all the complications I encountered in the life.

December 2021

Toulouse, France

Abbreviations

T_c	Cloud point temperature
LCST	Lower critical solution temperature
PNIPAM	Poly(*N*-isopropylacrylamide)
PNIPMAM	Poly(*N*-isopropylmethacrylamide)
PEAM	Poly(*N*-ethylacrylamide)
PEMAM	Poly(*N*,*N*-ethylmethylacrylamide)
PDEAM	Poly(*N*,*N*-diethylacrylamide)
PN*n*PAM	Poly(*N*-*n*-propylacrylamide)
PM*n*PAM	Poly(*N*-methyl-*N*-*n*-propylacrylamide)
PCPAM	Poly(*N*-cyclopropylacrylamide)
PNAEAA	Poly(*N*-acetoxylethyl acrylamide)
PNASME	Poly(*N*-acryloylsarcosine methyl ester)
PNAGME	Poly(*N*-acryloylglycine methyl ester)
PNAGEE	Poly(*N*-acryloylglycine ethyl ester)
P(MA-$_L$-Ala-OMe)	Poly(*N*-methacryloyl-$_L$-alanine methyl ester)
PDEAEAM	Poly(*N*,*N*-diethylamino ethyl acrylamide)
PEPyAM	Poly(*N*-ethylpyrrolidine acrylamide)
PMEMA	Poly(2-(*N*-morpholino) ethyl methacrylate)
PDMAEMA	Poly(2-(dimethylamino) ethyl methacrylate)
PDMAEEOMA	Poly(2-(2-(dimethylamino) ethoxy) ethyl methacrylate)
PEMAEEOMA	Poly(2-(2-(ethyl(methyl) amino) ethoxy) ethyl methacrylate)
PDEAEEOMA	Poly(2-(2-(diethylamino) ethoxy) ethyl methacrylate)
PDMAEEO_2MA	Poly(2-(2-(2-(dimethylamino) ethoxy) ethoxy) ethyl methacrylate)
PEMAEEO_2MA	Poly(2-(2-(2-(ethyl(methyl) amino) ethoxy) ethoxy) ethyl methacrylate)
PDEAEEO_2MA	Poly(2-(2-(2-(diethylamino) ethoxy) ethoxy) ethyl methacrylate)
PEMAEEO_4MA	Poly(2-(2-(2-(2-(2-(ethyl(methyl) amino) ethoxy) ethoxy) ethoxy) ethoxy) ethyl methacrylate)
PDEAEEO_4MA	Poly(2-(2-(2-(2-(2-(diethylamino) ethoxy) ethoxy) ethoxy) ethoxy) ethyl methacrylate)
PDEGMA	Poly(di(ethylene glycol) methyl ether methacrylate)

PTEGMA	Poly(tri(ethylene glycol) methyl ether methacrylate)
PPEGMA	Poly(penta(ethylene glycol) methyl ether methacrylate)
PTEGA	Poly(tri(ethylene glycol) methyl ether acrylate)
POEGA	Poly(oligoethylene oxide) acrylate)
PTEGEMA	Poly(tri(ethylene glycol) ethyl ether methacrylate)
PDEGA	Poly(di(ethylene glycol) ethyl ether acrylate)
PTEGEA	Poly(ethoxytri-(ethylene glycol) acrylate)
PMDEGA	Poly(methoxy diethylene glycol acrylate)
PVCL	Poly(*N*-vinyl caprolactam)
PVPip	Poly(*N*-vinylpiperidone)
PNVBA	Poly(*N*-vinyl-*n*-butyramide)
PNVIBA	Poly(*N*-vinylisobutyramide)
UCST	Upper critical solution temperature
OEGMEMA	Oligo(ethylene glycol) methyl ether methacrylate
OEGPhA	Oligo(ethylene glycol) phenyl ether acrylate
PNAGA	Poly(*N*-acryloylglycinamide)
PNAAAM	poly(*N*-acryloylasparaginamide)
PCNPCAVCP	Poly(1-cyano-*N*-propylcarboxyamido vinyl cyclopropane)
P*t*BMA	Poly(*tert*-butyl methacrylate)
POEGMEA	Poly(oligo(ethylene glycol) methyl ether acrylate)
PAEEO$_2$MA	Poly(2-(2-(2-acetoxyethoxy) ethoxy) ethyl methacrylate)
PAEEO$_3$MA	Poly(2-(2-(2-(2-hydroxyethoxy) ethoxy) ethoxy) ethyl methacrylate)
PAEEO$_4$MA	Poly(2-(2-(2-(2-(2-acetoxy) ethoxy) ethoxy) ethoxy) ethoxy) ethyl methacrylate)
PVEA	Poly(*N*-(4-vinylbenzyl)-*N*,*N*-diethylamine)
DLS	Dynamic Light Scattering
DSC	Differential Scanning Calorimetry
NMR	Nuclear Magnetic Resonance
FITR	Fourier Transform Infrared Spectroscopy
EO/EG	Ethylene oxide/ethylene glycol
BA	*n*-butyl acrylate
TMSPMA	3-(trimethoxysilyl) propyl methacrylate

D_H	Hydrodynamic diameter
OEOMA	Oligo(ethylene oxide) methyl ether methacrylate
PHIPPVTA	Poly(bis(*N*-hydroxyisopropyl pyrrolidone 2-vinylterephthalate))
ΔH	variation of enthalpy
PPO	Poly(propylene oxide)
PHPMAm	Poly(*N*-(2-hydroxypropyl) methacrylamide)
T_1	Spin-lattice relaxation time
T_2	Spin-spin relaxation time
PIPOx	Poly((2-isopropyl-2-oxazoline) methyl methacrylate)
PVME	Poly(vinyl methyl ether)
GMAm	*N*-propargylmethacrylamide
PEOx	Poly(2-ethyl-2-oxazoline)
PMeOx	Poly(2-methyl-2-oxazoline)
PCL	Poly(ε-caprolactone)
FTIR	Fourier Transform Infrared Spectroscopy
PDMAm	poly(*N*,*N*-dimethylacrylamide)
PcPA	Poly(*N*-cyclopropylamide)
P*n*PMA	Poly(*N*-*n*-propylmethacrylamide)
PbMoEA	Poly(*N*,*N*-bis(2-methoxyethyl) acrylamide)
PEoEA	Poly(*N*-(2-ethoxyethyl) acrylamide)
PEoEMA	Poly(*N*-(2-ethoxyethyl) methacrylamide)
PTHFA	Poly(*N*-tetrahydrofurfurylacrylamide)
PTHFMA	Poly(*N*-tetrahydrofurfurylmethacrylamide)
AN	Acrylonitrile
PdMMAEAPS	Poly(3-dimethyl(methacryloyloxyethyl) ammonium propane sulfonate)
MA	Methyl acrylate
VAc	Vinyl acetate
AA	Acrylic acid
PiPMAm	Poly(*N*-isopropyl,*N*-methylacrylamide)
OEtOxMA	Polymer based on oligo-2-ethyl-2-oxazoline side chains and a methacrylate backbone
ACMP	4-acryloylmorpholine

MAAm	Methacrylamide
MVA	*N*-methyl-*N*-vinylacetamide
NVA	*N*-vinylacetamide
VPL	*N*-vinyl-2-pyrrolidi-none
HIPAAm	2-hydroxyisopropylacrylamide
HMAAm	*N*-(hydroxymethyl) acrylamide)
HEAAm	*N*-hydroxyethylacrylamide
MASE	Methacrylic acid stearyl ester
PDEAEMA	Poly(2-(diethylamino) ethyl methacrylate)
Ac-6ACA	Acryloyl 6 amino caproic acid
HEMA	2-hydroxyethyl methacrylate
VL	Vinyl laurate
VP	*N*-vinylpyrrolidone
VOH	Vinyl alcohol
VPi	Vinyl pivalate
HA	*n*-hexyl acrylate
DMVP	Dimethyl vinylphosphonate
DPVP	Di-*n*-propyl vinylphosphonate
PPGMA	Poly(propylene glycol) methacrylate
PHTBAM	Poly(*N*-(2-hydroxyl-*tert*-butyl) acrylamide)
PEGMA	Poly(ethylene glycol) methacrylate
ATRP	Atom transfer radical polymerization
RAFT	Reversible addition-fragmentation chain-transfer
ATL	*N*-acryloylhomocysteine thiolactone
DEDA	Diethylethylenediamine
PEGA	Poly(ethylene glycol) methyl ether acrylate
EOVE	2-ethoxyethyl vinyl ether
MOVE	2-methoxyethyl vinyl ether
MMA	Methyl methacrylate
PEGMA	Obtained by transesterifing MMA into PEG methacrylate
PEGMMA	Poly((ethylene glycol) methyl methacrylate)
PBuMA	Poly(*n*-butyl methacrylate)
PHEGMA	Poly(hexa(ethylene glycol) methacrylate)

PBzMA	Poly(benzyl methacrylate)
CO_2	Carbon dioxide
EAA	Ethylacrylic acid
MAA	Methacrylic acid
mPEGV	(Ethylene glycol) methyl ether vinylphenyl
PAPy	Poly(*N*-acryloylpyrrolidine)
APi	*N*-acryloylpiperidine
BMAAm	*N*-(isobutoxymethyl)acrylamide
nPA	*N*-*n*-propylacrylamide
MVC	3-methyl-*N*-vinylcaprolactam
PSt	Polystyrene
P(A-Pro-OMe)	Poly(*N*-acryloyl-$_L$-proline methyl ester)
P(A-Hyp-OH)	Poly(*N*-acryloyl-4-*trans*-hydroxy-$_L$-proline)
NAG	*N*-acryloylglycine
NAGSP	*N*-acryloylglycine spiropyran ester
SPB	Sulfopropylbetaine
Bz	Benzylamine
THF	Tetrahydrofurfurylamine
PSBMA	Poly(sulfobetaine methacrylate)
PSPP	Poly(3-(*N*-(3-methacrylamidopropyl)-*N*,*N*-dimethyl) ammoniopropane sulfonate)
PSB	Polysulfobetaine
MPS	3-(*N*-(3methacrylamidopropyl)-*N*,*N*-dimethyl) ammoniopropane sulfonate
DMAPMA	*N*-(3-(dimethylamino) propyl) methacrylamide
MPDSAH	*N*-(3-(methacryloylamino)propyl)-*N*,*N*-dimethyl-*N*-(3-sulfopropyl) ammonium hydroxide
p	Packing parameter
α_0	Optimal area of head group
l_c	Length of hydrophobic tail
PLA	Poly($_{DL}$-lactide)
PVim	Poly(*N*-vinylimidazole)
PMAGP	Poly(6-O-methacryloyl-$_D$-galactopyranose)

PMVE	Poly(methyl vinyl ether)
PIBVE	Poly(isobutyl vinyl ether)
P(S-d_8)	Fully deuterated PSt block
PEP	Poly(ethylene-*alt*-propylene)
PI	Poly(isoprene)
PF	Poly(2,7-(9,9-dihexylfluorene))
EtMA	Ethyl methacrylate
HMA	Hexyl methacrylate
PSO	Poly(styrene oxide)
PVBA	Poly(4-vinylbenzoic acid)
PSSA	Poly(4-styrenesulfonic acid)
PVPA	Poly(vinylphosphonic acid)
PDPAEMA	Poly(2-(diisopropylamino) ethyl methacrylate)
P4VP	Poly(4-vinylpyridine)
P2VP	Poly(2-vinylpyridine)
*K*a	Acidic dissociation constant
IEP	Isoelectric point
PB	Poly(butadiene)
PGA	Poly($_L$-glutamic acid)
PLys	Poly($_L$-lysine)
PGMA	Poly(glycerol monomethacrlyate)
PHPMA	Poly(2-hydroxypropyl methacrylate)
PDVB	Poly(divinyl benzene)
PIMA	Poly(2-((3-(isopropylamino)-3-oxopropyl) (methyl) amino) ethyl acrylate)
PEPyM	Poly(*N*-ethylpyrrolidine methacrylate)
PMAME	Poly(*N*-methacryloyl-$_L$-alanine 2-(dimethylamino) ethylamide)
PMAEE	Poly(*N*-methacryloyl-$_L$-alanine 2-(diethylamino) ethylamide)
PMAMP	Poly(*N*-methacryloyl-$_L$-alanine 3-(dimethylamino) propylamide)
PMAEP	Poly(*N*-methacryloyl-$_L$-alanine 3-(diethylamino) propylamide)
P(MEO$_1$-DEAE-AM)	Poly(2-methoxyethyl 3-(*N*-(2-(diethylamino) ethyl) acrylamido) propanoate)

P(DEAE-NIPAM-AM)	Poly(*N*-(2-(diethylamino) ethyl)-*N*-(3-(isopropylamino)-3oxopropyl) acrylamide)
P(MA-iAsn-OH)	Poly(*N*-methacryloyl-$_L$-*β*-isopropylasparagine)
PAEVE	Poly(primary amino groups)
PEA	Poly(ethyl acrylate)
CMA	Coumarin methacrylate
PAD	Poly((*N*-amidino) dodecyl acrylamide)
PHIS	Poly(histamine acrylamido)
PHFBMA	Poly(2,2,3,4,4,4-hexafluorobutyl methacrylate)
PADS	*N'*-Propargyl-*N*,*N*-dimethylacetamidine modified poly(*p*-azidomethylstyrene)
Py	Pyrene group
NMP	Nitroxide-mediated radical polymerization
M	Monomer
Mt	Transition metal
P_n·	Reactive radicals
GTP	Group transfer polymerization
ROP	Ring opening polymerization
CMRP	Cobalt-mediated radical polymerization
PSBMA	Sulfobetaine modified poly(*N*,*N*-dimethylamino ethyl methacrylate)
AuNPs	Gold nanoparticles
AgNPs	Silver nanoparticles
MADIX	Macromolecular design by interchange of xanthates
TEM	Transmission Electronic Microscopy
SEC	Size Exclusion Chromatography
M_n	Molecular weight
Đ	Dispersity
DMF	Dimethylformamide
$NaBH_4$	Sodium borohydride
SPB	Surface plasmon band
TGA	Thermogravimetric analysis
k_{obs}	Pseudo-first order kinetic constant

AIBN	2,2'-azobisisobutyronitrile
xanthate X1	O-ethyl-S-(1-methoxycarbonyl)-ethyl dithiocarbonate
X2	Meso-2,5-di(O-ethyl xanthate) diethyladipate
C_{tr}	Transfer constant
T_g	Glass transition temperature
THF	Tetrahydrofuran
C_{ex}	Interchain transfer constant
SANS	Small Angle Neutron Scattering
R_h	Hydrodynamic radius
N_{agg}	Aggregation number
R_{core}	Radius of the core
M_{core}	Mean average molar mass of core block
N_A	Avogadro number
TS	Transparent solution
OS	Opaque solution
OG	Opaque gel
DG	Dehydrated gel
G’	Elastic/storage modulus
G”	Viscous/loss modulus
cryo-SEM	Cryo-Scanning Electron Microscopy
cac	Critical aggregation concentration
PNNBAM	Poly(*N*-*n*-butylacrylamide)
PDBEAM	Poly(*N*-(2-(dibutylamino) ethyl) acrylamide)
PDMAEA	Poly(2-dimethylamino) ethyl acrylate)
CDTPA	4-cyano-4-[(dodecylsulfanylthiocarbonyl) sulfanyl] pentanoic acid
CTA	Chain transfer agent
T_1	Longitudinal relaxation time
cryo-TEM	Cryogenic Transmission Electron Microscopy
TEA	Triethylamine
SAXS	Small-Angle X-Ray Scattering
Ar	Argon

Table of contents

Introduction

2 Introduction

Stimuli-responsive or so-called “smart” (co)polymers have aroused great attraction in recent years due to the alteration of their physicochemical properties (solubility, chain conformation, aggregation properties…) to adapt to the changes of the external environment. These rapid and reversible responsiveness endow such (co)polymers with multiple potential applications (such as drug delivery and controlled release, sensors, smart textiles, functionalized membranes…).

Responsive mechanism is attributed to the modification of inter- or intramolecular interactions induced by a response to the stimulus. Moreover, the level of response is strongly dependent on external conditions (such as the nature of stimulus and its intensity, selected solvents, presence of additives…) and (co)polymer structural parameters (such as architecture (block, statistical...), composition, (co)polymer concentration, molecular weight and dispersity).

The main objectives of this thesis are to study the relationship between composition, microstructure of different families of (co)polymers and their ability to respond to an external stimulus (temperature, pH or CO_2 addition). The modification of physicochemical properties of these (co)polymers in solution (solubility, self-organization ability) is more specifically studied. Moreover, this work will provide more insights to design multi stimuli-responsive (co)polymers and to understand the complex responsive mechanism.

A bibliographic overview of thermo-, pH- and CO_2-sensitive (co)polymers is presented in **Chapter I**. The first four sections summarize the concepts, categories and characterization techniques of thermo-, pH- and CO_2-responsive (co)polymers. Some examples are given to illustrate how (co)polymer structure and composition as well as other parameters (molecular weight, polymer concentration, stimuli intensity...) influence the pahse transition and self-assembly behavior of these (co)polymers in auqeous solution upon application of different stimuli. A short overview of the synthetic strategies and typical applications of such multi-stimuli responsive (co)polymers is given in the end of this chapter.

Chapter II investigates the effect of copolymer composition on the formation, stabilization and catalytical properties of gold nanoparticles (AuNPs) stabilized by thermoresponsive statistical copolymer, poly((*N*-vinylcaprolactam)-*stat*-(*N*-vinylpyrrolinone)) (P(VCL-*stat*-VP)), thermoresponsive VCL moieties endow the obtained nanohybrids with an organic shell with tunable properties. Two synthetic methods are proposed to obtain such thermoresponsive nanohybrids: (1) *in situ* formation and (2) coating of preformed AuNPs. The

effects of copolymer composition, concentration, system pH and ionic strength on the colloidal properties (size and stability) of Au@P(VCL-*stat*-VP) are discussed. To study the catalytic efficiency of such nanohybrids, reduction of *p*-nitrophenol to *p*-aminophenol by sodium borohydride is used as a model reaction to investigate how copolymer composition and temperature tune the reaction kinetics.

Chapter III focuses on the study of poly((*n*-butyl acrylate)-*co*-(*N*-isopropylacrylamide)) (P(BA-*co*-NIPAM)) copolymers with different microstructures (diblock, triblock and statistical) comprising thermosensitive NIPAM and hydrobic BA units. These copolymers with different structures and compositions are synthesized by reversible addition-fragmentation chain transfer polymerization/macromolecular design by interchange of xanthates (RAFT/MADIX). The effect of copolymer microstructures on their thermoresponsive properties and self-organization behavior in water is studied in dilute and in concentrated conditions.

Chapter IV aims at studying block copolymers comprising both thermo- and pH-responsive blocks. PNIPAM is chosen as a thermoresponsive block and poly(*N*,*N*-diethylamino ethyl acrylamide) (PDEAEAM) as a dual pH- and thermo-responsive block. All studied homopolymers and block copolymers with controlled molecular weight or composition are synthesized by RAFT polymerization. Thermoresponsiveness of PNIPAM and PDEAEAM homopolymers are first investigated along with pH change. Then the behavior of corresponding block copolymer in aqueous solution is studied as a function of pH and temperature, the effect of copolymer composition on thermosensitive properties and colloidal properties is also investigated under these two stimuli of temperature and pH.

Chapter V explores CO_2-responsiveness of PNIPAM-*b*-PDEAEAM in water. The effect of CO_2 (addition and removal) on the physiochemical properties of PDEAEAM homopolymer is first studied. Then the phase transition (T_c), self-organized nanostructures below and above T_c and reversibility are characterized upon exposure to CO_2/N_2 bubbling.

Chapter I

Literature Review

Contents

I.1 Introduction

Response to external stimuli is central to understanding how biological systems work, especially at the cellular level, with subsequent changes in properties and function from the molecular to the macroscopic level. Stimuli response is crucial for maintaining a normal function: the nervous system regulates the body's responses to internal and external stimuli by carrying information to and from all parts of the body through a vast network of nerve cells; membrane cell permeability and enzyme activity are modulated by concentration of molecular species in solution and so on.

The observation of various systems where such processes occur has indicated a certain number of directions for preparation of next generation systems capable of responding to stimuli in a controllable and predictable fashion.

Many (co)polymers have been designed to respond to external stimuli such as a change in solvent, temperature, pH, light, magnetic or electric field, ionic factors, (bio)molecules and mechanical stress. These responses are manifested as dramatic changes in materials properties, dimensions, structures and interactions and may lead to their rearrangement or changes in their aggregation state.

In this chapter, we first presented the main families of stimuli responsive (co)polymers (thermo-, pH- and CO_2-responsive), their corresponding responsive properties (phase transition temperature and self-organization behavior) upon stimuli applied/removal, impacts for affecting responsiveness, the main polymerization strategies used to obtain these (co)polymers and their applications in field of advanced science materials are described.

I.2 Thermoresponsive (co)polymers

Thermoresponsive (co)polymers in aqueous solution generally undergo a change of solubility in response to a modification of temperature. A fine hydrophobic-hydrophilic balance in their structure is responsible for this phenomenon. Small temperature changes around a critical value induce the collapse or expansion of

(co)polymer chains as a response to the new adjustments of hydrophobic-hydrophilic interactions between (co)polymer and water. The temperature at which the phase separation occurs is called cloud point temperature (T_c). According to the phase transition behavior, there are primarily two categories of thermosensitive (co)polymers.

(a) LCST-type (co)polymers

As illustrated in **Scheme I.1**, the first family concerns (co)polymer for which the phase diagram exhibits a transition from a monophasic to a biphasic region upon heating. This type of (co)polymers possesses a good solubility in water at low temperature because of hydrogen bonds between water molecules and polar groups of (co)polymers. As temperature increases, these hydrogen bonds are broken, water is released and intra- and intermolecular interactions between the (co)polymer chains become stronger, which induces the formation of aggregates and results in cloudy solution.

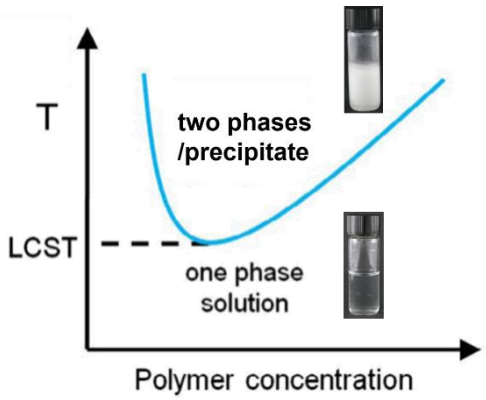

Scheme I.1 Phase diagram of thermoresponsive (co)polymers with LCST behavior.

The minimum temperature on the separation curve is called lower critical solution temperature (LCST). Strictly speaking, the LCST is not equal to T_c since LCST is the minimum value of T_c in the full phase diagram while T_c refers to the temperature at which the system changes from one-phase to two-phase state at a fixed (co)polymer concentration. It is therefore important to pay attention to the concentration-dependent T_c when comparing results issued from the literature. In this thesis, T_c refers to phase

transition temperature of thermoresponsive (co)polymers measured at a given concentration.

The most extensively reported LCST-type homopolymers with different T_c values are summarized in **Table I.1**.

Table I.1 Typical LCST-type homopolymers and their corresponding T_c values (T_c for LCST-type homopolymers determined at a specific homopolymer concentration, molecular weight, and end group).

***N*-alkyl substituted poly(meth)acrylamides**			
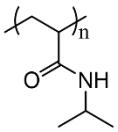 PNIPAM T_c: 32 °C [1]	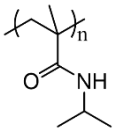 PNIPMAM T_c: 43 °C [2]	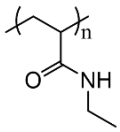 PEAM T_c: 32.2 °C [3]	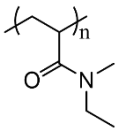 PEMAM T_c: 70 °C [4]
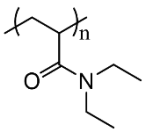 PDEAM T_c: 30 °C [5-8]	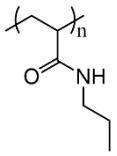 PN*n*PAM T_c: 22.56 °C [9]	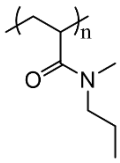 PM*n*PAM T_c: 29.3 °C [10]	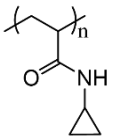 PCPAM T_c: 38 °C [8]
***N*-ester substituted poly(meth)acrylamides**			
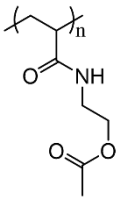 PNAEAA T_c: 51.5 °C [11]	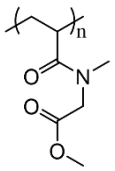 PNASME T_c: 44 °C [12]	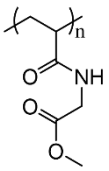 PNAGME T_c: 36.5 °C [13]	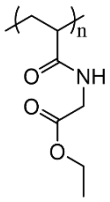 PNAGEE T_c: 20.5 °C [13]	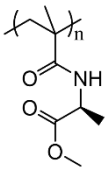 P(MA-$_L$-Ala-OMe) T_c: 35 °C [14]
Poly(*N*-dialkylamino ethyl (meth)acrylamide)s			
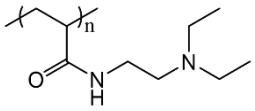 PDEAEAM T_c: 34.5 °C [15]		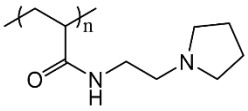 PEPyAM T_c: 30 °C [16]	
***N*-alkyl substituted poly(meth)acrylates**			
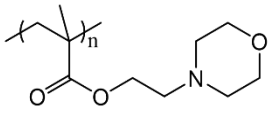 PMEMA T_c: 34 °C [17]		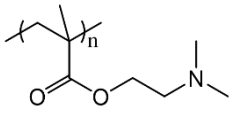 PDMAEMA T_c: 32.2 °C [17]	

Table I.1 (Continued)

Oligo(ethylene glycol) poly(*N*-dialkylamino) methacrylates			
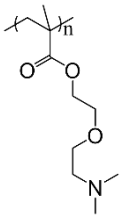	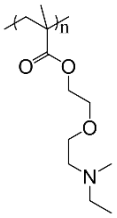	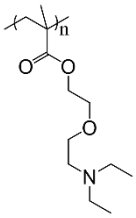	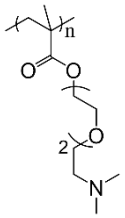
PDMAEEOMA T_c: 52 °C [18]	PEMAEEOMA T_c: 27 °C [18]	PDEAEEOMA T_c: 7 °C [18]	PDMAEEO$_2$MA T_c: 73 °C [18]
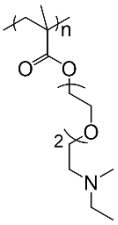	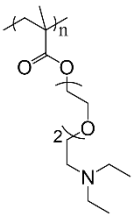	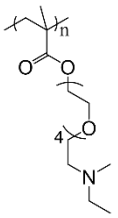	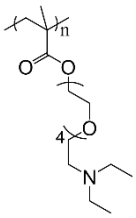
PEMAEEO$_2$MA T_c: 39 °C [18]	PDEAEEO$_2$MA T_c: 20 °C [18]	PEMAEEO$_4$MA T_c: 79 °C [18]	PDEAEEO$_4$MA T_c: 51 °C [18]
Oligo(ethylene glycol) poly(acrylates)			
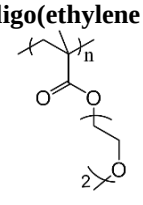	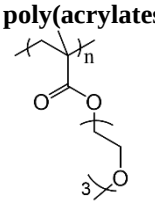	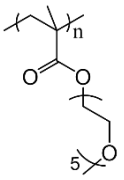	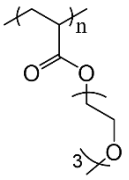
PDEGMA T_c: 27 °C [19, 20]	PTEGMA T_c: 49 °C [19, 20]	PPEGMA T_c: 71 °C [19]	PTEGA T_c: 58 °C [21]
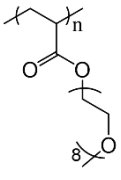			
POEGA T_c: 92 °C [22]			
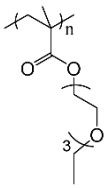	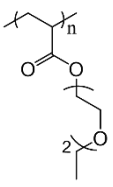	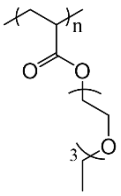	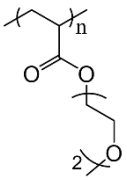
PTEGEMA T_c: 24 °C [19]	PDEGA T_c: ~ 10 °C [23, 24]	PTEGEA T_c: 36 °C [25]	PMDEGA T_c: 45 °C [26]
Other types			
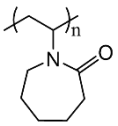	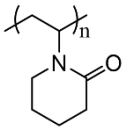	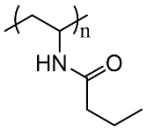	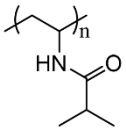
PVCL T_c: 33 °C [27]	PVPip T_c: 68 °C [28]	PNVBA T_c: 32 °C [29]	PNVIBA T_c: 39 °C [29]

Abbreviations: PNIPAM: poly(*N*-isopropylacrylamide), PNIPMAM: poly(*N*-isopropylmethacrylamide), PEAM: poly(*N*-ethylacrylamide), PEMAM: poly(*N*,*N*-ethylmethylacrylamide), PDEAM: poly(*N*,*N*-diethylacrylamide), PN*n*PAM: poly(*N*-*n*-propylacrylamide), PM*n*PAM: poly(*N*-methyl-*N*-*n*-propylacrylamide), PCPAM: poly(*N*-cyclopropylacrylamide), PNAEAA: poly(*N*-acetoxylethyl acrylamide), PNASME: poly(*N*-acryloylsarcosine methyl ester), PNAGME: poly(*N*-acryloylglycine methyl ester), PNAGEE: poly(*N*-acryloylglycine ethyl ester), P(MA-$_L$-Ala-OMe): poly(*N*-methacryloyl-$_L$-alanine methyl ester), PDEAEAM: poly(*N,N'*-diethylamino ethyl acrylamide), PEPyAM: poly(*N*-ethylpyrrolidine acrylamide), PMEMA: poly(2-(*N*-morpholino) ethyl methacrylate),

PDMAEMA: poly(2-(dimethylamino) ethyl methacrylate), PDMAEEOMA: poly(2-(2-(dimethylamino) ethoxy) ethyl methacrylate), PEMAEEOMA: poly(2-(2-(ethyl(methyl) amino) ethoxy) ethyl methacrylate), PDEAEEOMA: poly(2-(2-(diethylamino) ethoxy) ethyl methacrylate), PDMAEEO$_2$MA: poly(2-(2-(2-(dimethylamino) ethoxy) ethoxy) ethyl methacrylate), PEMAEEO$_2$MA: poly(2-(2-(2-(ethyl(methyl) amino) ethoxy) ethoxy) ethyl methacrylate), PDEAEEO$_2$MA: poly(2-(2-(2-(diethylamino) ethoxy) ethoxy) ethyl methacrylate), PEMAEEO$_4$MA: poly(2-(2-(2-(2-(2-ethyl(methyl) amino) ethoxy) ethoxy) ethoxy) ethoxy) ethyl methacrylate), PDEAEEO$_4$MA: poly(2-(2-(2-(2-(2-(diethylamino) ethoxy) ethoxy) ethoxy) ethoxy) ethyl methacrylate), PDEGMA: poly(di(ethylene glycol) methyl ether methacrylate), PTEGMA: poly(tri(ethylene glycol) methyl ether methacrylate), PPEGMA: poly(penta(ethylene glycol) methyl ether methacrylate), PTEGA: poly(tri(ethylene glycol) methyl ether acrylate), POEGA: poly(oligoethylene oxide) acrylate), PTEGEMA: poly(tri(ethylene glycol) ethyl ether methacrylate), PDEGA: poly(di(ethylene glycol) ethyl ether acrylate), PTEGEA: poly(ethoxytri(ethylene glycol) acrylate), PMDEGA: poly(methoxy diethylene glycol acrylate), PVCL: poly(*N*-vinyl caprolactam), PVPip: poly(*N*-vinylpiperidone), PNVBA: poly(*N*-vinyl-*n*-butyramide), PNVIBA: poly(*N*-vinylisobutyramide).

(b) UCST-type (co)polymers

The second family of thermorespnsive (co)polymers exhibits a transition from a biphasic to a monophasic region in the phase diagram upon heating (**Scheme I.2**). The maximum temperature on the separation curve is called upper critical solution temperature (UCST). UCST-type (co)polymers at low temperature generally involve inter- and/or intramolecular interactions between or within different (co)polymer chains. Therefore, this family of (co)polymers is immiscible with solvent. With an increase of temperature, these inter- and/or intramolecular interactions are broken, accompanied with enhanced hydrogen bonds between (co)polymer chains and solvent molecules. This causes an increased solubility in the chosen solvent and the system becomes a monophasic solution.

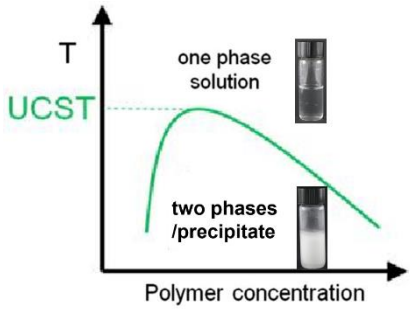

Scheme I.2 Phase diagram of thermoresponsive (co)polymers with UCST behavior.

Interestingly, the solvent plays a key role in studying solution behavior of thermoresponsive (co)polymers. Some (co)polymers, such as PNIPAM [30] and poly((oligo(ethylene glycol) methyl ether methacrylate)-*co*-(oligo(ethylene glycol) phenyl ether acrylate)) (P(OEGMEA-*co*-OEGPhEA)) [31] display typical LCST and UCST behaviors in different solvents.

In this chapter, we mainly focus on thermoresponsive (co)polymers with LCST behaviors, readers who are interested in UCST-type (co)polymers can refer to **Table I.2** where typical UCST-type homopolymers and their transition points are listed.

Table I.2 UCST-type homopolymers and their corresponding phase transition/clarification temperatures (T_{CL})[a].

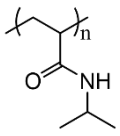	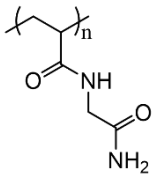	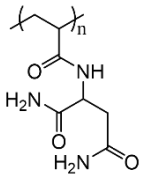	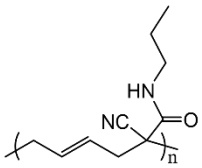
PNIPAM T_{CL}: 22 °C (d_8-[C_2mIm$^+$][TFSA$^-$]) [30]	PNAGA T_{CL}: ~20 °C (H_2O) [32-34]	PNAAAM T_{CL}: 24.3 °C (H_2O) [35]	PCNPCAVCP T_{CL}: ~67 °C (mixture of ethanol and H_2O) [36]
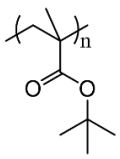	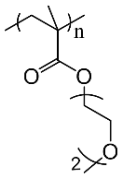	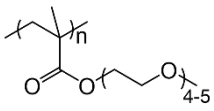	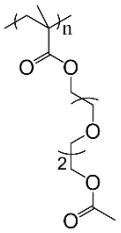
P*t*BMA T_{CL}: 35 °C (methanol) [37]	PDEGMA T_{CL}: 20.6/33.3 °C (ethanol/isopropanol) [38]	POEGMEA T_{CL}: 35.7 °C (isopropanol) [31, 39]	PAEEO$_2$MA T_{CL}: 26 °C (methanol) [40]
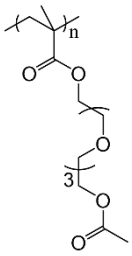		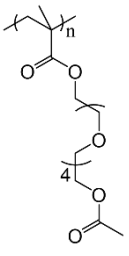	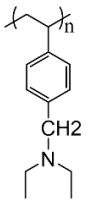
PAEEO$_3$MA T_{CL}: 16.2 °C (methanol) [40]		PAEEO$_4$MA T_{CL}: 4.5 °C (methanol) [40]	PVEA T_{CL}: 36.8 °C (isopropanol) [38]

[a]T_{CL} for UCST-type (co)polymers is temperature where solution changes from cloudy to transparent state. Abbreviations: PNAGA: poly(*N*-acryloylglycinamide), PNAAAM: poly(*N*-acryloylasparaginamide), PCNPCAVCP: poly(1-cyano-*N*-propylcarboxyamido vinyl

cyclopropane), P*t*BMA: poly(*tert*-butyl methacrylate), PDEGMA: poly(oligo(ethylene glycol) methyl ether methacrylate), POEGMEA: poly(oligo(ethylene glycol) methyl ether acrylate), $PAEEO_2MA$: poly(2-(2-(2-acetoxyethoxy) ethoxy) ethyl methacrylate), $PAEEO_3MA$: poly(2-(2-(2-(2-hydroxyethoxy) ethoxy) ethoxy) ethyl methacrylate), $PAEEO_4MA$: poly(2-(2-(2-(2-(2-acetoxy) ethoxy) ethoxy) ethoxy) ethoxy) ethyl methacrylate), PVEA: poly(*N*-(4-vinylbenzyl)-*N*,*N*-diethylamine).

I.2.1 Cloud point temperature (T_c): characterization techniques

T_c refers to the temperature where a phase transition of thermoresponsive (co)polymers at a fixed concentration takes place. Its determination is a prerequisite towards potential applications. Different techniques, including turbidimetry measurement, Dynamic Light Scattering (DLS), Differential Scanning Calorimetry (DSC), Nuclear Magnetic Resonance (NMR) spectroscopy and Fourier Transform Infrared Spectroscopy (FTIR) have been adopted in the literature and described in the following sections.

(i) Turbiditimetry measurement

Turbidimetry measurement is the most extensively applied method to determine T_c and is usually performed on a UV-vis spectrometer at a fixed wavelength to monitor the absorbance (or transmittance) change as a function of temperature. As illustrated in **Figure I.1**, T_c can be evaluated from this transmittance curve at different stages: onset temperature, temperature at which 90, 50 and 10% transmittance reach, inflection point. These different values are not significantly different for (co)polymers presenting a sharp transition, in the case of broad transition, as depicted in **Figure I.1A**, the deviation between the maximum ($T_{c,10\%\ transmittance}$) and minimum ($T_{c,onset}$) T_c values obtained by using different evaluation methods can reach up to 11.9 °C. Therefore, the way to evaluate the transmittance curve to obtain T_c should be treated carefully. [41]

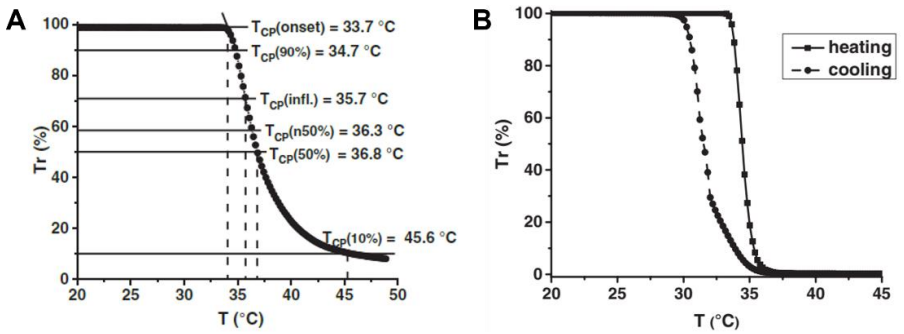

Figure I.1 Transmittance as a function of temperature for PNIPAM solutions: (A) Different evaluation methods for determination of T_c and (B) Thermal hysteresis observed in heating-cooling cycles (heating rate: 0.2 $^oC \cdot min^{-1}$, wavelength: 488 nm, PNIPAM concentration in (**A**) and (**B**) were 0.02 and 0.1 wt.% respectively). Copyright 2017. Reproduced with permission from WILEY-VCH Verlag GmbH & Co. kGaA. Ref. [41]

Ideally, the demixing (aggregation, dehydration) and remixing (dissolution, hydration) of thermoresponsive (co)polymers should appear at the same temperature. However, a thermal hysteresis, difference in phase transition points in heating-cooling cycles, is commonly observed in turbidimetry measurements, such as in the cases of PNIPAM (**Figure I.1B**), [41] poly(*N*-isopropylacrylamide)-*block*-poly(ethylene oxide)-*block*-poly(*N*-isopropylacrylamide) (PNIPAM-*b*-PEO-*b*-PNIPAM), [42] poly(*N*-isopropylacrylamide)-*block*-poly(*n*-butyl acrylate)-*block*-poly(*N*-isopropylacrylamide) (PNIPAM-*b*-PBA-*b*-PNIPAM), [43] PBA-*b*-PNIPAM, [43] PBA-*stat*-PNIPAM [34] and poly((*N*-isopropylacrylamide)-*co*-(3-(trimethoxysilyl) propyl methacrylate)) (P(NIPAM-*co*-TMSPMA)). [44] This phenomenon can be ascribed to the difficulty to rehydrate compact aggregates formed at high temperature due to intra-chain entanglement or limited diffusion of water molecules into hydrophobic aggregates. Only when sufficiently equilibrium time or a very low heating/cooling rate is applied, the same T_c in heating-cooling processes can be obtained. To limit this kinetic effect, T_c can be plotted as a function of heating or cooling rate and the value extrapolated to 0 $°C \cdot min^{-1}$ can be taken as the value of T_c.

(ii) Dynamic Light Scattering (DLS)

The presence of aggregates in solution results in a scattering phenomenon when this solution is irradiated with light. The intensity of scattered light is proportional to

D_H[6] (D_H: Hydrodynamic diameter). DLS enables to measure the scattered intensity and from this to evaluate particle size and size distribution (i.e. intensity-, number- and volume-distributed diameter) at a specific temperature.

DLS results for LCST-type (co)polymers generally show small D_H at temperature below T_c and large D_H above T_c due to the aggregation of thermoresponsive chains upon heating. Additionally, the evolution of scattered intensity or size as a function of temperature enables to estimate T_c (**Figure I.2**). By using this method, poly(di(ethylene oxide) methyl ether methacrylate) (PDEGMA) was reported with T_c at 27.5 °C, poly((di(ethylene oxide) methyl ether methacrylate)$_{81}$-*stat*-(oligo(ethylene oxide) methyl ether methacrylate)$_{19}$) (P(DEGMA$_{81}$-*stat*-OEOMA$_{19}$)) and P(DEGMA$_{80.5}$-*grad*-OEOMA$_{19.5}$) show LCST behaviors at 50.7 and 36.6 °C respectively. [45] Poly(bis(*N*-hydroxyisopropyl pyrrolidone 2-vinylterephthalate)) (PHIPPVTA) displays T_c in temperature range from 24 to 80.9 °C with molecular weight changing from 4700 to 44200 g·mol^{-1}. [46] T_c of PVCL-based (co)polymer varies from 27 to 42 °C depending on (co)polymer concentration, nature of comonomer and composition. [47]

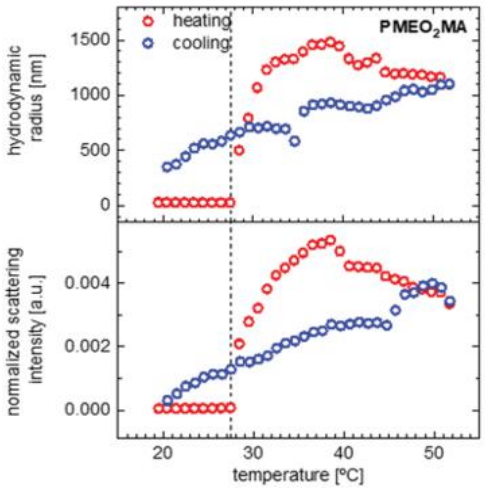

Figure I.2 Evolution of hydrodynamic diameter and normalized scattering intensity of $PMEO_2MA$ (or PDEGMA) as a function of temperature (M_n: 13660 g·mol^{-1}, concentration: 1 mg·mL^{-1}). Copyright 2020. Reproduced with permission from the Royal Society of Chemistry. Ref. [45]

(iii) Differential Scanning Calorimetry (DSC)

Thermal phase transition is accompanied with exchange of energy, which can be detected by DSC experiments. T_c is evaluated upon heating/cooling at onset

temperature or at temperature where maximum of measured peak occurs (**Figure I.3A**). In addition, the area of observed peak is equal to the variation of enthalpy (ΔH) which is regarded as the energy involved in this transition to break hydrogen bonds between water and (co)polymer chains. [48]

The endothermic peak significantly relies on sample concentration (**Figure I.3B**), it shifts to higher temperature and its peak shape becomes broader as (co)polymer concentration decreases. It is noteworthy that a very low concentration is detrimental to T_c determination whatever onset or maximum peak temperature selected due to the poor sensibility of this technique.

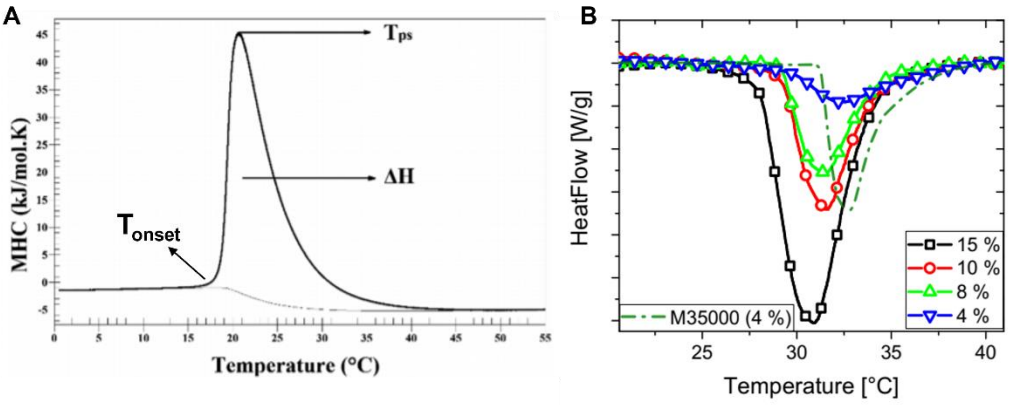

Figure I.3 Thermograms of (A) poly(propylene oxide) (PPO) aqueous solution (M_n: 2000 g·mol^{-1}, concentration: 0.5 wt.%, heating rate: 0.2 °C·min^{-1}) and (B) poly((*N*-isopropylacrylamine)-*stat*-(dopamine methacrylamide)) solution (M_n: 17900 g·mol^{-1}, heating rate: 5 °C·min^{-1}, dash-dot line was 4 wt.% PNIPAM with M_n of 35000 g·mol^{-1}). Copyright 2015 and 2019, respectively. Reproduced with permission from the American Chemical Society. Ref. [48, 49]

(iv) Nuclear Magnetic Resonance (NMR)

Upon heating, modification of interactions occurs in solution between the (co)polymer and the solvent that results in a decreasing solubility of (co)polymer. Therefore, thermal transition can be studied by NMR spectra by monitoring the changes in intensity and/or integration of characteristic peaks. In some extreme cases, no signals of thermoresponsive units can be detected when temperature rises over T_c. Through variable temperature ^{1}H NMR spectra, T_c of thermoresponsive (co)polymers can be calculated by plotting intensity or integration area of thermosensitive groups as a

function of temperature, the signal intensity at a given temperature depends on the degree of mobility of observed nuclei within aggregates as depicted in **Figure I.4**. [50]

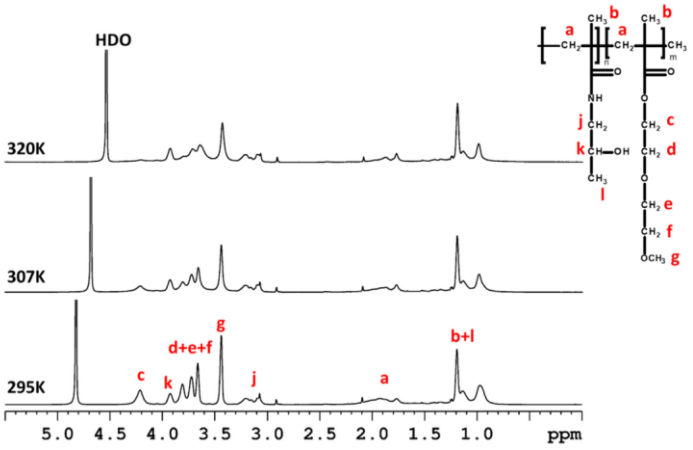

Figure I.4 ^{1}H NMR spectra of poly(*N*-(2-hydroxypropyl) methacrylamide)$_{53}$-*b*-poly(2-(2-methoxyethoxy) ethyl methacrylate)$_{53}$ (PHPMAm$_{53}$-*b*-PDEGMA$_{53}$) in D_2O at different temperatures ([PHPMAm$_{53}$-*b*-PDEGMA$_{53}$] = 0.67 wt.%, M_n = 17100 g·mol^{-1}, DEGMA content is 50 mol%, T_c = 308 K). Copyright 2020. Reproduced with permission from the Elsevier Ltd. Ref. [50]

In addition, to efficiently study the thermoresponsiveness, spin-lattice (T_1) or spin-spin (T_2) relaxation time can be measured since both are sensitive to changes in mobility of (co)polymer chains and solvent upon heating. Generally, for thermoresponsive groups, T_2 changes slightly along with temperature since the mobility of these groups is reduced due to hydrogen bonds at low temperature and is restricted by hydrophobic association among (co)polymer chains at high temperature. For water (HDO protons or D_2O deuterons), T_2 reflects water behavior and (co)polymer-water interaction upon heating. In the cases of PNIPAM, [51] PNIPMAM, [51] poly(2-isopropyl-2-oxazoline) (PIPOx), [52] PVCL, [53] poly(vinyl methyl ether) (PVME) [54, 55] and PEO-*b*-PNIPAM, [56] T_2 of HDO at low temperature is higher than the value at high temperature, which is ascribed to a small portion of HDO with restricted mobility confined within aggregation structure at temperature above T_c, the water releasing from inside of the aggregates makes T_2 increase over time, as shown in **Figure I.5A**. An inverse phenomenon is observed in the case of poly((2-(2-methoxyethoxy) ethyl methacrylate)-*stat*-(*N*-propargylmethacrylamide)) (P(DEGMA-*stat*-GMAm)) where larger T_2 value is observed at elevated temperature than that at low temperature (see

Figure I.5B), the possible reason may relate to the fact that raising temperature weakens the hydrogen bonding network and improves mobility of water. [50]

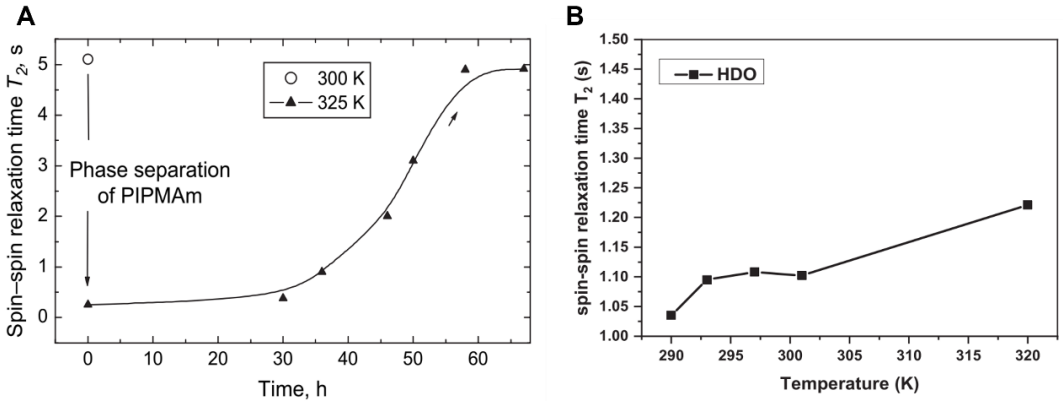

Figure I.5 (A) Time-dependence of T_2 of HDO of PNIPAM and (B) Temperature dependence of T_2 of HDO of P(DEGMA-*stat*-GMA) in D_2O solutions. Copyright 2006 and 2020, respectively. Reproduced with permission from the Elsevier Ltd. Ref. [50, 51]

Interestingly, in the cases of poly(2-ethyl-2-oxazoline) (PEOx), [57] $PHPMAm_{53}$-*b*-$PDEGMA_{78}$, [50] poly(2-ethyl-2-oxazoline)-*b*-poly(2-methyl-2-oxazoline) (PEOx-*b*-PMeOx), [52] $PIPOx_{86}$-*b*-$PMeOx_{14}$ [52] and Y-shape PEO_{44}-*b*-$PEOx_{252}$-*b*-(poly(ε-caprolactone)$_{87}$)$_2$ (PEO_{44}-*b*-$PEOx_{252}$-*b*-$(PCL_{87})_2$), [58] two T_2 values were measured corresponding to the existence of two types of water at elevated temperature (see **Figure I.6**): one is related to free water with long T_2 corresponding to the water in solution and the other is related to "bound" water with short T_2 corresponding to the water inside of aggregates. What's more, the exchange between "free" and "bound" water molecules is slow and both can keep their stabilities for a long time.

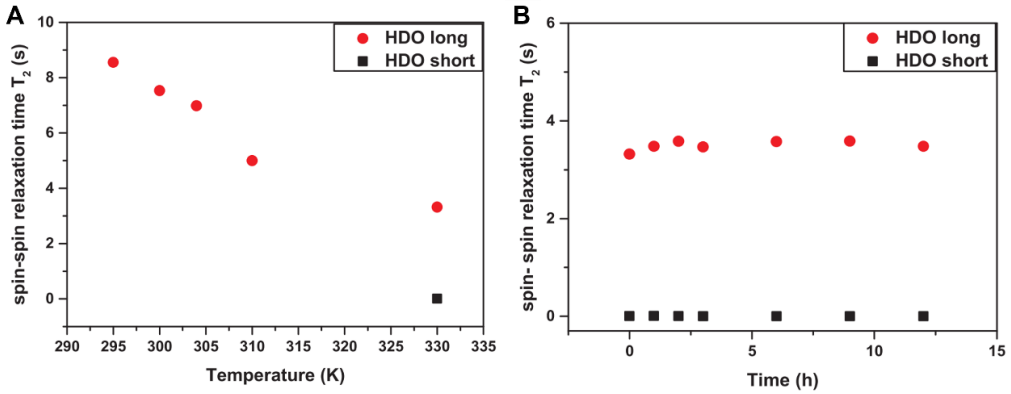

Figure I.6 (A) Temperature-dependence and (B) Time-dependence at 330 K of T_2 of HDO of $PHPMA_{53}$-*b*-$PDEGMA_{78}$ in D_2O. Copyright 2020. Reproduced with permission from the Elsevier Ltd. Ref. [50]

(v) Fourier Transform Infrared (FTIR) Spectroscopy

FTIR spectroscopy is a powerful tool to visualize changes in hydration state of individual groups upon heating since it is highly sensitive to the conformational change of thermoresponsive chains and to local environment of molecules and interaction between molecules. For instance, C=O stretching vibration of PNIPAM is observed at 1625 cm^{-1} corresponding to the hydrogen bonds between C=O and water at low temperature and shifts to 1650 cm^{-1} at high temperature due to the formation of C=O···H-N among PNIPAM chains. Therefore, the IR difference spectra calculated by subtracting IR spectrum at temperature below T_c from spectrum at temperature above T_c reflects the conformation and interaction changes in the system. Meanwhile, pairs of negative (representing absorption at low temperature) and positive (representing absorption at high temperature) peaks of these special groups appear in IR difference spectra (see **Figure I.7B**). To avoid the effect of baseline drift, the difference in ΔA at ν_1 (wavenumbers at positive peak) and ν_2 (wavenumbers at negative peak) instead of ΔA_{T-T0} at ν_1 or ν_2 is generally utilized to follow the phase transition behavior (**Figure I.7C**) and it is defined as:

$$\Delta\Delta A_{T-T0}(\nu_1 - \nu_2) = \Delta A_{T-T0}(\text{at } \nu_1) - \Delta A_{T-T0}(\text{at } \nu_2)$$

Where T and T_0 are high and low temperatures, respectively. By using this evaluation method, Yasushi Maeda and co-workers have obtained T_c values of a series of thermoresponsive homopolymers and copolymers, such as PNIPAM, [59] poly(*N*,*N*-dimethylacrylamide) (PDMAm), [60] PN*n*PAM, [61] poly(*N*-cyclopropylamide) (PcPA), [61] PVCL, [62] poly(*N*-*n*-propylmethacrylamide) (P*n*PMA), [63] PNIPMAM, [63] poly(*N*,*N*-bis(2-methoxyethyl) acrylamide) (PbMoEA), [64] PDEGMA, [65] poly(*N*-(2-ethoxyethyl) acrylamide) (PEoEA), [66] poly(*N*-(2-ethoxyethyl) methacrylamide) (PEoEMA), [66] poly(*N*-tetrahydrofurfurylacrylamide) (PTHFA), [67] poly(*N*-tetrahydrofurfurylmethacrylamide) (PTHFMA), [67] poly((*N*-isopropylacrylamide)-*co*-(acrylonitrile)) (P(NIPAM-*co*-AN_{20})), [68] poly((*N*-isopropylacrylamide)-*co*-(acrylamide) (P(NIPAM-*co*-AAm)), [68] poly(3-dimethyl(methacryloyloxyethyl) ammonium propane sulfonate)-*b*-poly(*N*,*N'*-

diethylacrylamide) (PdMMAEAPS-*b*-PDEAM), [69] poly((*N*-isopropylacrylamide)-*co*-(methyl acrylate)) (P(NIPAM-*co*-MA)), [70] poly((*N*-isopropylacrylamide)-*co*-(vinyl acetate)) (P(NIPAM-*co*-VAc)), [70] poly((*N*-isopropylacrylamide)-*co*-(acrylic acid)) (P(NIPAM-*co*-AA_5)) [71] and (P(DEAM-*co*-AA_5)). [71]

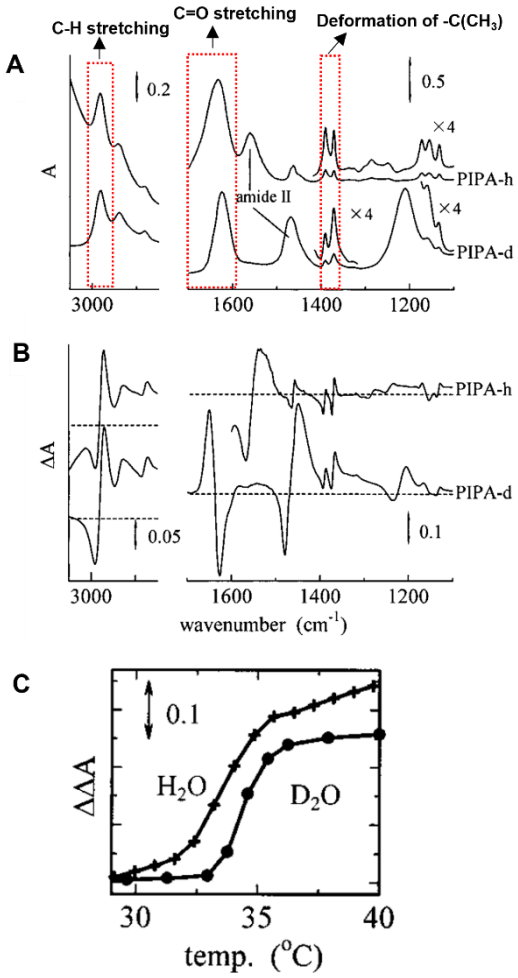

Figure I.7 (A) IR spectra of PNIPAM in H_2O and in D_2O at 25 °C. (B) IR difference spectra obtained by subtraction IR spectra measured at 25 °C from those measured at 40 °C. (C) Plots of $\Delta\Delta A_{T\text{-}25}$(2970-2991) (C-H stretching mode) in D_2O and in H_2O as a function of temperature. Copyright 2000. Reproduced with permission from the American Chemical Society. Ref. [59]

It is noteworthy that D_2O is usually used as solvent instead of H_2O in IR spectra measurement to avoid overlapping the water band (~1200 and 1640 cm^{-1} for D_2O and H_2O bands, respectively) with C=O stretching band (1600 cm^{-1}). Consequently, a higher T_c in D_2O than that in H_2O is obtained since hydrogen bonds formed from D_2O and (co)polymer chains are stronger than ones from H_2O.

I.2.2 Main parameters affecting T_c of (co)polymers

Finely tuning T_c is a key point to broaden the potential applications of thermoresponsive (co)polymers. In the literature, factors affecting T_c value have been reported, such as molecular weight, (co)polymer concentration, topology structure, incorporated comonomers, terminal groups, additives, etc. Here, we make a summary on how these impacts influence T_c of thermoresponsive (co)polymers in aqueous solution.

(i) Effect of molecular weight

Demixing point temperature of most thermoresponsive (co)polymers decreases with both increasing (co)polymer chain length and concentration. Typical examples are PDMAEMA, [17] PDEGMA, [72] poly(*N*-isopropyl-*N*-methylacrylamide) (PiPMAm), [73] PMEMA, [17] PEMAEEOMA, [18] PNAGME [13] and PVCL. [27, 74] In these cases, a clear decreasing trend of T_c is detected with increasing molecular weight.

Numerous efforts have been made to explore the relationship between T_c and molecular weight for PNIPAM homopolymers due to its extensive applications. However, this issue is still controversial. Stöver, Winnik and Nystrom have reported T_c of PNIPAM declines with an increase of molecular weight. In their work, PNIPAM homopolymers are ended with 2-propionamide, [75] ethyl 2-propionate, [75, 76] methyl 2-propionate, [77] phenyl 2-propionamide, [75] hydroxyethyl, [78] propargyl [78] and chloroethyl groups. [78] On the contrary, an increasing trend of T_c along with molecular weight has been reported by Warr and co-workers. In their work, T_c of dodecyl terminated PNIPAM increases from 14 to 33 ^{o}C as its corresponding molecular weight rises from 1110 to 7170 $g \cdot mol^{-1}$, [79] This phenomenon is also observed in PNIPAM terminated with *n*-hexyl [78] and *N*-triphenylmethyl 4-cyanovaleramide [80] groups in lower molecular weight range, after which T_c remains at a constant value and is not influenced by increasing molecular weight. Therefore, these different results on the relationship between T_c and molecular weight for PNIPAM homopolymer might be

ascribed to the effect of end groups introduced in the synthesis, the detailed information of effect of end groups on T_c will be described in **Section I.2.2 (v)**.

(ii) Effect of (co)polymer concentration

PNIPAM, [76, 81, 82] $PNASME_{170}$, [12] PNIPMAM, [2] PDEAEAM, [15] $PNAEAA_{113}$ [11] and $PEMAEEOMA_{108}$ [18] are reported to have lower T_c in concentrated solution than that in dilute solution: the density of (co)polymer chains in concentrated solution is high, which results in stronger hydrophobic intra- and interactions among (co)polymer chains at low temperature, although hydrogen bonds between water and (co)polymer chains dominate the system. Once temperature is raised, the hydrogen bonds in such conditions are easy to broke. Therefore, the thermal phase transition tends to take place at lower temperature. However, the intensity of concentration effect is less remarkable when concentration goes up to a critical value. For instance, T_c values of P($DEGA_{60}$-*stat*-$DMAm_{40}$) and P($DEGA_{50}$-*stat*-$DMAm_{50}$) do not change in concentration range from 6 to 20 $mg{\cdot}mL^{-1}$. [23] $PNASME_{170}$ solution maintains T_c around 44 ^oC as polymer concentration is over 0.5 wt.%, [12] T_c (36.5 ^oC) of $PNAGME_{177}$ starts to be independent on concentration change as concentration increases above 1 wt.%. [13]

(iii) Effect of additives

Considerable efforts have been taken into understanding the effect of additives (salts, organic solvents, surfactants, etc.) on T_c of thermoresponsive (co)polymers in water. The concepts of "salting in" effect (hydration) and "salting out" effect (dehydration) are proposed to analyze how salts influence T_c of thermoresponsive (co)polymer solution. Moreover, the influence of salts through their anions and cations and the amplitude of salt effect not only relate to the salt concentration, but also follow Hofmeister series, anions: $CO_3^{2-} > SO_4^{2-} > S_2O_3^{2-} > H_2PO_4^- > F^- > Cl^- > Br^- \sim NO_3^- > I^- > ClO_4^- > SCN^-$; cations: $Ba^+ > Zn^+ > Mg^{2+} > Ca^{2+} > Li^+ > Na^+ > Rb^+ > Cs^+ > NH_4^+ > N(CH_3)_4^+$. [83, 84] Generally, hydrated capacity of ions decreases along these two

series, ions on the left displaying "salting out" effect tends to lower T_c, while right ones showing "salting in" effect shifts T_c towards higher temperature. What's more, the anion effect within Hofmeister series is more pronounced than cations. With the guideline of Hofmeister series, the salt effect (especially the anions effect) on solubility behavior of thermoresponsive (co)polymers, such as PNIPAM, [85, 86] PNIPAM-*b*-PEO-*b*-PNIPAM, [42] $PNASME_{170}$, [12] $PNAEAA_{193}$, [11] PPO, [48] polymer based on oligo-2-ethyl-2-oxazoline side chains and a methacrylate backbone (POEtOxMA), [87] $P(DEGMA_{81}$-*stat*-$OEOMA_{19})$ [45] and $P(DEGMA_{80.5}$-*grad*-$OEOMA_{19.5})$ [45] can be easily analyzed.

Fatty acid sodium salts, such as sodium caproate, caprylate, caprate, undecylenoate, laurate, dodecyl sulfate and myristate salts are commonly regarded as surfactants with a long alkyl-substituted tail and a hydrophilic carboxylate or sulfate head group. The separated hydrophobic and hydrophilic structures of fatty acid sodium salts raising or lowering T_c of thermoresponsive (co)polymers depends on surfactant concentration and hydrocarbon tail length. [88, 89]

Freitas and co-workers found that LCST (34 ^oC) of PNIPAM in pure water shifts to 21.3 and -5 ^oC as molar fraction of acetone and methanol raises to 0.14 and 0.34, respectively (see **Figure I.8A**). Acetone and methanol are more likely to interact with water rather than with PNIPAM, the formation of organic solvent-water mixture reduces the hydrogen bonds formed between water and PNIPAM and leads to a decrease of enthalpy of LCST transition. To be specific, upon continuous addition of cosolvents, more water molecules are needed to form solvent-water mixture, which causes less free water are available to form hydrogen bonds between water and (co)polymers. The remaining free cosolvent molecules can bind to (co)polymer since hydrogen bonds are formed between PNIPAM and methanol (providing hydroxyl groups) or between PNIPAM and acetone (providing carbonyl groups), which helps to improve the solubility of PNIPAM. Therefore, an increasing T_c is observed at high concentration of methanol and acetone. [90] The similar phenomenon is also observed in the cases of PNIPAM in H_2O-THF and H_2O-dioxane systems. [91] However, an

unexpected UCST behavior occurred at higher concentration of organic solvents in the mixtures of water and ethanol (or methanol or propanol or DMSO or DMF), as shown in **Figure I.8B**. [90, 92] due to the large hydrophobic groups, hydrophobic interactions among non-polar groups in system overweight hydrogen bonds between PNIPAM and organic solvents. Thus, a UCST behavior occurs.

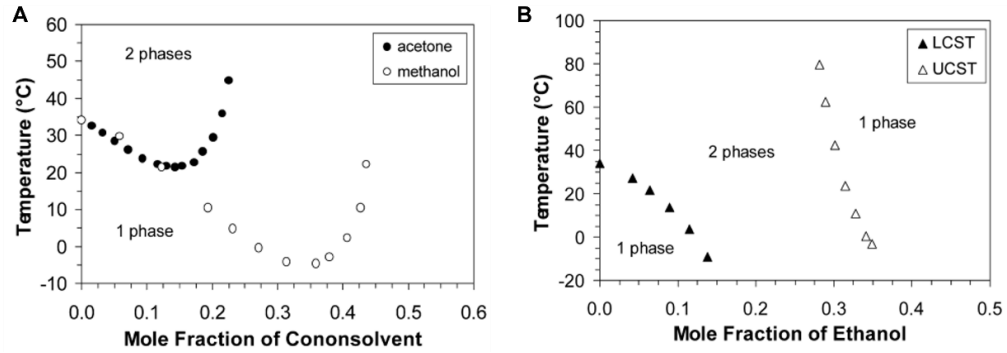

Figure I.8 Phase transition diagram of PNIPAM in (A) water-methanol (open cycles) and water-acetone (filled cycles) solutions, and in (B) water-ethanol (filled and open triangles representing LCST and UCST behaviors, respectively). Copyright 2002. Reproduced with permission from the Elsevier Science Ltd. Ref. [90]

(iv) Effect of polarity of incorporated comonomers

To precisely tune T_c of thermoresponsive homopolymers in aqueous solution over a broad temperature range, incorporation of hydrophilic or hydrophobic moieties is a common strategy. As depicted in **Scheme I.3**, the insertion of hydrophilic moieties generally enhances T_c while hydrophobic ones display an inverse effect. Moreover, the intensity in T_c change relates to the molar ratio of incorporated non-thermosensitive moieties in copolymers.

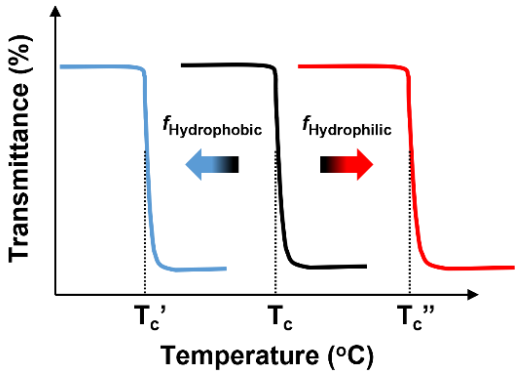

Scheme I.3 Schematic illustration for switchable T_c after incorporation of hydrophilic or hydrophobic comonomers measured by turbidimetry measurements.

(a) Hydrophilic comonomers

Introduction of hydrophilic moieties to thermosensitive homopolymers can help to increase the overall copolymer solvation in water since hydrogen bonds are formed not only between water and thermoresponsive groups but also between water and hydrophilic units, which shifts the hydrophilic/hydrophobic balance of the copolymers towards hydrophilicity. Consequently, a higher temperature is needed to release water.

(b) Hydrophobic comonomer

Hydrophobic moieties suppress hydrogen bonds between water and (co)polymer chains but enhances hydrophobic association between (co)polymer chains. These two effects tend to lower the miscibility of homopolymers modified with hydrophobic moieties in water and decrease their corresponding T_c values. **Table I.3** summarizes typical examples of enhanced/lowered T_c values by copolymerization with hydrophilic/hydrophobic comonomers.

Table I.3 T_c shifted by incorporation of hydrophilic/hydrophobic comonomers.

Thermoresponsive homopolymer	Incorporated hydrophilic comonomer	Incorporated hydrophobic comonomer
PNIPAM	DMAm, [93-95] ACMP, [96] MAAm, [96] MVA, [96] NVA, [96] VPL, [96] HIPAAm, [97], AAm, [94, 96] HMAAm, [98] HEAAm [99]	MASE, [100] BA, [101] Ac-6ACA, [102] CL, [103] HEMA, [94] VL [1]
PVCL	MVA, [104] NVA, [104] VP, [47, 105-107] VOH [108]	VAc, [104] VPi, [104] HA [47]
PDEGA	DMAm [23]	/
PDEVP	DMVP [109]	DPVP [109]
PHTBAM	HEAAm [110]	/
PM*n*PAM	DMAm [10]	/
PEGMA	/	PPGMA [111]

Abbreviations: ACMP: 4-acryloylmorpholine, MAAm: methacrylamide, MVA: *N*-methyl-*N*-vinylacetamide, NVA: *N*-vinylacetamide, VPL: *N*-vinyl-2-pyrrolidi-none, HIPAAm: 2-hydroxyisopropylacrylamide, HMAAm: *N*-(hydroxymethyl) acrylamide), HEAAm: *N*-hydroxyethylacrylamide, MASE: methacrylic acid stearyl ester, Ac-6ACA: acryloyl 6 amino

caproic acid, HEMA: 2-hydroxyethyl methacrylate, VL: vinyl laurate, VP: *N*-vinylpyrrolidone, VOH : vinyl alcohol, VPi: vinyl pivalate, HA: *n*-hexyl acrylate, DMVP: dimethyl vinylphosphonate, DPVP: di-n-propyl vinylphosphonate, PHTBAM: poly(*N*-(2-hydroxyl-*tert*-butyl) acrylamide), PEGMA: poly(ethylene glycol) methacrylate, PPGMA: poly(propylene glycol) methacrylate.

(v) Effect of end group

To prepare well-defined (co)polymers, people usually synthesize thermoresponsive (co)polymers by using controlled radical polymerization, such as atom transfer radical polymerization (ATRP), reversible addition-fragmentation chain-transfer (RAFT) polymerization. As a result, the initiators, terminators (or chain-transfer agents) as the end groups are inevitably introduced into (co)polymers, the transition points of which in aqueous solution are therefore affected due to the different polarities, especially for those (co)polymers with low molecular weights.

Many efforts have been devoted to exploring the effect of end groups on T_c of PNIPAM, such as hydrophilic (i.e. amino, hydroxyethyl, propargyl, chloroethyl terminated groups) and hydrophobic (i.e. alkyl substituted end groups: propyl, isobutyl hexyl, octyl, dodecyl and octadecyl) groups. [78, 79, 100, 112] Dodecyl terminated PNIPAM has a lower T_c around 25 ^oC, whereas T_c in the case without hydrophobic terminal is much higher (38 ^oC). [79] Another typical example was reported by Stöver and coworkers shown in **Figure I.9.**

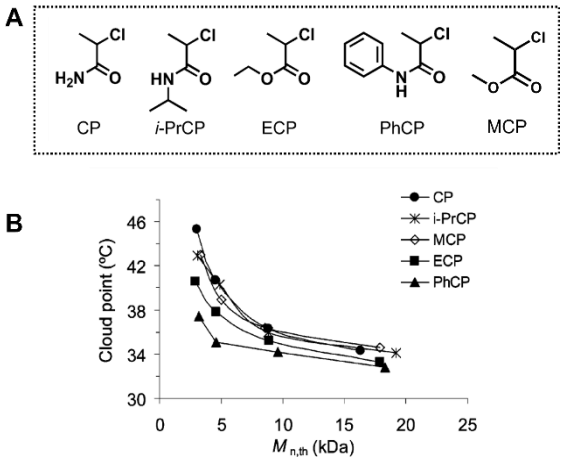

Figure I.9 (A) Chemical structure of initiators providing terminal groups to PNIPAM and (B) cloud point as a function of molecular weight for PNIPAM terminated with end groups

of varying polarities. Copyright 2006. Reproduced with permission from the American Chemical Society. Ref. [75]

PNIPAM ended with five groups deriving from initiators with variable polarities. The effect of termini on T_c at low molecular weight (3000 g·mol^{-1}) is dramatic, compared to T_c of PNIPAM-*i*-PrCP (42.9 ^{o}C, this end group has the similar chemical structure to PNIPAM units), hydrophilic propionamide group (PNIPAM-CP), hydrophobic ethoxypropionate (PNIPAM-ECP) and phenylpropionamide groups (PNIPAM-PhCP) shift T_c to 45.3, 40.6 and 37.4 ^{o}C, respectively. As molecular weight of PNIPAM raises to 16000 g·mol^{-1}, the end group effect is less remarkable. Additionally, due to the weak hydrophobicity, methylpropionate group (PNIPAM-MCP) displays a similar T_c to PNIPAM-*i*-PrCP at molecular weight of 3000 g·mol^{-1}, which suggests that methylpropionate group has a slight or no effect on T_c in the given range of molecular weight. [75]

Additionally, T_c is also influenced by the number of end groups. T_c of P(NIPAM-*stat*-DMAm) terminated with one hydrophobic dodecyl group is detected at 46 ^{o}C, one more dodecyl group can reduce T_c to 30 ^{o}C. [113] In the case of PNIPAM, two octadecyl end groups can dramatically drop T_c by 6.7 ^{o}C compared to the unmodified PNIPAM. [82]

As evidenced by these examples, the modification of thermoresponsive (co)polymer chain termini shows a similar effect on T_c as the effect of incorporation of hydrophilic/hydrophobic comonomers on T_c. In details, the thermoresponsive (co)polymers ended with hydrophilic groups tend to possess higher solvation and mobility, which results in a higher T_c, whereas the hydrophobic end groups are prone to lower T_c. Moreover, the magnitude of these effects relies on the nature of terminals.

(vi) Effect of topological structure

Taking advantage of controlled polymerization techniques, a great number of (co)polymers with different topologies, such as star, branched, dendritic and cyclic typed structures, are designed and successfully synthesized, these different topologies

strongly affect the bulk and solution properties (glass transition temperature, thermal phase transition, micellization, etc.). Investigation on topological effect on T_c of thermoresponsive (co)polymers allows us to gain a deep insight into modulation the complex thermoresponsiveness and to exploit better performing (co)polymeric materials.

Cyclic (also called ring) (co)polymers, compared to the linear counterparts, have no free chain ends in the (co)polymer backbone. Generally, the cyclic thermoresponsive (co)polymers exhibit lower T_c than linear ones at the same molecular weight and concentration, which was detected in the cases of PNIPAM, [114, 115] PDEAm [116] and PVCL. [117] This phenomenon can be explained by the existence of steric constraints especially in smaller rings, compared to the linear (co)polymers, cyclic ones are restricted in the ring and less stretched in dimensions, which favors the interaction hydrogen bonds between cyclic (co)polymer units instead of interactions between water and (co)polymer chains, that is to say, the water molecules bound to the (co)polymer chains are easy to release with rising temperature. In addition, the number of hydrogen bonds formed between water and (co)polymer chains inside of the ring is less than those formed outside, which leads to a gradual dehydration in a broader temperature range.

However, there are some exceptions of cyclic (co)polymers with enhanced T_c values than linear counterparts. For instance, the cyclic (co)polymers of PBA-*b*-PEO, [118] PDMAEMA, [119] PIPOx, [120] poly((*N*-isopropylamide)-*co*-(*N*-acryloylhomocysteine thiolactone)) P(NIPAM-*co*-ATL) [121] and poly((*N*-isopropylamide)-*co*-(*N*-acryloylhomocysteinethiolactone))-*graf*-(diethylethylenediamine) /(poly(ethylene glycol) methyl ether acrylate) (P(NIPAM-*co*-ATL)-*graf*-DEDA/PEGA) [121] were observed with elevated T_c compared to their corresponding analogues. Feng and co-workers found cyclic, diblock and triblock copolymer composing of poly(2-(diethylamino) ethyl methacrylate) (PDEAEMA) and PEO blocks follow a T_c decreasing order: $T_{c,cyclic} > T_{c,diblock} > T_{c,triblock}$. [122] These phenomena may be related to the repulsive force between the rings or cyclic grafts. Winnik reported cyclic PNIPAM shows higher T_c than the linear analogue under the similar molecular weight

and concentration, [123] the possible explanation is the introduction of different groups in synthesis of polymer, the effect of chain termini on T_c of linear polymers is believed more crucial than that of cyclic analogues.

Star (co)polymers basically are composed of one core and a certain number of arms in structure. The limited space near or in the core region restricts dispersion of water molecules. The hydrogen bonds formed between water and (co)polymer chains are relatively less, and they are broken more easily upon heating, therefore, the T_c of such thermoresponsive (co)polymers tends to be lower than linear counterparts at the same molecular weight and concentration. This explanation is evidenced by the case of star typed PDEAM. [116, 124] What's more, in the cases where molecular weight is sufficiently high and T_c is no longer dependent on molecular weight, such as PNASME, [125] PNIPAM [126] and PDMAEMA, [127] increasing arm numbers in star typed thermoresponsive (co)polymers means higher chain density. Compared to those analogues with less arms, the hydrophobic intra-interaction in the core region become very strong with increasing temperature. Therefore, the corresponding T_c values are detected at lower temperature.

(vii) Effect of (co)polymer microstructure

Linear thermoresponsive copolymers are usually designed with different microstrutures, such as block, gradient, and statistical structures. Generally, block copolymers possess at least two separated segments, gradient copolymers display a gradual distribution change in composition along a single chain, while the distribution of repeating units in statistical copolymers are random. The difference among these architectures is clearly illustrated in **Scheme I.4.**

For block and statistical copolymers with identical composition (bearing one thermoresponsive moieties), the non-thermoresponsive units in statistical structures disrupt the homogeneous distribution of thermoresponsive block and results in a formation of several thermosensitive blocks with different lengths, which generally endows themselves with variable thermosensitivity since T_c of each block is strongly

affected by chain length and neighboring segments. Consequently, statistical copolymers exhibit different T_c values compared to block counterparts even though their molecular weights and compositions are identical. The T_c of statistical copolymers higher or lower than block analogues depends on the polarity of non-thermoresponsive moieties, as mentioned in **Section I.2.2 (iv)**.

Due to the gradual distribution of repeating units in gradient structures, stepwise dehydration tends to take place along a copolymer chain. Although their composition distributions resemble statistical copolymers, the different thermoresponsive behaviors are observed. Aoshima et al. reported only one T_c at 39 °C was observed in poly((2-ethoxyethyl vinyl ether)$_{300}$-*stat*-(2-methoxyethyl vinyl ether)$_{300}$ P(EOVE$_{300}$-*stat*-MOVE$_{300}$), [128] whereas P(EOVE$_{300}$-*grad*-MOVE$_{300}$) displays a two-step transmittance decrease. Compared to PEOVE$_{300}$-*b*-PMOVE$_{300}$, the gradient structures show a gradual transmittance decrease in temperature range from 20 to 50 °C, while the block ones have a sharp transition. [128, 129] Additionally, P(MMA$_{100}$-*stat*-PEGMA$_{100}$) (MMA: methyl methacrylate, PEGMA: obtained by transesterifing MMA into PEG methacrylate), PMMA$_{100}$-*grad*-PEGMA$_{100}$ and PEGMA$_{50}$-*grad*-PMMA$_{100}$-*grad*-PEGMA$_{50}$ at the similar molecular weight and composition exhibit different T_c values at 58, 65 and 66 °C, respectively. [130]

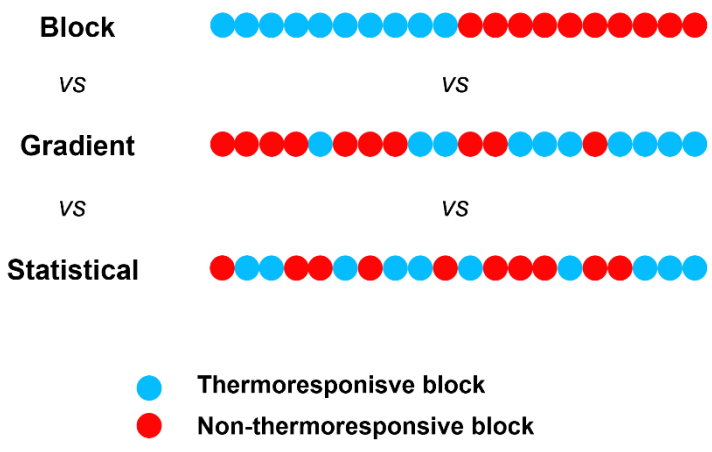

Scheme I.4 Schematic illustration of thermoresponsive block, gradient, and statistical copolymers (terminal groups are omitted).

For a chosen composition, different block sequences can be obtained as illustrated in **Scheme I.5**. Indeed, changing block order means different blocks are connected to a defined terminal group and this will influence measured T_c of thermoresponsive (co)polymers, especially in diblock copolymers.

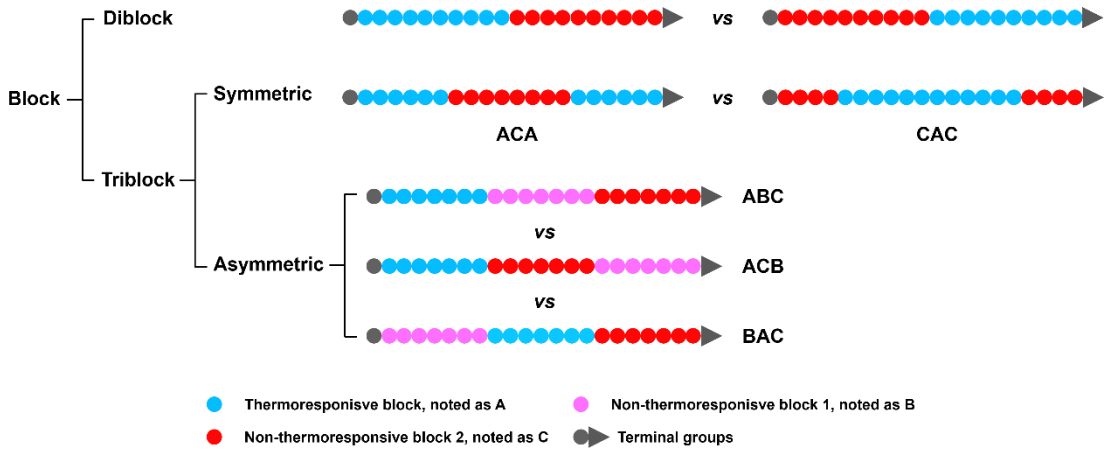

Scheme I.5 Schematic representation of thermoresponsive block copolymers with different block sequences.

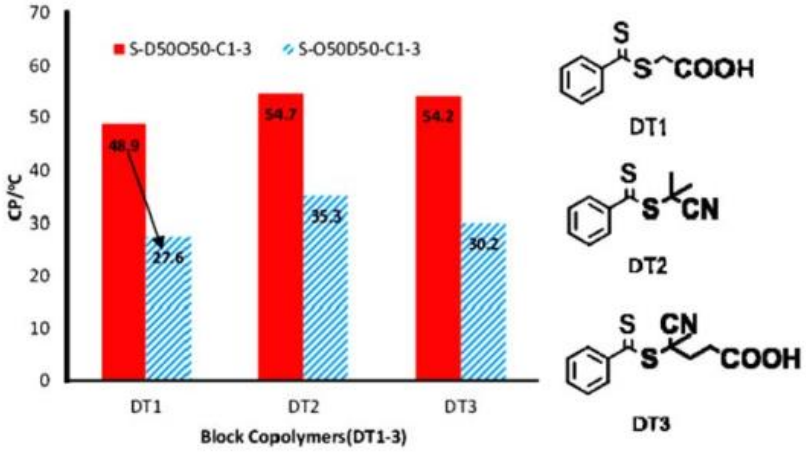

Figure I.10 T_c of diblock copolymer of PDEGMA and POEGA with different end groups and sequences. Copyright 2015. Reproduced with permission from the Wiley Periodicals, Inc. Ref. [131]

Hence, for $PVCL_{155}$-*b*-PVP_{164} (T_c: 42.5 °C) and PVP_{128}-*b*-$PVCL_{165}$ (T_c: 41.9 °C) ended with double hydrophilic asymmetric groups a variation of T_c equal to 0.6 °C is found. [107] However, this difference can be significantly higher in the case of copolymer illustrated in **Figure I.10**. At the same composition, $PDEGMA_{50}$-*b*-$POEGA_{50}$ in which more hydrophilic block of POEGA is connected to hydrophilic

end groups of alkyl carboxylic acid or alkyl nitrile show significantly higher T_c than $POEGA_{50}$-*b*-$PDEGMA_{50}$ where less hydrophilic block of PDEGMA is connected to the same end groups. [131] The same phenomenon was also observed in $PDEGMA_{50}$-*b*-P($DEGMA_{25}$-*stat*-$OEGA_{25}$) (T_c: 43.5 °C) and P($DEGMA_{25}$-*stat*-$OEGA_{25}$)-*b*-$PDEGMA_{50}$ (T_c: 31 °C) ended with amphiphilic phenyl dithioester and alkyl carboxylic acid. [132]

For triblock thermoresponsive copolymers, the effect of block order on T_c is considered in terms of symmetric (ABA- and BAB-type) and asymmetric (ABC-, ACB- and BAC-type) structures. For symmetric triblock copolymers, Heiden and co-workers found T_c relates to the matching of polarities between outer block and end group (matched polarity: outer blocks have the same polarity to end groups. Mismatched polarity: the polarities of outer block and end groups are opposite). When hydrophilic alkyl carboxylic acid is utilized as end groups, matched $POEGA_{25}$-*b*-$PDEGMA_{50}$-*b*-$POEGA_{25}$ has lower T_c (29.2 °C) than mismatched $PDEGMA_{25}$-*b*-$POEGA_{50}$-*b*-$PDEGMA_{25}$ (T_c: 31.8 °C). In the case where hydrophobic phenyl trithioester is taken as end group, matched $PDEGMA_{25}$-*b*-$POEGA_{50}$-*b*-$PDEGMA_{25}$ and mismatched $POEGA_{25}$-*b*-$PDEGMA_{50}$-*b*-$POEGA_{25}$ display T_c at 25.2 and 40.5 °C, respectively. [131]

For asymmetrical triblock structures (ABC, A: thermoresponsive block, B: hydrophilic block and C: hydrophobic block) Georgiou and co-workers found T_c values of ABC and ACB (A: $PDMAEMA_{30}$, B: poly((ethylene glycol) methyl methacrylate)$_9$ ($PEGMMA_9$), C: poly(*n*-butyl methacrylate)$_{13}$ ($PBuMA_{13}$)) are 60 and 57 °C, respectively, while BAC is insoluble in water. [133] Patrickios reported ABC, ACB and BAC (A: $PDMAEMA_{10}$, B: poly(hexa(ethylene glycol) methacrylate)$_{10}$ ($PHEGMA_{10}$), C: $PMMA_{10}$) display T_c at 80, 80.7 and 89.5 °C, respectively. [134] These three types in another triblock copolymer (A: $PDMAEMA_{11}$, B: $PHEGMA_5$, C: poly(benzyl methacrylate)$_{10}$ ($PBzMA_{10}$)) have different T_c values at 66.6, 59.6 and 65.8 °C, respectively. [135]

(viii) Effect of pH/CO_2

T_c of (co)polymers comprising pH-/CO_2- and thermo-sensitive groups can be adjusted by changing system pH or by addition of CO_2. For instance, T_c of PDEAEAM increases from 33.1 to 50.2 ^oC as pH decreases from 11.0 to 8.5. [15] $PNAGME_{177}$ changes T_c from 31.5 to 39 ^oC with pH ranging from 1 to 10, [13] T_c of PDMAEMA shows a pronounced increasing tendency along with pH decline. [127] $PEMAEEOMA_{108}$ displays a LCST behavior in pH range from 12 to 8.5 but loses thermoresponsiveness at pH lower than 8.5. [18] Additionally, T_c values of amino-terminated PHEMA (end groups: primary amine, dimethyl and diethyl amino groups) are variable at different pH values. [136] These phenomena are attributed to the protonation degree. In basic environment, the tertiary amine groups in PDMAEMA and PDEAEAM are more and more protonated with decreasing pH, which results in a shift of T_c towards higher temperature. In acidic solution, all the amine- or amino-based (co)polymer chains are protonated and become positively charged, the existed electrostatic repulsion among the charged units prevents chains from aggregation upon heating. Hence, no thermoresponsive behaviors in PDMAEMA and PDEAEAM are detected. CO_2 treatment has a similar effect on T_c, bubbling CO_2 causes the protonation of CO_2-responsive moieties, which can improve the solubility of overall (co)polymers in aqueous solution. As a consequence, T_c of (co)polymers shifts towards higher value (i.e. T_c values of P(NIPAM-*co*-DMAEMA), P(DEGMA-*co*-DMAEMA), P(DEGMA-*co*-AA), poly((2-(2-methoxyethoxy) ethyl methacrylate)-*co*-(ethylacrylic acid)) (P(DEGMA-*co*-EAA)) and poly((2-(2-methoxyethoxy) ethyl methacrylate)-*co*-(methacrylic acid)) (P(DEGMA-*co*-MAA)) upon bubbling CO_2 shift from 31, 25, 20, 20 and 18 ^oC to 40, 40, 24, 22 and 32 ^oC, respectively. [137, 138] Additionally, P(NIPAM-*co*-DEAEMA) [137] and P($DEGMA_{180}$-*co*-$DMAEMA_{38}$)-*b*-PEO_{455}-*b*-P($DEGMA_{180}$-*co*-$DMAEMA_{38}$) [138] lose their thermoresponsiveness after aeration CO_2. However, T_c of P($DEGMA_{160}$-*co*-MAA_{36})-*b*-PEO_{455}-*b*-P($DEGMA_{160}$-*co*-MAA_{36}) declines from a higher temperature (above 50 ^oC) to 24 ^oC after CO_2 treatment.

I.2.3 Dual thermoresponsive (co)polymers

Copolymers comprising two or more thermoresponsive monomers within their structure have attracted tremendous attention in order to obtain materials with stepwise phase transition or self-assembly behavior. Nevertheless, due to the difficulty to synthesize well-defined multiple thermoresponsive copolymers, [4, 139] most reported works focused on dual thermosensitive copolymers with LCST-LCST, LCST-UCST or UCST-UCST typed behavior.

(i) Copolymers with LCST-LCST behavior

In this case, both thermoresponsive segments are soluble at low temperature with two distinct cloud point temperatures: $T_{c,1}$ and $T_{c,2}$. Above $T_{c,1}$, the first thermoresponsive block collapses and the overall copolymer changes from a double hydrophilic to an amphiphilic state. Further heating above $T_{c,2}$ induces a transition of second block, which eventually causes the formation of aggregates that are prone to precipitate from the system.

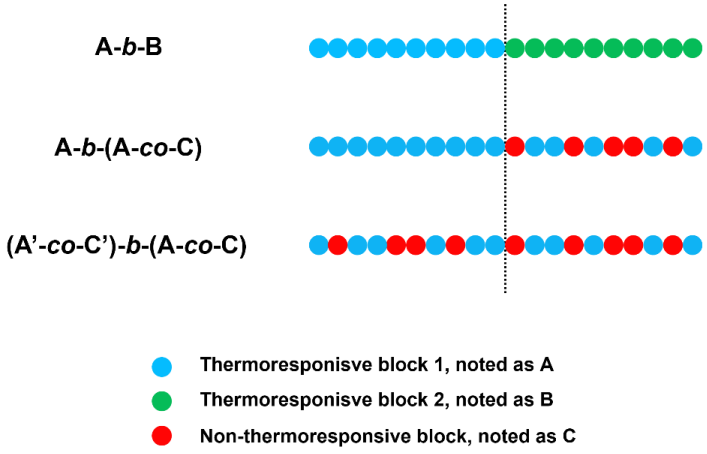

Scheme I.6 Different microstructures of diblock copolymers with LCST-LCST behavior (terminal groups are omitted, dot line separates block copolymers into two blocks).

Different strategies enable to obtain such LCST-LCST typed diblock copolymers with separate T_c values as illustrated in **Scheme I.6.** The first one is based on the copolymerization of two different thermoresponsive blocks A and B. Alternatively, as T_c can be readily tuned by incorporation of non-thermoresponsive moieties C, a

hydrophilically or hydrophobically modified copolymer (A-*co*-C) acting as an individual thermoresponsive block can be combined with thermosensitive block A to form A-*b*-(A-*co*-C), or combined with the similar copolymer of (A'-*co*-C') but different compositions to generate (A'-*co*-C')-*b*-(A-*co*-C) copolymers. Triblock copolymers with symmetric (comprising of two different LCST-type blocks) or asymmetric (one non-thermoresponsive block and two different LCST-type blocks) microstructures can also be obtained. Typical examples of such structures with LCST-LCST behavior are summarized in **Table I.4**.

Table I.4 Thermoresponsive (co)polymers with LCST-LCST behavior in water.

Copolymer	$T_{c,1}$ (°C)[a]	$T_{c,2}$ (°C)[a]	Ref.
$PNIPAM_{137}$-*b*-$PEAM_{67}$	17	62	[140]
$PNIPAM_{34}$-*b*-$PEAM_{94}$	27	58	
$PEOVE_{300}$-*b*-$PMOVE_{300}$	20	50	[128]
$PNASME_{170}$-*b*-$PNIPAM_{63}$	38	43	[12]
$PDMAEMA_{51}$-*b*-$PDEGMA_{49}$	34.4	46.1	[141]
PN*n*PAM_{84}-*b*-$PEMAM_{42}$	32	60	[142]
$P(mPEGV_{466})_{18}$-*b*-$PNIPAM_{60}$	35	54	[143]
$PDMAEEOMA_{137}$-*b*-$PEMAEEOMA_{78}$	32.5	48.3	[18]
$PNIPAM_{115}$-*b*-$PNAEAA_{230}$	41.9	56.8	[11]
$PNIPAM_{450}$-*b*-$P(NIPAM_{244}$-*co*-$HMAAm_{70})$	35	47	[98]
PAPy-*b*-P(APi-*co*-APy)	15-25	43-47	[144]
PNIPAM-*b*-P(NIPAM-*co*-BMAAm)	25	32	[145]
$PVCL_{315}$-*b*-$P(MVA_{215}$-*stat*-$VCL_{143})$	37	70	[104]
$P(nPA_{0.7}$-*co*-$EAM_{0.3})$-*b*-$P(nPA_{0.4}$-*co*-$EAM_{0.6})$	41.5	53	[146]
P(MVC-*co*-VCL)-*b*-P(VCL-*co*-VP)	27	42	[147]
$P(mPEGV)_{32}$-*b*-$PNIPAM_{170}$-*b*-PSt_{166}	37.6	55.1	[148]
$PDMAEMA_{30}$-*b*-$PNIPAM_{68}$-*b*-PSt_{482}	43	63	[149]
$PNIPAM_{54}$-*b*-$PDMAEMA_{46}$-*b*-PSt_{460}	50	67	
$PMOVE_{58}$-*b*-$PNIPAM_{170}$-*b*-$PMOVE_{58}$	31.8	64.7	[150]
$PDEGA_{48}$-*b*-$PDMAm_{150}$-*b*-$PVCL_{113}$	21	37	[151]
PEO_{45}-*b*-$PNIPAM_{380}$-*b*-$P(NIPAM_{423}$-*co*-$HEAAm_{42})$	37	48	[152]

[a] $T_{c,1}$ and $T_{c,2}$ determined at a specific molecular weight and copolymer concentration. Abbreviations: mPEGV: poly(ethylene glycol) methyl ether vinylphenyl, PAPy: poly(*N*-

acryloylpyrrolidine), APi: *N*-acryloylpiperidine, BMAAm: *N*-(isobutoxymethyl)acrylamide, nPA: *N*-*n*-propylacrylamide, MVC: 3-methyl-*N*-vinylcaprolactam, mPEGV: (ethylene glycol) methyl ether vinylphenyl, PSt: polystyrene.

The combination of multiple thermoresponsive blocks with different T_c values is expected to exhibit sequential phase transitions upon heating. Nevertheless, different factors influence the number of transition points observed:

(1) *Cooperative dehydration.* PNIPAM (T_c: ~ 32 ^oC) and PVCL (T_c: ~ 30-50 ^oC, depending on molecular weight) are well-known LCST-typed homopolymers. However, in PNIPAM-*b*-PVCL only one T_c was observed upon heating, which is attributed to a cooperative contribution from both two blocks triggering phase transition. [153, 154] A single T_c (15 °C) was also measured in PDEGA-*b*-PVCL. Nevertheless, the incorporation of a PDMAm block as a middle block can prevent the cooperative dehydration of PDEGA and PVCL blocks. Thus, for $PDEGA_{48}$-*b*-$PDMAm_{150}$-*b*-$PVCL_{113}$ two distinct T_c values were observed at 21 and 37 ^oC. [151]

(2) *Polarity of non-thermoresponsive block*. Three T_c values were clearly detected in PN*n*PAM_{129}-*b*-$PNIPAM_{52}$-*b*-$PEMAM_{63}$ but only one T_c was observed in PN*n*PAM_{129}-*b*-$PNIPAM_{52}$-*b*-$PEMAM_{63}$-*b*-$PDMAm_{184}$. In the latter case the insertion of a hydrophilic PDMAm block increases the solubility of the whole copolymer and restrains the influence of other blocks. [4]

(3) *Block sequence*. As mentioned in **Section I.2.2 (vii)**, position of different blocks plays a crucial role on thermoresponsiveness, Adjacent segment not only influences T_c but also affects the number of transition points upon heating. For instance, a two-step thermal transition was observed in both $PNIPAM_{110}$-*b*-$PAPy_{70}$-*b*-$PDMAm_{64}$ and $PNIPAM_{110}$-*b*-$PDMAm_{52}$-*b*-$PAPy_{69}$, whereas one T_c was measured in $PDMAm_{139}$-*b*-$PNIPAM_{52}$-*b*-$PAPy_{28}$. [155]

(ii) Copolymers with LCST-UCST behavior

The combination of LCST and UCST behaviors is commonly realized by block copolymerization of one LCST-type block (with a cloud point temperature T_c) with one

UCST-type block (with a clarification point temperature T_{CL}). Therefore, two distinguishable transition points are expected to exist in LCST-UCST typed (co)polymers upon heating. As illustrated in **Scheme I.7**, two types of phase diagrams can be differentiated depending on the relative position of T_c and T_{CL}.

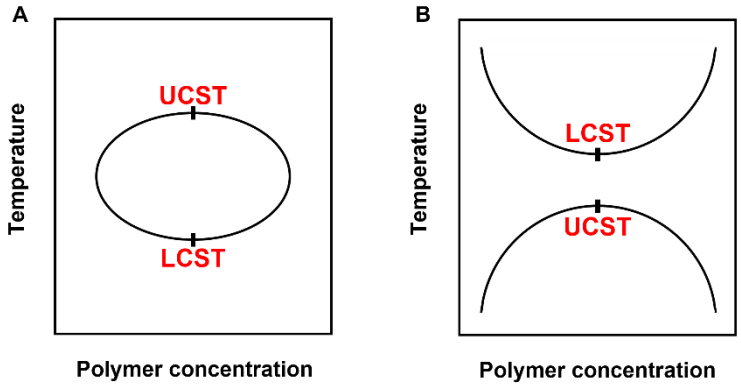

Scheme I.7 Phase diagrams of LCST-UCST typed thermoresponsive copolymers (A: $T_c < T_{CL}$, B: $T_c > T_{CL}$).

(1) $T_c < T_{CL}$. In this case, copolymers are soluble at temperature below T_c and at temperature above T_{CL}, and both blocks exhibit poor solubilities or precipitate in the intermediate temperature range.

(2) $T_c > T_{CL}$. In this case, copolymers display an inverse behavior: they are soluble in the intermediate temperature range ($T_{CL} < T < T_c$) whereas poor solubilities occur at temperature below T_{CL} and above T_c. Typical examples of LCST-UCST typed copolymers are listed in **Table I.5**.

Table I.5 Thermoresponsive (co)polymers with LCST-UCST behavior.

Copolymer	Solvent	T_c (°C)[a]	T_{CL} (°C)[a]	Ref.
$T_c < T_{CL}$				
P(A-Pro-OMe)$_{27}$-*b*-P(A-Hyp-OH)$_{73}$	Acidic water (containing NaCl)	20	40	[156]
PNIPAM$_{94}$-*b*-P(NAG$_{19}$-*co*-NAGSP$_{30}$)	H_2O	42.5	63	[157]
P(SPB$_{0.51}$-*co*-Bz$_{0.23}$-*co*-THF$_{0.26}$)	H_2O	37.9	67.8	[158]
P(amido thioether) (containing *N*-diethylaminoethylamido and *N*-hydroxyethylamido)	H_2O (pH=8.14)	36.4	66.3	[159]
PEO$_{45}$-*b*-P(AAm-*stat*-AN)	H_2O	30	50	[160]

Table I.5 (Continued)

Copolymer	Solvent	T_c (°C)[a]	T_{CL} (°C)[a]	Ref.
$T_c > T_{CL}$				
P*t*BMA$_{329}$-*b*-PVEA$_{142}$	methanol	53	32	[37]
PBA$_{5k}$-*b*-PNIPAM$_{5k}$	[C_2mim][NTf_2]	53	16	[161]
PDMAEMA-*b*-PSBMA	H_2O (pH=9.0)	55	41	[162]
PNIPAM$_{95}$-*b*-PSPP$_{33}$	H_2O	33.4	8.6	[163]
PdMMAEAPS-*b*-PDEAM	D_2O	31	22	[69]
PSB$_{430}$-*b*-PNIPAM$_{200}$	D_2O	32.3 ± 0.5	21.2 ± 0.5	[164]
P(AAm$_{231}$-*co*-AN$_{78}$)-*b*-PDMAEMA$_{319}$	PBS	45.86	20.9	[165]
P(DEGMA$_{60}$-*stat*-OEGMA$_{40}$)$_{27}$-*b*-PMAAm$_{440}$	H_2O	66	56	[166]
P(OEGMA-*co*-DEGMA)-*b*-P(MPS-*co*-DMAPMA)	H_2O	61	21	[167]
PEO$_{17}$-*b*-PNIPAM$_{87}$-*b*-PNAGA$_{83}$	PBS	36.5	10	[168]
PEO$_{17}$-*b*-PNAGA$_{99}$-*b*-PNIPAM$_{63}$	PBS	32.6	20.6	
PMPDSAH$_{50}$-*b*-PDEGMA$_{100}$-*b*-PMPDSAH$_{50}$	H_2O	23	16	[169]
P(AAm$_{89}$-*co*-AN$_{23}$)-*b*-PDMAm$_{475}$-*b*-PNIPAM$_{57}$	H_2O	31	20	[170]

[a]T_{CL} and T_c determined at a specific copolymer concentration and molecular weight. Abbreviations: P(A-Pro-OMe): poly(*N*-acryloyl-L-proline methyl ester), P(A-Hyp-OH): poly(*N*-acryloyl-4-*trans*-hydroxy-L-proline), NAG: *N*-acryloylglycine, NAGSP: *N*-acryloylglycine spiropyran ester, SPB: sulfopropylbetaine, Bz: benzylamine, THF: tetrahydrofurfurylamine, PSBMA: poly(sulfobetaine methacrylate), PSPP: poly(3-(*N*-(3-methacrylamidopropyl)-*N*,*N*-dimethyl) ammoniopropane sulfonate), PSB: polysulfobetaine, MPS: 3-(*N*-(3methacrylamidopropyl)-*N*,*N*-dimethyl) ammoniopropane sulfonate, DMAPMA: *N*-(3-(dimethylamino) propyl) methacrylamide, MPDSAH: *N*-(3-(methacryloylamino) propyl)-*N*,*N*-dimethyl-*N*-(3-sulfopropyl) ammonium hydroxide.

(iii) Copolymers with a UCST-UCST behavior

UCST-UCST typed copolymers, consisting of two individual UCST-type blocks, undergo a (double hydrophobic)-to-amphiphilic-to-(double hydrophilic) transition with increasing temperature. This behavior is opposite to that of LCST-LCST typed copolymers. Unfortunately, there are few reports of such type copolymers involving

the thermoresponsive property in dilute solution (phase transition temperature and self-assembly).

I.2.4 Self-assembly of thermoresponsive (co)polymers

The self-organization behavior of amphiphilic copolymers, resulting from the inherent molecular structure, can be predicted based on a "packing parameter" of copolymer chains, *p*, which is calculated by the following formula,

$$p = \frac{\nu}{\alpha_0 l_c}$$

where ν is volume of hydrophilic chains, α_0 is optimal area of head group and l_c is length of hydrophobic tail. **Scheme I.8** illustrates the relation between the value of *p* and the aggregate geometry. [171]

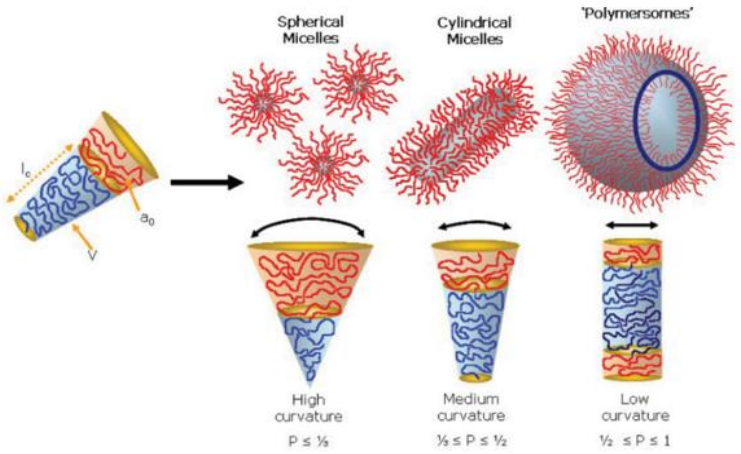

Scheme I.8 Evolution of morphologies of aggregates depending on the value of packing parameter *p*. Copyright 2009. Reproduced with permission from the WILEY-VCH Verlag GmbH & Co. KGaA, Weinheim. Ref. [171]

As stated above, thermoresponsive (co)polymers usually undergo a modification of their solubility in aqueous solution in response to a change of temperature. Depending on the microstructure of the studied (co)polymer, this modification can result in the formation/modification of aggregates. The formation of such assemblies and the effect of temperature on aggregates structure can be studied through scattering (light, neutrons, and X-ray) and microscopy measurements. Only thermoresponsive block (co)polymers are discussed in this section.

(i) Self-assembly of mono thermoresponsive (co)polymers

Thermoresponsive (co)polymers in different concentration regions display various aggregation states, such as unimers, nanoparticles with spherical, worm-like micellar and vesicular geometry in dilute solution as well as sol and gel in concentrated solution. Here, temperature-induced morphological transition will be discussed with respect to (co)polymer concentrations.

Table I.7 Morphological transition of thermoresponsive diblock copolymer in dilute solution.

Morphological transition upon heating & Examples Thermoresponsive block Hydrophilic block Hydrophobic block
Hydrophobically modified polymers 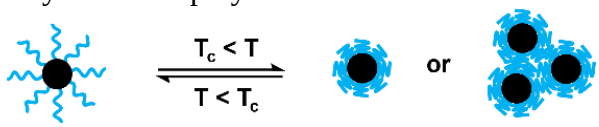 PSt-*b*-PNIPAM, [172, 173] PSt-*b*-PMDEGA, [172] PNIPAM-*b*-PMMA, [174, 175] $PNIPAM_{8k}$-*b*-PBA_{2k}, [101] PNIPAM-*b*-PLA, [176] PVAc-*b*-PVCL [108]
Hydrophilically modified polymers 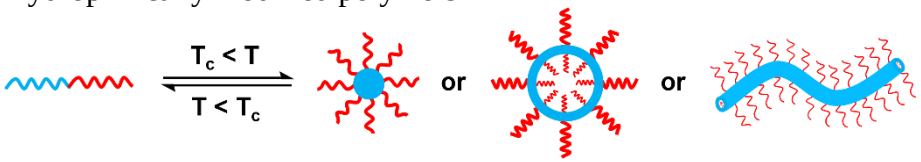 PVCL-*b*-PVP, [107] PVOH-*b*-PVCL, [108] PEO-*b*-PNIPAM, [177-180] PNIPAM-*b*-PVP, [181] PNIPAM-*b*-PVim, [182] PNIPAM-*b*-PHEAAm [99]

Abbreviations: PLA: poly($_{DL}$-lactide), PVim: poly(*N*-vinylimidazole).

(a) In dilute solution

Block copolymer structures containing an additional hydrophobic or hydrophilic block can be easily synthesized. When a thermoresponsive block is associated with a hydrophobic structure either by incorporation of hydrophobic comonomer or by modification with hydrophobic end groups the amphiphilic block copolymers are obtained. These (co)polymers are prone to assemble in dilute solution with a corona of thermoresponsive block. Upon heating, the thermoresponsive block undergo a coil-to-(meso)globule transition and the whole copolymer becomes hydrophobic or precipitates from the system, this induces an aggregation of existing assemblies in a

more or less controlled fashion. When a thermoresponsive homopolymer is associated with a hydrophilic block, the block copolymer undergoes a hydrophilic-to-amphiphilic transition upon heating, and a unimers-to-(core-corona structure) transition can be observed at the same time. Typical temperature-induced morphological transitions of diblock copolymers are summarized in **Table I.7**.

Table I.8 Morphological transition of triblock copolymers in dilute solution upon heating.[a]

Triblock copolymer	Morphological transition upon heating & Examples A: Thermoresponsive block B: Hydrophilic block C: Hydrophobic block
ABA	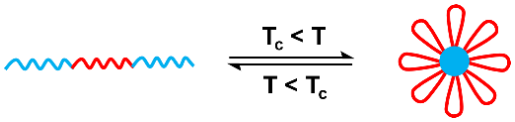 PDMAEMA-*b*-PMAGP-*b*-PDMAEMA, [183] PNIPAM-*b*-PDMAm-*b*-PNIPAM, [184] PNIPAM$_{53}$-*b*-PDMAm$_{105}$-*b*-PNIPAM$_{53}$, [185] PNIPAM$_{16k}$-*b*-PEO$_{4k}$-*b*-PNIPAM$_{16k}$ [186]
ACA	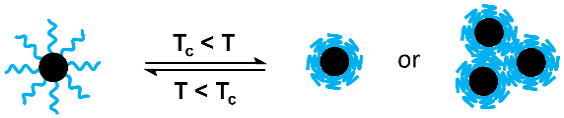 PNIPAM$_{4k}$-*b*-PBA$_{2k}$-*b*-PNIPAM$_{4k}$, [43] PMVE-*b*-PIBVE-*b*-PMVE, [187] a$_{12}$-*b*-i$_{10}$-*b*-a$_{12}$ [188]
CAC	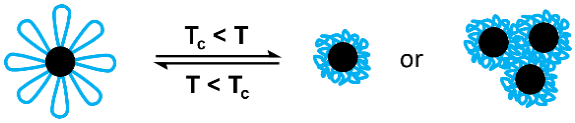 i$_2$-*b*-a$_{28}$-*b*-i$_2$, [188] PSt-*b*-PNIPAM-*b*-PSt, [189] P(St-*d*$_8$)$_{10}$-*b*-PNIPAM$_{390}$-*b*-P(St-*d*$_8$)$_{10}$ [190]
ABC	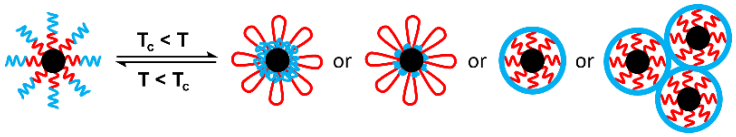 PCL$_{4k}$-*b*-PEO$_{0.6k}$-*b*-PNIPAM$_{9.7k}$, [191] PSt$_{135}$-*b*-PDMAm$_{80}$-*b*-PNIPAM$_{76}$, [192] PEP-*b*-PEO-*b*-PNIPAM [193]
BAC	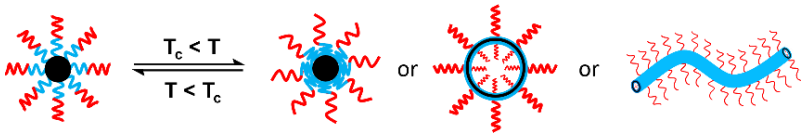 PEO$_{43}$-*b*-PNIPAM$_{82}$-*b*-PCL$_{87}$, [194] PEO-*b*-PNIPA-*b*-PI, [195] PEO$_{45}$-*b*-PNIPAM$_{168}$-*b*-PSt$_{46}$, [196] PF-*b*-PNIPAM-*b*-PHEAAm [99]

[a]Size of assembled aggregates is omitted. Abbreviations: PMAGP: poly(6-O-methacryloyl-D-galactopyranose), PMVE: poly(methyl vinyl ether), PIBVE: poly(isobutyl vinyl ether), a: atactic PNIPAM, i: isotactic PNIPAM, P(S-*d*$_8$): fully deuterated PSt block, PEP: poly(ethylene-*alt*-propylene), PI: poly(isoprene), PF: poly(2,7-(9,9-dihexylfluorene)).

The self-organization behavior of thermoresponsive triblock copolymers is more complex and is related to the copolymer specific microstructures (i.e. symmetric and asymmetric structures). For symmetric structure, according to the polarity of non-thermoresponsive block, two transitions of unimers-to-(core-corona structure) and (core-corona structure)-to-(core-shell structure) are commonly observed. In the case of triblock copolymers, bearing one thermoresponsive and two double hydrophilic blocks or one thermoresponsive and two double hydrophobic blocks, their temperature-triggered morphological transition is similar to hydrophilic or hydrophobic modified diblock copolymers. For asymmetric triblock copolymers with different block sequences, the self-assembly behavior upon heating depends on the block order. The morphological transition of triblock copolymers with different microstructures is summarized in **Table I.8**.

(b) In concentrated solution

The self-assembly behavior of thermoresponsive (co)polymers in concentrated solution is basically studied in terms of macrophase transition. The detailed mechanism of thermoresponsive block (co)polymers is depicted in **Scheme I.9.**

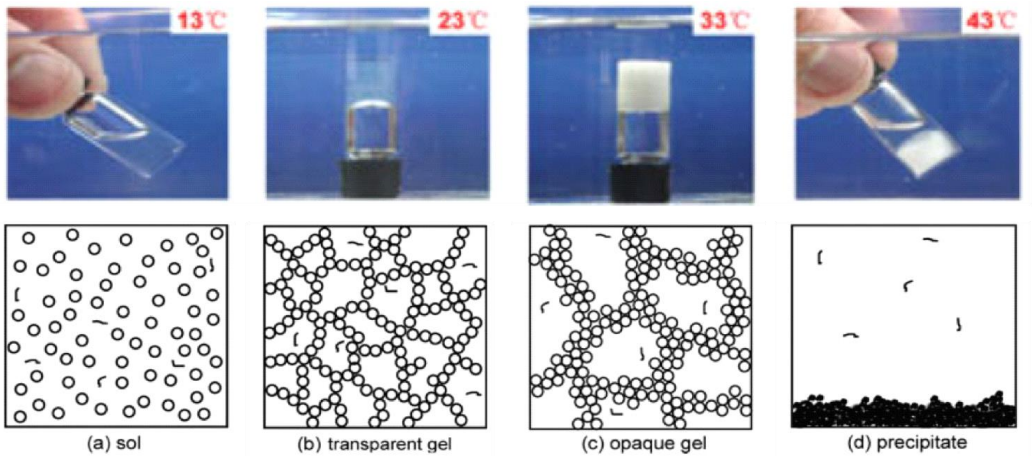

Scheme I.9 Schematic illustration of temperature-induced gelation for block copolymers in water via micelle packing and entanglement. A micelle is shown as a circle. Copyright 2007. Reproduced with permission from the Wiley Periodicals, Inc. Ref. [197]

In concentrated solution, thermoresponsive (co)polymer are well dispersed in water either as micelles (for amphiphilic structures) or as unimers (for double hydrophilic structures). Increasing temperature leads to the formation of a three-

dimensional networks with orderly arrangements, which is generally defined as transparent gel. This network result either from the packing of preexisting micelle or from the aggregation of (co)polymer. With a further increase of temperature, the size of clusters or the distance between clusters reaches the range of wavelength of visible light, the gels become opaque to eyes. Continuously increasing temperature, due to the over-hydrophobicity, the micellar network is broken with volume shrinkage by expelling water, and a macrophase separation occurs, which is noted as gel with syneresis or dehydrated gel. The temperature-induced gel via micelle packing and entanglement, should be distinguished with chemical crosslinked gel formed through covalent bonds. Indeed, the former one displays a good reversibility of sol-to-gel transition upon heating/cooling. [197]

The transparent, opaque and syneresis gels are not always observed sequentially upon heating for all thermoresponsive (co)polymers. Their appearances are dependent on the degree of entanglement at a specific temperature, relating to (co)polymer composition and concentration. For instance, these three types of gel were all observed in PNIPAM$_{38}$-*b*-PEO$_{114}$ in concentration range from 5 to 7 wt.%, whereas only opaque and syneresis gels occur in PNIPAM$_{228}$-*b*-PEO$_{114}$ and PNIPAM$_{143}$-*b*-PEO$_{114}$ at the same concentration. [198] Additionally, P(BA-*stat*-NIPAM)$_{21k}$ displays three gel phases at concentration of 30 wt.% upon heating it loses transparent gel phase at 20 wt.%. What's more, only transparent gel exists at 10 wt.%, and no sol-to-gel transition is detected when concentration declines to 5 wt.%. [199]

The gelation temperature can be easily tuned for a specific application by adjusting molecular weight, composition and/or architecture. [197] For instance, an increase of hydrophobic BuMA ratio in PEGMA-*b*-PBuMA-*b*-PDMAEMA drives formation temperature and concentration of transparent gel shift towards lower value. [133] Statistical copolymers of P(DMAEMA$_{30}$-*co*-BuMA$_{13}$-*co*-EGMA$_{9}$), P(EGMA$_{2}$-*co*-BuMA$_{14}$-*co*-DMAEMA$_{16}$), P(EGMA$_{2}$-*co*-EtMA$_{18}$-*co*-DMAEMA$_{16}$) (EtMA: ethyl methacrylate) and P(EGMA$_{2}$-*co*-HMA$_{12}$-*co*-DMAEMA$_{16}$) (HMA: hexyl methacrylate) cannot form gels or form gels with weak or unstable properties compared to triblock

analogues at the same composition. [133, 200] Additionally, the gel formed in triblock structure of poly(ethylene oxide)$_{69}$-*b*-poly(styrene oxide)$_8$-*b*-poly(ethylene oxide)$_{69}$ (PEO$_{69}$-*b*-PSO$_8$-*b*-PEO$_{69}$) is more difficult at low concentration than in diblock analogue of PSO$_{10}$-*b*-PEO$_{135}$. [201]

(ii) Self-assembly of dual thermoresponsive (co)polymers

Thermoresponsive (co)polymers comprising of two thermoresponsive blocks have two different transition temperature values. The hydrophilic/hydrophobic ratio of overall copolymers in each temperature regime is different, which drives these copolymers self-organize into different morphologies with various sizes. Although the study of such system is complex, the sensitivity and specificity are higher than that of mono-thermoresponsive (co)polymers.

(a) Self-assembly of copolymers with LCST-LCST behavior

Copolymers with LCST-LCST behavior undergo a gradual dehydration with an increase of temperature. For dual thermosensitive diblock copolymers and symmetric triblock copolymers, the copolymers change from double hydrophilic ($T < T_{c,1}$) to amphiphilic ($T_{c,1} < T < T_{c,2}$) to double hydrophobic ($T > T_{c,2}$) state, such copolymers tend to undergo a unimer ($T < T_{c,1}$) to core-corona aggregates ($T_{c,1} < T < T_{c,2}$) to core-shell micelles or aggregate clusters ($T > T_{c,2}$) transition.

The solubility change of triblock copolymers containing an additional hydrophilic or hydrophobic block (ABC-type) is more complex. Copolymers bearing one hydrophilic block undergo (triple hydrophilic)-to-amphiphilic change upon heating, while those copolymers with one hydrophobic block exhibit amphiphilic-to-(triple hydrophobic) transition under continuously increasing temperature. Besides the hydrophilic-hydrophobic ratio at a fixed temperature, the block sequence and copolymer structure also matter morphologies as mentioned above. The typical self-assembly behavior of LCST-LCST typed copolymers trigged by temperature is summarized in **Table I.9**.

Table I.9 Morphological transition of LCST-LCST typed copolymers.[a]

Morphological transition upon heating & Examples Thermoresponsive block 1 (smaller T_c) Hydrophilic block Thermoresponsive block 2 (larger T_c) Hydrophobic block
Diblock LCST-LCST typed copolymers 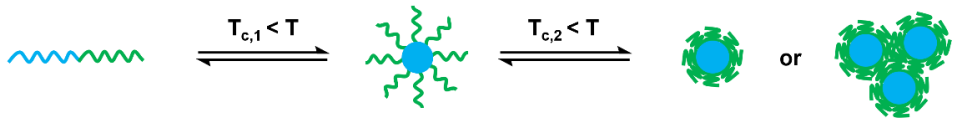   PNIPAM-*b*-PEAM, [140] PDMAEEOMA$_{137}$-*b*-PEMAEEOMA$_{78}$, [18] P(mPEGV$_{466}$)$_{18}$-*b*-PNIPAM$_{60}$, [143] PEOVE-*b*-PMOVE, [128] PNIPAM$_{115}$-*b*-PNAEAA$_{230}$ [11] PN*n*PAM$_{84}$-*b*-PEMAM$_{42}$, [142] PAPy-*b*-P(APi-*co*-APy), [144] PNIPAM-*b*-P(NIPAM-*co*-BMAAm), [145] PVCL$_{315}$-*b*-P(MVA$_{215}$-*stat*-VCL$_{143}$), [104] PVCL$_{132}$-*b*-P(VCL$_{40}$-*stat*-VP$_{172}$), [106] P(1-*alt*-5)$_6$-*b*-P1)$_{20}$,[b] [202] P(1-*alt*-4)$_{26}$-*b*-P1$_{63}$,[b] [202] PNIPAM$_{450}$-*b*-P(NIPAM$_{244}$-*co*-HMAAm$_{70}$), [98] P(nPA$_{0.7}$-*co*-EAM$_{0.3}$)-*b*-P(nPA$_{0.4}$-*co*-EAM$_{0.6}$), [146] P(MVC-*co*-VCL)-*b*-P(VCL-*co*-VP) [147]
Triblock LCST-LCST typed copolymers with symmetric structures 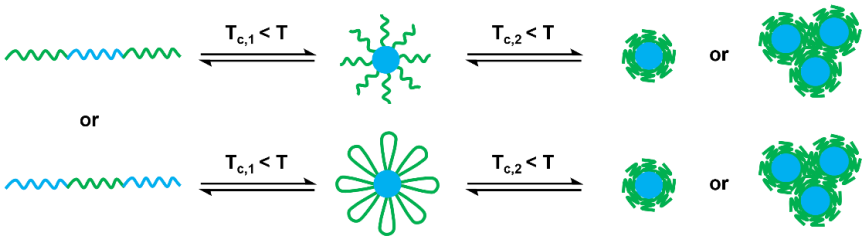   PMOVE$_{58}$-*b*-PNIPAM$_{170}$-*b*-PMOVE$_{58}$, [150] PVCL$_{132}$-*b*-P(VCL$_{80}$-*stat*-VP$_{344}$)-*b*-PVCL$_{132}$ [106]
Triblock LCST-LCST typed copolymers containing one hydrophilic block 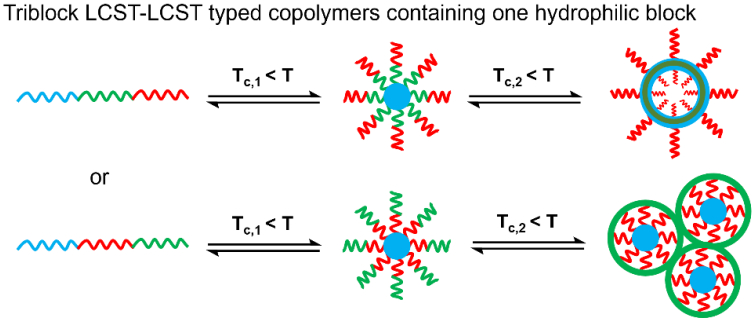   PEO$_{45}$-*b*-PNIPAM$_{380}$-*b*-P(NIPAM$_{423}$-*co*-HEAAm$_{42}$), [152] PDEGA$_{48}$-*b*-PDMAm$_{150}$-*b*-PVCL$_{113}$ [151]
Triblock LCST-LCST typed copolymers containing one hydrophobic block 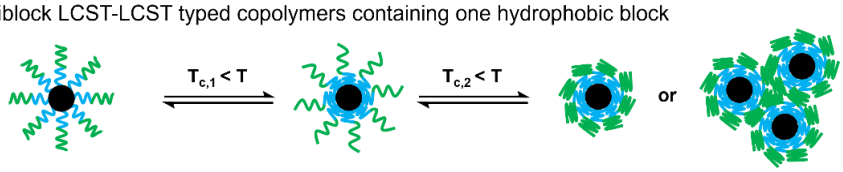   PNIPAM$_{54}$-*b*-PDMAEMA$_{46}$-*b*-PSt$_{460}$, [149] P(mPEGV)$_{32}$-*b*-PNIPAM$_{170}$-*b*-PSt$_{166}$ [148]

[a]Effects of block sequence and structure on morphological transition of triblock copolymers upon heating are omitted. [b]1: methoxytetraethylene glycol-4-vinylbenzyl ether, 5: *N*-(3-Trimethylsilyl) propylmaleimide, 4: *N*-decylmaleimide.

(b) Self-assembly of copolymers with LCST-UCST behavior

LCST-UCST copolymers with $T_c < T_{CL}$ or $T_c > T_{CL}$ present amphiphilic characters at lower and higher temperature and are therefore prone to display "schizophrenic"

behavior via formation of two distinct core-shell structures upon temperature adjustment. In the intermediate temperature window, these copolymers are soluble or insoluble depending on the respective T_c and T_{CL} values. This inversibility of polarity of aggregate nucleus provides insights to encapsulate and to release different compounds in solution by simply modulation of temperature. Morphological transition of LCST-UCST typed copolymers upon heating is summarized in **Table I.10**.

Concerning the fact that some (co)polymers in organic solvent or mixture of water and organic solvent display UCST behavior, it is worth noting the solvents selected in the cases of LCST-UCST typed copolymers.

Table I.10 Self-assembly of LCST-UCST typed copolymers in different temperature regions.

Morphological transition & Examples[a] LCST block UCST block
$T_c < T_{CL}$ 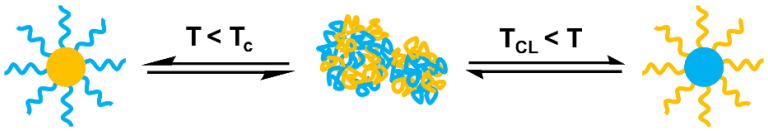   P(A-Pro-OMe)$_{27}$-*b*-P(A-Hyp-OH)$_{73}$ (acidic water with NaCl), [156] PEO$_{45}$-*b*-P(AAm-*stat*-AN) (H_2O) [160]
$T_c > T_{CL}$    P*t*BMA$_{329}$-*b*-PVEA$_{142}$ (methanol), [37] P(DEGMA$_{60}$-*stat*-OEGMA$_{40}$)$_{27}$-*b*-PMAAm$_{440}$ (H_2O), [166] P(OEGMA-*co*-DEGMA)-*b*-P(MPS-*co*-DMAPMA) (H_2O), [167] PdMMAEAPS-*b*-PDEAM (H_2O), [69] P(AAm$_{231}$-*co*-AN$_{78}$)-*b*-PDMAEMA$_{319}$ (H_2O), [165] P(AM$_{89}$-*co*-AN$_{23}$)-*b*-PDMA$_{475}$-*b*-PNIPAM$_{57}$ (H_2O), [170] PSPP$_{430}$-*b*-PNIPAM$_{200}$ (D_2O), [164] PDMAEMA$_{33}$-*b*-PSBMA$_{36}$ (basic water), [162] PEO$_{17}$-*b*-PNAGA$_{99}$-*b*-PNIPAM$_{63}$ (PBS), [168] PEO$_{17}$-*b*-PNIPAM$_{87}$-*b*-PNAGA$_{83}$ (PBS) [168]

[a]In the cases of LCST-UCST typed triblock copolymers, the effect of non-thermoresponsive block on self-assembly is not considered.

I.3 pH-responsive (co)polymers

In the case of pH-sensitive polymers, the key element in such system is the presence of ionizable weak acidic or basic moieties attached to the hydrophobic backbone. Upon ionization, the coiled chains stretch dramatically responding to the electrostatic repulsions among generated anions or cations. However, complete

ionization of polyelectrolytes is more difficult due to electrostatic effects exerted by other adjacent ionized groups. This transition between tightly coiled and expanded state is influenced by any condition that modifies electrostatic repulsion, such as ionic strength and counterions type. Consequently, it has to be kept in mind that after several cycles of protonation/deprotonation by addition of acids or bases, the accumulation of salt has a detrimental effect on the organization of (co)polymers in aqueous solution.

I.3.1 Main families of pH-responsive homopolymers

According to the functional groups, pH-responsive (co)polymers are divided into two categories: (co)polymers with acidic groups (carboxylic, sulfonic, phosphonic, boronic acid groups) and (co)polymers with basic groups (tertiary amine, morpholine, pyrrolidine, imidazole, piperazine and pyridine groups).

Table I.11 Chemical structures and p*K*a values of pH-responsive homopolymers.

Polyacids				
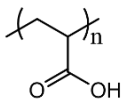	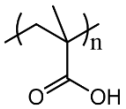	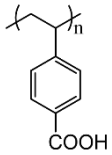	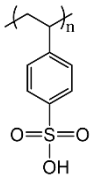	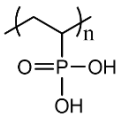
PAA p*K*a: 4.52- 4.55 [203]	PMAA p*K*a: 4.86 [204]	PVBA p*K*a: 7.1 [205]	PSSA p*K*a: 0.94 [206]	PVPA p*K*a: 3.02 [207]
Polybases				
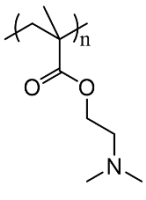	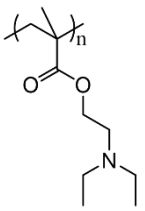	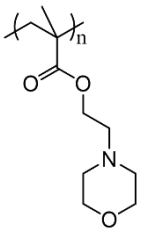	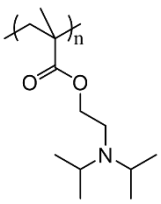	
PDMAEMA p*K*a: 7.4 [17, 208]	PDEAEMA p*K*a: 7.5 [17, 208]	PMEMA p*K*a: 4.9 [17]	PDPAEMA p*K*a: 6.0 [17]	
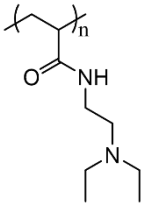	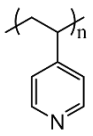	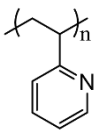		
PDEAEAM p*K*a*	P4VP p*K*a: 4.4 [209]	P2VP p*K*a: 4.5 [210]		

*value measured in **Chapter IV**.

Abbreviations: PVBA: poly(4-vinylbenzoic acid), PSSA: poly(4-styrenesulfonic acid), PVPA: poly(vinylphosphonic acid), PDPAEMA: poly(2-(diisopropylamino) ethyl methacrylate), P4VP: poly(4-vinylpyridine), P2VP: poly(2-vinylpyridine).

Polyacids are deionized at low pH and ionized with negative charges at neutral and high pH, while polybases have an opposite behavior, being protonated at low pH values and deprotonated at high pH. For these pH-responsive (co)polymers, it is therefore crucial to determine the acidic dissociation constant, *K*a (or its negative log: p*K*a) to know at which pH the ionic/non-ionic transition occurs. The most extensively investigated pH-responsive homopolymers and their corresponding p*K*a values are summarized in **Table I.11**.

When both acidic and basic groups coexist within one chain, (co)polymers are defined as polyampholytes, which experience multiple protonation states in different pH regimes separated by isoelectric point (IEP). This IEP depends on the polyampholyte composition and the corresponding p*K*a values of acid and basic units. At pH below IEP, due to the protonated polybase segments and deionized polyacid block, the positive charges domain the system. By contrast, at pH above IEP, it is governed by the negative charges because of deprotonation of polybase units and ionized polyacid block. At a narrow pH window around IEP, the polyampholytes tend to precipitate due to the electrostatic attraction among charged groups.

I.3.2 Impacts on self-assembly of pH-responsive (co)polymers

pH adjustment alters the protonation/deprotonation (or ionization/deionization) degree of pH-sensitive moieties and the electrostatic repulsion among the charged chains, which influences the hydrogen bonding network, ionic/hydrophobic interactions in the system, and further causes solubility change of (co)polymers in aqueous solution. To well understand and control the self-assembly behavior of pH-responsive (co)polymers, apart from hydrophilic/hydrophobic ratio at a specific pH, the impacts of different parameters such as pH, pH-sensitive chain length, concentration of salt and (co)polymer architecture on the aggregates shape and size should be considered.

(i) Effect of chain length of pH-responsive segment

The effect of chain length on the self-assembly of pH-responsive (co)polymers is ascribed to the ionization degree of pH-sensitive blocks. In other word, pH-sensitive segments with different chain lengths at a fixed pH imply variable ionization degrees. Meanwhile, for those (co)polymers with identical chain length but at different pH values, their electrostatic repulsions between charged chains are variable and make the corona volume swell or deswell with pH change. Therefore, a profound change in morphology and size takes place as pH-responsive units are not completely ionized. Once these units are totally ionized, adjusting system pH no longer exert significant effect on aggregates structure and size. Typical examples are poly(butadiene)-*b*-poly(L-glutamic acid) (PB-*b*-PGA) and poly(isoprene)-*b*-poly(L-lysine) (PI-*b*-PLys) (**Figure I.11**), in which micelles and vesicles are formed and their sizes display an increasing and decreasing tendency in pH range of 4 - 7 and 6 - 10, respectively. Whereas, in other pH ranges, no remarkable change in sizes is detected. [211-213]

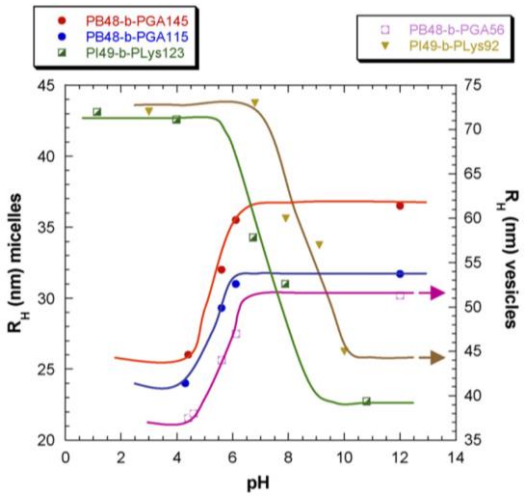

Figure I.11. Size of micelles and vesicles as a function of pH for PB-*b*-PGA and PI-*b*-PLys block copolymers having pH-responsive segments with different chain lengths (no addition of salt). Copyright 2007. Reproduced with permission from the Elsevier B. V. Ref. [213]

(ii) Effect of ionic strength

In ionized state, the addition of salt into pH-responsive (co)polymers solution tends to shield the intra-corona repulsion among the charged (co)polymer chains due to

the association of salt with charged chains, this causes a change of morphology towards structure with lower curvature. For instance, poly(glycerol monomethacrlyate)$_{50}$-*b*-poly(2-hydroxypropyl methacrylate)$_{140}$ (MPETTC-PGMA$_{50}$-*b*-PHPMA$_{140}$) formed spherical micelles at pH 3 and it transformed into worm-like micelles upon addition of KCl. [214]

The addition of salt has another more unexpected consequence called "salting out" effect, this term is used to describe the decreasing solubility, which results from the addition of salts or electrolytes to solute-solvent system. When salt concentration increases, some of water molecules are attracted by the salt ions, which leads to a decrease of the number of water molecules available to interact with charged part of (co)polymer. The "salting out" effect is responsible for a change of solubility of (co)polymers in aqueous solution or induces a modification of the morphology of these (co)polymer aggregates.

PMEMA is a polybase which has good solubility in neutral and acidic aqueous solution. Meanwhile, it is sensitive to the presence of electrolytes and displays "salting out" effect in presence of 0.2 - 0.3 M Na_2SO_4 at room temperature. [17] Consequently PMEMA-based pH-responsive block copolymers (i.e. PDEAEMA$_{34}$-*b*-PDMAEMA$_{67}$-*b*-PMEMA$_{39}$, [215] PMEMA-*b*-PDEAEMA [216, 217] and PVBA$_{63}$-*b*-PMEMA$_{123}$ [205]) exhibit "schizophrenic" behavior in response to addition of salt and pH change. As illustrated in **Scheme I.10**, starting from a block copolymer at pH value where both blocks are completely hydrated, the addition of salt with a sufficient high level causes the formation of micelles due to "salting out" effect of PMEMA block. Once the addition of salt is replaced with pH change, inverse micelles with a core of pH sensitive block and a shell of PMEMA block.

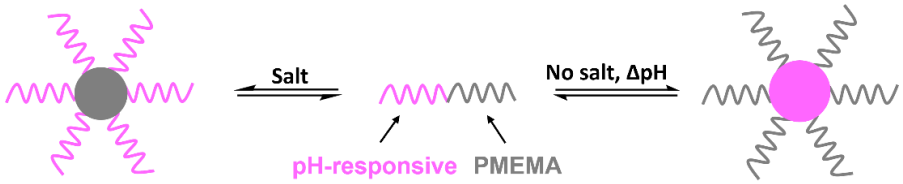

Scheme I.10 Micelle-to-(inverse micelle) transition of PMEMA-based pH-responsive copolymers in response to addition of salt and pH change.

(iii) Effect of charge balance within the (co)polymer

The effect of charge balance within block copolymer on self-organization is remarkable in the cases of polyampholytes. pH change drives structure of PAA_{134}-*b*-$P2VP_{628}$-*b*-PAA_{134} transfer from unimers at pH below IEP to micelles with P2VP core and PAA corona at pH above. [218] Additionally, the multiarm star-shaped terpolymer with 9 arms, poly(styrene)$_9$-poly(divinyl benzene)-(poly(2-vinyl-pyridine)$_{126}$-*b*-poly(acrylic acid)$_{69}$)$_9$ ((PSt_{33})$_9$-PDVB-($P2VP_{126}$-*b*-PAA_{69})$_9$) was reported with the formation of unimolecular, worm-like and multicore micelles at lower pH range, as well as irregular multistar aggregates, network-like assemblies and compartmentalized micelles at higher pH region (**Scheme I.11**). [219]

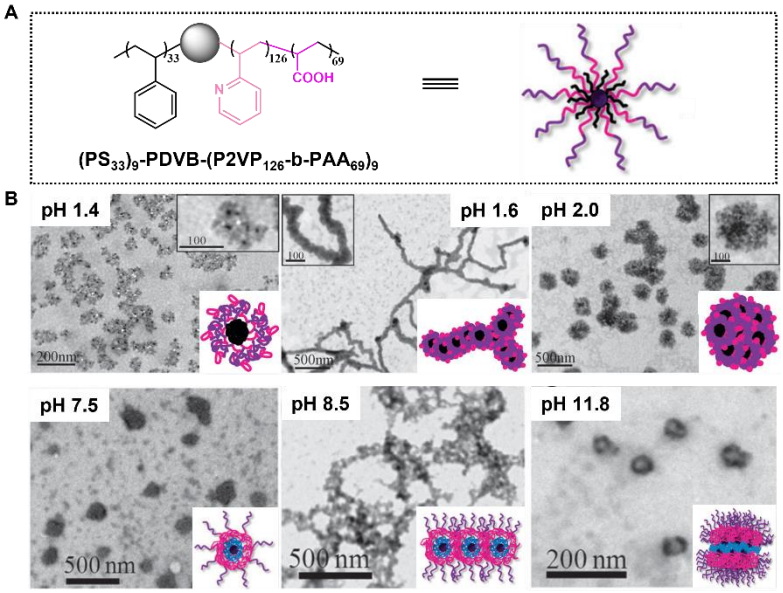

Scheme I.11 Chemical structure and TEM images at different pH values of star-shaped (PSt_{33})$_9$-PDVB-($P2VP_{126}$-*b*-PAA_{69})$_9$. Copyright 2011. Reproduced with permission from the Royal Society of Chemistry. Ref. [219]

(iv) Effect of architecture

Based on the synthetic process adopted, the architectures of pH-responsive (co)polymers can be linear, star, graft, branched and network. Depending on (co)polymer concentration and hydrophilic-hydrophobic ratio, these (co)polymers can self-assemble into unimers, micelles, vesicles and hydrogels. Changes in aggregates

morphology and size of different families of pH-responsive copolymers upon pH modulation are depicted in **Scheme I.12**. [220]

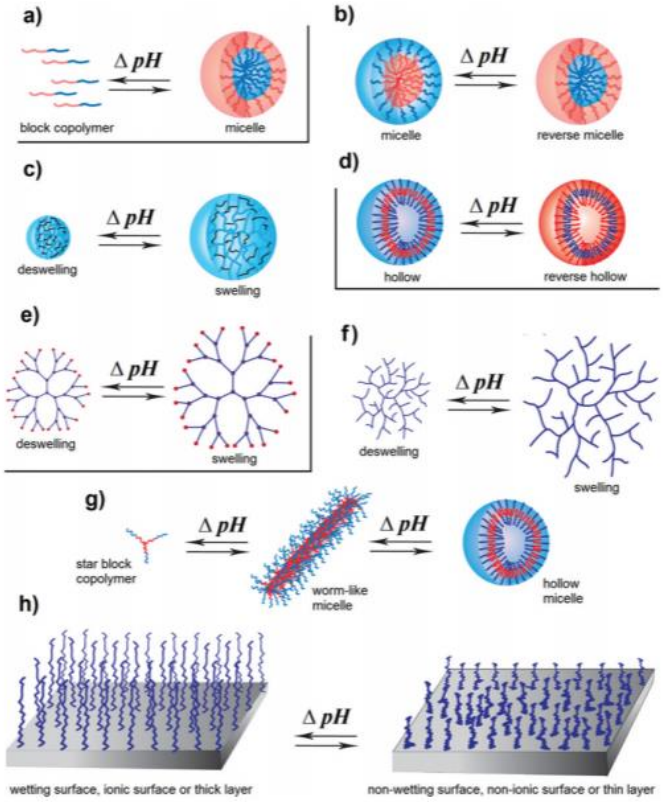

Scheme I.12 Morphological transition triggered by pH change for pH-responsive (co)polymers with (a), (b), (c), (d) linear, (e) dendrimer, (f) hyperbranched, (g) star and (h) brushes structures. Copyright 2017. Reproduced with permission from the Royal Society of Chemistry. Ref. [220]

pH-induced morphological transition of linear (co)polymers (such as block, statistical, gradient, etc.) is the most extensively studied project. Except pH-triggered unimers-to-micelle, micelle-to-(reverse micelle) and vesicle-to-(reverse vesicle) transitions mentioned in **Scheme I.12**, the vesicle-to-cylinder-to-sphere, [221] unimers-to-(mixture of micelles and micelles cluster), [222] spheres-to-(mixture of worm-like micelles and vesicles), [223] and sphere-to-vesicle [223] transitions have also been reported in the literature.

I.3.3 Dual temperature- and pH-responsive (co)polymers

The behavior of such dual thermo- and pH-responsive (co)polymers are relatively complex to study since each stimulus needs to be considered as stated above.

Some pH-responsive homopolymers also possess thermoresponsive properties at a given pH depending on the degree of protonation. Such family are regarded as dual thermo- and pH-responsive homopolymers, typical examples are listed in **Table I.12**.

Table I.12 Thermo- and pH-responsive homopolymers.

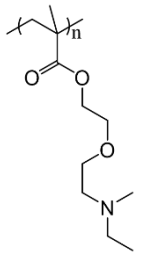 PEMAEEOMA[18]	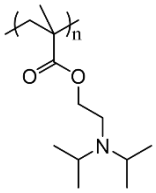 PDPAEMA[224]	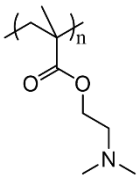 PDMAEMA[127]	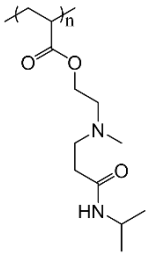 PIMA[225]	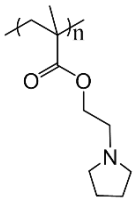 PEPyM[226]
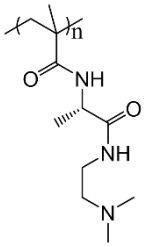 PMAME [227]	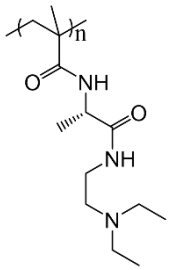 PMAEE [227]	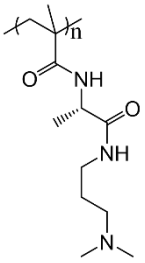 PMAMP [227]	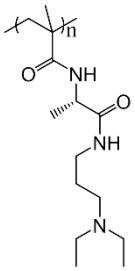 PMAEP [227]	
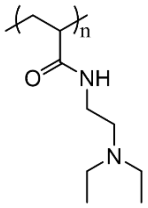 PDEAEAM [15]	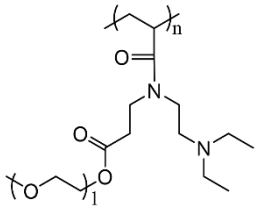 P(MEO$_1$-DEAE-AM) [228]	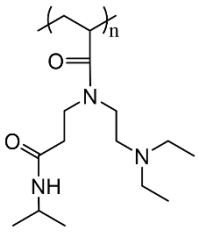 P(DEAE-NIPAM-AM) [229]	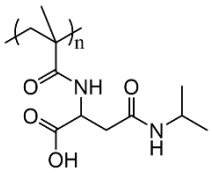 P(MA-iAsn-OH) [230]	

Abbreviations: PIMA: poly(2-((3-(isopropylamino)-3-oxopropyl)(methyl)amino) ethyl acrylate), PEPyM: poly(*N*-ethylpyrrolidine methacrylate), PMAME: poly(*N*-methacryloyl-$_L$-alanine 2-(dimethylamino) ethylamide), PMAEE: poly(*N*-methacryloyl-$_L$-alanine 2-(diethylamino) ethylamide), PMAMP: poly(*N*-methacryloyl-$_L$-alanine 3-(dimethylamino) propylamide), PMAEP: poly(*N*-methacryloyl-$_L$-alanine 3-(diethylamino) propylamide), P(MEO$_1$-DEAE-AM): poly(2-methoxyethyl 3-(*N*-(2-(diethylamino) ethyl) acrylamido) propanoate), P(DEAE-NIPAM-AM): poly(*N*-(2-(diethylamino) ethyl)-*N*-(3-(isopropylamino)-3oxopropyl) acrylamide), P(MA-iAsn-OH): poly(*N*-methacryloyl-$_L$-*β*-isopropylasparagine).

For instance, PDEAEAM and PDMAEMA homopolymers, are fully soluble at pH below p*K*a whatever the temperature since electrostatic repulsion among the charged chains prevent chains from aggregation upon heating. At pH above p*K*a, these

homopolymers are thermoresponsive and behave coil-to-globule or clear-to-cloud transition with increasing temperature.

Block copolymers comprising of one thermo-responsive block and one pH-responsive block have been extensively studied. The study of organization properties in aqueous solution of such thermo- and pH-responsive copolymers is complex. In general, pH adjustment alters ionization/deionization (or protonation/deprotonation) state of pH-sensitive segments, while temperature change shifts hydrophilic/hydrophobic balance of thermoresponsive moieties. Both changes influence the morphology of copolymers. Some examples of dual thermo- and pH-responsive diblock copolymers are listed in **Table I.13**.

Table I.13 Examples for pH- and temperature-controlled morphological transition.

Morphological transition triggered by pH and temperature[a] & Examples Thermoresponsive block pH-responsive block
polyacid-based diblock copolymers 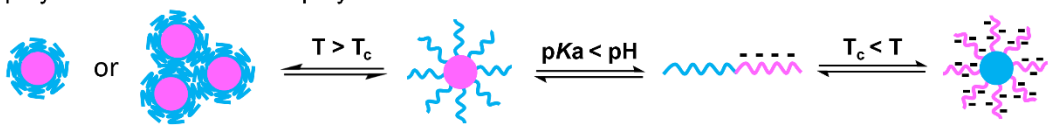
PNIPAM-*b*-PVBA, [231] PNIPAM$_{38}$-*b*-(PGMA$_{48}$-*graf*-PGA$_9$) [232]
polybase-based diblock copolymers 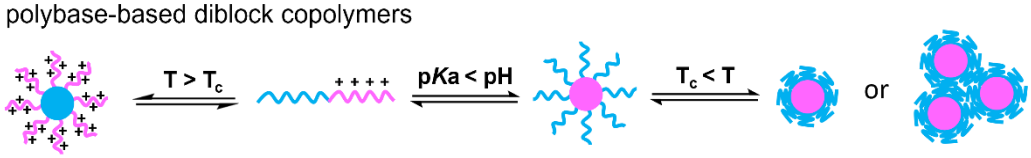
Star PNIPAM-*b*-(PDEAEMA)$_4$, [233] PDEAEMA$_{98}$-*b*-PNIPAM$_{209}$, [234] PNIPAM-*b*-P4VP, [235] PPO$_{33}$-*b*-PDEAEMA$_{42}$, [236] PMOVE$_{200}$-*b*-PAEVE$_{50}$, [237] PNIPAM-*b*-(PEA-*graf*-P2VP), [238] POEGMA-*b*-P4VP, [239] P2VP-*b*-PNIPAM [240]

[a]Polyacids are insoluble at low pH and soluble at high pH, while polybases are insoluble at high pH and soluble at low pH. Abbreviations: PAEVE: poly(primary amino groups), PEA: poly(ethyl acrylate).

I.4 CO_2-responsive (co)polymers

CO_2-responsive (co)polymers are (co)polymers that are prone to react with CO_2 in aqueous solution, this reaction can be reversed upon alternate bubbling CO_2/inert gases. As a stimulus, CO_2 has promising prospects due to its abundance, nonflammability, low

toxicity and biocompatibility. Moreover, CO_2 is easy to be removed without any accumulations or contaminations in the system upon repeated cycles. CO_2-responsiveness of (co)polymers is realized by incorporation of CO_2-sensitive functional groups along the (co)polymer chains. The most reported CO_2-responsive functional groups are organobases, such as amine, amidine, guanidine and imidazole, whose structures are shown in **Scheme I.13**.

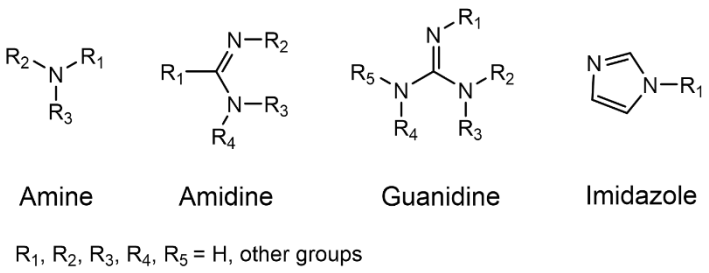

Scheme I.13 Structures of CO_2-responsive groups.

I.4.1 CO_2-responsive mechanism

The trigger of CO_2-responsiveness is regarded as the protonation of CO_2-sensitive groups within (co)polymers, which changes from uncharged to positively charged state after reaction with CO_2, this is similar to pH-responsive mechanism of polybases. The corresponding p*K*a value is an important parameter to judge the feasibility of CO_2-switchability. The detailed mechanism of each CO_2-sensitive group is demonstrated in **Scheme I.14**.

For CO_2-responsive groups containing N-H bonds, such as poly(allylamine) bearing two N-H bonds, when less quantity of CO_2 is added, amine groups react with CO_2 to form ammonium carbamates, with increasing CO_2 concentration in the system, carbamates then hydrolyze into bicarbonate salt. These two products can be distinguished by signals in ^{13}C NMR spectra where characteristic peaks at 165 and 160 ppm are attributed to carbamate and bicarbonate, respectively. [241] When bulky groups are attached to nitrogen atom in amine groups, the carbamate formation is restricted due to the steric effect, hence, bicarbonate salts are more readily to generate.

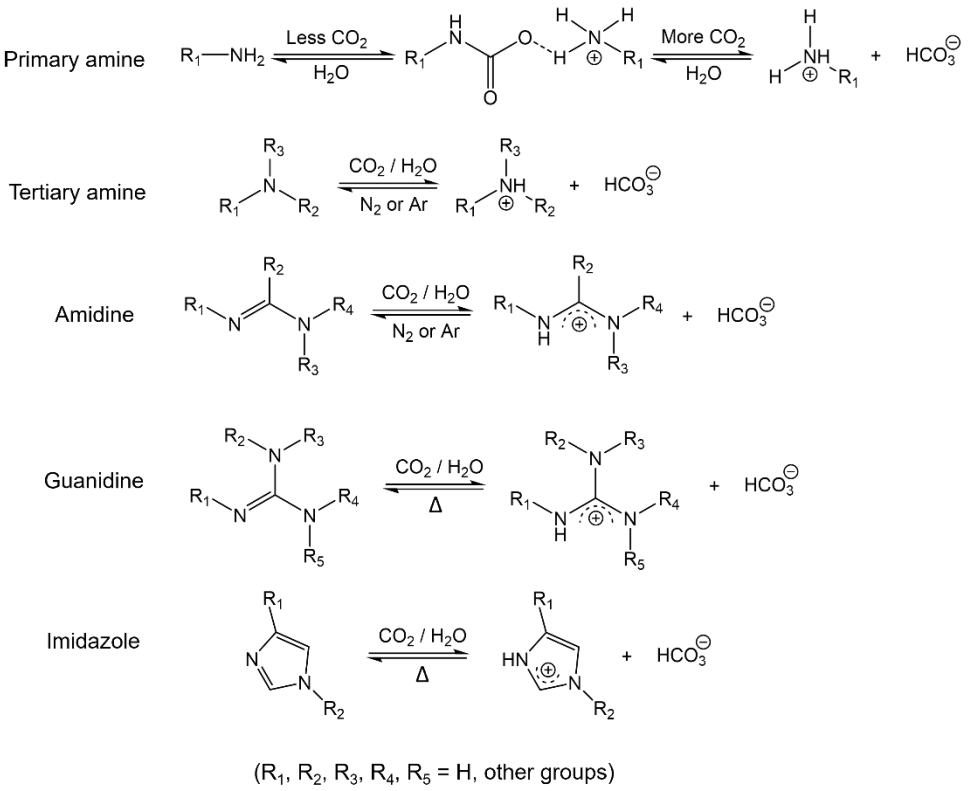

Scheme 14. CO_2-responisve mechanism.

For CO_2-responsive groups without N-H bonds, like tertiary amines, amidines, guanidines and imidazoles, they typically react with CO_2 to form bicarbonate salts instead of carbamates. In general, tertiary amines have p*K*a around 6.5 - 8.0, the protonation/deprotonation by gas treatment is easily accessible. Moreover, monomers bearing tertiary amines, such as DEAEMA and DMAEMA, are commercially available. Amidines have an average p*K*a value around 9.0, which provides themselves with stronger basicity and higher CO_2-sensitivity as well as faster responsive speed. Guanidine structures contain three nitrogen atoms attached to one carbon and have a p*K*a around 13.5. The chemical structure of imidazoles is generally regarded as cyclic amidines with a five-membered ring, alkyl substituted imidazoles possess higher p*K*a values of 10 - 14.5. Due to the higher p*K*a values of guanidines and imidazoles, inverting bicarbonate salts to neutral states by aeration inertial gases to remove CO_2 is not efficient, a common approach is heating the aqueous solution. [242, 243]

I.4.2 Self-assembly behavior of CO_2-responisve (co)polymers

The solubility of CO_2-responsive (co)polymers in aqueous solution is significantly influenced by the protonation/deprotonation upon CO_2 treatment/removal. Due to the shift of hydrophilic/hydrophobic balance in the system, these (co)polymers can assemble into different aggregates with variable geometries and sizes. In addition, the impacts of (co)polymer architecture, block sequence and (co)polymer composition should also be taken into account during the analysis of aggregation of (co)polymer. **Table I.14** summarizes some examples of CO_2-induced morphological transition.

Table I.14 Morphological transition of CO_2-responsive (co)polymers.

Morphological transition triggered by CO_2 & Examples
CO_2-responsive block Hydrophilic block Hydrophobic block
Diblock copolymers
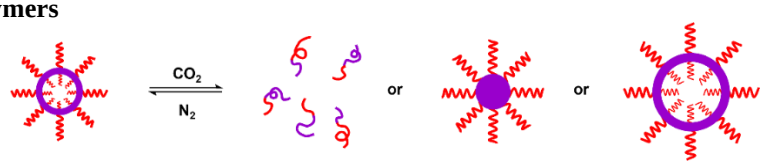
PDMAm$_{30}$-*b*-PDEAEMA$_{400}$, [244] PEO$_{45}$-*b*-P(DEAEMA$_{100}$-*co*-CMA$_6$), [244] PEO$_{45}$-*b*-P(DEAEMA$_{90}$-*co*-St$_{66}$), [245] PEO-*b*-PAD [246, 247]
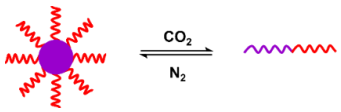
PDEAEMA-*b*-PEO [122], PDMAm-*b*-PHIS [248]
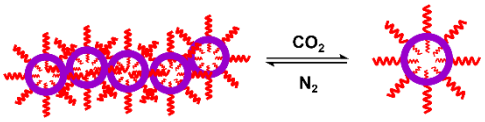
PEO$_{113}$-*b*-P(4VP$_{90}$-*co*-DEAEMA$_{30}$) [249]
Triblock copolymers
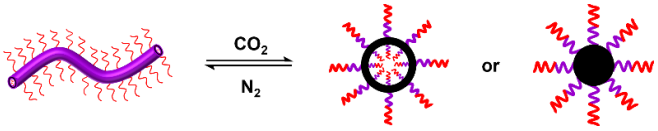
PEO$_{23}$-*b*-PAD$_{79}$-*b*-PSt$_{151}$ [250]
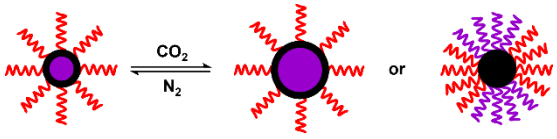
PEO$_{113}$-*b*-PHFBMA$_{110}$-*b*-PDEAEMA$_{212}$ [251] PEO$_{113}$-*b*-PSt$_{30}$-*b*-PDEAEMA$_{52}$, [252]
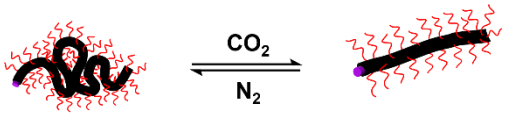
PEO$_{113}$-*b*-PSt$_{72}$-*b*-PDEAEMA$_{61}$ [252]

Table I.14 (Continued)

Morphological transition triggered by CO_2 & Examples CO_2-responsive block Hydrophilic block Hydrophobic block
Triblock copolymers
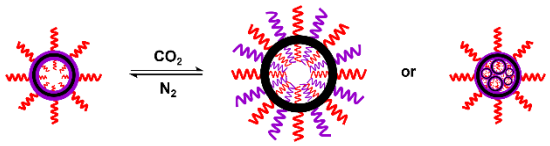 PEO_{45}-*b*-$PDEAEMA_{93}$-*b*-PSt_{66}, [245] PEO_{113}-*b*-PSt_{211}-*b*-$PDEAEMA_{59}$, [252] $POEGMEMA_{33}$-*b*-$PBzMA_{400}$-*b*-$PDEAEMA_{100}$ [253]
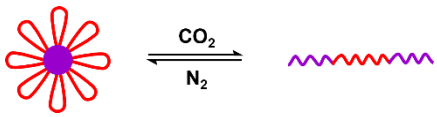 PDEAEMA-*b*-PEO-*b*-PDEAEMA [122]

Abbreviations: CMA: coumarin methacrylate, PAD: poly((*N*-amidino) dodecyl acrylamide), PHIS: poly(histamine acrylamido), PHFBMA: poly(2,2,3,4,4,4-hexafluorobutyl methacrylate).

I.4.3 Self-assembly of thermo- and CO_2-responsive (co)polymers

Dual thermo- and CO_2-responsive (co)polymers are generally based on one thermosensitive and one CO_2-responsive groups within (co)polymer chains. Some homopolymers with dual responsive properties have been reported in the literature and are listed in **Table I.15**.

Table I.15 Homopolymers with dual thermo- and CO_2-responsive properties.

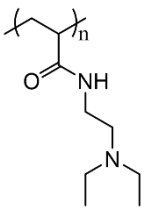	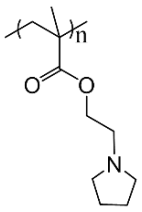	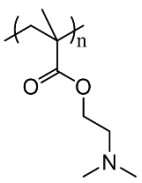	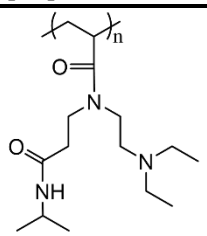
PDEAEAM [15]	PEPyM [16]	PDMAEMA [137]	P(DEAE-NIPAM-AM) [229]
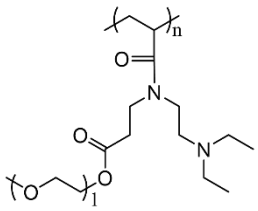	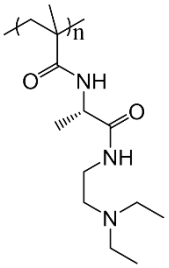	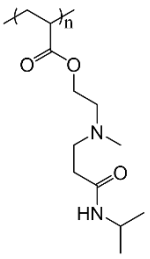	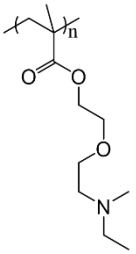
P(MEO_1-DEAE-AM) [228]	PMAEE [227]	PIMA [225]	PEMAEEOMA [18]

Table I.16 Examples of temperature- and CO_2-switchable morphological transition.

Morphological transition triggered upon heating/cooling and CO_2 treatment/removal & Examples Thermoresponsive block; Hydrophilic block; CO_2-responsive block; Hydrophobic block
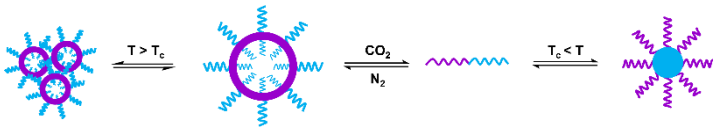 PDEAEMA$_{60}$-*b*-PNIPAM$_{40}$ [254]
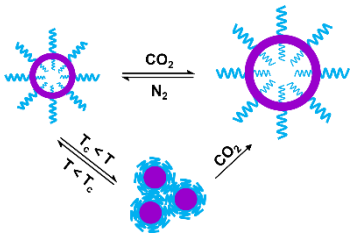 PADS-*b*-PDMAEMA [255]
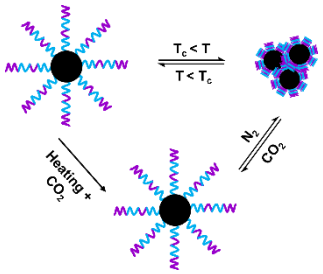 Py-PCL-*b*-P(NIPAM-*co*-DMAEMA) [256]
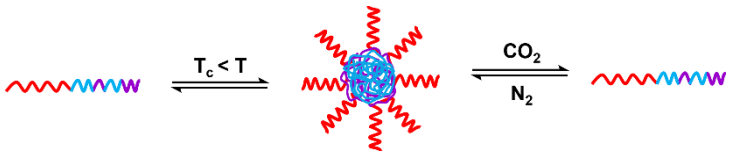 PEO$_{45}$-*b*-P(NIPAM$_{220}$-*co*-DEAEMA$_{90}$) [137]
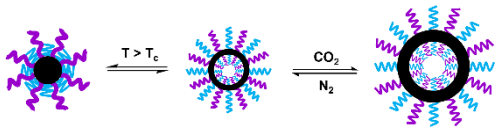 PNIPAM-*b*-PCL-*b*-PDMAEMA [257]
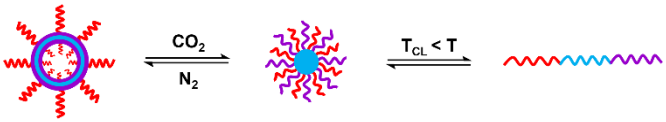 PEG$_{45}$-*b*-P(AAm$_{223}$-*co*-AN$_{103}$)-*b*-PDEAEMA$_{83}$* [258]

*Thermoresponsive block with a UCST behavior. Abbreviations: PADS: *N'*-Propargyl-*N*,*N*-dimethylacetamidine modified poly(*p*-azidomethylstyrene), Py: pyrene group.

Regarding the relative tedious synthetic routes of such multi-responsive monomers (and their corresponding homopolymers) and the access to obtain aggregates

with different structures and morphologies, many studies have been reported the combination of thermoresponsive units and CO_2-responsive moieties in (co)polymers with different structures via controlled radical polymerization. Some examples of temperature- and CO_2-tuned self-assemblies are presented in **Table I.16**. It is noteworthy that analysis of responsiveness in presence of CO_2 at high temperature should be taken care since CO_2 is not stable in aqueous solution at relatively high temperature, which influences the protonation degree of CO_2-responsive units to a certain extent.

I.5 Synthetic methods to prepare multi-stimuli (co)polymers

The precise synthesis of well-defined (co)polymers is a prerequisite to achieve desired properties, such as precisely tuning T_c values over a broad temperature range or controlling self-assembly behaviors triggered by external stimuli. To achieve such goal, controlled radical polymerization methods such as nitroxide-mediated radical polymerization (NMP), [259] atom transfer radical polymerization (ATRP), [260] reversible addition-fragmentation chain transfer (RAFT) polymerization [261-263] are the tools of choice. Indeed, the rapid development of controlled radical polymerization provides insights to design and synthesize (co)polymers with controlled molecular weight, narrow polydispersity and advanced microstructure. Thanks to these sophisticated techniques and post-polymerization modification, a great number of multi-stimuli responsive (co)polymers have been synthesized. In this section, we primarily make a short introduction on the synthesis of stimuli-responsive (co)polymers by using RAFT polymerization and/or ATRP since these two methods have been extensively reported in the literature.

I.5.1 RAFT polymerization

RAFT polymerization is an effective and versatile method to synthesize (co)polymers with controlled structures and compositions through a reversible chain transfer process, in which the number of radicals and occurrence of termination

reactions are reduced to achieve (co)polymer chains with controlled growth. In a typical RAFT polymerization, three important components are included: monomer, initiator and RAFT agent (or chain transfer agent). **Scheme I.15** depicts key steps of chain transfer and main equilibria processes in RAFT polymerization, the initiation and termination steps are similar to free radical polymerization, and they are not discussed here. In pre-equilibrium step, initial RAFT agent reacts with reactive radicals (propagating radicals) to yield a macro-RAFT agent (or dormant species), which further exchanges functionality with reactive radicals in main equilibrium step to form a new macro-RAFT agent, whose polymerization degree is different from the one's in pre-equilibrium step.

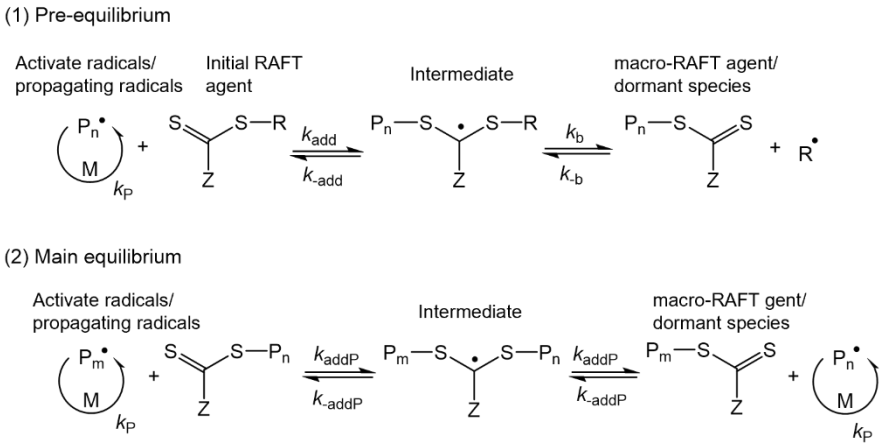

Scheme I.15 Chain transfer and main equilibria in RAFT polymerization mechanism.

Synthesis of multi-stimuli responsive block copolymers by RAFT polymerization basically includes at least two consecutive controlled radical procedures. In each step, the chosen RAFT agent should be able to effectively mediate the controlled polymerization of different monomers. Therefore, a key point in RAFT polymerization is the selection of RAFT agent, whose effectiveness is determined by the nature of activating and leaving groups. Additionally, some properties of synthesized (co)polymers may be influenced by the residual groups of RAFT agents as end groups attaching to the (co)polymer main chains. For instance, the polarity of end groups influences T_c of synthesized thermoresponsive (co)polymers and their colloidal properties in water. [75, 214, 264]

All in all, RAFT polymerization has been successfully and extensively employed in synthesis of multi-stimuli responsive (co)polymers due to its unique advantages: (1) good compatibility over a wide range of monomers; (2) mild polymerization conditions. **Table I.17** gives some examples of stimuli-responsive (co)polymers synthesized by RAFT polymerization.

Table I.17 Synthesis of stimuli-responsive (co)polymers by RAFT polymerization.

(Co)polymer	Stimulus type	Experimental conditions[a]		Ref.
		Initial RAFT agent	Initiator	
PDMAEEOMA$_{137}$-*b*-PEMAEEOMA$_{78}$	Dual temperature (LCST-LCST)	CDTPA	AIBN	[18]
P(DEGA-*stat*-DMAm)	Temperature	DMP	AIBN	[23]
PNIPAM$_{94}$-*b*-P(NAG$_{19}$-*co*-NAGSP$_{30}$)	Dual temperature (LCST-UCST)	CDTPA	AIBN	[157]
P(mPEGV)$_{32}$-*b*-PNIPAM$_{170}$-*b*-PSt$_{166}$	Dual temperature (LCST-LCST)	EMP	ACPA(AIBN)	[148]
PNIPAM$_{54}$-*b*-PDMAEMA$_{46}$-*b*-PSt$_{460}$	Dual temperature (LCST-LCST)	CDTPA	AIBN	[149]
PNASME$_{170}$-*b*-PNIPAM$_{63}$	Dual temperature (LCST-LCST)	DMAT	AIBN	[12]
PNIPAM$_{115}$-*b*-PNAEAA$_{230}$	Dual temperature (LCST-LCST)	ECT	AIBN	[11]
PDEAEMA-*b*-PNIPAM	Temperature, pH	CEP	V-501(VA-044)	[234]
PDMA-*b*-PDEAEMA	CO_2	CPDB	AIBN	[244]
PDEAEMA$_{60}$-*b*-PNIPAM$_{40}$	Temperature, CO_2	DMP	AIBN	[254]
PEO$_{113}$-*b*-PHFBMA$_{110}$-*b*-PDEAEMA$_{212}$	CO_2	macro PEO	ACPA	[251]
PEO$_{45}$-*b*-P(DEAEMA$_{90}$-*co*-St$_{66}$)	CO_2	macro PEO$_{45}$	ACVA	[245]
PEO$_{45}$-*b*-PDEAEMA$_{93}$-*b*-PSt$_{66}$	CO_2	macro PEO$_{45}$	ACVA	
PEO$_{113}$-*b*-P(4VP$_{90}$-*co*-DEAEMA$_{30}$)	CO_2	macro PEO$_{113}$	ACVA	[249]
POEGMA$_{33}$-*b*-PBzMA$_{400}$-*b*-PDEAEMA$_{100}$	CO_2	CPADB	AIBN	[253]
PEO-*b*-P(AAm-*co*-AN)-*b*-PDEAMA	Temperature (UCST), CO_2	macro PEO$_{45}$	AIBN	[258]

[a]Only RAFT agent and initiator are presented, other polymerization conditions like solvents, polymerization temperature, reaction time and post-modification can be referred to the corresponding references.

I.5.2 ATRP

ATRP is a catalytic process involving a transition-metal complex to create equilibria between growing and dormant radicals. As illustrated in **Scheme I.16**, an ATRP system primarily consists of monomer (M), alkyl halide initiator and transition-metal catalyst (Mt). The polymerization reaction is usually initiated by the latter two components. In details, the catalyst can activate alkyl halide initiator (dormant species) via a transfer of halide atom, leading to the formation of reactive radicals ($P_n\cdot$), which reacts with monomer to extend (co)polymer chains (P_n-X). Meanwhile, these reactive radicals are deactivated and become dormant species by transferring a halide atom from Mt^{z+1}-X. This reversible step can be adjusted to reduce concentration of dormant species and to minimize termination reaction as well as to realize (co)polymer chains with controlled grow. [260]

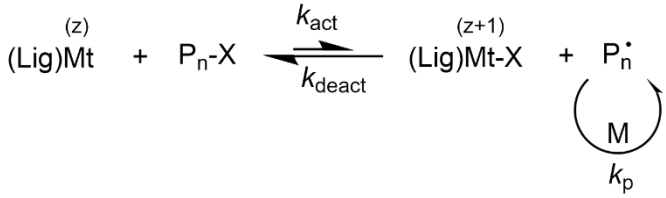

Scheme I.16 Reversible activation/deactivation in ATRP mechanism.

Table I.18 Some examples of stimuli-responsive (co)polymers synthesized through ATRP reaction.

(Co)polymer	Stimulus type	Experimental conditions[a]		Ref.
		Catalyst	Initiator	
$PNIPAM_{450}$-*b*-P($NIPAM_{244}$-*co*-$HMAAm_{70}$)	Dual temperature (LCST-LCST)	CuBr/Me_6TREN	EBB	[98]
PEO_{45}-*b*-$PNIPAM_{380}$-*b*-P($NIPAM_{423}$-*co*-$HEAAm_{42}$)	Dual temperature (LCST-LCST)	CuCl/Me_6TREN	PEO_{45}-Br	[152]
PEO-*b*-PSt-*b*-PDEAEMA	CO_2	CuBr/PMDETA (CuCl/$CuCl_2$/PMDETA)	PEO-Br	[252]
PEO-*b*-P(DEAEMA-*co*-CMA)	CO_2	CuBr/PMDETA	PEO-Br	[244]
P($DEGMA_{180}$-*co*-$DMAEMA_{38}$)-*b*-PEO_{455}-*b*-P($DEGMA_{180}$-*co*-$DMAEMA_{38}$)	Temperature, CO_2	CuCl/PMDETA	Br-PEO-Br	[138]
P($DEGMA_{160}$-*co*-MAA_{36})-*b*-PEO_{455}-*b*-P($DEGMA_{160}$-*co*-MAA_{36})	Temperature, CO_2	CuCl/PMDETA	Br-PEO-Br	

[a]Only catalyst and initiator are presented, other polymerization conditions like solvents, polymerization temperature, reaction time and post-modification can be referred to the corresponding references.

ATRP has appealing characters, such as good tolerance over a wide range of functional monomers, readily mono- and multi-functionalized initiators and concurrent growth of all chains. However, some limitations should be noted: (1) the final obtained (co)polymers typically contain a small amount of residual metal, which may influence the applications, (2) transition-metal catalysts at lower state are easy to be oxidized. Some examples of stimuli-responsive (co)polymers synthesized via ATRP are summarized in **Table I.18**.

I.5.3 Other methods

In addition to these two synthetic methods mentioned above, other methods, such as nitroxide-mediated radical polymerization (NMP), group transfer polymerization (GTP), living anionic/cationic polymerization, ring opening polymerization (ROP) and cobalt-mediated radical polymerization (CMRP) are also used or combined with post-polymerization modification to synthesize stimuli-responsive (co)polymers with controlled molecular weight and well-defined structure. Interested reader can refer to the examples summarized in **Table I.19**.

Table I.19 Examples of stimuli-responsive (co)polymers synthesized via different methods.

(Co)polymer	Stimulus type	Synthesized method	Ref.
P2VP-*b*-PNIPAM	Temperature, pH	NMP	[240]
PPO-*b*-P(DMAEMA-*stat*-2VP)	Temperature, pH	NMP	[265]
$PDPAEMA_{23}$-*b*-$PDMAEMA_{150}$-*b*-$PDPAEMA_{20}$	pH	GTP	[266]
PMEMA-*b*-PDEAEMA	pH	GTP	[216]
$PMEMA_{60}$-*b*-$PDEAEMA_{40}$	pH	GTP	[217]
$PDEAEMA_{34}$-*b*-$PDMAEMA_{67}$-*b*-$PMEMA_{39}$	pH	GTP	[215]
P(iPMAm-*stat*-DMAm)	Temperature	GTP	
PiPMAm-*b*-PDMAm	Temperature	GTP	[73]
PiPMAm-*b*-PDMAm-*b*-PiPMAm	Temperature	GTP	

Table I.19 (Continued)

(Co)polymer	Stimulus type	Synthesized method	Ref.
PDMAm-*b*-PiPMAm-*b*-PDMAm	Temperature	GTP	[73]
PDMAEMA-*b*-PEGMA-*b*-PBuMA	Temperature, pH	GTP	[133]
PSBMA-*b*-PMEMA	Dual temperature (UCST-LCST)	GTP + Selective quaternization	[267]
PB_{24}-*b*-$PMAA_{10}$	pH	Sequential anionic polymerization	[221]
PVP-*b*-PEO	pH	Stepwise anionic polymerization	[268]
$PMOVE_{107}$-*b*-$PNIPAM_{210}$	Dual temperature (LCST-LCST)	Living cationic polymerization + RAFT	[269]
$PMOVE_{58}$-*b*-$PNIPAM_{170}$-*b*-$PMOVE_{58}$	Dual temperature (LCST-LCST)	Living cationic polymerization + RAFT	[150]
P2VP-*b*-PDMAEMA	Temperature, pH	Living anionic polymerization	[270]
PGA_{15}-*b*-$PLys_{15}$	pH	ROP	[271]
PVCL-*stat*-PVP	Temperature	CMRP	[106]
PVCL-*b*-P(VCL-*stat*-VP)	Dual temperature (LCST-LCST)	CMRP	
PVCL-*b*-P(VCL-*stat*-VP)-*b*-PVCL	Dual temperature (LCST-LCST)	CMRP + cobalt-mediated reaction coupling	
PVAc-*b*-PVCL	Temperature	CMRP	[108]
PVOH-*b*-PVCL	Temperature	CMRP + Hydrolysis	
P(VCL-*stat*-VAc)	Temperature	CMRP	[104]
P(VCL-*stat*-MVA)	Temperature	CMRP	
P(VCL-*stat*-NVA)	Temperature	CMRP	
P(VCL-*stat*-VPi)	Temperature	CMRP	

Abbreviations: PSBMA: sulfobetaine modified poly(*N*,*N*-dimethylamino ethyl methacrylate).

I.6 Applications

Multi-stimuli responsive (co)polymers are one kinds of smart materials and have attracted great interest in recent years. Due to their physiochemical property change (such as solubility, chain conformation, dimension, configuration…) in response to the

subtle external environment change, these (co)polymers can be used as drug carriers, functionalized surface and sensors, etc. in the potential fields of biotechnology, nanotechnology, functional membranes and smart coatings.

I.6.1 Drug carrier

Self-organization and particle size are the most important parameters to realize controlled drug delivery and release. As stated above, the morphology of stimuli-responsive (co)polymers can be triggered by specific stimuli, which provides possibilities on design of stimuli-sensitive materials as drug carriers with regard to the problems of solubility, enzymatic degradation and non-toxicity of drugs. These intelligent carriers can be designed with micelle or vesicle or hydrogel structures to load drugs, to reduce the side effects and to maximize the efficiency of drugs (**Scheme I.17**). [272]

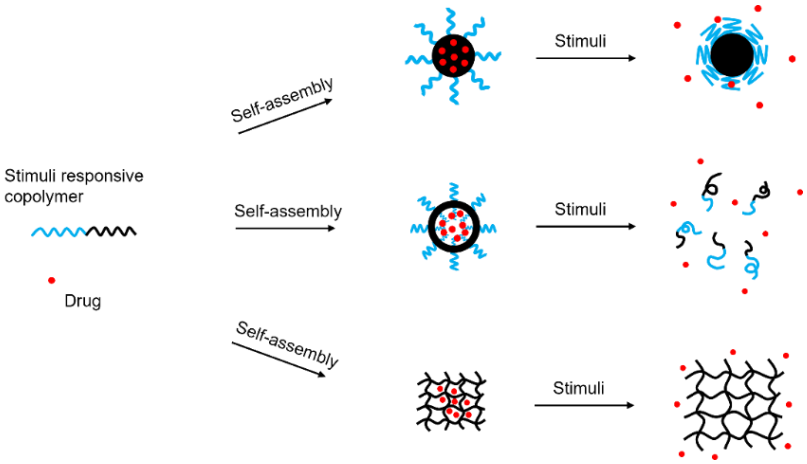

Scheme I.17. Schematic representation of stimuli-responsive (co)polymers used for drug delivery and controlled release.

Since hydrophobic micelle core can associate some lipophilic drugs, the highly hydrated corona provides stabilizing interface between hydrophobic cores and aqueous solution, which helps to improve the dispersion of micelles and to suppress the intermicellar aggregation. Once the external environment changes, the micellar structure is destabilized and drives drug diffuse out quickly from the micelle cores. [174, 273] Additionally, vesicular structures have high loading capacity, the hydrophilic drugs can be placed inside of vesicles while the hydrophobic molecules are

integrated into bilayer, as stimuli applied, vesicular structures dissociate and drugs are released. [274] Meanwhile, internal space in 3D network structure endows hydrogels with high efficiency to encapsulate and release drugs via volume compaction and expansion, which can be modulated by external stimuli. [275]

I.6.2 Functionalized surface

Metal nanoparticles, such as gold and silver nanoparticles (AuNPs and AgNPs), have obtained ever-increasing interest due to their unique properties and extensive applications as smart sensors. However, bare metal nanoparticles undergo aggregation in response to a subtle change of ionic strength or pH in system. Hence, the stabilization of such particles in solution is required to use some stabilizing agent such as (co)polymer. These hybrid materials can be obtained through different strategies (*in situ* formation, ligand exchange, "grafting from" or "grafting to" strategies). In addition, modification of stimuli-responsive (co)polymers to metal NPs surface confers to the obtained hybrid materials with specific additional properties. Indeed, such obtained hybrid nanoparticles not only keep the unique properties of bare nanoparticles (such as optical, catalytic properties…), but also own the special properties of (co)polymers, especially the stimuli-responsiveness and processibility. For instance, the system stability of coating $PNIPAM_{10k}$ on AuNPs at room temperature is improved over a broad pH range (1-13) and high ionic strength (up to 1 wt.%). And its catalytic efficiency in reduction of *p*-nitrophenol to *p*-aminophenol is influenced by temperature change due to the thermoresponsive PNIPAM, the reaction rate increases along with temperature until T_c reaches, which is followed by a decreasing tendency. [276] Additionally, AgNPs coated with CO_2-responsive PDEAEMA has a reversible dispersion/aggregation transition in water upon CO_2 treatment/removal, and its catalytic activity after bubbling CO_2 is higher in reduction of *p*-nitrophenol to *p*-aminophenol than that in absence of CO_2 (**Scheme I.18**). [277]

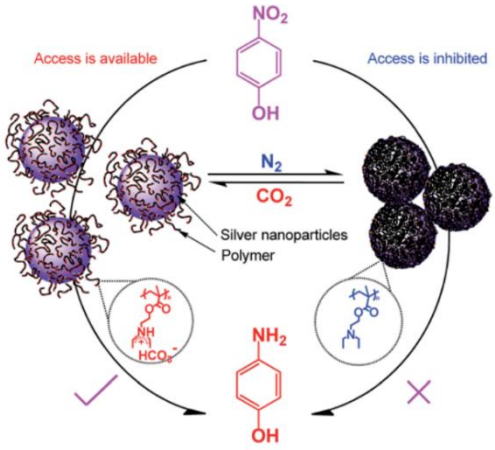

Scheme I.18 Tunable catalytic activity of AgNPs coated with PDEAEMA in reduction of *p*-nitrophenol to *p*-aminophenol upon bubbling CO_2/N_2. Copyright 2017. Reproduced with permission from the Royal Society of Chemistry. Ref. [277]

I.6.3 Sensors

Sensors are a type of smart devices with capacity of transferring some specific analytes from its surroundings into output signals which is processed and readable. Design of stimuli-responsive (co)polymer-based sensors is of great interest due to its rapid and efficient response. For instance, Minko and co-workers designed a pH-responsive nanosensor based on the real-time determination of shrinkage/expansion of pH-sensitive polymer brush, the signals are detected by surface plasmon resonance spectroscopy of AuNPs. As pH alters, electrostatic repulsion is caused by charges within polymer brush, this drives brush to stretch and swell, as a result, surface plasmon bands are shifted (**Scheme I.19**). [278]

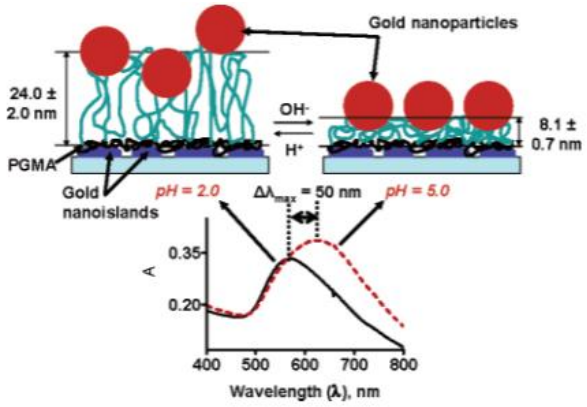

Scheme I.19 Schematic illustration pH-sensor of AuNPs coated with P2VP polymer brush. Copyright 2004. Reproduced with permission from the American Chemical Society. Ref. [278]

I.7 Conclusions

The latest development of multi-stimuli (thermo-, pH- and CO_2-) responsive (co)polymers is reviewed in this chapter. Some (co)polymer molecular parameters (such as microstructures, molecular weight, concentration, composition...) affecting phase transition behavior and self-organization of such (co)polymers solution upon stimuli treatment/removal are discussed. Meanwhile, a short introduction of synthetic methods (ATRP, RAFT polymerization) and applications is presented in the end of this chapter.

I.8 References

[1] Z. Cao, W. Liu, P. Gao, K. Yao, H. Li, G. Wang, Polymer 46 (2005) 5268-5277.

[2] C.-H. Ko, K.-L. Claude, B.-J. Niebuur, F.A. Jung, J.-J. Kang, D. Schanzenbach, H. Frielinghaus, L.C. Barnsley, B. Wu, V. Pipich, A. Schulte, P. Müller-Buschbaum, A. Laschewsky, C.M. Papadakis, Macromolecules 53 (2020) 6816-6827.

[3] H.Y. Liu, X.X. Zhu, Polymer 40 (1999) 6985-6990.

[4] Y. Cao, X.X. Zhu, J. Luo, H. Liu, Macromolecules 40 (2007) 6481-6488.

[5] I. Idziak, D. Avoce, D. Lessard, D. Gravel, X.X. Zhu, Macromolecules 32 (1999) 1260-1263.

[6] M. Matsumoto, R. Wakabayashi, T. Tada, T.-A. Asoh, T. Shoji, N. Kitamura, Y. Tsuboi, Macromol. Chem. Phys. 217 (2016) 2576-2583.

[7] D.G. Lessard, M. Ousalem, X.X. Zhu, A. Eisenberg, P.J. Carreau, J Polym Sci B Polym Phys 41 (2003) 1627-1637.

[8] E. Uğuzdoğan, E.B. Denkbaş, O.S. Kabasakal, J. Appl. Polym. Sci. 127 (2013) 4374-4384.

[9] D. Ito, K. Kubota, Macromolecules 30 (1997) 7828-7834.

[10] J. Li, S. Mizutani, S.-I. Sato, A. Narumi, O. Haba, S. Kawaguchi, T. Kakuchi, X. Shen, Polymer 202 (2020) 122678.

[11] Y. Hou, Y. Guo, S. Qian, H. Khan, G. Han, W. Zhang, Polymer 167 (2019) 159-166.

[12] S. Chen, K. Wang, W. Zhang, Polym. Chem. 8 (2017) 3090-3101.

[13] S. Chen, Y. Zhang, K. Wang, H. Zhou, W. Zhang, Polym. Chem. 7 (2016) 3509-3519.

[14] D. Yu, C. Luo, W. Fu, Z. Li, Polym. Chem. 5 (2014) 4561-4568.

[15] Z. Song, K. Wang, C. Gao, S. Wang, W. Zhang, Macromolecules 49 (2016) 162-171.

[16] K. Wang, Z. Song, C. Liu, W. Zhang, Polym. Chem. 7 (2016) 3423-3433.

[17] V. Bütün, S.P. Armes, N.C. Billingham, Polymer 42 (2001) 5993-6008.

[18] K. Wang, S. Chen, W. Zhang, Macromolecules 50 (2017) 4686-4698.

[19] Q. Li, A.P. Constantinou, T.K. Georgiou, J. Polym. Sci. 59 (2021) 230-239.

[20] S. Han, M. Hagiwara, T. Ishizone, Macromolecules 36 (2003) 8312-8319.

[21] F. Hua, X. Jiang, D. Li, B. Zhao, J Polym Sci A Polym Chem 44 (2006) 2454-2467.

[22] C. Boyer, M.R. Whittaker, K. Chuah, J. Liu, T.P. Davis, Langmuir 26 (2010) 2721-2730.

[23] P. De, B.S. Sumerlin, Macromol. Chem. Phys. 214 (2013) 272-279.

[24] C. Boyer, M.R. Whittaker, M. Luzon, T.P. Davis, Macromolecules 42 (2009) 6917-6926.

[25] X. Jiang, C.A. Lavender, J.W. Woodcock, B. Zhao, Macromolecules 41 (2008) 2632-2643.

[26] Q. Zhong, W. Wang, J. Adelsberger, A. Golosova, A.M.B. Koumba, A. Laschewsky, S.S. Funari, J. Perlich, S.V. Roth, C.M. Papadakis, P. Müller-Buschbaum, Colloid Polym Sci 289 (2011) 569-581.

[27] M. Beija, J.-D. Marty, M. Destarac, Chem. Commun. 47 (2011) 2826-2828.

[28] N.S. Ieong, M. Redhead, C. Bosquillon, C. Alexander, M. Kelland, R.K. O'Reilly, Macromolecules 44 (2011) 886-893.

[29] K. Suwa, K. Morishita, A. Kishida, M. Akashi, J Polym Sci A Polym Chem 35 (1997) 3087-3094.

[30] H. Asai, K. Fujii, T. Ueki, S. Sawamura, Y. Nakamura, Y. Kitazawa, M. Watanabe, Y.-S. Han, T.-H. Kim, M. Shibayama, Macromolecules 46 (2013) 1101-1106.

[31] P.J. Roth, M. Collin, C. Boyer, Soft Matter 9 (2013) 1825-1834.

[32] J. Seuring, S. Agarwal, Macromol. Chem. Phys. 211 (2010) 2109-2117.

[33] W. Sun, Z. An, P. Wu, Macromolecules 50 (2017) 2175-2182.

[34] J. Seuring, F.M. Bayer, K. Huber, S. Agarwal, Macromolecules 45 (2011) 374-384.

[35] S. Glatzel, A. Laschewsky, J.-F. Lutz, Macromolecules 44 (2010) 413-415.

[36] D.H. Seuyep N., D. Szopinski, G.A. Luinstra, P. Theato, Polym. Chem. 5 (2014) 5823-5828.

[37] S. Li, F. Huo, Q. Li, C. Gao, Y. Su, W. Zhang, Polym. Chem. 5 (2014) 3910-3918.

[38] Y. Su, M. Dan, X. Xiao, X. Wang, W. Zhang, J Polym Sci A Polym Chem 51 (2013) 4399-4412.

[39] P.J. Roth, F.D. Jochum, P. Theato, Soft Matter 7 (2011) 2484-2492.

[40] K. Wang, Q. Liu, G. Liu, Y. Zeng, Polymer 203 (2020) 122746.

[41] Z. Osváth, B. Iván, Macromol. Chem. Phys. 218 (2017) 1600470.

[42] P.O. Stănescu, L.C. Radu, C. Drăghici, M. Teodorescu, React Funct Polym 152 (2020) 104610.

[43] F. Yin, J.S. Behra, M. Beija, A. Brûlet, J. Fitremann, B. Payré, S. Gineste, M. Destarac, N. Lauth-de Viguerie, J.-D. Marty, J Colloid Interface Sci 578 (2020) 685-697.

[44] Z. Osváth, T. Tóth, B. Iván, Polymer 108 (2017) 395-399.

[45] M. Bozorg, B. Hankiewicz, V. Abetz, Soft Matter 16 (2020) 1066-1081.

[46] P. Liu, H. Xie, H. Tang, G. Zhong, H. Zhang, J Polym Sci A Polym Chem 50 (2012) 3664-3673.

[47] S.M. Ponce-Vargas, N.A. Cortez-Lemus, A. Licea-Claveríe, Macromol. Symp. 325 (2013) 56-70.

[48] S. Z. Moghaddam, E. Thormann, Phys. Chem. Chem. Phys. 17 (2015) 6359-6366.

[49] A. García-Peñas, C.S. Biswas, W. Liang, Y. Wang, P. Yang, F.J. Stadler, Polymers 11 (2019) 991.

[50] R. Konefał, J. Spěváček, G. Mužíková, R. Laga, Eur. Polym. J. 124 (2020) 109488.

[51] L. Starovoytova, J. Spěváček, Polymer 47 (2006) 7329-7334.

[52] R. Konefał, P. Černoch, M. Konefał, J. Spěváček, Polymers 12 (2020) 1879.

[53] J. Spěváček, J. Dybal, L. Starovoytova, A. Zhigunov, Z. Sedláková, Soft Matter 8 (2012) 6110-6119.

[54] J. Spěváček, L. Hanková, L. Starovoytova, Macromolecules 37 (2004) 7710-7718.

[55] J. Spěváček, L. Hanyková, Macromol. Symp. 203 (2003) 229-238.

[56] J. Spěváček, R. Konefał, J. Dybal, E. Čadová, J. Kovářová, Eur. Polym. J. 94 (2017) 471-483.

[57] R. Konefał, J. Spěváček, P. Černoch, Eur. Polym. J. 100 (2018) 241-252.

[58] R. Konefał, J. Spěváček, E. Jäger, S. Petrova, Colloid Polym Sci 294 (2016) 1717-1726.

[59] Y. Maeda, T. Higuchi, I. Ikeda, Langmuir 16 (2000) 7503-7509.

[60] Y. Maeda, T. Nakamura, I. Ikeda, Macromolecules 35 (2002) 10172-10177.

[61] Y. Maeda, T. Nakamura, I. Ikeda, Macromolecules 34 (2001) 1391-1399.

[62] T. Liu, J. Chen, S. Sugihara, Y. Maeda, Colloid Polym Sci 290 (2012) 763-767.

[63] Y. Maeda, T. Nakamura, I. Ikeda, Macromolecules 34 (2001) 8246-8251.

[64] T. Hidaka, S. Sugihara, Y. Maeda, Eur. Polym. J. 49 (2013) 675-681.

[65] Y. Maeda, T. Nakamura, H. Yamauchi, T. Nakaji, H. Kitano, Langmuir 23 (2007) 11259-11265.

[66] Y. Maeda, J. Sakamoto, S.-Y. Wang, Y. Mizuno, J. Phys. Chem. B 113 (2009) 12456-12461.

[67] Y. Maeda, S. Takaku, J. Phys. Chem. B 114 (2010) 13110-13115.

[68] Y. Maeda, T. Higuchi, I. Ikeda, Langmuir 17 (2001) 7535-7539.

[69] Y. Maeda, H. Mochiduki, I. Ikeda, Macromol. Rapid. Commun. 25 (2004) 1330-1334.

[70] Y. Maeda, M. Tsubota, I. Ikeda, Colloid Polym Sci 281 (2003) 79-83.

[71] Y. Maeda, H. Yamamoto, I. Ikeda, Colloid Polym Sci 282 (2004) 1268-1273.

[72] S.I. Yamamoto, J. Pietrasik, K. Matyjaszewski, J Polym Sci A Polym Chem 46 (2008) 194-202.

[73] J. Li, S. Mizutani, S.-I. Sato, A. Narumi, O. Haba, S. Kawaguchi, M. Kikuchi, T. Kakuchi, X. Shen, Polym. Chem. 11 (2020) 2346-2359.

[74] A. Laukkanen, L. Valtola, F.M. Winnik, H. Tenhu, Macromolecules 37 (2004) 2268-2274.

[75] Y. Xia, N.A.D. Burke, H.D.H. Stöver, Macromolecules 39 (2006) 2275-2283.

[76] R. Pamies, K. Zhu, A.-L. Kjøniksen, B. Nyström, Polym. Bull. 62 (2008) 487-502.

[77] Y. Xia, X. Yin, N.A.D. Burke, H.D.H. Stöver, Macromolecules 38 (2005) 5937-5943.

[78] X. Qiu, T. Koga, F. Tanaka, F.M. Winnik, Sci China Chem 56 (2013) 56-64.

[79] P.A. FitzGerald, S. Gupta, K. Wood, S. Perrier, G.G. Warr, Langmuir 30 (2014) 7986-7992.

[80] S. Furyk, Y. Zhang, D. Ortiz-Acosta, P.S. Cremer, D.E. Bergbreiter, J Polym Sci A Polym Chem 44 (2006) 1492-1501.

[81] C. Boutris, E.G. Chatzi, C. Kiparissdes, Polymer 38 (1997) 2567-2570.

[82] P. Kujawa, F. Segui, S. Shaban, C. Diab, Y. Okada, F. Tanaka, F.M. Winnik, Macromolecules 39 (2006) 341-348.

[83] W. Kunz, P. Lo Nostro, B.W. Ninham, Curr Opin Colloid Interface Sci 9 (2004) 1-18.

[84] M.G. Cacace, E.M. Landau, J.J. Ramsden, Q. Rev. Biophys. 30 (1997) 241-277.

[85] R. Freitag, F. Garret-Flaudy, Langmuir 18 (2002) 3434-3440.

[86] Y. Zhang, S. Furyk, D.E. Bergbreiter, P.S. Cremer, J. Am. Chem. Soc. 127 (2005) 14505-14510.

[87] M.M. Bloksma, D.J. Bakker, C. Weber, R. Hoogenboom, U.S. Schubert, Macromol. Rapid. Commun. 31 (2010) 724-728.

[88] F. Eeckman, A.J. Moës, K. Amighi, J Control Release 88 (2003) 105-116.

[89] F. Eeckman, K. Amighi, A.J. Moës, Int. J. Pharm. 222 (2001) 259-270.

[90] R.O.R. Costa, R.F.S. Freitas, Polymer 43 (2002) 5879-5885.

[91] H.G. Schild, M. Muthukumar, D.A. Tirrell, Macromolecules 24 (1991) 948-952.

[92] I. Bischofberger, D.C.E. Calzolari, V. Trappe, Soft Matter 10 (2014) 8288-8295.

[93] K. Bauri, S.G. Roy, S. Arora, R.K. Dey, A. Goswami, G. Madras, P. De, J. Therm. Anal. Calorim. 111 (2013) 753-761.

[94] Z. Shen, K. Terao, Y. Maki, T. Dobashi, G. Ma, T. Yamamoto, Colloid Polym Sci 284 (2006) 1001-1007.

[95] I.C. Barker, J.M.G Cowie, T.N. Huckerby, D.A. Shaw, I. Soutar, L. Swanson, Macromolecules 36 (2003) 7765-7770.

[96] F. Eeckman, A.J. Moës, K. Amighi, Eur. Polym. J. 40 (2004) 873-881.

[97] T. Maeda, K. Yamamoto, T. Aoyagi, J Colloid Interface Sci 302 (2006) 467-474.

[98] Y. Kotsuchibashi, Y. Kuboshima, K. Yamamoto, T. Aoyagi, J Polym Sci A Polym Chem 46 (2008) 6142-6150.

[99] S.-T. Lin, K. Fuchise, Y. Chen, R. Sakai, T. Satoh, T. Kakuchi, W.-C. Chen, Soft Matter 5(2009) 3761-3770.

[100] J.E. Chung, M. Yokoyama, T. Aoyagi, Y. Sakurai, T. Okano, J Control Release 53 (1998) 119-130.

[101] S. Sistach, M. Beija, V. Rahal, A. Brûlet, J.-D. Marty, M. Destarac, C. Mingotaud, Chem. Mater. 22 (2010) 3712-3724.

[102] M.V. Deshmukh, A.A. Vaiya, M.G. Kulkarni, P.R. Rajamohanan, S. Ganapathy, Polymer 41 (2000) 7951-7960.

[103] C. Choi, S.Y. Chae, J.-W. Nah, Polymer 47 (2006) 4571-4580.

[104] A. Kermagoret, C.-A. Fustin, M. Bourguignon, C. Detrembleur, C. Jérôme, A. Debuigne, Polym. Chem. 4 (2013) 2575-2583.

[105] X. Zhao, O. Coutelier, H.H. Nguyen, C. Delmas, M. Destarac, J.-D. Marty, Polym. Chem. 6 (2015) 5233-5243.

[106] A. Kermagoret, K. Mathieu, J.-M. Thomassin, C.-A. Fustin, R. Duchêne, C. Jérôme, C. Detrembleur, A. Debuigne, Polym. Chem. 5 (2014) 6534-6544.

[107] X. Liang, V. Kozlovskaya, C.P. Cox, Y. Wang, M. Saeed, E. Kharlampieva, J Polym Sci A Polym Chem 52 (2014) 2725-2737.

[108] M. Hurtgen, J. Liu, A. Debuigne, C. Jerome, C. Detrembleur, J Polym Sci A Polym Chem 50 (2012) 400-408.

[109] N. Zhang, S. Salzinger, B. Rieger, Macromolecules 45 (2012) 9751-9758.

[110] Q. Cui, Y. Wang, F. Wu, E. Wang, Polymer 54 (2013) 4521-4527.

[111] W. Wang, H. Liang, R.C.A. Ghanami, L. Hamilton, M. Fraylich, K.M. Shakesheff, B. Saunders, C. Alexander, Adv. Mater. 21 (2009) 1809-1813.

[112] J.E. Chung, M. Yokoyama, K. Suzuki, T. Aoyagi, Y. Sakurai, T. Okano, Colloids Surf. B 9 (1997) 37-48.

[113] M.L. Ohnsorg, J.M. Ting, S.D. Jones, S. Jung, F.S. Bates, T.M. Reineke, Polym. Chem. 10 (2019) 3469-3479.

[114] J. Ye, J. Xu, J. Hu, X. Wang, G. Zhang, S. Liu, C. Wu, Macromolecules 41 (2008) 4416-4422.

[115] J. Xu, J. Ye, S. Liu, Macromolecules 40 (2007) 9103-9110.

[116] S. Kikuchi, Y. Chen, E. Ichinohe, K. Kitano, S.-I. Sato, Q. Duan, X. Shen, T. Kakuchi, Macromolecules 49 (2016) 4828-4838.

[117] Y. Yang, G. Tang, M. Hu, L. Shao, J. Li, Y. Bi, Polymer 68 (2015) 213-220.

[118] S. Honda, T. Yamamoto, Y. Tezuka, J. Am. Chem. Soc. 132 (2010) 10251-10253.

[119] X. An, Q. Tang, W. Zhu, K. Zhang, Y. Zhao, Macromol. Rapid. Commun. 37 (2016) 980-986.

[120] Y. Jung, J.-H. Kim, W.-D. Jang, Eur. Polym. J. 88 (2017) 605-612.

[121] H. Zhang, W. Wu, X. Zhao, Y. Zhao, Macromolecules 50 (2017) 3411-3423.

[122] Y. Jiang, T. Zhang, Z. Yi, Y. Han, X. Su, Y. Feng, Polymers 12 (2020) 984.

[123] X.-P. Qiu, F. Tanaka, F.M. Winnik, Macromolecules 40 (2007) 7069-7071.

[124] J. Li, S. Kikuchi, S.-I. Sato, Y. Chen, L. Xu, B. Song, Q. Duan, Y. Wang, T. Kakuchi, X. Shen, Macromolecules 52 (2019) 7207-7217.

[125] M. Cao, G. Han, W. Duan, W. Zhang, Polym. Chem. 9 (2018) 2625-2633.

[126] J. Xu, S. Liu, J Polym Sci A Polym Chem 47 (2009) 404-419.

[127] F.A. Plamper, M.Ruppel, A. Schmalz, O. Borisov, M. Ballauff, A.H.E. Müller, Macromolecules 40 (2007) 8361-8366.

[128] K.-I. Seno, I. Tsujimoto, T. Kikuchi, S. Kanaoka, S. Aoshima, J Polym Sci A Polym Chem 46 (2008) 6151-6164.

[129] S. Okabe, K.-I. Seno, S. Kanaoka, S. Aoshima, M. Shibayama, Macromolecules 39 (2006) 1592-1597.

[130] Y. Ogura, T. Terashima, M. Sawamoto, Macromolecules 50 (2017) 822-831.

[131] X. Xiang, X. Ding, N. Chen, B. Zhang, P.A. Heiden, J Polym Sci A Polym Chem 53 (2015) 2838-2848.

[132] N. Chen, X. Xiang, A. Tiwari, P.A. Heiden, J Colloid Interface Sci 391 (2013) 60-69.

[133] M.A. Ward, T.K. Georgiou, J Polym Sci A Polym Chem 48 (2010) 775-783.

[134] A.I. Triftaridou, M. Vamvakaki, C.S. Patrickios, Polymer 43 (2002) 2921-2926.

[135] M.S. Kyriacou, S.C. Hadjiyannakou, M. Vamvakaki, C.S. Patrickios, Macromolecules 37 (2004) 7181-7187.

[136] S.-H. Jung, H.-Y. Song, Y. Lee, H.M. Jeong, H.-I. Lee, Macromolecules 44 (2011) 1628-1634.

[137] D. Han, X. Tong, O. Boissière, Y. Zhao, ACS Macro Lett. 1 (2012) 57-61.

[138] D. Han, O. Boissiere, S. Kumar, X. Tong, L. Tremblay, Y. Zhao, Macromolecules 45 (2012) 7440-7445.

[139] Y. Cao, N. Zhao, K. Wu, X. X. Zhu, Langmuir 25 (2009) 1699-1704.

[140] J. Weiss, C. Böttcher, A. Laschewsky, Soft Matter 7 (2011) 483-492.

[141] C. Pietsch, U. Mansfeld, C. Guerrero-Sanchez, S. Hoeppener, A. Vollrath, M. Wagner, R. Hoogenboom, S. Saubern, S.H. Thang, C.R. Becer, J. Chiefari, U.S. Schubert, Macromolecules 45 (2012) 9292-9302.

[142] Y.-G. Jia, X.X. Zhu, Polym. Chem. 5 (2014) 4358-4364.

[143] Y. Su, Q. Li, S. Li, M. Dan, F. Huo, W. Zhang, Polymer 55 (2014) 1955-1963.

[144] S. Eggers, T. Eckert, V. Abetz, J Polym Sci A Polym Chem 56 (2018) 399-411.

[145] Y. Kotsuchibashi, M. Ebara, K. Yamamoto, T. Aoyagi, J Polym Sci A Polym Chem 48 (2010) 4393-4399.

[146] M.T. Savoji, S. Strandman, X.X. Zhu, Macromolecules 45 (2012) 2001-2006.

[147] X. Liang, F. Liu, V. Kozlovskaya, Z. Palchak, E. Kharlampieva, ACS Macro Lett. 4 (2015) 308-311.

[148] Q. Li, F. Huo, Y. Cui, C. Gao, S. Li, W. Zhang, J Polym Sci A Polym Chem 52 (2014) 2266-2278.

[149] Q. Li, C. Gao, S. Li, F. Huo, W. Zhang, Polym. Chem. 5 (2014) 2961-2972.

[150] S. Sugihara, K. Iwata, S. Miura, A.H. Ma'Radzi, Y. Maeda, Polymer 54 (2013) 1043-1052.

[151] Z. Ye, Y. Li, Z. An, P. Wu, Langmuir 32 (2016) 6691-6700.

[152] H. Wei, S. Perrier, S. Dehn, R. Ravarian, F. Dehghani, Soft Matter 8 (2012) 9526-9528.

[153] L. Hou, P. Wu, Soft Matter 10 (2014) 3578-3586.

[154] L. Hou, P. Wu, Soft Matter 11 (2015) 2771-2781.

[155] K. Skrabania, J. Kristen, A. Laschewsky, Ö. Akdemir, A. Hoth, J.-F. Lutz, Langmuir 23 (2007) 84-93.

[156] H. Mori, I. Kato, S. Saito, T. Endo, Macromolecules 43 (2010) 1289-1298.

[157] Y. Zhang, S. Chen, M. Pang, W. Zhang, Polym. Chem. 7 (2016) 6880-6884.

[158] Y. Zhu, R. Batchelor, A.B. Lowe, P.J. Roth, Macromolecules 49 (2016) 672-680.

[159] H. Zhang, J. Zhang, W. Dai, Y. Zhao, Polym. Chem. 8 (2017) 5749-5760.

[160] F. Käfer, F. Liu, U. Stahlschmidt, V. Jérôme, R. Freitag, M. Karg, S. Agarwal, Langmuir 31 (2015) 8940-8946.

[161] H.H. Nguyen, M. El Ezzi, C. Mingotaud, M. Destarac, J.-D. Marty, N. Lauth-de Viguerie, Soft Matter 12 (2016) 3246-3251.

[162] H. Sun, X. Chen, X. Han, H. Liu, Langmuir 33 (2017) 2646-2654.

[163] M. Arotçaréna, B.Heise, S. Ishaya, A. Laschewsky, J. Am. Chem. Soc. 124 (2002) 3787-3793.

[164] N.S. Vishnevetskaya, V. Hildebrand, B.-J. Niebuur, I. Grillo, S.K. Filippov, A. Laschewsky, P. Müller-Buschbaum, C.M. Papadakis, Macromolecules 49 (2016) 6655-6668.

[165] H. Zhang, X. Tong, Y. Zhao, Langmuir 30 (2014) 11433-11441.

[166] J. Xu, V. Abetz, Macromol. Rapid. Commun. 42 (2021) 2000648.

[167] H.-Y. Tian, J.-J. Yan, D. Wang, C. Gu, Y.-Z. You, X.-S. Chen, Macromol. Rapid. Commun. 32 (2011) 660-664.

[168] L. Mäkinen, D. Varadharajan, H. Tenhu, S. Hietala, Macromolecules 49 (2016) 986-993.

[169] F. Dai, P. Wang, Y. Wang, L. Tang, J. Yang, W. Liu, H. Li, G. Wang, Polymer 49 (2008) 5322-5328.

[170] C. Zhou, Y. Chen, M. Huang, Y. Ling, L. Yang, G. Zhao, J. Chen, New J. Chem. 45. (2021) 5925-5932.

[171] A. Blanazs, S.P. Armes, A.J. Ryan, Macromol. Rapid. Commun. 30 (2009) 267-277.

[172] D. Aravopoulou, K. Kyriakos, A. Miasnikova, A. Laschewsky, C.M. Papadakis, A. Kyritsis, J. Phys. Chem. B 122 (2018) 2655-2668.

[173] J. Adelsberger, A. Meier-Koll, A.M. Bivigou-Koumba, P. Busch, O. Holderer, T. Hellweg, A. Laschewsky, P. Müller-Buschbaum, C.M. Papadakis, Colloid Polym Sci 289 (2011) 711-720.

[174] H. Wei, X.-Z. Zhang, Y. Zhou, S.-X. Cheng, R.-X. Zhuo, Biomaterials 27 (2006) 2028-2034.

[175] C.-H. Ko, C. Henschel, G.P. Meledam, M.A. Schroer, P. Müller-Buschbaum, A. Laschewsky, C.M. Papadakis, Macromolecules 54 (2021) 384-397.

[176] F. Kohori, K. Sakai, T. Aoyagi, M. Yokoyama, Y. Sakurai, T. Okano, J. Controlled Release 55 (1998) 87-98.

[177] A. Papagiannopoulos, J. Zhao, G. Zhang, S. Pispas, A. Radulescu, Polymer 54 (2013) 6373-6380.

[178] S. Qin, Y. Geng, D.E. Discher, S. Yang, Adv. Mater. 18 (2006) 2905-2909.

[179] W. Zhang, L. Shi, K. Wu, Y. An, Macromolecules 38 (2005) 5743-5747.

[180] P. Pramanik, S. Ghosh, J Polym Sci A Polym Chem 53 (2015) 2444-2451.

[181] S.-I. Yusa, S. Yamago, M. Sugahara, S. Morikawa, T. Yamamoto, Y. Morishima, Macromolecules 40 (2007) 5907-5915.

[182] Z. Ge, D. Xie, D. Chen, X. Jiang, Y. Zhang, H. Liu, S. Liu, Macromolecules 40 (2007) 3538-3546.

[183] H. Arslan, O. Zirtil, V. Bütün, Eur. Polym. J. 49 (2013) 4118-4129.

[184] K. Skrabania, W. Li, A. Laschewsky, Macromol. Chem. Phys. 209 (2008) 1389-1403.

[185] Y. Zhou, K. Jiang, Q. Song, S. Liu, Langmuir 23 (2007) 13076-13084.

[186] A.J. de Graaf, K.W. Boere, J. Kemmink, R.G. Fokkink, C.F. van Nostrum, D.T.S. Rijkers, J. van der Gucht, H. Wienk, M. Baldus, E. Mastrobattista, T. Vermonden, W.E. Hennink, Langmuir 27 (2011) 9843-9848.

[187] B. Verdonck, J.-F. Gohy, E. Khousakoun, R. Jérôme, F. Du Prez, Polymer 46 (2005) 9899-9907.

[188] M. Nuopponen, K. Kalliomäki, V. Aseyev, H. Tenhu, Macromolecules 41 (2008) 4881-4886.

[189] A. Papagiannopoulos, J. Zhao, G. Zhang, S. Pispas, A. Radulescu, Eur. Polym. J. 56 (2014) 59-68.

[190] J. Adelsberger, A.Kulkarni,A. Jain, W. Wang, A.M. Bivigou-Koumba, P. Busch, V. Pipich, O. Holderer, T. Hellweg, A. Laschewsky, P. Müller-Buschbaum, C.M. Papadakis, Macromolecules 43 (2010) 2490-2501.

[191] P. Sun, Y. Zhang, L. Shi, Z. Gan, Macromol. Biosci. 10 (2010) 621-631.

[192] Y. Qu, F. Huo, Q. Li, X. He, S. Li, W. Zhang, Polym. Chem. 5 (2014) 5569-5577.

[193] C. Zhou, M.A. Hillmyer, T.P. Lodge, Macromolecules 44 (2011) 1635-1641.

[194] J. Chen, M. Liu, H. Gong, Y. Huang, C. Chen, J. Phys. Chem. B 115 (2011) 14947-14955.

[195] A. Sundararaman, T. Stephan, R.B. Grubbs, J. Am. Chem. Soc. 130 (2008) 12264-12265.

[196] W. Zhang, X. Jiang, Z. He, D. Xiong, P. Zheng, Y. An, L. Shi, Polymer 47 (2006) 8203-8209.

[197] L. Yu, G. Chang, H. Zhang, J. Ding, J Polym Sci A Polym Chem 45 (2007) 1122-1133.

[198] R. Motokawa, K. Morishita, S. Koizumi, T. Nakahira, M. Annaka, Macromolecules 38 (2005) 5748-5760.

[199] B. Li, M.E. Thompson, Phys. Chem. Chem. Phys. 20 (2018) 13623-13631.

[200] M.A. Ward, T.K. Georgiou, Polym. Chem. 4 (2013) 1893-1902.

[201] S. Barbosa, M.A. Cheema, P. Taboada, V. Mosquera, J. Phys. Chem. B 111 (2007) 10920-10928.

[202] J. Weiss, A. Laschewsky, Macromolecules 45 (2012) 4158-4165.

[203] T. Swift, L. Swanson, M. Geoghegan, S. Rimmer, Soft Matter 12 (2016) 2542-2549.

[204] A. Katchalsky, N. Shavit, H. Eisenberg, J Polym Sci, 13 (1954) 69-84.

[205] S. Liu, S.P. Armes, Langmuir 19 (2003) 4432-4438.

[206] J. Shen, S. Shahid, A. Sarihan, D.A. Patterson, E.A.C. Emanuelsson, Sep. Purif. Technol. 204 (2018) 336-344.

[207] B.L. Rivas, E. Pereira, P. Gallegos, D. Homper, K.E. Geckeler, J Appl Polym Sci 92 (2004) 2917-2922.

[208] P. van de Wetering, E.E. Moret, N.M.E. Schuurmans-Nieuwenbroek, M.J. van Steenbergen, W.E. Hennink, Bioconjug. Chem. 10 (1999) 589-597.

[209] S. Mendrek, A. Mendrek, H.-J. Adler, A. Dworak, D. Kuckling, J Polym Sci A Polym Chem 47 (2009) 1782-1794.

[210] N. Tantavichet, M.D. Pritzker, C.M. Burns, J. Appl. Polym. Sci. 81 (2001) 1493-1497.

[211] F. Chécot, A. Brûlet, J. Oberdisse, Y. Gnanou, O. Mondain-Monval, S. Lecommandoux, Langmuir 21 (2005) 4308-4315.

[212] J. Babin, J. Rodriguez-Hernandez, S. Lecommandoux, H.-A. Klok, M.-F. Achard, Faraday Discuss. 128 (2005) 179-192.

[213] F. Chécot, J. Rodríguez-Hernández, Y. Gnanou, S. Lecommandoux, Biomol. Eng. 24 (2007) 81-85.

[214] N.J.W. Penfold, J.R. Lovett, N.J. Warren, P. Verstraete, J. Smets, S.P. Armes, Polym. Chem. 7 (2016) 79-88.

[215] V. Bütün, S.P. Armes, N.C. Billingham, Polymer 42 (2001) 5993-6008.

[216] V. Bütün, R.B. Top, S. Ufuklar, Macromolecules 39 (2006) 1216-1225.

[217] V. Bütün, S.P. Armes, N.C. Billingham, Z. Tuzar, A. Rankin, J. Eastoe, R.K. Heenan, Macromolecules 34 (2001) 1503-1511.

[218] V. Sfika, C. Tsitsilianis, Macromolecules 36 (2003) 4983-4988.

[219] Z. Iatridi, C. Tsitsilianis, Chem. Commun. 47 (2011) 5560-5562.

[220] G. Kocak, C. Tuncer, V. Bütün, Polym. Chem. 8 (2017) 144-176.

[221] C. Fernyhough, A.J. Ryan, G. Battaglia, Soft Matter 5 (2009) 1674-1682.

[222] L. Liu, J. Zhang, W. Lv, Y. Luo, X. Wang, J Polym Sci A Polym Chem 48 (2010) 3350-3361.

[223] J. Zhang, B. Farias-Mancilla, I. Kulai, S. Hoeppener, B. Lonetti, S. Prévost, J. Ulbrich, M. Destarac, O. Colombani, U.S. Schubert, C. Guerrero-Sanchez, S. Harrisson, Angew. Chem. Int. Ed. 60 (2021) 4925-4930.

[224] T. Thavanesan, C. Herbert, F.A. Plamper, Langmuir 30 (2014) 5609-5619.

[225] J. Huang, H. Qin, B. Wang, Q. Tan, J. Lu, Polym. Chem. 10 (2019) 6379-6384.

[226] N. González, C. Elvira, J.S. Roman, Macromolecules 38 (2005) 9298-9303.

[227] C. Luo, W. Fu, Z. Li, B. Zhao, Polymer 101 (2016) 319-327.

[228] X. Jiang, C. Feng, G. Lu, X. Huang, Polymer 64 (2015) 268-276.

[229] X. Jiang, C. Feng, G. Lu, X. Huang, ACS Macro Lett. 3 (2014) 1121-1125.

[230] C. Luo, Y. Liu, Z. Li, Macromolecules 43 (2010) 8101-8108.

[231] A.B. Lowe, M. Torres, R. Wang, J Polym Sci A Polym Chem 45 (2007) 5864-5871.

[232] Y. Tang, L. Liu, J. Wu, J. Duan, J Colloid Interface Sci 397 (2013) 24-31.

[233] Z. Ge, Y. Cai, J. Yin, Z. Zhu, J. Rao, S. Liu, Langmuir 23 (2007) 1114-1122.

[234] A.E. Smith, X. Xu, S.E. Kirkland-York, D.A. Savin, C.L. McCormick, Macromolecules 43 (2010) 1210-1217.

[235] Y. Xu, L. Shi, R. Ma, W. Zhang, Y. An, X.X. Zhu, Polymer 48 (2007) 1711-1717.

[236] S. Liu, N.C. Billingham, S.P. Armes, Angew. Chem. 113 (2001) 2390-2393.

[237] Y. Oda, S. Kanaoka, S. Aoshima, J Polym Sci A Polym Chem 48 (2010) 1207-1213.

[238] C. Feng, Y. Li, D. Yang, Y. Li, J. Hu, S. Zhai, G. Lu, X. Huang, J Polym Sci t A Polym. Chem. 48 (2010) 15-23.

[239] M. Topuzogullari, V. Bulmus, E. Dalgakiran, S. Dincer, Polymer 55 (2014) 525-534.

[240] C. Corten, K. Kretschmer, D. Kuckling, Beilstein J Org Chem 6 (2010) 756-765.

[241] D. Nagai, A. Suzuki, Y. Maki, H. Takeno, Chem. Commun. 47 (2011) 8856-8858.

[242] A. Darabi, P.G. Jessop, M.F. Cunningham, Chem. Soc. Rev. 45 (2016) 4391-4436.

[243] Q. Yan, Y. Zhao, Chem. Commun. 50 (2014) 11631-11641.

[244] B. Yan, D. Han, O. Boissière, P. Ayotte, Y. Zhao, Soft Matter 9 (2013) 2011-2016.

[245] H. Liu, Z. Guo, S. He, H. Yin, C. Fei, Y. Feng, Polym. Chem. 5 (2014) 4756-4763.

[246] Q. Yan, R. Zhou, C. Fu, H. Zhang, Y. Yin, J. Yuan, Angew. Chem. Int. Ed. 50 (2011) 4923-4927.

[247] Q. Yan, J. Wang, Y. Yin, J. Yuan, Angew. Chem. Int. Ed. 52 (2013) 5070-5073.

[248] J.Y. Quek, P.J. Roth, R.A. Evans, T.P. Davis, A.B. Lowe, J Polym Sci A Polym Chem 51 (2013) 394-404.

[249] W. Wang, H. Liu, M. Mu, H. Yin, Y. Feng, Polym. Chem. 6 (2015) 2900-2908.

[250] Q. Yan, Y. Zhao, Angew. Chem. 125 (2013) 10132-10135.

[251] H. Liu, Y. Zhao, C.A. Dreiss, Y. Feng, Soft Matter 10 (2014) 6387-6391.

[252] Q. Yan, Y. Zhao, J. Am. Chem. Soc. 135 (2013) 16300-16303.

[253] M. Zeng, M. Huo, Y. Feng, J. Yuan, Macromol. Rapid. Commun. 39 (2018) 1800291.

[254] A. Feng, C. Zhan, Q. Yan, B. Liu, J. Yuan, Chem. Commun. 50 (2014) 8958-8961.

[255] H. Zou, W. Yuan, Polym. Chem. 6 (2015) 2457-2465.

[256] W. Yuan, J. Shen, H. Zou, RSC Adv. 5 (2015) 13145-13152.

[257] B.-W. Liu, H. Zhou, S.-T. Zhou, H.-J. Zhang, A.-C. Feng, C.-M. Jian, J. Hu, W.-P. Gao, J.-Y. Yuan, Macromolecules 47 (2014) 2938-2946.

[258] S. Lin, J. Shang, P. Theato, Polym. Chem. 8 (2017) 2619-2629.

[259] J. Nicolas, Y. Guillaneuf, C. Lefay, D. Bertin, D. Gigmes, B. Charleux, Prog. Polym. Sci. 38 (2013) 63-235.

[260] K. Matyjaszewski, Macromolecules 45 (2012) 4015-4039.

[261] D.J. Keddie, G. Moad, E. Rizzardo, S.H. Thang, Macromolecules 45 (2012) 5321-5342.

[262] C. Boyer, V. Bulmus, T.P. Davis, V. Ladmiral, J. Liu, S. Perrier, Chem. Rev. 109 (2009) 5402-5436.

[263] G. Moad, Y.K. Chong, A. Postma, E. Rizzardo, S.H. Thang, Polymer 46 (2005) 8458-8468.

[264] J.R. Lovett, N.J. Warren, L.P.D. Ratcliffe, M.K. Kocik, S.P. Armes, Angew. Chem. Int. Ed. 54 (2015) 1279-1283.

[265] C. Zhang, M. Maric, J Polym Sci A Polym Chem 50 (2012) 4341-4357.

[266] F.F. Taktak, V. Bütün, Polymer 51 (2010) 3618-3626.

[267] J.V.M. Weaver, S.P. Armes, V. Bütün, Chem. Commun. 18 (2002) 2122-2123.

[268] T.J. Martin, K. Procházka, P. Munk, S.E. Webber, Macromolecules 29 (1996) 6071-6073.

[269] S. Sugihara, K. Yamashita, K. Matsuzuka, I. Ikeda, Y. Maeda, Macromolecules 45 (2012) 794-804.

[270] J.-F. Gohy, S. Antoun, R. Jérôme, Macromolecules 34 (2001) 7435-7440.

[271] J. Rodriguez-Hernandez, S. Lecommandoux, J. Am. Chem. Soc. 127 (2005) 2026-2027.

[272] M.A. Ward, T.K. Georgiou, Polymers 3 (2011) 1215-1242.

[273] N. Rapoport, Prog. Polym. Sci. 32 (2007) 962-990.

[274] F. Meng, Z. Zhong, J. Feijen, Biomacromolecules 10 (2009) 197-209.

[275] L. Zha, B. Banik, F. Alexis, Soft Matter 7 (2011) 5908-5916.

[276] M. Beija, E. Palleau, S. Sistach, X. Zhao, L. Ressier, C. Mingotaud, M. Destarac, J.-D. Marty, J. Mater. Chem. 20 (2010) 9433-9442.

[277] Z. Guo, H. Gu, W. Ma, Q. Chen, Z. He, J. Zhang, Y. Liu, L. Zheng, Y. Feng, RSC Adv. 7 (2017) 49777-49786.

[278] I. Tokareva, S. Minko, J.H. Fendler, E. Hutter, J. Am. Chem. Soc. 126 (2004) 15950-15951.

Chapter II

(*N*-vinylcaprolactam / *N*-vinylpyrrolidone) statistical copolymers - Effect of copolymer composition on the formation, stabilization, thermoresponsiveness and catalytic properties of gold nanoparticles

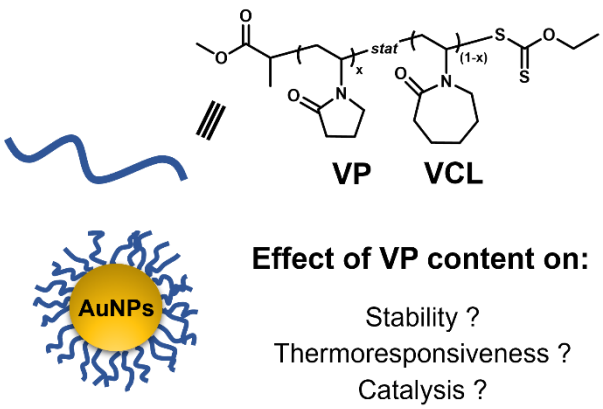

Contents

II.1 Introduction

Metal nanoparticles, [1] especially gold nanoparticles (AuNPs), have attracted much attention because of their unique electronic, optical and catalytic properties resulting in their wide applications ranging from optoelectronics to biology. [2, 3] These properties strongly depend on the particle size and shape, the nature of the protecting organic shell and the interparticle distance. [4] AuNPs are colloidally unstable and are susceptible to irreversible aggregation, but they can be stablized through the grafting or adsorption of small organic molecules such as citrates, surfactants, ligands or polymers. These organic molecules provide an additional tool to modulate physicochemical properties. To this end, polymers have proved to be ideal material of choice due to their flexibility for tailoring specific uses and also for their greater long-term stabilizing properties compared to small molecules (such as citrates). Notable examples include responsive polymers. Indeed, coating AuNPs with stimuli-responsive polymers is a convenient way to reversibly change the properties of AuNPs. Thermoresponsive (co)polymers with LCST-typed behavior have been grafted on AuNPs without losing their thermoresponsiveness. [5-9]

These obtained hybrid materials not only show a steric stability, but also have a capacity to control the NPs properties (electronic, optical and catalytic properties…) in response to a change of temperature. [10-12] Hence different families of thermoresponsive polymers like poly(*N*-isopropylacrylamide), [13-18] poly(methyl vinyl ether), [19] poly(*N*-acryloyl-*N*'-propyl piperazine) [20] and copolymers based on oligo(ethylene glycol) (meth)acrylate [21-23] or poly(*N*-vinyl caprolactam) (PVCL) [24, 25] have been used to obtain such hybrid nanoparticles. The use of this last family is of special interest for the formation of hybrids presenting a sharp reversible response to temperature. Moreover, the cloud point temperature (T_c) of PVCL and corresponding hybrid materials can be easily tuned either by adjusting polymer chain length or by changing polymer concentration. [24]

PVCL belongs to the family of poly(*N*-vinyl lactams) like poly(*N*-vinylpyrrolidone) (PVP), which is not thermoresponsive but is one of the most commonly used polymers for stabilizing NPs with different natures for diverse applications. [26] The structure of *N*-vinyl caprolactam (VCL) monomer only differs from *N*-vinylpyrrolidone (VP) by the inclusion of two additional methylene groups. Reversible addition-fragmentation chain transfer (RAFT) polymerization has recently made it possible to synthesize copolymers of VCL and VP with variable architectures and tunable thermoresponsive properties. [25, 27-29] Detrembleur and coworkers synthesized PVCL-*b*-P(VCL-*stat*-VP)-*b*-PVCL with adjustable hydration/dehydration

properties by cobalt-mediated radical polymerization followed by a radical coupling reaction, and then studied their solution behaviors. [28, 29] Hoogenboom et al. used RAFT-derived P(VCL-*stat*-VP) to stabilize preformed AuNPs surrounded by citrate via a "grafting to" approach. The polymer coating AuNPs showed a larger hydrodynamic size in comparison to pristine citrate@AuNPs. In presence of 0.1 M NaCl, a color change depending on the copolymer composition and T_c value of the polymer were observed. [25]

The objective of this chapter is to study the influence of composition of narrowly dispersed P(VCL-*stat*-VP)$_{20k}$ copolymers with controlled molecular weight for the formation, stabilization and modulation of the properties of AuNPs. For this purpose, a series of VCL/VP statistical copolymers containing variable amounts of VP (molar content changes from 0 to 100%) was synthesized by RAFT/MADIX polymerization (MADIX standing for macromolecular design by interchange of xanthates). Then two methods (*in situ* formation and coating of preformed AuNPs) were used to prepare nanohybrids, whose stabilization, thermoresponsiveness and catalytic properties were investigated by transmission electronic microscopy (TEM) and UV-visible spectroscopy.

II.2 Synthesis and characterization of copolymers

The synthesis of homopolymers and copolymers of VCL and VP used in this chapter was previously performed by X. Zhao in IMRCP lab. [27] It concerns a series of P(VCL-*stat*-VP)$_{20k}$ copolymers with predetermined molecular weight (20000 g·mol^{-1}) and various compositions, which were synthesized by RAFT/MADIX polymerization (**Scheme II.1**) using adequate reactivity of xanthates towards *N*-vinyl monomers. These synthesized (co)polymers were characterized by nuclear magnetic resonance (NMR) spectroscopy, size exclusion chromatography (SEC) and differential scanning calorimetry (DSC), the main characteristics are summarized in **Table II.1**.

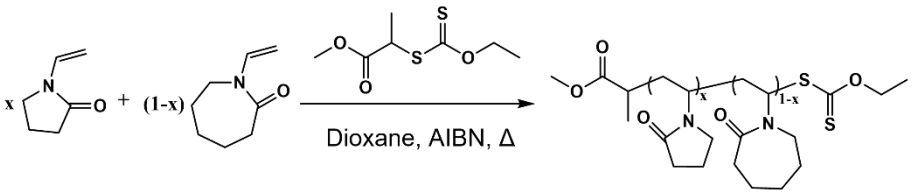

Scheme II.1 Synthesis of P(VCL-*stat*-VP)$_{20k}$ by RAFT/MADIX polymerization (synthesis was done by X. Zhao in IMRCP, Toulouse, France).

Taking ^{1}H NMR spectrum of purified P(VCL$_{75}$-*stat*-VP$_{25}$) as an example (**Figure II.1A**), its composition can be calculated by integration area ratio of broad signal at 4 - 4.4 ppm corresponding to the methine proton in VCL units and signal at 2.8 - 3.5 ppm corresponding to

-CH_2 group in both units. Molecular weights of all P(VCL-*stat*-VP)$_{20k}$ were analyzed by SEC analysis. Copolymers containing less than 50% of VP could be eluted in THF (**Table II.1**, Entry 1-3) while the whole range of composition could be eluted in DMF (containing LiBr). **Figure II.1B** represents the superposition of SEC traces in DMF for copolymers with targeted molecular weight of 20000 g·mol^{-1}. Thanks to the MALS detector, we could not only access the accurate values of molecular weights but also follow the evolution of molecular weights within the chromatogram. Therefore, we can conclude that the difference of elution time observed should be attributed to an important variation of hydrodynamic volume when changing VCL/VP ratio. MALS detector enables to determine molecular weights, which are given in **Table II.1**.

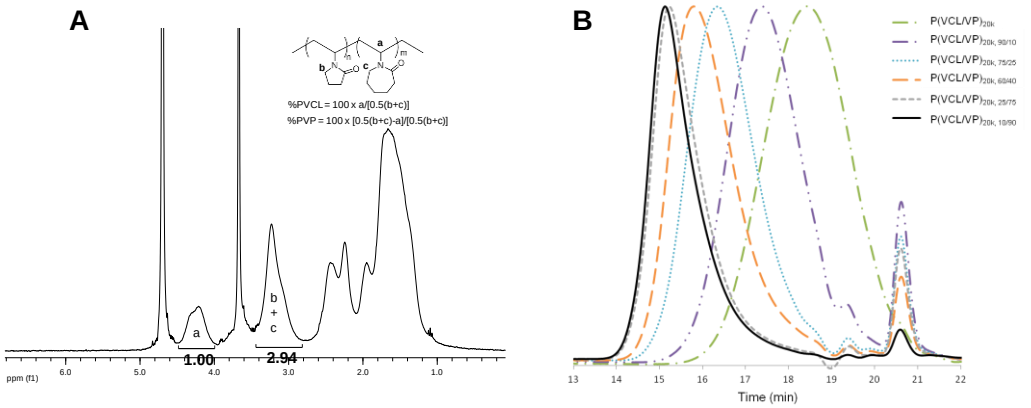

Figure II.1 (A) ^{1}H NMR spectrum of P(VCL$_{75}$-*stat*-VP$_{25}$) in D_2O and (B) SEC traces for P(VCL-*stat*-VP)$_{20k}$ with different compositions in DMF (containing LiBr) with a flow rate of 1 mL·min^{-1} (^{1}H NMR and SEC analyses were performed by X. Zhao in IMRCP, Toulouse, France).

Table II.1 Copolymer composition and main characteristics of the synthesized (co)polymers.

Entry	Theoretical copolymer structure	Composition		M_n (g·mol^{-1}) THF(DMF)	Dispersity (Đ) THF(DMF)	DSC (solution 2%)	
		VCL/VP weight ratio[a]	VCL/VP molar ratio[a]			T_c (°C)[b]	ΔH (J·g^{-1} of VCL)[c]
1	PVCL	100/00	100/00	14350	1.09	36.7	-30
2	P(VCL$_{75}$-*stat*-VP$_{25}$)	75/25	70/30	16000 (13850)	1.04 (1.12)	50.8	-8
3	P(VCL$_{60}$-*stat*-VP$_{40}$)	63/37	58/42	17000 (18500)	1.04 (1.19)	62.0	-3
4	P(VCL$_{50}$-*stat*-VP$_{50}$)	51/49	45/55	(18400)	(1.07)	/[d]	/[d]
5	P(VCL$_{25}$-*stat*-VP$_{75}$)	26/74	22/78	(19000)	(1.13)	/[d]	/[d]
6	P(VCL$_{10}$-*stat*-VP$_{90}$)	10/90	8/92	(23200)	(1.12)	/[d]	/[d]
7	PVP	0/100	0/100	(22000)		/[d]	/[d]

[a]Determined by ^{1}H NMR spectra. [b]Evaluated by extrapolation to 0 °C·min^{-1} of the maximum of observed peak upon heating processes with different heating rates, standard deviation on T_c = ± 0.2 J·g^{-1}. [c]Obtained with a heating

rate of 2.5 °C·min^{-1}, standard deviation on ΔH = ± 2 J·g^{-1}. [d]No transition detectable. (^{1}H NMR and DSC measurements were done by X. Zhao in IMRCP, Toulouse, France)

The cloud point temperature increases non-linearly from 36.7 to 50.8 and 62.0 °C for P(VCL-*stat*-VP)$_{20k}$ with VP content changing from 0 to 25 and 40% respectively (Entry 1-3 in **Table II.1**), which results from the introduction of the hydrophilic VP units. No transition occurs as VP content is higher than 40%. Further insight on the effect of VP introduction within PVCL chain is obtained through the measurement of associated variation of enthalpy (ΔH) normalized with respect to VCL content. When VP fraction in copolymer increases, a strong decrease of ΔH is measured (**Table II.1**). This variation is clearly not proportional to VCL content, which is ascribed to a mechanism of dehydration involving the whole macromolecule structure, and not short sequences of VCL units. Indeed, insertion of VP units within the PVCL backbone strongly impedes dehydration phenomenon by preventing release of water molecules from the polymer chains and therefore the formation of hydrophobic regions is responsible for the aggregation process and the formation of mesoglobules. [27] Consequently, only copolymers with low VP content (below 40%) present thermoresponsive behaviors in solution.

II.3 Formation of nanohybrids

To study the stabilization, thermoresponsiveness and catalytic properties of hybrid nanoparticles, two methods shown in **Scheme II.2** were used to obtain nanohybrids: (1) *in situ* formation and (2) coating of preformed AuNPs.

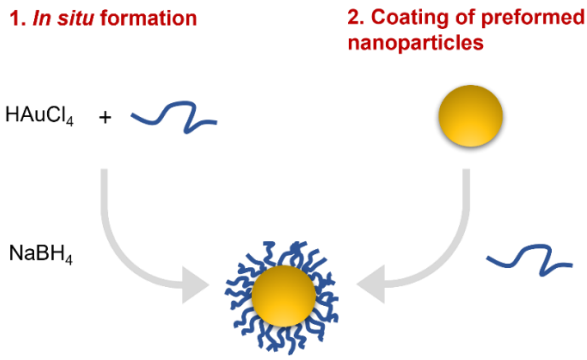

Scheme II.2 Two synthetic pathways used for formation of nanohybrids (*in situ* formation and coating of preformed nanoparticles).

II.3.1 *In situ* formation

The first evidence of the interaction of different polymers with AuNPs is given by performing *in-situ* growth of AuNPs. Whereas PVP-based polymers can act as both reducing agent and stabilizer, their use as reductants lead to the formation of large particles with broad

size distribution poorly adapted to catalytic applications. [30] Therefore, sodium borohydride ($NaBH_4$) is used here as a reducing agent to have fast access to AuNPs with better control of particle size and dispersity. For this, a $NaBH_4$ solution was added to a mixture of gold salt and P(VCL-*stat*-VP)$_{20k}$ at different (co)polymer concentrations (0.001, 0.01, 0.1 and 0.5 wt.%), the formation of AuNPs was detected by TEM and UV-vis measurements. Different colors of the colloidal solutions are observed in **Figure II.2**, which indicating that polymer concentration drastically modifies the particles growth. At the lowest polymer concentration (0.001 wt.%), a sharp surface plasmon band (SPB) is visible for all nanohybrids (blue curve in **Figure II.3**).

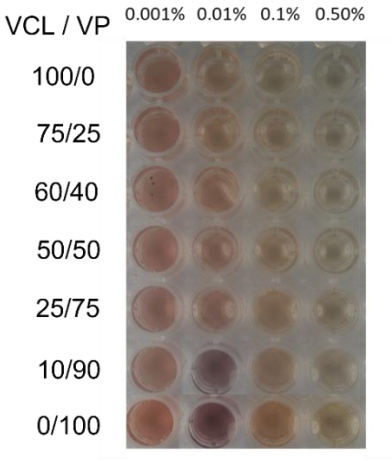

Figure II.2 Effect of (co)polymer concentration and (co)polymer composition on *in-situ* formation of nanohybrids. The formation of AuNPs was induced by the addition of $NaBH_4$ in $NaAuCl_4{\cdot}2H_2O$ in presence of P(VCL-*stat*-VP)$_{20k}$ at different concentrations ($[NaBH_4] = [Au]_{final} = 5\times10^{-4}$ mol·L^{-1}. Photos of colloidal solutions were taken by H.H. Nguyen in IMRCP, Toulouse, France).

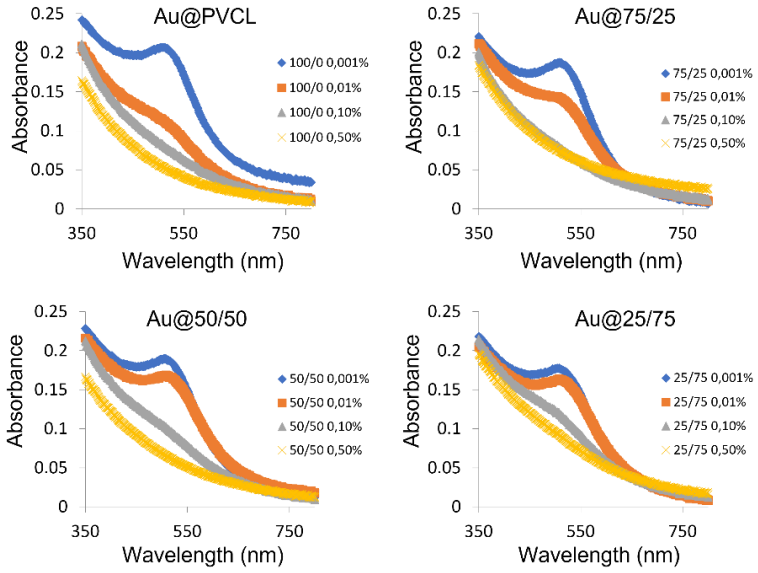

Figure II.3. UV-vis spectra of nanohybrids at different (co)polymer compositions and (co)polymer concentrations detected five days after *in-situ* formation ($[Au]_{final} = 5\times10^{-4}$ mol·L^{-1}, [P(VCL-*stat*-VP)$_{20k}$] = 0.001, 0.01, 0.1 and 0.5 wt.%. UV-vis spectra were performed by H.H. Nguyen in IMRCP, Toulouse, France).

TEM analysis evidenced the formation of AuNPs with an average size smaller than 4 nm close to that of AuNPs obtained in the absence of polymers (5 ± 2 nm). Increasing P(VCL-*stat*-VP)$_{20k}$ concentration leads to a progressive decrease of intensity of the plasmon band whatever the nature of polymer (**Figure II.3**). This decrease results from the formation of smaller NPs as demonstrated by TEM measurements. The difference in size as a function of P(VCL-*stat*-VP)$_{20k}$ concentration confirms that the presence of (co)polymer plays an important role in the control of NPs growth by interacting with the gold nuclei/gold precursor at early stage of NPs growth, which is favored on the one hand by the interactions of the thioester groups present at the end of (co)polymer chains [18] and on the other hand by the interactions of (co)polymer chain with the surface of AuNPs. The latter interaction occurs from carbonyl group and nitrogen atom within the lactam ring as demonstrated in PVP-based (co)polymers by combination of X-ray photoelectron spectroscopy, Fourier-transform infrared spectroscopy and Raman spectroscopy. [30]

The effect of P(VCL-*stat*-VP)$_{20k}$ composition at a given polymer concentration is then considered. As illustrated in **Figure II.4A**, an increase of the intensity of measured plasmon band with an increase of VP fraction in copolymer is observed. TEM analysis (**Figures II.4B** and **II.4C**) confirms that the observed trend is related to a progressive increase of average size of formed Au@P(VCL-*stat*-VP)$_{20k}$ from 1.5 to 3.2 nm when VP content increases from 0 to 100%. The different copolymers have the same end groups, thus the difference observed can only be attributed to a difference in composition: a higher VCL content leading to a better control of NPs growth. In comparison with VP, VCL presents two additional methylene group per monomer in the lactam ring. The increased hydrophobicity of VCL (i.e. a lower hydration level in solution) thus favors the interaction with surface of AuNPs and blocks the growth of particles at early stage. TGA measurement on purified AuNPs enables to evaluate roughly a polymer content of 20 wt.% corresponding to density coverage of 0.3 polymer per nm^2 in agreement with previous published from literature. [30]

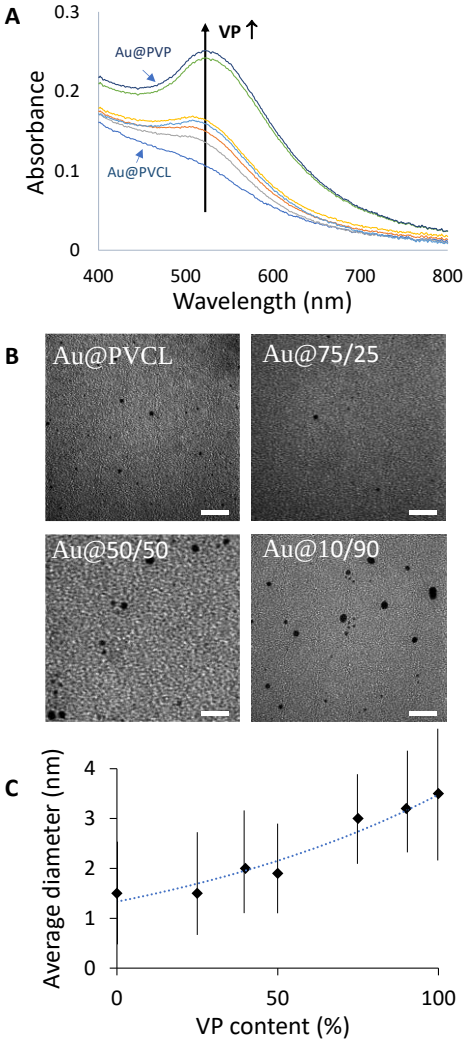

Figure II.4 (A) UV-vis spectra of nanohybrids detected five days after *in-situ* formation ($[Au]_{final}$ = 5×10^{-4} mol·L^{-1}, [P(VCL-*stat*-VP)$_{20k}$] = 0.01 wt.%, VP contents are 0, 25, 40, 50, 75, 90 and 100%), (B) TEM images for Au@PVCL, Au@P(VCL$_{75}$-*stat*-VP$_{25}$), Au@P(VCL$_{50}$-*stat*-VP$_{50}$) and Au@P(VCL$_{10}$-*stat*-VP$_{90}$) and (C) Evolution of average size as a function of VP content (the line is only a guide for the eyes). (UV-vis spectra and TEM analyses were performed by H.H. Nguyen in IMRCP, Toulouse, France)

II.3.2 Coating of preformed AuNPs

Sole evaluation of the effect of copolymer composition on the different properties of AuNPs (stabilization, catalysis and optical properties...) is of interest, a second series of nanohybrids was prepared by coating preformed AuNPs with a chosen amount of P(VCL-*stat*-VP)$_{20k}$ (**Scheme II.2**). Pristine AuNPs were synthesized by reduction of $NaAuCl_4{\cdot}2H_2O$ by using $NaBH_4$. [13, 31] Whereas no additional stabilizing agent was added, experimental conditions including pH (around 8.0) and gold precursor concentration (2.5×10^{-4} mol·L^{-1}) were carefully adjusted to yield AuNPs with good colloidal stability and controlled size (5 ± 2 nm). These NPs were then coated by different copolymer families presented in **Table II.1**. As stated above, interactions with preformed AuNPs come from both lactam ring and thioester group.

[18, 30] Four different (co)polymer concentrations were used for each (co)polymer (final concentration equals to 10^{-4}, 10^{-3}, 5×10^{-3} and 10^{-2} wt.%). As illustrated in **Figure II.5**, all solutions remain stable in absence of NaOH or NaCl after coating AuNPs with P(VCL-*stat*-VP)$_{20k}$ (columns A_1, B_1, C_1 and D_1).

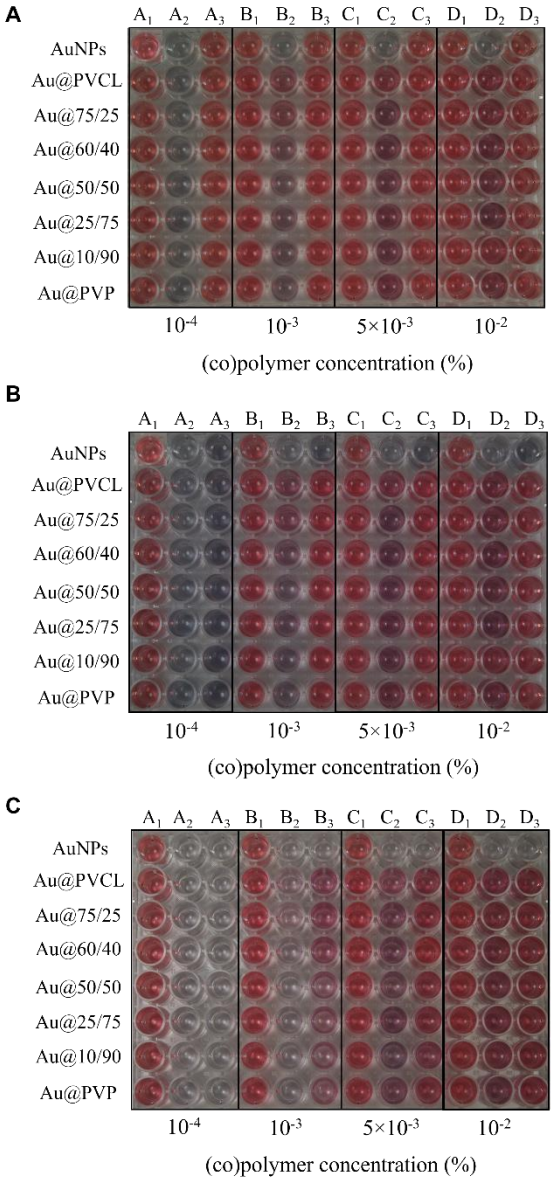

Figure II.5 Colloidal stability of aqueous solutions of Au@P(VCL-*stat*-VP)$_{20k}$ observed at four different (co)polymer concentrations and different (co)polymer compositions (A) immediately (B) after 2 hours and (C) after 2 weeks after addition of NaOH (A_2, B_2, C_2, D_2, pH_{final} = 10) and after addition of NaCl (A_3, B_3, C_3, D_3, $[NaCl]_{final}$ = 1 mol·L^{-1}) compared to a control (A_1, B_1, C_1, D_1). (A_n: 10^{-4} wt.%, B_n: 10^{-3} wt.%, C_n: 5×10^{-3} wt.%, D_n: 10^{-2} wt.%, $[Au]_{final}$ = 2.5×10^{-4} mol·L^{-1})

Moreover, the average hydrodynamic diameters of Au@P(VCL-*stat*-VP)$_{20k}$ measured by DLS measurements are around 9 ± 2 nm (see **Figure II.6**), which is larger than that of bare AuNPs (5 ± 2 nm) and corresponds to colloidal solutions made of AuNPs surrounded by a polymer corona preventing aggregation through steric hindrance. Additionally, the evolutions

of absorption spectra of bare AuNPs and Au@P(VCL-*stat*-VP)$_{20k}$ solution with a copolymer concentration of 0.001 wt.% were monitored after two hours and after two weeks as shown in **Figure II.7 (**column B_1**)**, the surface plasmon resonance band reveals a slight red shift (2 nm) after coating AuNPs due to a decrease in local polarity. These nanohybrids obtained from preformed AuNPs were further studied to evaluate the effect of copolymer composition on their colloidal stability, thermoresponsiveness and catalytic activity.

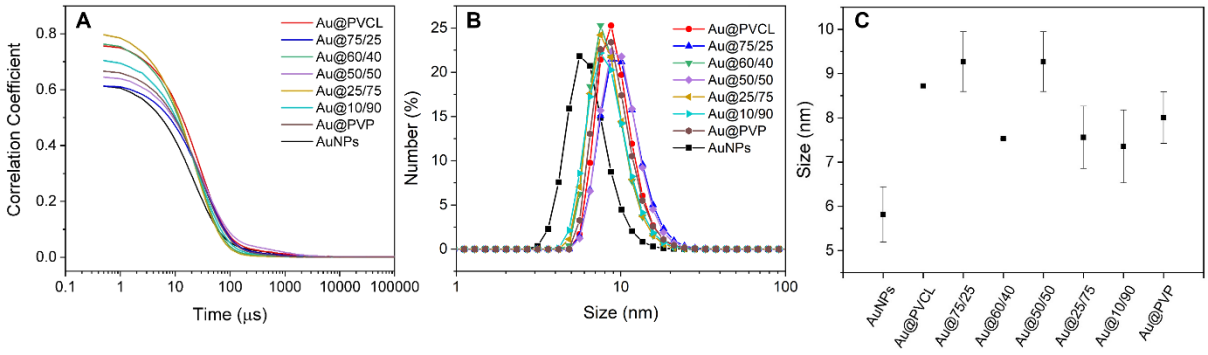

Figure II.6 (A) Correlograms, (B) size distribution (number-averaged) and (C) corresponding averaged hydrodynamic diameter of AuNPs coated by P(VCL-*stat*-VP)$_{20k}$ copolymers at 25 °C (column B_1 in **Figure II.5**, $[Au]_{final} = 2.5\times10^{-4}$ mol·L^{-1}, [(co)polymer] = 10^{-3} wt.%).

(i) Colloidal stability

The effect of copolymer composition on the colloidal stabilization of particles solution subjected to an increase in pH or ionic strength was then evaluated after addition of NaOH (columns A_2, B_2, C_2, D_2) or NaCl solution (columns A_3, B_3, C_3, D_3) as shown in **Figures II.5** and **II.7**. In this experiment, a progressive change of color relates to the modification of plasmon band of the particles due to the fact that aggregation or sedimentation phenomena reflects a low colloidal stability. After addition of NaOH, at copolymer concentration of 10^{-4} wt.%, the system is not stable and the nanoparticles aggregate to form larger aggregates cluster (column A_2 in **Figure II.5**). As copolymer concentration raises to 10^{-3} wt.%, the effect of copolymer composition on colloidal stability is clearly detected by column B_2 in **Figure II.5** and by evolution of absorbance spectra in **Figure II.7**, with an increase of VP content, the solution stabilization is weakened gradually. After two weeks, only Au@PVCL and Au@P(VCL$_{75}$-*stat*-VP$_{25}$) remain very weak stability, the nanohybrids in other cases flocculates. Further increasing copolymer concentration, the colloidal solution becomes more stable even after two weeks whatever copolymer used (see columns C_2 and D_2 in **Figure II.5**). The addition of NaCl shifts Au@P(VCL-*stat*-VP)$_{20k}$ stability towards higher copolymer concentration (columns A_3, B_3, C_3 and D_3 in **Figure II.5**). For a given copolymer concentration (i.e. 10^{-3} wt.%), the system

maintains stable (column B_3 in **Figures II.5** and **II.7**) after 2 h. However, the color of solution after two weeks fades gradually along with increased VP content, which is in agreement with stronger interactions of VCL than VP toward the surface of AuNPs as previously evidenced for the *in situ* formation of Au@P(VCL-*stat*-VP)$_{20k}$.

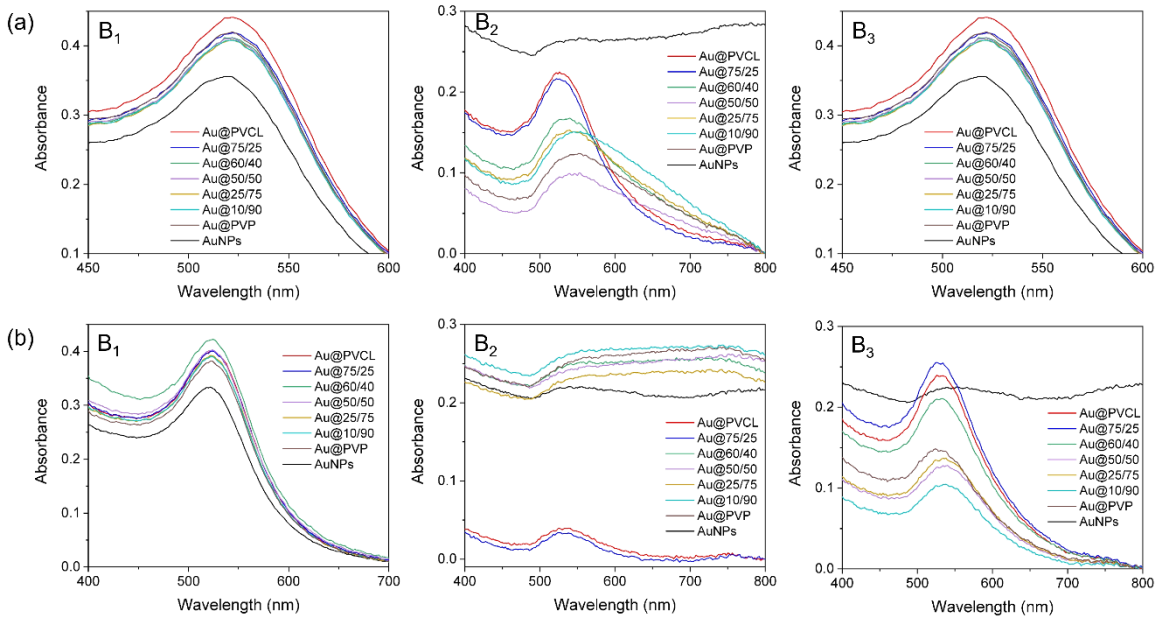

Figure II.7 UV-vis absorption spectra of nanohybrids at different copolymer composition between 400 and 800 nm (a) after two hours and (b) after two weeks detected after addition of NaOH (column B_2, pH_{final} = 10) and NaCl (column B_3, $([NaCl]_{final}$ = 1 mol·L^{-1}) compared to a control (column B_1). ([(co)polymer] = 10^{-3} wt.%, $[Au]_{final} = 2.5\times10^{-4}$ mol·L^{-1})

(ii) Effect of temperature on Au@P(VCL-*stat*-VP)$_{20k}$ properties

The effect of temperature on the resulted hybrid materials was then evaluated as shown in **Figure II.8** by measuring the absorbance of solutions at 520 nm between 20 and 70 °C as a function of the copolymer composition.

Only Au@PVCL and Au@P(VCL$_{75}$-*stat*-VP$_{25}$) systems present a significant increase of absorbance induced by an increase of temperature (**Figures II.8** and **II.9A**). Increasing VP content induces two main effects on thermoresponsive properties: (1) a shift of transition temperature to higher values as observed in **Figure II.8** and (2) a lower variation of enthalpy during the phase transition. As a result, only nanohybrids coated by copolymers with VP content below 40% present thermoresponsive properties in solution at a chosen concentration. Additionally, only colloidal solution of Au@PVCL shows a significant change in the wavelength of the maximum absorbance when temperature increases from 20 to 70 °C (**Figure II.9B**) as previously observed. [27] Thus, increasing VP content in P(VCL-*stat*-VP)$_{20k}$ is detrimental to thermoresponsive property and to the aggregation of NPs.

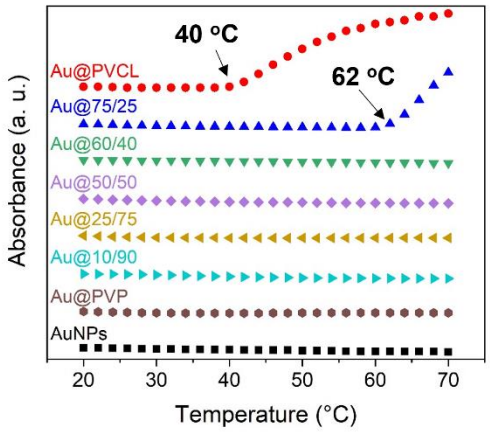

Figure II.8 Evolution of absorbance (an arbitrary unit was chosen) at 520 nm as a function of temperature for pristine AuNPs and AuNPs coated by different copolymers ([P(VCL-*stat*-VP)$_{20k}$] = 2.5×10^{-2} wt.%, $[Au]_{final} = 2.5\times10^{-4}$ mol·L^{-1}).

In addition, temperature change is likely to induce changes in the aggregation state of colloidal solutions. In order to evaluate the ability of different copolymers to effectively and reversibly stabilize AuNPs, the absorbance spectra at 20 °C are compared before and after temperature rises to 70 °C (**Figure II.9C**). The two homopolymer-based colloidal solutions Au@PVCL and Au@PVP show the smallest variation in absorbance and are therefore the least sensitive to temperature variation.

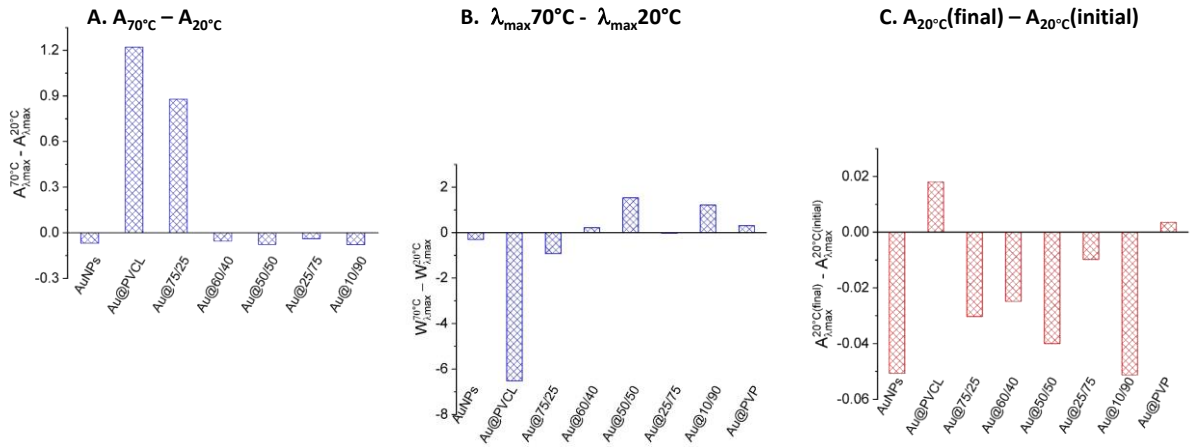

Figure II.9 (A) Variation of absorbance observed at 70 °C compared to the one measured at 20 °C. (B) Variation of wavelength corresponding to the maximum of absorbance observed at 70 °C compared to the one measured at 20 °C. (C) Variation of absorbance observed at 20 °C before and after increasing temperature to 70 °C ([P(VCL-*stat*-VP)$_{20k}$] = 2.5×10^{-2} wt.%, $[Au]_{final} = 2.5\times10^{-4}$ mol·L^{-1}).

(iii) Catalytic efficiency of Au@P(VCL-*stat*-VP)$_{20k}$

The catalytic performances of all Au@P(VCL-*stat*-VP)$_{20k}$ systems were further tested at different temperatures (20, 30, 40, 50, 60 and 70 °C) in the reduction of *p*-nitrophenol to *p*-

aminophenol in water using $NaBH_4$ (**Scheme II.3**). [12] The color change of the system associated with the conversion of *p*-nitrophenol to *p*-aminophenol enables researchers to easily monitor the reaction kinetics by UV-vis spectroscopy at 400 nm. As expected, the catalytic reduction is not triggered when only $NaBH_4$ is present.

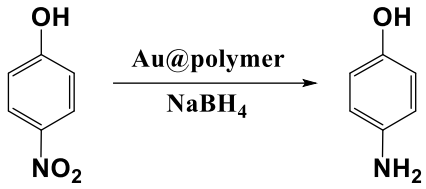

Scheme II.3 Reduction of *p*-nitrophenol to *p*-aminophenol by $NaBH_4$ (system pH around 8).

Figures II.10A and II.10C show the absorbance spectra of catalytic reaction system of *n*-nitrophenol at different reaction time in the presence of Au@P(VCL$_{75}$-*stat*-VP$_{25}$) and Au@PVCL at 20 °C respectively.

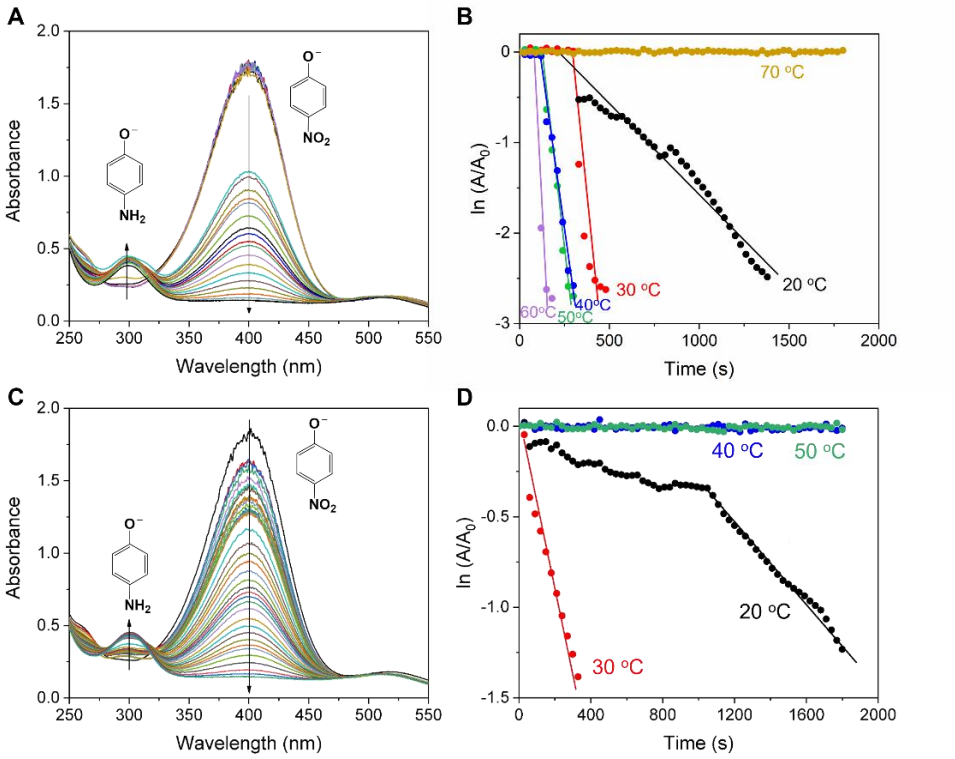

Figure II.10 UV-vis spectra of the reduction of *p*-nitrophenol to *p*-aminophenol by $NaBH_4$ catalyzed by (A) Au@P(VCL$_{75}$-*stat*-VP$_{25}$) and (C) Au@PVCL at 20 °C. Plots of ln(A/A$_0$) *vs* time for (B) Au@P(VCL$_{75}$-*stat*-VP$_{25}$) and (D) Au@PVCL at different temperatures ([*p*-nitrophenol] = 10^{-4} mol·L^{-1}, [Au] = 5×10^{-5} mol·L^{-1}, [$NaBH_4$] = 3×10^{-3} mol·L^{-1}, [(co)polymer] = 5×10^{-3} wt.%).

The observed rate constants (k_{obs}) for all kinetics were extracted from linear relationship between ln (A_t/A_0) *versus* time t assuming pseudo first-order kinetics for this reaction in the presence of an excess of $NaBH_4$. **Figures II.10B** and **II.10D** display the fits of the experimental data obtained at different temperatures for Au@P(VCL$_{75}$-*stat*-VP$_{25}$) and Au@PVCL catalysts,

respectively. At the beginning of reaction stage, there is an induction period which is related to a surface restructuring of the nanoparticles before the catalytic reaction starts. [32] The reaction can occur only between species adsorbed on the surface. The evolutions of pseudo-first order kinetic constant (k_{obs}) as a function of temperature for Au@P(VCL$_{75}$-*stat*-VP$_{25}$) and Au@PVCL are given in **Figure II.11**. Results suggest that the catalytic activity increases with temperature until the cloud point is reached after which no catalytic efficiency is observed.

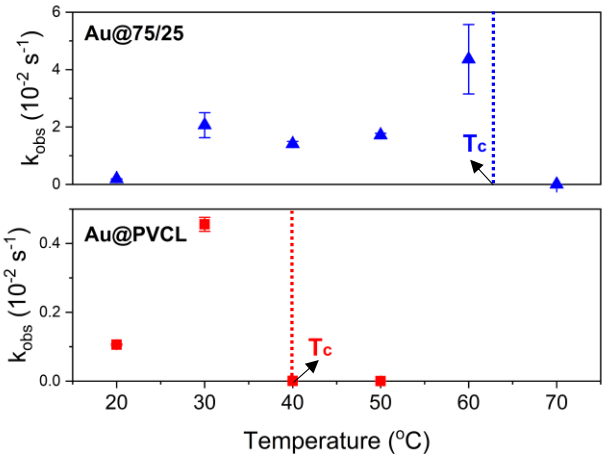

Figure II.11 Pseudo-first order kinetic constant (k_{obs}) as a function of temperature for Au@P(VCL$_{75}$-*stat*-VP$_{25}$) and Au@PVCL ([*p*-nitrophenol] = 10^{-4} mol·L^{-1}, [Au] = 5×10^{-5} mol·L^{-1}, [$NaBH_4$] = 3×10^{-3} mol·L^{-1}, [(co)polymer] = 5×10^{-3} wt.%).

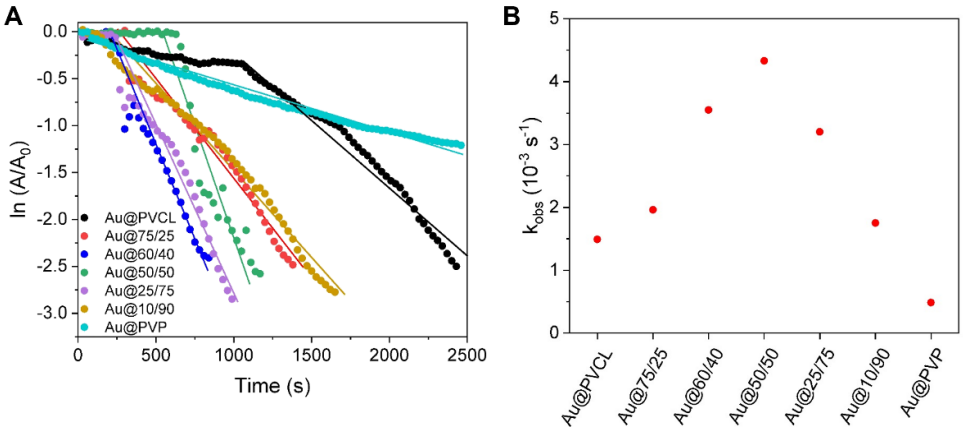

Figure II.12 (A) Plots of ln(A/A$_0$) *vs* time for the reduction of *p*-nitrophenol by $NaBH_4$ catalyzed by AuNPs stabilized by different statistical polymers at 20 °C and (B) corresponding pseudo-first order kinetic constant (k_{obs}) as a function of polymer composition ([Au] = 5×10^{-5} mol·L^{-1}, [P(VCL-*stat*-VP)$_{20k}$] = 5×10^{-3} wt.%, [*p*-nitrophenol] = 10^{-4} mol·L^{-1}, [$NaBH_4$] = 3×10^{-3} mol·L^{-1}).

Additional results obtained at 20 °C for different Au@P(VCL-*stat*-VP)$_{20k}$ systems are given in **Figure II.12**. At 20 °C, hybrid nanoparticles based on statistical copolymers present higher k_{obs} values than those evaluated for Au@PVCL and Au@PVP. Moreover, an optimum k_{obs} is measured when VP content equals to 50%. The observed trend of catalytic efficiency as a function of copolymer composition can be rationalized as a compromise between two opposite

effects. On the one hand, higher VCL content increases the hydrophobic character of organic shell surrounding AuNPs and thus favors the diffusion of reactants towards the AuNPs surface. On the other hand, the stronger adsorption of VCL compared to VP limits the catalytic efficiency of resulting nanohybrids.

II.4 Conclusions

The stabilization of AuNPs based on PVCL enables the access to hybrid thermosensitive materials with modular properties. [24, 25] Though structurally close to PVP, studies on PVCL are much less prevalent. In order to compare the ability of these two families for the formation, stabilization and modulation of the properties of AuNPs, a series of VCL/VP statistical copolymers with controlled molecular weights and low dispersity, containing variable amounts of VP (ranging from 0 to 100%), was synthesized by RAFT/MADIX polymerization. The effect of the copolymer composition was evaluated both on the growth of AuNPs prepared in the presence of the polymers (*in situ* route) and on the properties (stabilization, optical and catalytic properties...) of preformed nanoparticles coated by these (co)polymers. With two additional methylene group per monomer unit in comparison with PVP, PVCL demonstrates strong differences concerning its ability to interact with and stabilize AuNPs. As demonstrated through this chapter, its increased hydrophobic character enables PVCL to act as a more effective stabilizing and growth control agent than PVP for the *in situ* synthesis of AuNPs. Moreover, whatever the method of preparation of nanohybrids used (*in situ* formation or coating of preformed AuNPs), statistical copolymerization of VCL and VP makes it possible to modulate to some extent the properties of polymer, and thus of the obtained hybrid materials. Hence, at a molar fraction of VP in copolymer less than 40%, it is possible to increase the transition temperature of the hybrid material and improve catalytic property compared to counterparts comprising PVP and PVCL homopolymers. In addition, incorporation of higher fraction of VCL units in P(VCL-*stat*-VP)$_{20k}$ promotes an increased colloidal stability of AuNPs.

The results obtained on AuNPs in this chapter can be used to extend the scope of PVCL-based copolymers for the synthesis of functional colloidal materials based on the different inorganic supports as described for PVP [30] or for the formation of thermosensitive hybrid nanogels [33, 34].

II.5 References

[1] K.K. Harish, V. Nagasamy, B. Himangshu, K. Anuttam, Biomed J Sci Tech Res 4 (2018) 3765-3775.

[2] M.-C. Daniel, D. Astruc, Chem. Rev. 104 **(**2004) 293-346.

[3] C.-C. You, A. Verma, V.M. Rotello, Soft Matter 2 (2006), 190-204.

[4] J. Shan, H. Tenhu, Chem. Commun. 44 (2007) 4580-4598.

[5] M.-Q. Zhu, L.-Q. Wang, G.J. Exarhos, A.D.Q. Li, J. Am. Chem. Soc. 126 (2004) 2656-2657.

[6] A. Housni, Y. Zhao, Langmuir 26 (2010) 12933-12939.

[7] O.J. Cayre, N. Chagneux, S. Biggs, Soft Matter 7 (2011) 2211-2234.

[8] S. Salmaso, P. Caliceti, V. Amendola, M. Meneghetti, J.P. Magnusson, G. Pasparakis, C. Alexander, J. Mater. Chem. 19 (2009) 1608-1615.

[9] J. Shan, Y. Zhao, N. Granqvist, H. Tenhu, Macromolecules 42 (2009) 2696-2701.

[10] M. Beija, J.-D. Marty, M. Destarac, Prog. Polym. Sci. 36 (2011) 845-886.

[11] S. Maji, B. Cesur, Z. Zhang, B.G. De Geestb, R. Hoogenboom, Polym. Chem. 7 (2016) 1705-1710.

[12] M. Beija, E. Palleau, S. Sistach, X. Zhao, L. Ressier, C. Mingotaud, M. Destarac, J.-D. Marty, J. Mater. Chem. 20 (2010) 9433-9442.

[13] S. Sistach, M. Beija, V. Rahal, A. Brûlet, J.-D. Marty, M. Destarac, C. Mingotaud, Chem. Mater. 22 (2010) 3712-3724.

[14] C. Boyer, M.R. Whittaker, K. Chuah, J. Liu, T.P. Davis, Langmuir 26 (2010) 2721-2730.

[15] A. Aqil, H. Qiu, J.-F. Greisch, R. Jérôme, E. De Pauw, C. Jérôme, Polymer 49 (2008) 1145-1153.

[16] J. Raula, J. Shan, M. Nuopponen, A. Niskanen, H. Jiang, E.I. Kauppinen, H. Tenhu, Langmuir 19 (2003) 3499-3504.

[17] H.H. Nguyen, A. Brûlet, D. Goudounèche, P. Saint-Aguet, N. Lauth-de Viguerie, J.-D. Marty, Polym. Chem. 6 (2015) 5838-5850.

[18] A. Glaria, M. Beija, R. Bordes, M. Destarac, J.-D. Marty, Chem. Mater. 24 (2013) 1868-1876.

[19] B. Verdonck, E.J. Goethals, F.E. Du Prez, Macromol. Chem. Phys. 204 (2003) 2090-2098.

[20] L.H. Gan, Y.Y. Gan, G.R. Deen, Macromolecules 33 (2000) 7893-7897.

[21] J.-F. Lutz, Ö. Akdemir, A. Hoth, J. Am. Chem. Soc. 128 (2006) 13046-13047.

[22] J.-F. Lutz, A. Hoth, Macromolecules 39 (2006) 893-896.

[23] G. Vancoillie, D. Frank, R. Hoogenboom, Prog. Polym. Sci. 39 (2014) 1074-1095.

[24] M. Beija, J.-D. Marty, M. Destarac, Chem. Commun. 47 (2011) 2826-2828.

[25] S. Maji, Z. Zhang, L. Voorhaar, S. Pieters, B. Stubbe, S. Van Vlierberghe, P. Dubruel, B.G. De Geest, R. Hoogenboom, RSC Adv. 5 (2015) 42388-42398.

[26] H. Wang, X. Qiao, J. Chen, X. Wang, S. Ding, Mater. Chem. Phys. 94 (2005) 449-453.

[27] X. Zhao, O. Coutelier, H.H. Nguyen, C. Delmas, M. Destarac, J.-D. Marty, Polym. Chem. 6 (2015) 5233-5243.

[28] A. Kermagoret, K. Mathieu, J.-M. Thomassin, C.-A. Fustin, R. Duchêne, C. Jérôme, C. Detrembleur, A. Debuigne, Polym. Chem. 5 (2014) 6534-6544.

[29] J.-M. Thomassin, K. Mathieu, A. Kermagoret, C.-A. Fustin, C. Jérôme, A. Debuigne, Polym. Chem. 6 (2015) 1856-1864.

[30] K.M. Koczkur, S. Mourdikoudis, L. Polavarapu, S.E. Skrabalak, Dalton Trans. 44 (2015) 17883-17905.

[31] S. Sistach, K. Rahme, N. Pérignon, J.-D. Marty, N. Lauth-de Viguerie, F. Gauffre, C. Mingotaud, Chem. Mater. 20 (2008) 1221-1223.

[32] S. Wunder, Y. Lu, M. Albrecht, M. Ballauff, ACS Catal. 1 (2011) 908-916.

[33] J. Siirilä, M. Karesoja, P. Pulkkinen, J.-M. Malho, H. Tenhu, Eur. Polym. J. 115 (2019) 59-69.

[34] A. Pich, A. Tessier, V. Boyko, Y. Lu, H.-J.P. Adler, Macromolecules 39 (2006) 7701-7707.

Chapter III

(*n*-butyl acrylate / *N*-isopropylacrylamide) copolymers - Effect of microstructure on the thermoresponsiveness, self-organization and gel properties in water

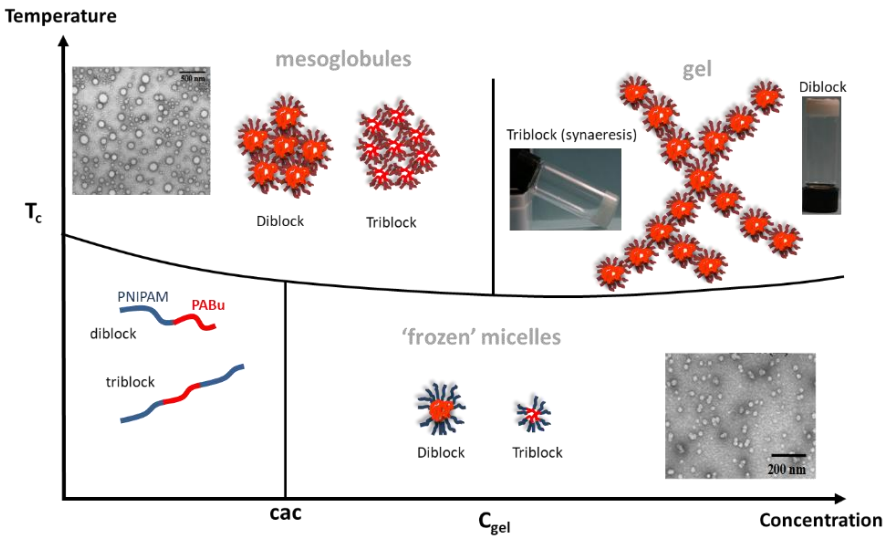

Contents

III.1 Introduction

Synthetic materials capable of responding in a controllable and predictable fashion to small changes in their environment (temperature, pH, mechanical stress…) have aroused great interest in the last decades. This response induces changes in the properties of these materials such as dimensions, internal structure or aggregation state. [1] In that context, thermosensitive systems, obtained by dissolving a polymer in aqueous solution, have been extensively studied. They present a characteristic transition temperature called cloud point temperature (T_c) at which the interactions between the polymer chains and the aqueous media dramatically change. This results in the collapse or expansion of polymer chains. If, in the phase diagram, a change from a two-phase to a single-phase system is observed when the temperature is increased, an upper critical solution temperature (UCST) is defined. In the opposite case, a lower critical solution temperature can be defined (LCST). Among all polymers presenting LCST, like poly(*N*-vinylcaprolactam) (PVCL), [2, 3] poly(oligo(ethylene glycol) methacrylate), [4] etc…, poly(*N*-isopropylacrylamide) (PNIPAM) is by far the most commonly described. [5, 6] Their thermoresponsive properties are used in stimuli responsive drug nanocarriers and functional surfaces with tunable hydrophobicity. [2, 7-9]

Interestingly, the choice of the macromolecular parameters of a chosen polymer (composition, molar mass, architecture…) greatly influences the properties of obtained materials. The T_c remains almost constant whatever the molar mass in the case of PNIPAM, [2] but changes along with a strong, concentration-dependent polymer-solvent interaction. However, this temperature can be precisely controlled by the adjustment of molecular weight (M_n) in the case of PVCL with a value tending to increase with the decrease of copolymer chain length. Polymer architecture (linear, branched, hyperbranched, grafted…) also influences thermoresponsiveness of these polymers. For example, four-arm PNIPAM stars collapse to form denser globules than the ones observed for linear PNIPAM [10] and PNIPAM-based branched thermoresponsive gels do not show the same kinetics of hydration and rheological properties when compared to their linear counterparts. [11, 12]

Incorporation of hydrophilic or hydrophobic comonomers within random or block copolymers enables to finely tune LCST values: [13] random copolymerization with a 82/18 molar ratio of NIPAM with hydrophilic acrylamide monomer increases T_c value from 32 to 45 °C. [14] Similarly, random copolymerization of VCL with hydrophilic comonomers (i.e. *N*-vinyl formamide, *N*-methyl-*N*-vinylacetamide or vinylpyrrolidone (VP)) induces a significant increase of T_c. [15, 16] Thus copolymerization appears to be an effective means of modulating

T_c, even if, in most case, this variation does not depend linearly on the comonomer ratio. [15] Moreover, this incorporation can lead to a rapid loss of heat-sensitive properties. [15, 16] On the contrary, an incorporation of a hydrophobic monomer tends to decrease the observed transition temperature. Thus, statistical copolymerization of NIPAM with hydrophobic acrolein using a 80/20 molar ratio induced a decrease of T_c value down to 26 °C, [14] a similar tendency was observed in cases of block copolymers. In addition, below T_c, their specific microstructure confers an amphiphilic character to this block structure, this results in the formation of self-assemblies such as micellar structures or polymersomes. [13] Above T_c, the dehydration of the thermoresponsive block induces aggregation of the preformed nanoobjects.

In this chapter, copolymers of NIPAM and hydrophobic *n*-butyl acrylate (BA) were considered. Whereas this family of copolymers can act as stabilizers for nanoparticles [13] or emulsion systems, [17] few studies have described their properties in aqueous solution yet. [13, 17-20] For instance, P(BA-*stat*-NIPAM) statistical copolymers have been used to form hydrogels for which a decrease of T_c from 34.3 to 29.5 °C was observed when BA content increased up to 20 mol.%. [21] The specific structure of PBA-*b*-PNIPAM block copolymer enabled the formation of stable nanospheres both below and above T_c [13, 19] with a significant increase of diameter above T_c. [13] Here, we aimed at further studying the properties of this family of copolymers at different temperatures and concentrations in relation with their composition and microstructure. For this, polymers with statistical, diblock and triblock microstructures were synthesized by reversible addition-fragmentation chain transfer (RAFT)/macromolecular design by interchange of xanthates (MADIX) copolymerization of NIPAM and BA. [13, 17] The ability of different copolymer structures to associate as colloids in dilute solution and to form gels at higher concentration, and the temperature dependence of these properties were studied with turbidimetry measurements, differential scanning calorimetry, electronic microscopy, rheology and scattering experiments.

III.2 Synthesis and characterization of copolymers

In order to study the influence of copolymer composition and architecture on the thermoresponsive properties, three families of copolymers were investigated: P(BA-*stat*-NIPAM) statistical copolymers, PBA-*b*-PNIPAM diblock copolymers and PNIPAM-*b*-PBA-*b*-PNIPAM triblock copolymers. For each family of them, a similar M_n value of 10000 g·mol^{-1} (abbreviated as 10k) was selected.

III.2.1 Synthesis of P(BA-*co*-NIPAM) copolymers

The structures of diblock, triblock and statistical copolymers synthesized by RAFT/MADIX polymerization are given in **Scheme III.1**.

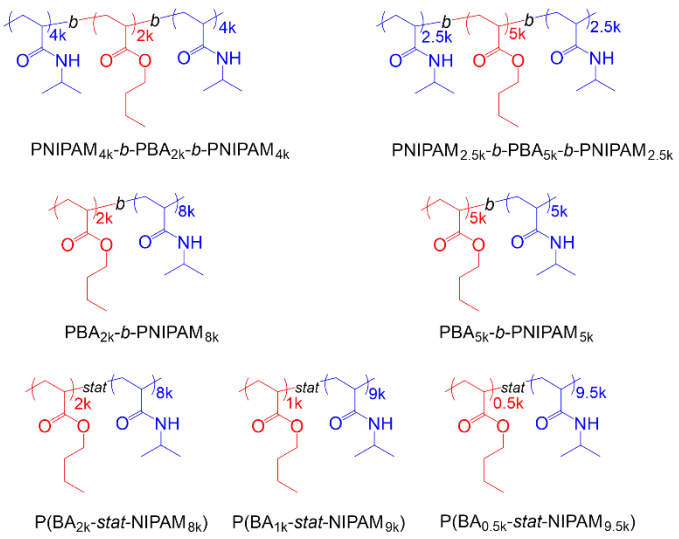

Scheme III.1. Structures of P(BA-*co*-NIPAM) synthesized in this chapter.

(i) Synthesis of PBA-*b*-PNIPAM diblock copolymers

Well-defined diblock copolymers with targeted structures corresponding to PBA_{2k}-*b*-$PNIPAM_{8k}$ and PBA_{5k}-*b*-$PNIPAM_{5k}$ (2k and 5k for theoretical M_n values of PBA blocks equal to 2000 and 5000 g·mol^{-1} respectively) were selected. These block copolymers were synthesized in the presence of xanthate **X1** [13] via two-step polymerizations initiated by 2,2'-azobis(isobutyronitrile) (AIBN) in ethanol at 62 °C without purification of intermediate PBA block (see **Scheme III.2)**.

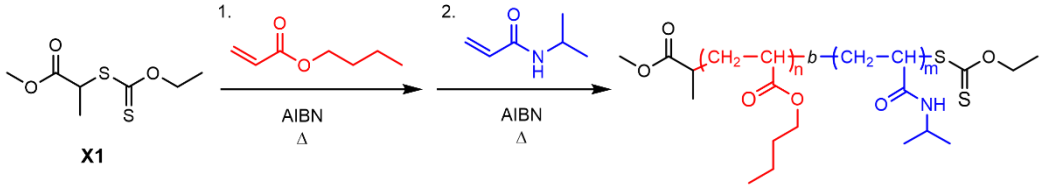

Scheme III.2 Synthesis of PBA-*b*-PNIPAM diblock copolymers (Synthesis was performed by V. Rahal in IMRCP, Toulouse, France).

(ii) Synthesis of PNIPAM-*b*-PBA-*b*-PNIPAM triblock copolymers

Triblock copolymers were obtained in a similar two-step way in the presence of *bis*-xanthate **X2** (its synthesis was described in **Experimental Section**) as shown in **Scheme III.3**. PNIPAM-*b*-PBA-*b*-PNIPAM copolymers with targeted structures corresponding to

PNIPAM$_{4k}$-*b*-PBA$_{2k}$-*b*-PNIPAM$_{4k}$ and PNIPAM$_{2.5k}$-*b*-PBA$_{5k}$-*b*-PNIPAM$_{2.5k}$ were selected. In the conditions used, conversions of BA and NIPAM are greater than 97% in each polymerization step.

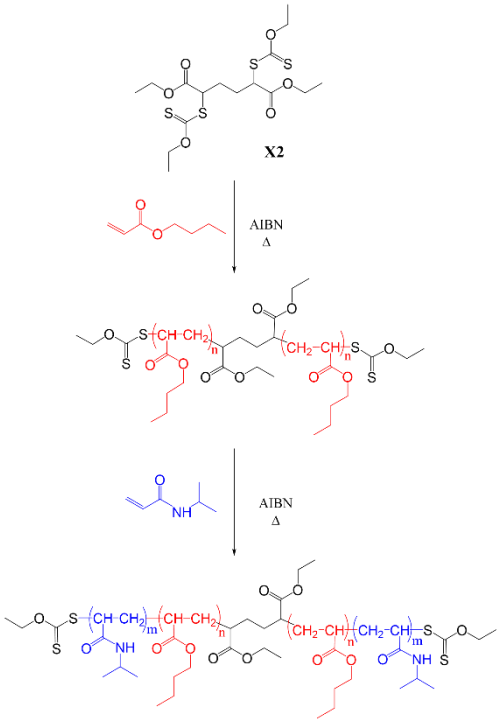

Scheme III.3 Synthesis of PNIPAM-*b*-PBA-*b*-PNIPAM triblock copolymers (Synthesis was performed by J.S. Behra and N. Lauth-de Viguerie in IMRCP, Toulouse, France).

(iii) Synthesis of P(BA-*stat*-NIPAM) statistical copolymers

Three P(BA-*stat*-NIPAM) statistical copolymers: P(BA$_{2k}$-*stat*-NIPAM$_{8k}$), P(BA$_{1k}$-*stat*-NIPAM$_{9k}$) and P(BA$_{0.5k}$-*stat*-NIPAM$_{9.5k}$) with similar molecular weights but different BA/NIPAM ratios were also synthesized by RAFT/MADIX polymerization in the presence of xanthate **X1** (**Scheme III.4**).

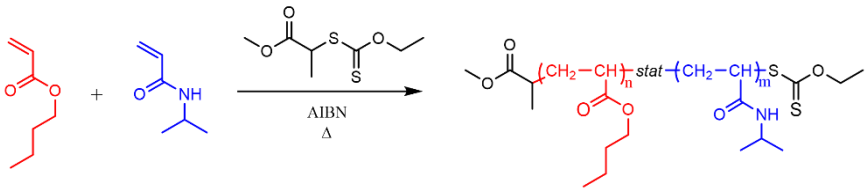

Scheme III.4 Synthesis of P(BA-*stat*-NIPAM) statistical copolymers.

III.2.2 Characterization of copolymers

These three families of copolymers were characterized by Nuclear Magnetic Resonance (NMR) Spectra, Size Exclusion Chromatography (SEC) and Differential Scanning Calorimetry

(DSC). The ^{1}H NMR spectra of triblock, diblock and statistical copolymers are shown in **Figures III.1**, **III.2** and **III.3**, respectively.

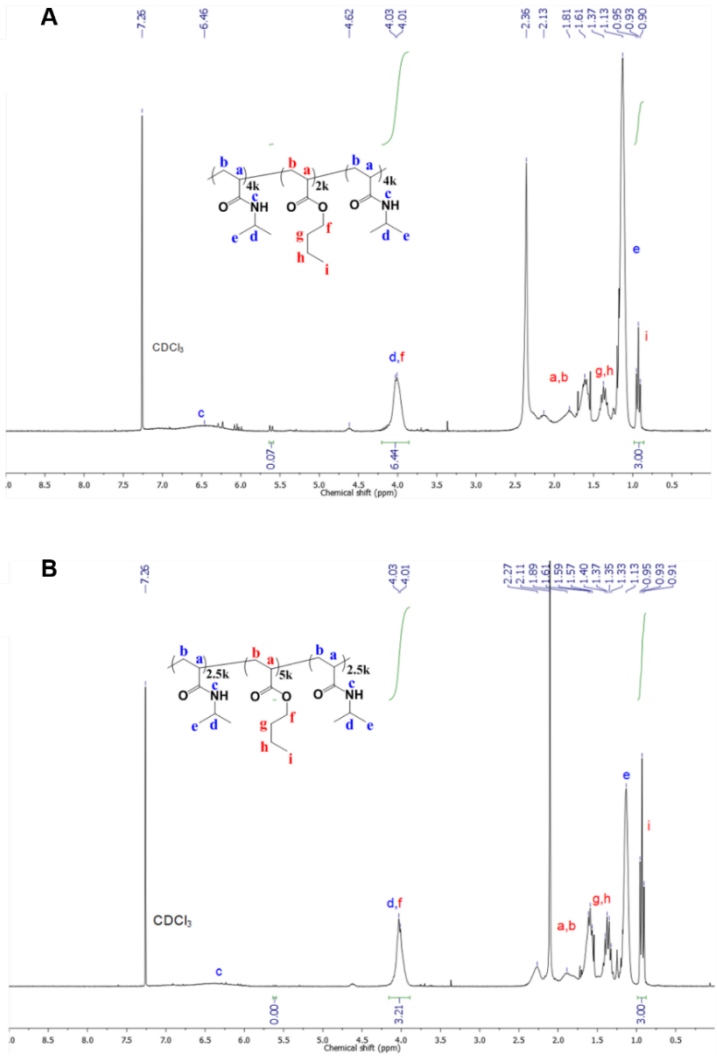

Figure III.1 ^{1}H NMR spectra of (A) PNIPAM$_{4k}$-*b*-PBA$_{2k}$-*b*-PNIPAM$_{4k}$ and (B) PNIPAM$_{2.5k}$-*b*-PBA$_{5k}$-*b*-PNIPAM$_{2.5k}$ in $CDCl_3$.

In the case of PNIPAM$_{4k}$-*b*-PBA$_{2k}$-*b*-PNIPAM$_{4k}$, the signals at 4.0 ppm are attributed to the methylene in α position of the ester group of PBA block and isopropyl methine of PNIPAM block, the peaks at 0.9 ppm are attributed to methyl group in PBA, the signals of unreacted NIPAM are about 5.5 - 6.0 ppm. According to the integrals of these special groups in ^{1}H NMR spectrum (**Figure III.1A**), the NIPAM conversion is calculated above 99%, and the molar ratio of NIPAM and BA is 4.37, suggesting the PNIPAM$_{4k}$-*b*-PBA$_{2k}$-*b*-PNIPAM$_{4k}$ was successfully synthesized. The same treatment method is used to calculate NIPAM conversion and molar ratio of NIPAM/BA in other cases, the detailed information is shown in **Tables ES.2** and **ES.3** in **Experimental Section**.

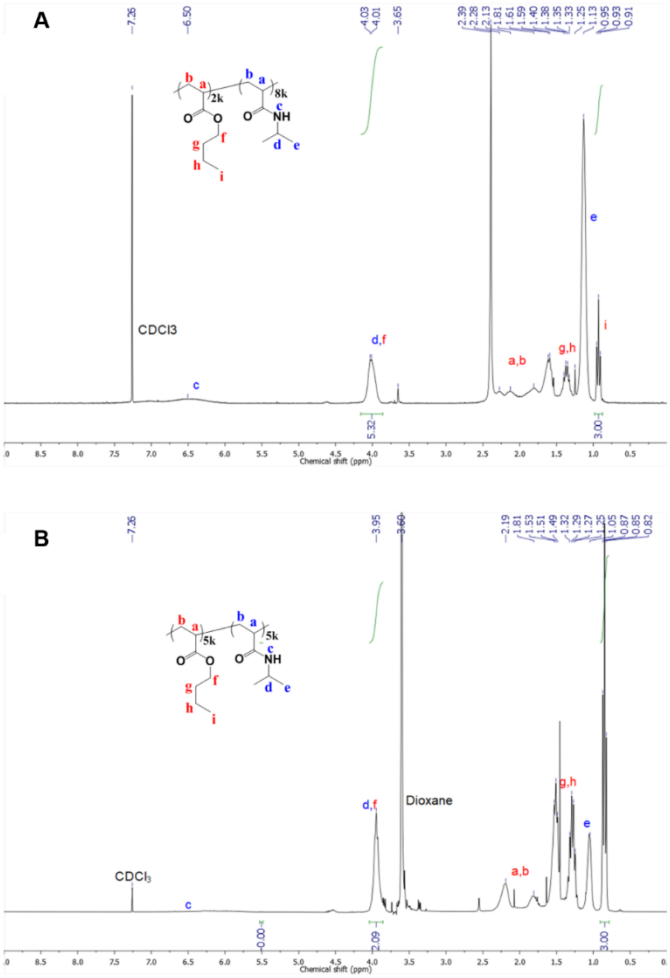

Figure III.2 ^{1}H NMR spectra of (A) PBA_{2k}-*b*-$PNIPAM_{8k}$ and (B) PBA_{5k}-*b*-$PNIPAM_{5k}$ in $CDCl_3$.

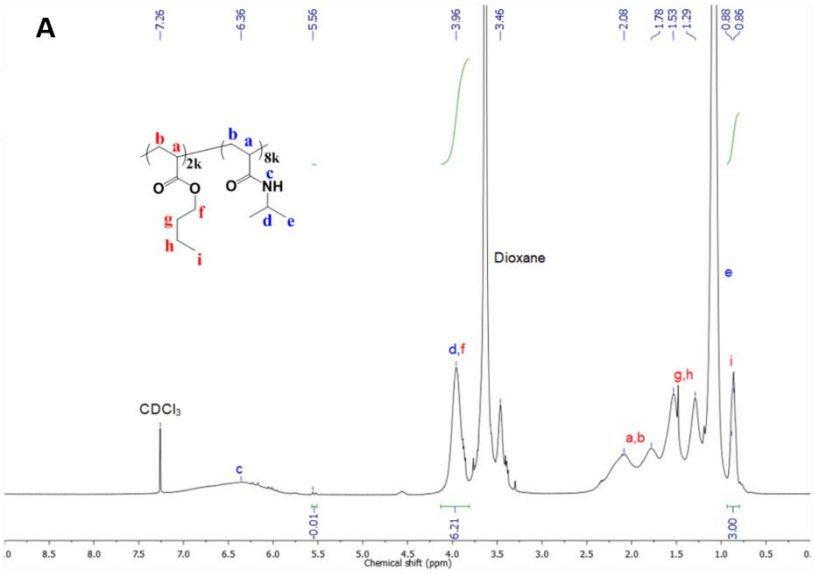

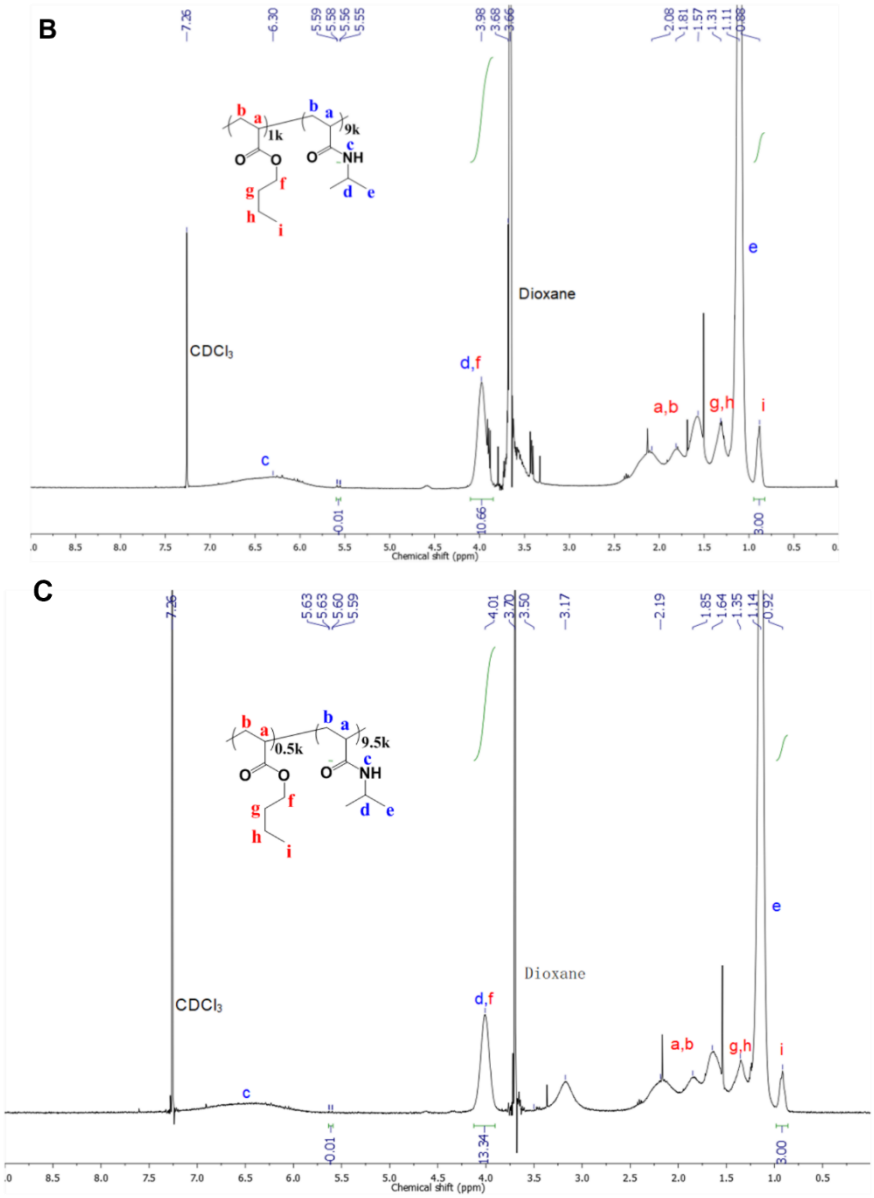

Figure III.3 ^{1}H NMR spectra of (A) P(BA_{2k}-*stat*-$NIPAM_{8k}$), (B) P(BA_{1k}-*stat*-$NIPAM_{9k}$) and (C) P($BA_{0.5k}$-*stat*-$NIPAM_{9.5k}$) in $CDCl_3$.

Number-average molecular weights (M_n) and dispersity (Đ) of all the copolymers were evaluated by SEC measurements (**Figure III.4**). The detailed information of all PBA precursors and BA/NIPAM copolymers is reported in **Table III.1**. In all cases, the M_n values are very close to theoretical expectations for a controlled RAFT/MADIX polymerization, which is in agreement with known values of transfer constants (C_{tr}) of BA and NIPAM to xanthate **X1** ($C_{tr,X1}$ = 2.7 [22] and 3.3 [23] for BA and NIPAM in ethanol, respectively). The M_n of PNIPAM synthesized in the presence of **X1** or **X2** is nearly twice as high as the theoretical M_n value when SEC analysis was performed in DMF. We attribute these differences in M_n to differences in hydrodynamic volumes between PMMA and PNIPAM in DMF/LiBr eluent, as the $C_{tr,X1}$ value

of 3.3 for NIPAM rules out the possibility for the xanthate to be partially reacted at the end of the polymerization.

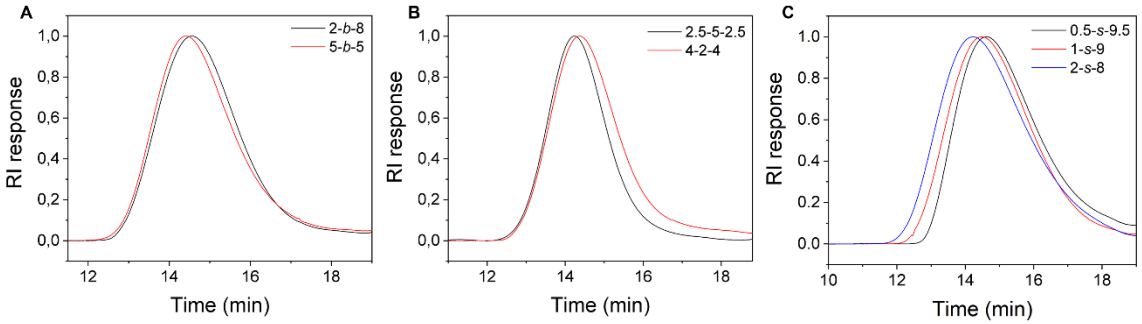

Figure III.4 SEC curves of (A) diblock, (B) triblock and (C) statistical copolymers in THF (copolymer concentration was 10 mg·mL^{-1}, eluent flow rate was 1 mL·min^{-1}).

Table III.1 Characteristics of various copolymers prepared by RAFT/MADIX polymerization: M_n, Đ and glass transition temperatures (T_g).

PBA /PNIPAM	Sample	M_n (g·mol^{-1})	Đ	T_g [c] (°C)	ΔC_p [c] (J·g^{-1}·K^{-1})
0.5k/9.5k	P(BA$_{0.5k}$-*stat*-NIPAM$_{9.5k}$)	10620[a]	1.30[a]	111.90	0.74
1k/9k	P(BA$_{1k}$-*stat*-NIPAM$_{9k}$)	11230[a]	1.57[a]	114.20	0.71
2k/8k	PBA$_{2k}$-*b*-PNIPAM$_{8k}$	10000[a]	1.16[a]	108.90	0.20
	P(BA$_{2k}$-*stat*-NIPAM$_{8k}$)	9100[a]	1.81[a]	100.40	0.63
	PNIPAM$_{4k}$-*b*-PBA$_{2k}$-*b*-PNIPAM$_{4k}$	8960[a]	1.40[a]	100.60	0.28
5k/5k	PBA$_{5k}$-*b*-PNIPAM$_{5k}$	9400[a]	1.25[a]	-48.00 106.70	0.10 0.20
	PNIPAM$_{2.5k}$-*b*-PBA$_{5k}$-*b*-PNIPAM$_{2.5k}$	11000[a]	1.23[a]	-35.20 86.21	0.10 0.28
8k/2k	PBA$_{8k}$-*b*-PNIPAM$_{2k}$	10100[a]	1.20[a]	-44.00 133.00	0.40 0.10
	PNIPAM$_{1k}$-*b*-PBA$_{8k}$-*b*-PNIPAM$_{1k}$	9900[a]	1.36[a]	-41.70	0.56
PBA	PBA$_{2k}$	2400[a]	1.38[a]	-50.70	0.50
	PBA$_{5k}$	5750[a]	1.35[a]	-50.60	0.50
	PBA$_{8k}$	9500[a]	1.30[a]	-50.70	0.50
PNIPAM	PNIPAM$_{8k}$	17600[b]	1.27[b]	127.90	0.40
	PNIPAM$_{10k}$	21300[b]	1.31[b]	126.20	0.46

[a]SEC analyses performed in THF with RI-MALS detection. [b]SEC analyses performed in DMF and calibrated with PMMA standards. The chosen conditions led to an overestimate of given mass by a factor of two. [c]Glass transitions measured by DSC technique with a heating rate of 10 °C·min^{-1}.

As reported in **Table III.1**, the dispersity values are close to 1.3 for PNIPAM and lie in the range of 1.3 - 1.4 for PBA. By approximating at the end of polymerization process Đ to

$1+1/C_{ex}$ (C_{ex} is interchain transfer constant), [24] the xanthate exchange can be considered as relatively slow in both cases (C_{ex} ~ 3 in line with $C_{tr,X1}$ values) and slightly slower in the case of BA than NIPAM. Concerning these copolymers, their experimental M_n values are very close to theoretical estimations. Đ values of block copolymers tend to slightly decrease compared to that of PBA block precursor (1.16 < Đ < 1.40). Most importantly, as illustrated in the case of PNIPAM$_{2.5k}$-*b*-PBA$_{5k}$-*b*-PNIPAM$_{2.5k}$, the overlay of SEC chromatograms of PBA precursor and resulting diblock or triblock copolymers in THF shows that in both cases, PBA is successfully incorporated in the final copolymer (**Figure III.5**).

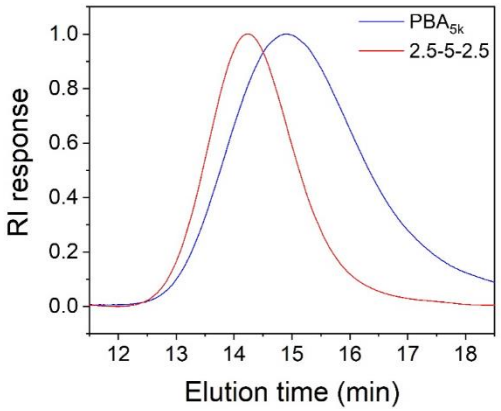

Figure III.5 Size exclusion chromatograms (RI response) of PNIPAM$_{2.5k}$-*b*-PBA$_{5k}$-*b*-PNIPAM$_{2.5k}$ (red line) and PBA$_{5k}$ (blue line) in THF.

Thermal properties of block copolymers. DSC analysis was performed for all homopolymers, statistical and block copolymers. As expected glass transition temperature of statistical polymer decreases from 111.9 to 100.4 °C when BA content increases from 5 to 20 wt.% within the copolymer (see **Table III.1**). Whereas block copolymers with 50/50 weight composition show two glass transitions temperatures (around -50 and 100 °C), 2k/8k copolymers present only one around 100 °C. In the latter case, the lower weight fraction of BA within the copolymer prevents the possibility to undergo the transition corresponding to this block. Interestingly, the observed T_g values for triblock copolymers are found at lower temperature than the one observed for corresponding diblock or statistical copolymers, this suggests there is a different phase separation of two blocks in the solid state.

III.3 Determination of cloud point temperatures of copolymer solutions

In order to evaluate the influence of composition and microstructure on T_c values, the behavior of polymer solutions was studied as a function of temperature at concentration ranging from 0.1 to 20 wt.%. Among synthesized (co)polymers, only those with a minimum PNIPAM

content of 50 wt.% make it possible to obtain perfectly transparent solutions at room temperature. Subsequently, the behavior of these copolymer solutions was studied by turbidimetry, DLS and DSC measurements. **Figures III.6 - III.12** and **Table III.2** give T_c values of all synthesized (co)polymers.

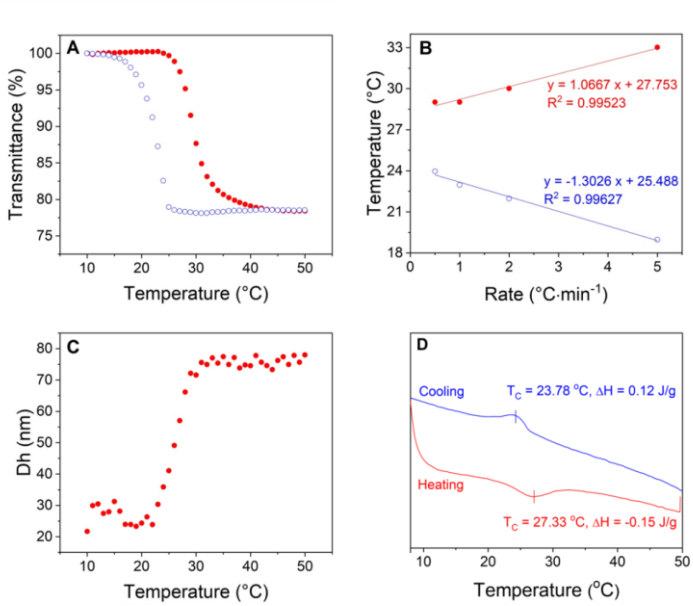

Figure III.6 Turbidimetry, DLS and DSC measurements of PNIPAM$_{4k}$-*b*-PBA$_{2k}$-*b*-PNIPAM$_{4k}$ solution. (A) Transmittance curves recorded at 500 nm as a function of temperature with a heating/cooling rate of 1 °C·min^{-1}. (B) Extrapolation of inflection points determined from turbidimetry curves at different heating/cooling rates. (C) Hydrodynamic diameter obtained from DLS measurements upon heating. (D) DSC thermograms recorded upon heating and cooling at a rate of 1 °C·min^{-1}. (Polymer concentrations used for turbidimetry, DLS and DSC measurements were 0.1, 0.1 and 1 wt.%, respectively)

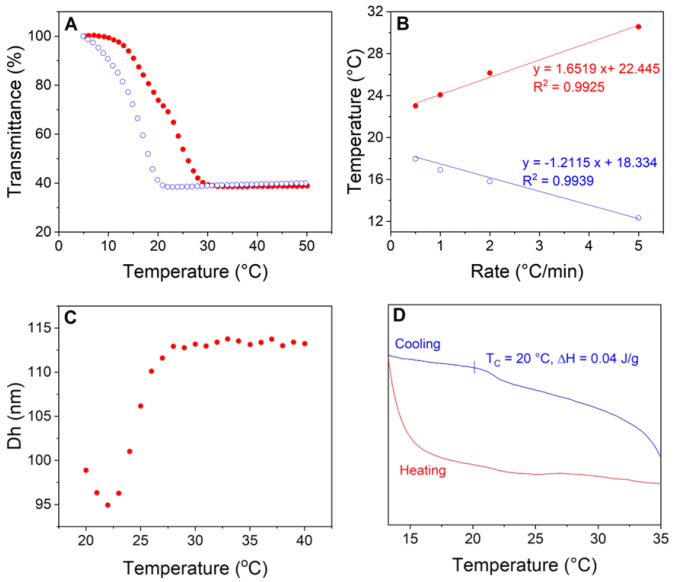

Figure III.7 Turbidimetry, DLS and DSC measurements of PNIPAM$_{2.5k}$-*b*-PBA$_{5k}$-*b*-PNIPAM$_{2.5k}$ aqueous solution. (A) Transmittance curves recorded at 500 nm as a function of temperature with a heating/cooling rate of 1 °C·min^{-1}. (B) Extrapolation of inflection points determined from turbidimetry curves at different heating/cooling rates. (C) Hydrodynamic diameter obtained from DLS measurements

upon heating. (D) DSC thermograms recorded upon heating and cooling processes with a rate of 1 °C·min^{-1}. (Polymer concentrations used for turbidimetry, DLS and DSC measurements were 0.1, 0.1 and 1 wt.%, respectively)

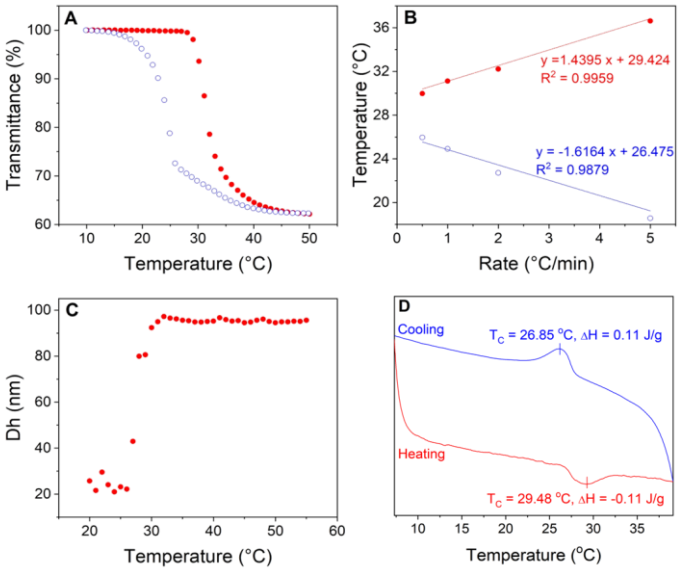

Figure III.8 Turbidimetry, DLS and DSC measurements of PBA_{2k}-*b*-$PNIPAM_{8k}$ solution. (A) Transmittance curves recorded at 500 nm as a function of temperature with a heating/cooling rate of 1 °C·min^{-1}. (B) Extrapolation of inflection points determined from turbidimetry curves at different heating/cooling rates. (C) Hydrodynamic diameter obtained from DLS measurements upon heating. (D) DSC thermograms recorded upon heating and cooling at a rate of 1 °C·min^{-1}. (Polymer concentrations used for turbidimetry, DLS and DSC measurements were 0.1, 0.1 and 1 wt.%, respectively)

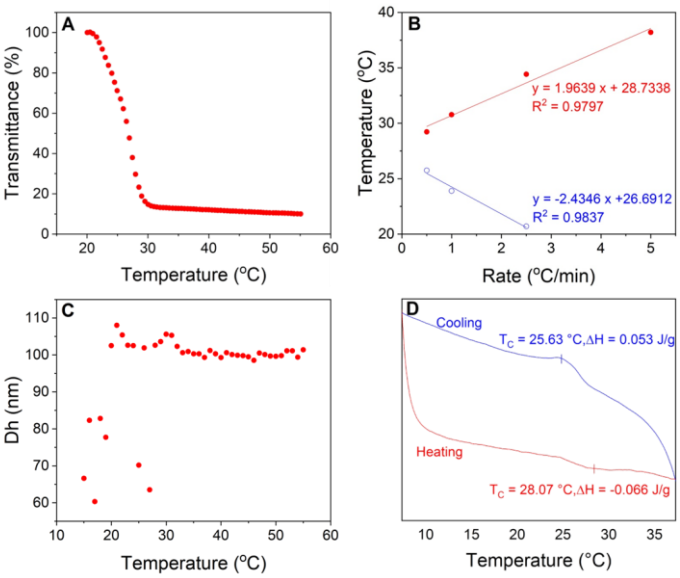

Figure III.9 Turbidimetry, DLS and DSC measurements of PBA_{5k}-*b*-$PNIPAM_{5k}$ solution. (A) Transmittance curves recorded at 500 nm as a function of temperature with a heating/cooling rate of 1 °C·min^{-1}. (B) Extrapolation of inflection points determined from turbidimetry curves at different heating/cooling rates. (C) Hydrodynamic diameter obtained from DLS measurements upon heating. (D) DSC thermograms recorded upon heating and cooling at a rate of 1 °C·min^{-1}. (Polymer concentrations used for turbidimetry, DLS and DSC measurements were 0.1, 0.1 and 1 wt.%, respectively)

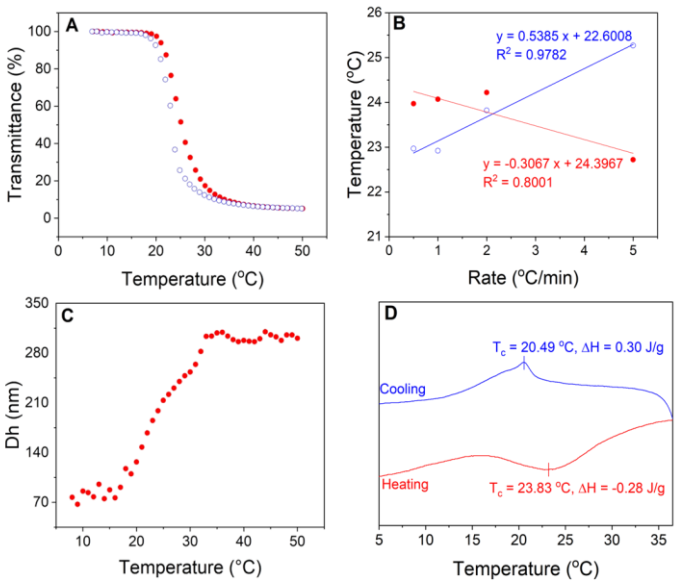

Figure III.10 Turbidimetry, DLS and DSC measurements of P($BA_{0.5k}$-*stat*-$NIPAM_{9.5k}$) solution. (A) Transmittance curves recorded at 500 nm as a function of temperature with a heating/cooling rate of 1 °C·min^{-1}. (B) Extrapolation of inflection points determined from turbidimetry curves at different heating/cooling rates. (C) Hydrodynamic diameter obtained from DLS measurements upon heating. (D) DSC thermograms recorded upon heating and cooling at a rate of 1 °C·min^{-1}. (Polymer concentrations used for turbidimetry, DLS and DSC measurements were 0.1, 0.1 and 1 wt.%, respectively)

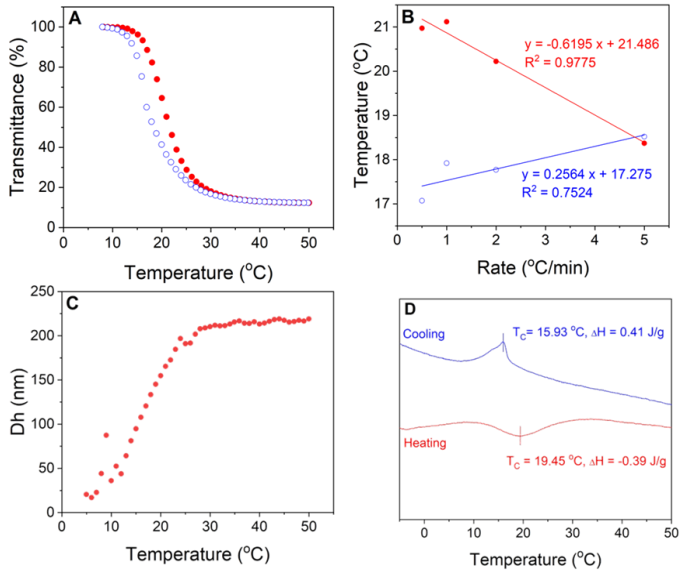

Figure III.11 Turbidimetry, DLS and DSC measurements of P(BA_{1k}-*stat*-$NIPAM_{9k}$) solution. (A) Transmittance curves recorded at 500 nm as a function of temperature with a heating/cooling rate of 1 °C·min^{-1}. (B) Extrapolation of inflection points determined from turbidimetry curves at different heating/cooling rates. (C) Hydrodynamic diameter obtained from DLS measurements upon heating. (D) DSC thermograms recorded upon heating and cooling at a rate of 1 °C·min^{-1}. (Polymer concentrations used for turbidimetry, DLS and DSC measurements were 0.1, 0.1 and 1 wt.%, respectively)

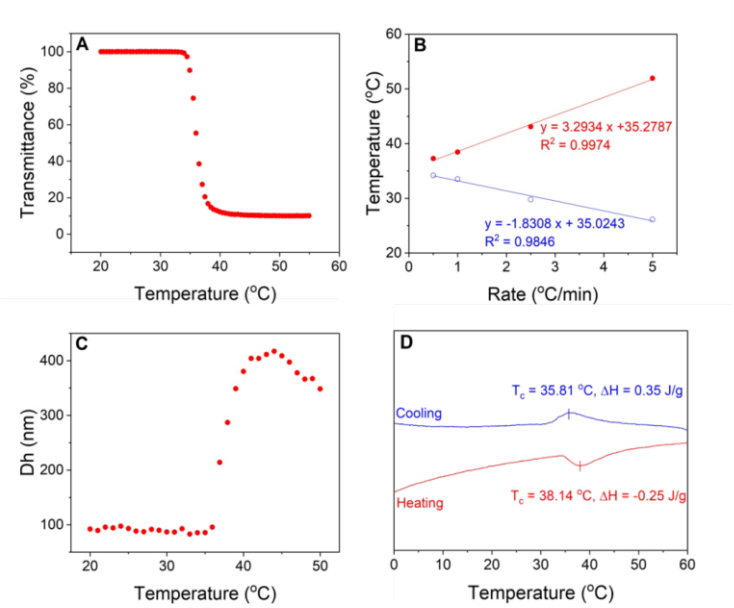

Figure III.12 Turbidimetry, DLS and DSC measurements of $PNIPAM_{10k}$ solution. (A) Transmittance curves recorded at 500 nm as a function of temperature with a heating/cooling rate of 1 °C·min^{-1}. (B) Extrapolation of inflection points determined from turbidimetry curves at different heating/cooling rates. (C) Hydrodynamic diameter obtained from DLS measurements upon heating. (D) DSC thermograms recorded upon heating and cooling at a rate of 1 °C·min^{-1}. (Polymer concentrations used for turbidimetry, DLS and DSC measurements were 0.1, 0.1 and 1 wt.%, respectively)

Table III.2 Cloud points of copolymer aqueous solutions obtained by visual assessment, DSC, DLS and turbidimetry measurements.

PNIPAM weight fraction (%)	(Co)polymer	Visual assessment T_c(°C)	DSC				DLS	Turbidimetry	
			heating		Cooling		heating	heating	cooling
			T_c (°C)[a]	ΔH (J·g^{-1})	T_c (°C)[a]	ΔH (J·g^{-1})	T_c (°C)	T_c (°C)[b]	T_c (°C)[b]
100	$PNIPAM_{10k}$	30	37.67	-14.00	36.16	18.00	37.00	35.28	35.02
95	$P(BA_{0.5k}$-*stat*-$PNIPAM_{9.5k})$	19	23.15	-29.47	21.24	31.58	21.00	24.40	22.60
90	$P(BA_{1k}$-*stat*-$NIPAM_{9k})$	insoluble	17.75	-18.89	15.45	13.33	17.00	21.49	17.28
80	PBA_{2k}-*b*-$PNIPAM_{8k}$	32	28.80	-13.75	27.60	13.75	27.00	29.42	26.48
	$P(BA_{2k}$-*s*-$NIPAM_{8k})$	insoluble	/[c]	/[c]	9.62	2.25	/[c]	/[c]	/[c]
	$PNIPAM_{4k}$-*b*-PBA_{2k}-*b*-$PNIPAM_{4k}$	25	26.00	-18.75	25.13	15.00	26.00	27.70	25.50
50	PBA_{5k}-*b*-$PNIPAM_{5k}$	28	27.35	-13.20	26.44	10.60	24.00	28.73	26.69
	$PNIPAM_{2.5k}$-*b*-PBA_{5k}-*b*-$PNIPAM_{2.5k}$	20	/[c]	/[c]	21.74	8.00	24.00	22.45	18.33

[a]Determined by extrapolation to 0 °C·min^{-1} of peak values on the thermogram upon heating/cooling at different rates. [b]Determined by extrapolation to 0 °C·min^{-1} of inflection points of transmittance curves at different heating/cooling rates. [c]Not determined. (Copolymer concentrations used for visual

assessment, DSC, DLS and turbidimetry measurements were 1, 1, 0.1 and 0.1 wt.%, respectively. ΔH values calculated per gram of PNIPAM present in the considered copolymers.)

Whatever the technique used, a sharp and reversible phase transition was observed. In addition, when comparing the behavior of polymer solutions upon cooling or heating, a hysteresis phenomenon whose amplitude depending on the chosen heating/cooling rate is observed. This phenomenon is related to the difficulty of swelling compact aggregates formed at higher temperatures due to intra-chain entanglement. [25] In the case of PNIPAM$_{4k}$-*b*-PBA$_{2k}$-*b*-PNIPAM$_{4k}$ T_c values equal to 27.7, 26.0 and 26.0 °C are obtained upon heating thanks to turbidimetry, DLS and DSC measurements respectively. It should be noted that for these polymers with low molecular weight, the study of thermal properties by using UV-visible spectroscopy leads to a systematic overestimation of T_c values compared to those obtained from DSC or DLS measurements, regardless of the studied polymer family. Such effect can be attributed to the fact that aggregates with sufficient size can be detected by these techniques. Thus, even as the dehydration of the polymer chain begins, as evidenced by DSC measurements, the formation of aggregates with sufficient size able to scatter light at a sufficient level requires a certain amount of time and/or greater dehydration level. Therefore, DSC was performed on the different families of copolymers in order to compare the T_c and corresponding enthalpy variations (ΔH). **Figure III.13** shows T_c values obtained by DSC upon heating or cooling for the different families of copolymers at a concentration of 1, 5 and 20 wt.%.

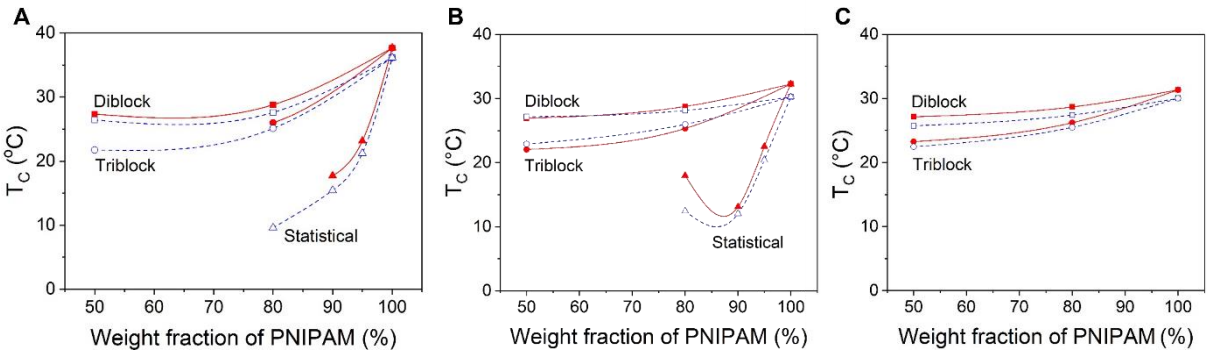

Figure III.13 Cloud point temperatures T_c (peak maximum) obtained by DSC measurements on heating (red plain marks) or cooling (blue open marks) for PNIPAM homopolymer and statistical, diblock and triblock PNIPAM-based copolymers at a concentration of (A) 1, (B) 5 and (C) 20 wt.%.

As can be seen in **Figure III.13**, it has to be noted that for most (co)polymers, there is no significant difference in T_c values measured at different concentrations. Only PNIPAM shows a significantly different value at 1 wt.% compared to the values assessed at 5 and 10 wt.% (i.e. 36, 32 and 32 °C respectively). Moreover, compared to PNIPAM homopolymer, incorporation of a hydrophobic monomer in the PNIPAM chain leads to a significant decrease in T_c values

regardless of the considered structure, i.e. diblock, triblock or statistical. This trend is expected, as insertion of a hydrophobic moiety significantly decreases the level of hydration of polymer chain and thus decreases the T_c values. At the same time, the measured enthalpy variations (ΔH) reported for a constant amount of PNIPAM decrease significantly when the amount of PNIPAM decreases. Hence, in the case of statistical copolymers, ΔH values equal to 31.58, 13.33 and 2.25 $J \cdot g^{-1}$ of PNIPAM are reported for a PBA content of 5, 10 and 20 wt.% respectively. Similar trends were observed for diblock and triblock copolymers but, as expected, in a lesser extent. Indeed, for these copolymers, disruption of hydrogen network is less expected due to the presence of large PNIPAM moieties. In addition to this composition effect, the effect of the microstructure is highly pronounced. Hence, for a given composition (i.e. 80 wt.% of PNIPAM), the T_c measured for a statistical copolymer is well below the one measured for triblock and diblock structures (9.62, 25.13 and 27.60 °C, respectively). In the case of a statistical copolymer, its specific microstructure seems to strongly disadvantage the hydration of the copolymer. It also does not enable to study copolymers containing BA fractions greater than 20 wt.%. Lastly, the slightly lower values of T_c for triblock structures compared to diblock ones might be related to a similar phenomenon: indeed, for a given composition, triblock structures present one supplementary transition between PBA and PNIPAM blocks.

III.4 Properties of block copolymer in dilute aqueous solution

In addition to effect on cloud point temperature, the microstructure also strongly impacts the solubility of the different studied copolymers. Hence copolymers with a statistical structure present a low solubility in aqueous solutions (limited to 1 wt.%), whereas diblock and triblock copolymers thanks to their specific amphiphilic structure enable to obtain clear solution for weight fraction up to 20 wt.%. This observation might be related to the formation of nanometric colloidal suspensions and will be studied in the following section.

III.4.1 Phase behavior in water at low temperature ($T < T_c$)

As evidenced by DLS measurements, block copolymers behave as isolated chains at concentration of 0.1 wt.%. When they are transferred from organic solvent into aqueous solutions, a significant increase of their hydrodynamic radii are observed by DLS whereas only a slight change is seen for homopolymers (**Table III.3**), suggesting that they have the ability to self-assemble. Additionally, Transmission Electronic Microscopy (TEM) and Small Angle Neutron Scattering (SANS) measurements were carried out to analyze the size and

conformation as a function of the architecture of copolymers at lower temperature. All results are reported in **Table III.3**.

Table III.3. Cloud points (T_c) and DLS, TEM and SANS results on polymer aqueous solutions at 20 and 40 °C.

Copolymer	Cloud point (T_c, °C)[a]	Radius at 20 °C (nm)			Radius at 40 °C (nm)		
		$R_{h,TEM}$	$R_{h,DLS}$	$R_{h,SANS}$	$R_{h,TEM}$	$R_{h,DLS}$	$R_{h,SANS}$
$PNIPAM_{10k}$	32.3	/[b]	3 ± 2	/[b]	/[b]	243 ± 97	/[b]
PBA_{2k}-*b*-$PNIPAM_{8k}$	27.6	11 ± 1.5	14 ± 3	8 ± 1	/[b]	57 ± 3	52 ± 7
$PNIPAM_{4k}$-*b*-PBA_{2k}-*b*-$PNIPAM_{4k}$	25.1	10.6 ± 2.3	10.5 ± 2.0	4.9 ± 2.0[c]	21.6 ± 3.5	78 ± 2	39 ± 11
PBA_{5k}-*b*-$PNIPAM_{5k}$	26.4	20.5 ± 5	31 ± 6	20.5 ± 3.5	/[b]	66 ± 1	53 ± 8
$PNIPAM_{2.5k}$-*b*-PBA_{5k}-*b*-$PNIPAM_{2.5k}$	21.7	/[b]	53.5 ± 2.5	9 ± 5[c]	/[b]	123 ± 2	46 ± 7

[a]Obtained from DSC measurements (1 wt.% in cooling mode). [b]Not determined. [c]Lognormal distribution. (Copolymer concentration for size determination was 0.1 wt.%. R_h is not influenced by preparation methods such as direct solubilization, liposomes-like…. Note: Errors in DLS results were calculated by multiplying polydispersity index values by the mean hydrodynamic radius values. Error in the fits results from SANS were calculated by multiplying the distribution by the radius values.)

For $PNIPAM_{4k}$-*b*-PBA_{2k}-*b*-$PNIPAM_{4k}$ a hydrodynamic radius equal to 10.5 ± 2.0 nm is measured. TEM images of dried aqueous solutions show very regular monodisperse spherical structures with average radius equal to 10.6 ± 2.3 nm (**Figure III.14B**) in fair agreement with DLS results. This suggests the formation of spherical-like micellar structures for copolymer, as confirmed by SANS measurements shown in **Figure III.14A**. Data are well fitted by a simple model of polydisperse sphere, which gives the mean micelle radius and its Gaussian distribution (**Table III.3**). In this case, the PNIPAM corona surrounding the PBA core is also swollen by the solvent. Its contribution to the SANS signal is very weak. Thus, with this assumption, the micelle radius deduced from SANS is the radius of the hydrophobic PBA core alone. The micelles radii of $PNIPAM_{2.5k}$-*b*-PBA_{5k}-*b*-$PNIPAM_{2.5k}$ copolymers measured by DLS and SANS are twice as large as those of $PNIPAM_{4k}$-*b*-PBA_{2k}-*b*-$PNIPAM_{4k}$. Such an increase of micelle size related to the length of the hydrophobic block might be related to the strong aggregation limit case predicted and observed for the aggregation of diblock copolymer. [26] In this case, the hydrophobic blocks are mainly located in the core of the micelles. Longer hydrophobic block leads to the formation of micelles with a higher aggregation number and a

larger micelle size. The average aggregation number (N_{agg}) of these micelles can be assessed from the following formula by considering a dense and solvent excluded core:

$$N_{agg} = 4\pi\rho_{core}R_{core}^3 N_A/(3M_{core}) \quad (1)$$

Where R_{core} is radius of the core, M_{core} is the mean average molar mass of core block (here $M_{core} = M_{PBA}$), ρ_{core} is 1.1 g·cm^{-3}, block density of the core, N_A is Avogadro number. From this, average aggregation number N_{agg} = 163 and 405 are found for copolymer micelles of PNIPAM$_{4k}$-*b*-PBA$_{2k}$-*b*-PNIPAM$_{4k}$ and PNIPAM$_{2.5k}$-*b*-PBA$_{5k}$-*b*-PNIPAM$_{2.5k}$ respectively. By noting N_A is the number of monomers of the hydrophobic block, the observed increase of N_{agg} is in good agreement with the expected scaling law $N_{agg} \propto N_A^2$. [26] The surface area per chain calculated from $A_c = 4\pi R_{core}^2/N_{agg}$ gives values of 1.85 and 2.52 nm^2 respectively.

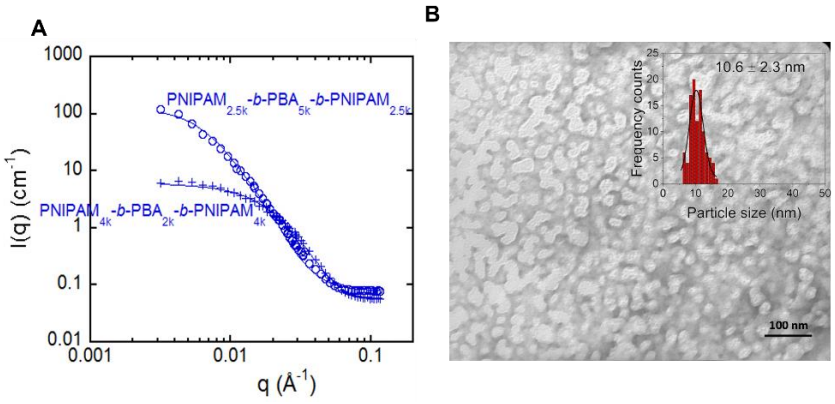

Figure III.14 (A) Scattering intensity in absolute units (cm^{-1}) of D_2O solutions of (0.1 wt.%) PNIPAM$_{4k}$-*b*-PBA$_{2k}$-*b*-PNIPAM$_{4k}$ (+) and PNIPAM$_{2.5k}$-*b*-PBA$_{5k}$-*b*-PNIPAM$_{2.5k}$ (o) measured at 20 °C. Lines are the best fits to a model of polydisperse sphere with a Lognormal distribution. (B) Representative TEM micrograph of aggregates formed by PNIPAM$_{4k}$-*b*-PBA$_{2k}$-*b*-PNIPAM$_{4k}$ at 20 °C stained with uranyl acetate (TEM deposit was performed below T_c). (SANS measurement was done by N. Lauth-de Viguerie and A. Brûlet in LLB, Gif sur Yvette Cedex, France. TEM image was taken by H.H. Nguyen in IMRCP, Toulouse, France.)

Diblock copolymers show the same tendency: an increase of size and aggregation number with an increase of BA content [13] with N_{agg} = 710 and 4800 respectively for copolymer micelles of PBA$_{2k}$-*b*-PNIPAM$_{8k}$ and PBA$_{5k}$-*b*-PNIPAM$_{5k}$ with a surface area per chain in the corona for the two micellar systems gives values of 1.13 and 1.10 nm^2 respectively. Thus, at 20 °C, both diblock and triblock structures enable the formation of micellar structures. For a given composition, these specific structures favor their solubility and are responsible for higher T_c values compared to the statistical microstructure. In addition, compared to diblock copolymers, triblock counterparts lead to smaller and less dense structures.

III.4.2 Self-assembly in water at high temperature ($T > T_c$)

As shown in **Figure III.15**, when a 0.1 wt.% solution of $PNIPAM_{4k}$-*b*-PBA_{2k}-*b*-$PNIPAM_{4k}$ is heated, hydrodynamic radius determined from DLS measurements evolves from 10.5 ± 2.0 nm below T_c to 78 ± 2 nm above T_c (**Table III.3**). The formation of spherical aggregates with a narrow size distribution was further confirmed by TEM experiments (negative staining) and SANS measurements as shown in **Figure III.15**. The estimated radius distribution from TEM measurements is equal to 21.6 ± 3.5 nm. The large distribution observed by TEM might be caused by drying and/or the staining process which leads to local overconcentration and, consequently, induces the formation of objects with different sizes. However, samples prepared using the same procedure at room temperature do not show such large objects (see **Figure III.14B**). Since the aggregates appear to be spherical, it is consistent to fit the SANS data (see **Figure III.15A**) above T_c with the polydisperse sphere model, which gives a mean radius of 39 ± 11 nm for $PNIPAM_{4k}$-*b*-PBA_{2k}-*b*-$PNIPAM_{4k}$. At this temperature, PNIPAM is poorly solvated and both blocks contribute to scattering signal. This behavior inducing the formation of large aggregates with increasing temperature is observed whatever the structure and composition studied. Hence, from SANS measurements, $PNIPAM_{2.5k}$-*b*-PBA_{5k}-*b*-$PNIPAM_{2.5k}$ forms aggregates with a similar radius within experimental error (46 ± 7 nm).

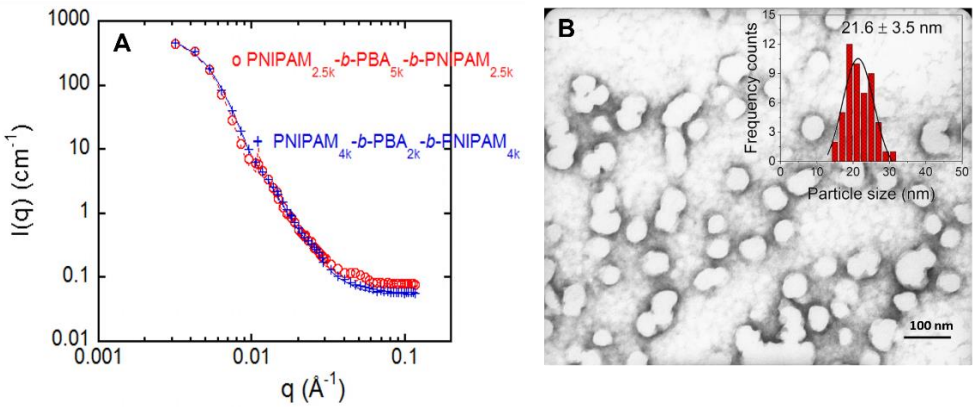

Figure III.15 (A) Scattering intensity in absolute units (cm^{-1}) of D_2O solutions of (0.1 wt.%) $PNIPAM_{4k}$-*b*-PBA_{2k}-*b*-$PNIPAM_{4k}$ (+) and $PNIPAM_{2.5k}$-*b*-PBA_{5k}-*b*-$PNIPAM_{2.5k}$ (o) measured at 36 °C. Lines are the best fits to a model of polydisperse sphere with Gaussian distribution. (B) TEM image of aggregates formed above the cloud point for $PNIPAM_{4k}$-*b*-PBA_{2k}-*b*-$PNIPAM_{4k}$ (TEM deposit was performed above T_c, followed by a negative staining with uranyl acetate. SANS measurement was done by N. Lauth-de Viguerie and A. Brûlet in LLB, Gif sur Yvette Cedex, France. TEM image was taken by H.H. Nguyen in IMRCP, Toulouse, France.)

Moreover, for diblock copolymers, radii are equal to 52 ± 7 nm and 53 ± 8 nm for PBA_{2k}-*b*-$PNIPAM_{8k}$ and PBA_{5k}-*b*-$PNIPAM_{5k}$ respectively. Thus, at temperature above T_c, these aggregates have similar size whatever the nature of microstructure (diblock or triblock). The formation of spherical aggregates also named mesoglobules has been previously described in

the case of PNIPAM homopolymers [27, 28] as well as of hydrophobically modified PNIPAM polymers and PNIPAM-based amphiphilic block copolymers. [13] These mesoglobules are stable in aqueous solution and they spontaneously transform into spherical micelles when the solution is cooled below T_c: formation of larger aggregates is prevented by the low probability of Brownian collisions in dilute solutions. [27] At temperature above T_c, polymer chains dehydrate and as a result intrachain contraction and interchain association occur, which gives rise to the formation of large aggregates with poorly hydrated property. Consecutively to the further ejection of water molecule to bulk water, very dense and rigid mesoglobules are formed. The probability of merging of different mesoglobules might be very low due to the very short contact time between two mesoglobules during a collision or due to partial vitrification taking place within the dense mesoglobules. [29]

III.5 Formation and characterization of thermosensitive hydrogels

The behavior of polymer solutions for concentrations ranging from 0.1 to 20 wt.% was then studied. For this range of concentration, DSC measurements do not show significant changes in the measured transition temperatures T_c whatever the considered structures (diblock or triblock). Related enthalpy variation normalized with respect to PNIPAM content shows a strong decrease when the concentration increases. As such a decrease is not observed in dilute conditions, it tends to demonstrate a clear difference between the different polymers concerning the polymer/polymer and polymer/solvent interactions in gel solution. Interestingly, the concentration effect is proved to have a strong impact on the rheological properties of the studied solutions.

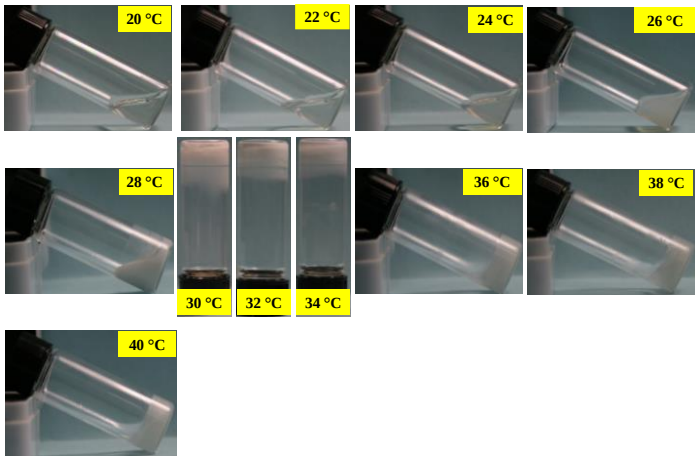

Figure III.16 Photographs of phase states of PNIPAM$_{4k}$-*b*-PBA$_{2k}$-*b*-PNIPAM$_{4k}$ (20 wt.% in water) as a function of temperature (Experiment was carried out in a dry box ranging from 20 to 40 °C at 2 °C intervals, the sample was equilibrated for 5 min at a given temperature before visual observation, then the same procedure was operated at higher temperature after sample recovered to transparent state).

An initial visual assessment of the effect of temperature for different (co)polymer structures, compositions or concentrations was performed. **Figure III.16** shows phase states of $PNIPAM_{4k}$-*b*-PBA_{2k}-*b*-$PNIPAM_{4k}$ aqueous solution with a concentration of 20 wt.% in temperature range from 20 to 40 °C.

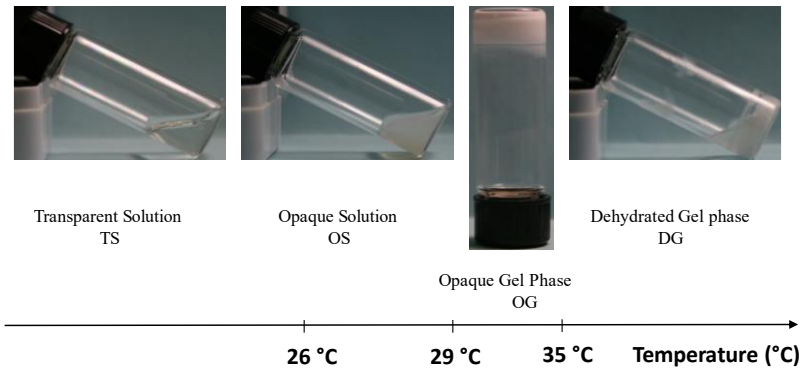

Figure III.17 Photographs of the observed phase transition for $PNIPAM_{4k}$-*b*-PBA_{2k}-*b*-$PNIPAM_{4k}$ triblock structure at a concentration of 20 wt.% as a function of temperature: transparent solution (TS) → opaque solution (OS) → opaque gel phase (OG) → dehydrated gel phase (DG).

As shown in **Figure III.17**, below T_c, i.e. 26 °C, the transparent polymer solution looks like a free-flowing liquid independently of the concentration so that we name this phase as transparent solution (TS). As the solution is heated above the transition temperature, the solution rapidly becomes white and turbid but remain freely mobile. This phase is noted OS as opaque solution. Then heating more, an opaque gel phase (OG) appears: this gel phase is identified by gently tilting the vials [30] when no fluidity is visually observed on tilting after 5 min. As temperature increases, macrophase separation (synaeresis) with volume shrinkage by expelling water occurs and forms the final dehydrated gel phase (DG). The similar observations of $PNIPAM_{4k}$-*b*-PBA_{2k}-*b*-$PNIPAM_{4k}$ were made at different concentrations (5, 10 and 15 wt.%, see **Figures III.18 - III.20**).

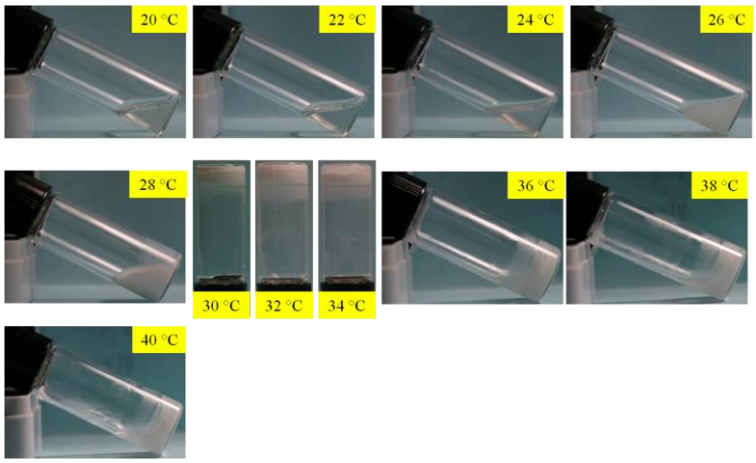

Figure III.18 Photographs of phase states of $PNIPAM_{4k}$-*b*-PBA_{2k}-*b*-$PNIPAM_{4k}$ (15 wt.% in water) as a function of temperature (Experiment was carried out in a dry box ranging from 20 to 40 °C at 2 °C

intervals, the sample was equilibrated for 5 min at a given temperature before visual observation, then the same procedure was operated at higher temperature after sample recovered to transparent state).

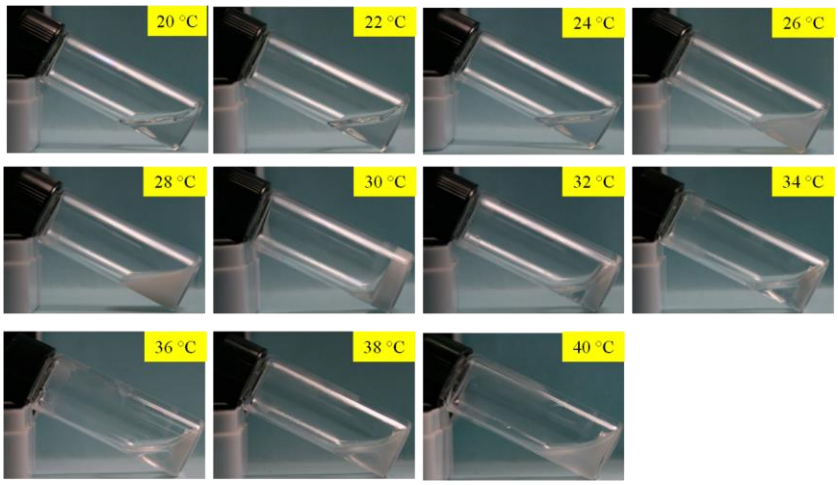

Figure III.19 Photographs of phase states of $PNIPAM_{4k}$-*b*-PBA_{2k}-*b*-$PNIPAM_{4k}$ (10 wt.% in water) as a function of temperature (Experiment was carried out in a dry box ranging from 20 to 40 °C at 2 °C intervals, the sample was equilibrated for 5 min at a given temperature before visual observation, then the same procedure was operated at higher temperature after sample recovered to transparent state).

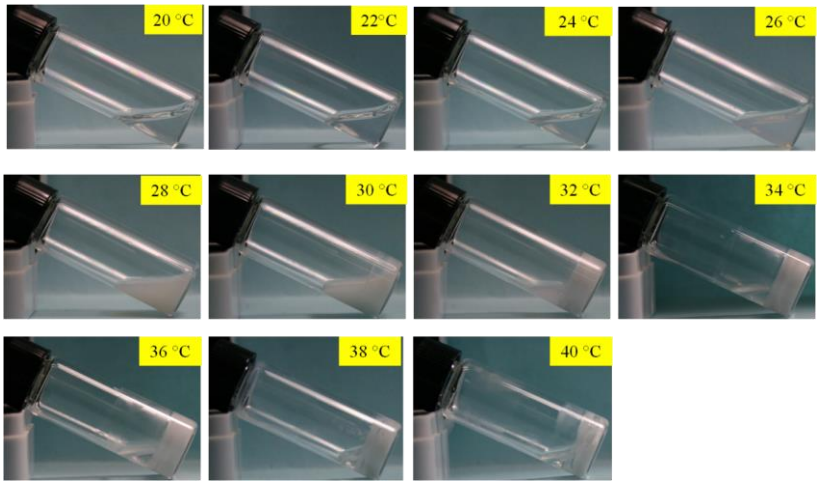

Figure III.20 Photographs of phase states of $PNIPAM_{4k}$-*b*-PBA_{2k}-*b*-$PNIPAM_{4k}$ (5 wt.% in water) as a function of temperature (Experiment was carried out in a dry box ranging from 20 to 40 °C at 2 °C intervals, the sample was equilibrated for 5 min at a given temperature before visual observation, then the same procedure was operated at higher temperature after sample recovered to transparent state).

To compare temperature-/concentration-dependent phase transition temperatures of different (co)polymer structures, the similar procedures were operated in other (co)polymer samples, the photographs of PBA_{2k}-*b*-$PNIPAM_{8k}$ in concentration range from 5 to 20 wt.% are showed in **Figures III.21 - III.24**.

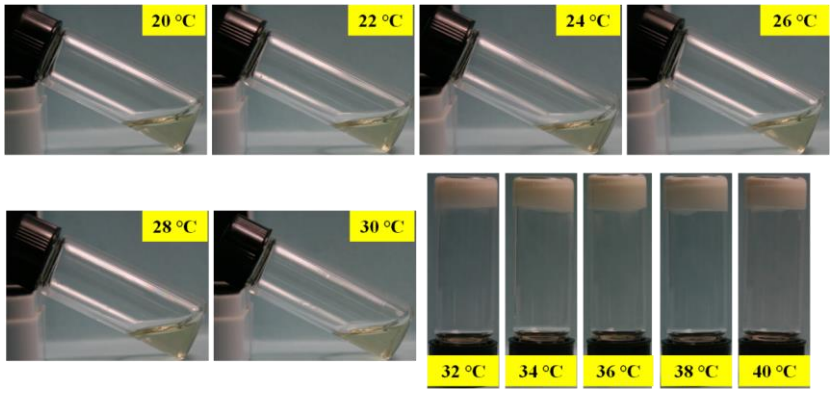

Figure III.21 Photographs of phase states of PBA_{2k}-*b*-$PNIPAM_{8k}$ (20 wt.% in water) as a function of temperature (Experiment was carried out in a dry box ranging from 20 to 40 °C at 2 °C intervals, the sample was equilibrated for 5 min at a given temperature before visual observation, then the same procedure was operated at higher temperature after sample recovered to transparent state).

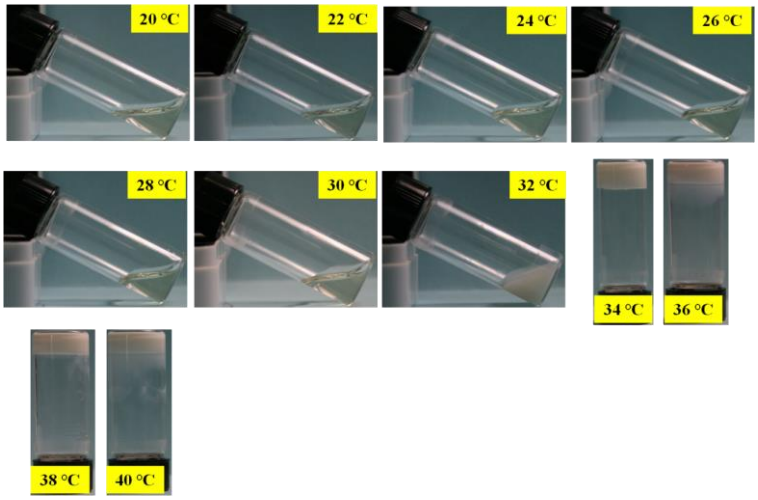

Figure III.22 Photographs of phase states of PBA_{2k}-*b*-$PNIPAM_{8k}$ (15 wt.% in water) as a function of temperature (Experiment was carried out in a dry box ranging from 20 to 40 °C at 2 °C intervals, the sample was equilibrated for 5 min at a given temperature before visual observation, then the same procedure was operated at higher temperature after sample recovered to transparent state).

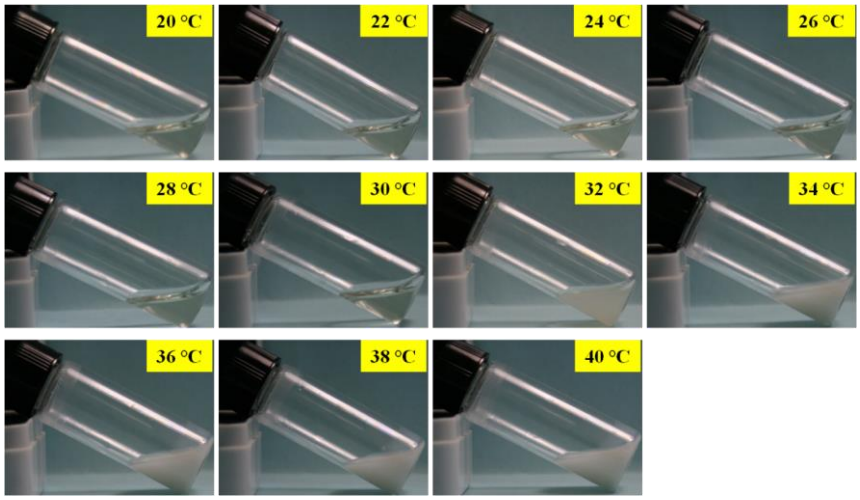

Figure III.23 Photographs of phase states of PBA_{2k}-*b*-$PNIPAM_{8k}$ (10 wt.% in water) as a function of

temperature (Experiment was carried out in a dry box ranging from 20 to 40 °C at 2 °C intervals, the sample was equilibrated for 5 min at a given temperature before visual observation, then the same procedure was operated at higher temperature after sample recovered to transparent state).

Figure III.24 Photographs of phase states of PBA_{2k}-*b*-$PNIPAM_{8k}$ (5 wt.% in water) at 30, 32 and 34 °C (The sample was equilibrated in a dry box for 5 min at a given temperature before visual observation, then the same procedure was operated at higher temperature after sample recovered to transparent state).

The photographs of phase states for $PNIPAM_{10k}$ in concentration range of 5 - 20 wt.% are showed in **Figures III.25 - III.28**.

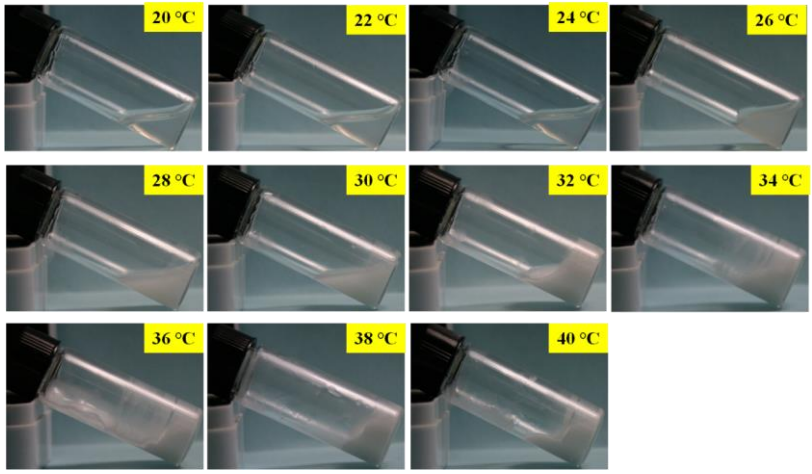

Figure III.25 Photographs of phase states of $PNIPAM_{10k}$ (20 wt.% in water) as a function of temperature (Experiment was carried out in a dry box ranging from 20 to 40 °C at 2 °C intervals, the sample was equilibrated for 5 min at a given temperature before visual observation, then the same procedure was operated at higher temperature after sample recovered to transparent state).

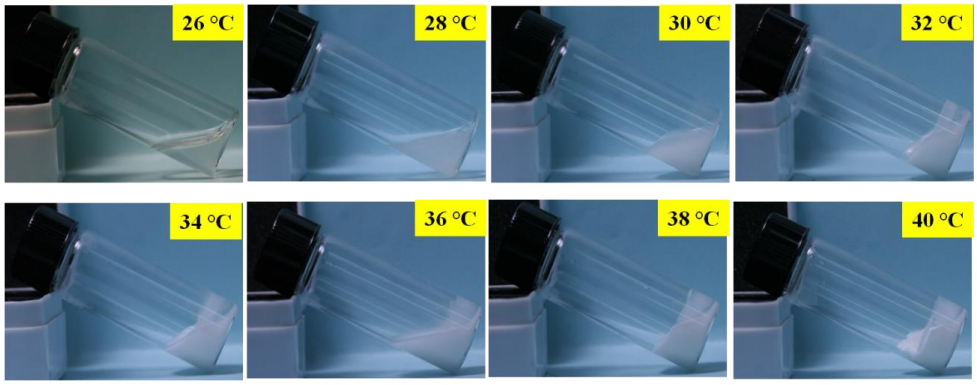

Figure III.26 Photographs of phase states of $PNIPAM_{10k}$ (15 wt.% in water) as a function of temperature (Experiment was carried out in a dry box ranging from 26 to 40 °C at 2 °C intervals, the sample was equilibrated for 5 min at a given temperature before visual observation, then the same procedure was operated at higher temperature after sample recovered to transparent state).

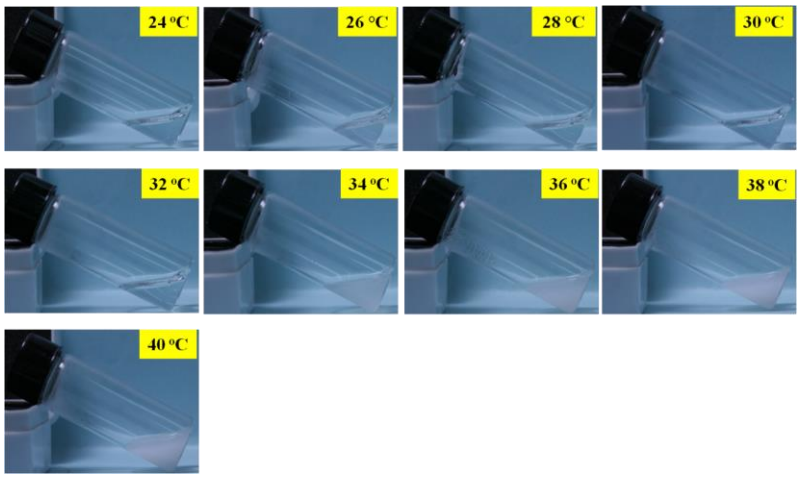

Figure III.27 Photographs of phase states of $PNIPAM_{10k}$ (10 wt.% in water) as a function of temperature (Experiment was carried out in a dry box ranging from 24 to 40 °C at 2 °C intervals, the sample was equilibrated for 5 min at a given temperature before visual observation, then the same procedure was operated at higher temperature after sample recovered to transparent state).

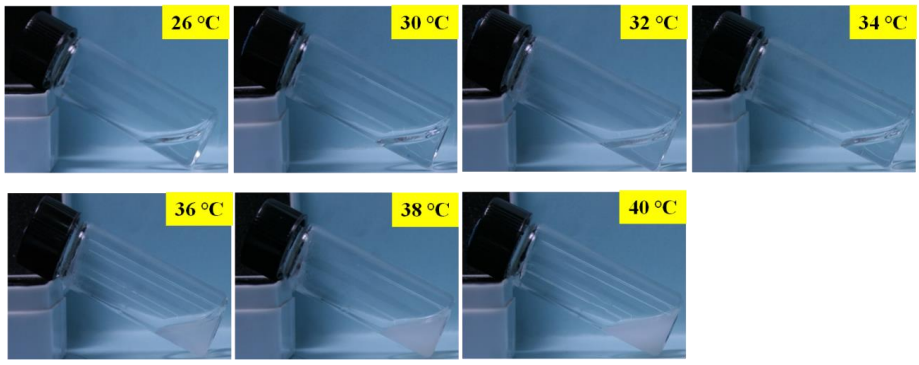

Figure III.28 Photographs of phase states of $PNIPAM_{10k}$ (5 wt.% in water) as a function of temperature (Experiment was carried out in a dry box ranging from 26 to 40 °C at 2 °C intervals, the sample was equilibrated for 5 min at a given temperature before visual observation, then the same procedure was operated at higher temperature after sample recovered to transparent state).

Photographs of $PNIPAM_{2.5k}$-*b*-PBA_{5k}-*b*-$PNIPAM_{2.5k}$ in concentration range of 5 - 20 wt.% are shown in **Figures III.29 - III.32**.

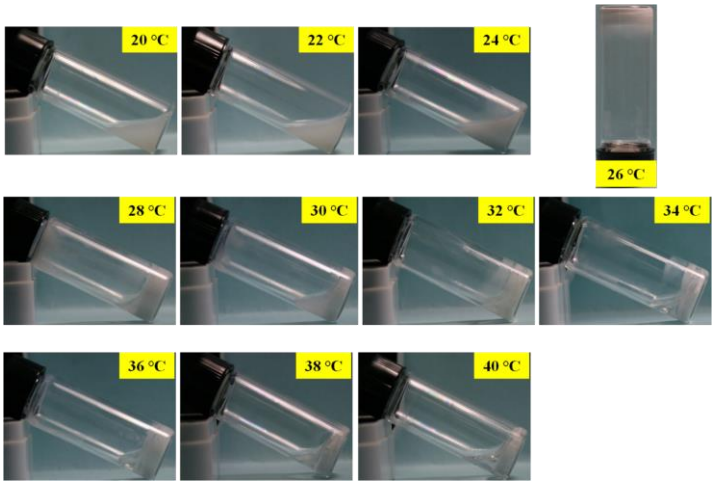

Figure III.29 Photographs of phase states of $PNIPAM_{2.5k}$-*b*-PBA_{5k}-*b*-$PNIPAM_{2.5k}$ (20 wt.% in water) as a function of temperature (Experiment was carried out in a dry box ranging from 20 to 40 °C at 2 °C

intervals, the sample was equilibrated for 5 min at a given temperature before visual observation, then the same procedure was operated at higher temperature after sample recovered to transparent state).

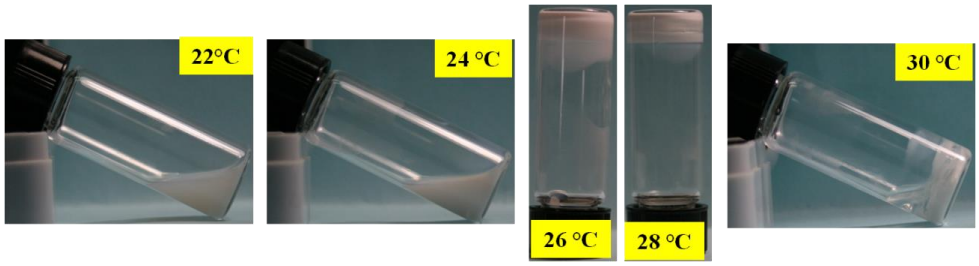

Figure III.30 Photographs of phase states of PNIPAM$_{2.5k}$-*b*-PBA$_{5k}$-*b*-PNIPAM$_{2.5k}$ (15 wt.% in water) as a function of temperature (Experiment was carried out in a dry box ranging from 22 to 30 °C at 2 °C intervals, the sample was equilibrated for 5 min at a given temperature before visual observation, then the same procedure was operated at higher temperature after sample recovered to transparent state).

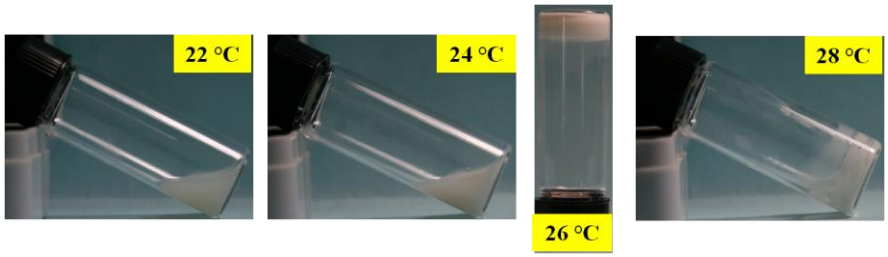

Figure III.31 Photographs of phase states of PNIPAM$_{2.5k}$-*b*-PBA$_{5k}$-*b*-PNIPAM$_{2.5k}$ (10 wt.% in water) as a function of temperature (Experiment was carried out in a dry box ranging from 22 to 28 °C at 2 °C intervals, the sample was equilibrated for 5 min at a given temperature before visual observation, then the same procedure was operated at higher temperature after sample recovered to transparent state).

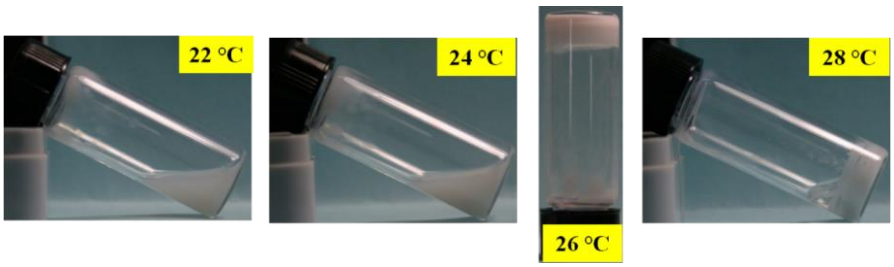

Figure III.32 Photographs of phase states of PNIPAM$_{2.5k}$-*b*-PBA$_{5k}$-*b*-PNIPAM$_{2.5k}$ (5 wt.% in water) as a function of temperature (Experiment was carried out in a dry box ranging from 22 to 28 °C at 2 °C intervals, the sample was equilibrated for 5 min at a given temperature before visual observation, then the same procedure was operated at higher temperature after sample recovered to transparent state).

Based on these measurements, a phase diagram describing the behavior of aqueous polymer solutions as a function of concentration was established and compared to the ones of PBA$_{2k}$-*b*-PNIPAM$_{8k}$ diblock copolymer (see **Figure III.33**).

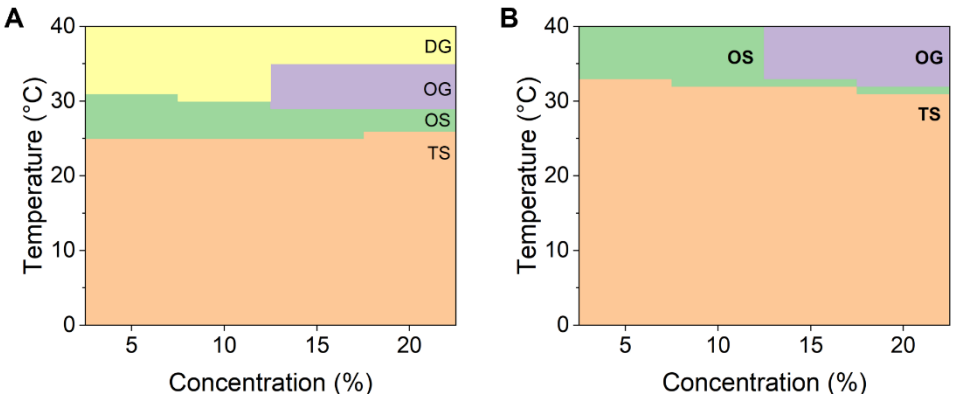

Figure III.33 Phase diagram of aqueous polymer solutions for $PNIPAM_{4k}$-*b*-PBA_{2k}-*b*-$PNIPAM_{4k}$ (A) and PBA_{2k}-*b*-$PNIPAM_{8k}$ (B) as a function of concentration.

Whereas for the homopolymer $PNIPAM_{10k}$, the formation of gel is only observed at concentrations of 15 and 20 wt.% (**Figure III.34**), for the diblock and triblock structures gel formation occurred at lower concentrations. In all cases, those gelation concentrations are found to be much higher than the entanglement concentration which can be evaluated around 3 wt.% in the case of $PNIPAM_{10k}$. [31] Interestingly the synaeresis effect inducing the formation of dehydrated gel is strongly related to the chemical structure of the (co)polymer. Whereas homopolymer and triblock copolymers present a pronounced synaeresis effect after only few minutes, diblock structure is less prone to demonstrate such an effect. Results from literature also demonstrate that gels obtained from branched or statistical structure favor the formation of gels without pronounced synaeresis effect. [12, 15] In addition to the structure effect, the effect of composition was also studied. As shown in **Figure III.34**, triblock structure of $PNIPAM_{2.5k}$-*b*-PBA_{5k}-*b*-$PNIPAM_{2.5k}$ with a higher PBA content favors the formation of gel at lower concentration (down to 5 wt.%) and displays a highly pronounced synaeresis phenomenon. This first set of experiments enables us to evidence the effect of microstructure on the macroscopic behavior in concentrated solution.

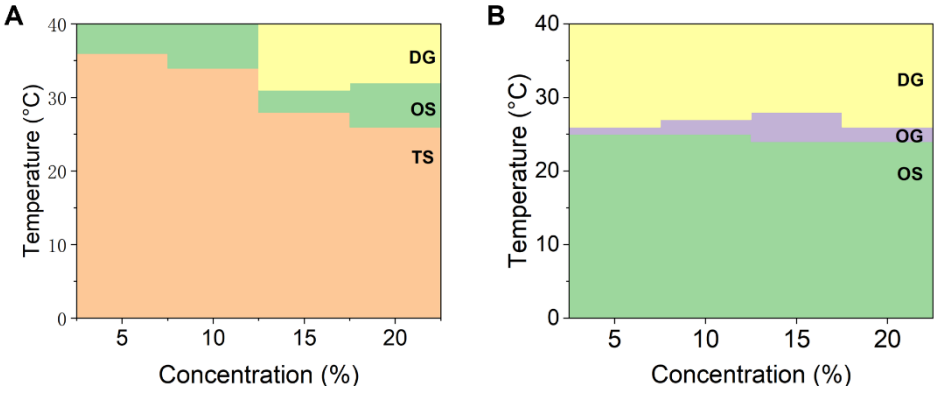

Figure III.34 Phase diagram of aqueous polymer solutions for $PNIPAM_{10k}$ (A) and $PNIPAM_{2.5k}$-*b*-PBA_{5k}-*b*-$PNIPAM_{2.5k}$ (B) as a function of concentration.

Rheological measurements provided a quantitative characterization of the mechanical changes during sol-gel transition. The elastic modulus (G') and the viscous modulus (G") were monitored from 20 to 31 °C for PNIPAM$_{4k}$-*b*-PBA$_{2k}$-*b*-PNIPAM$_{4k}$ and from 20 to 35 °C for PBA$_{2k}$-*b*-PNIPAM$_{8k}$ with 1 °C·min^{-1} heating ramp. The maximal temperatures have been selected within the OG domain, so that the gels do not undergo synaeresis during the experiment. The oscillatory stress amplitude was set at 1 Pa (**Figure III.35**) with frequency of 1 Hz. **Figure III.36** shows the variation of G' and G" along with temperature for 20 wt.% of aqueous solution of PNIPAM$_{4k}$-*b*-PBA$_{2k}$-*b*-PNIPAM$_{4k}$ and PBA$_{2k}$-*b*-PNIPAM$_{8k}$.

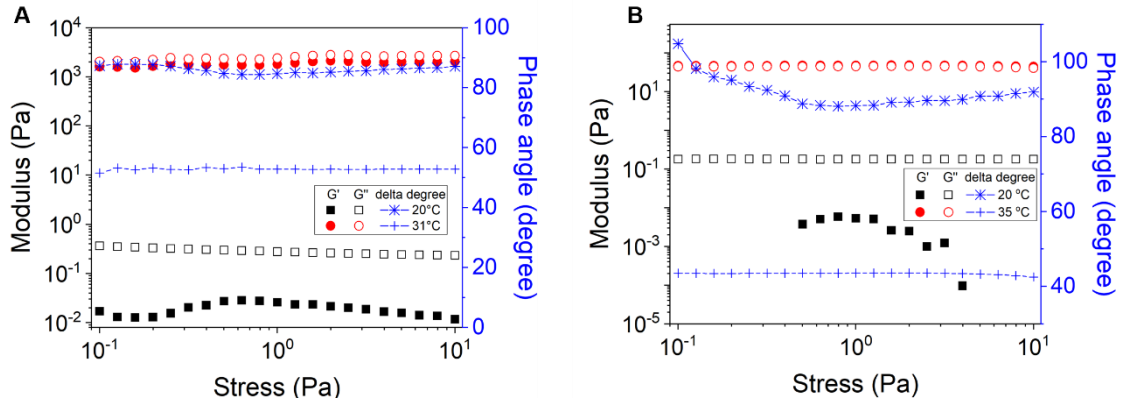

Figure III.35 Stress-dependent storage and loss moduli for (A) PNIPAM$_{4k}$-*b*-PBA$_{2k}$-*b*-PNIPAM$_{4k}$ and (B) PBA$_{2k}$-*b*-PNIPAM$_{8k}$ at lower and higher temperatures. (Copolymer concentration was 20 wt.%, heating rate was 1 °C·min^{-1}, frequency was 1 Hz. Storage modulus G': filled marks, loss modulus G": empty marks, dephasing in blue marks. These measurements highlight a large linear viscoelastic region (LVR), showing that the moduli are not affected by stress amplitude changes up to at least 10 Pa for the gel phase. For solutions at 20 °C, the LVR is shorter, extending up to around 1-2 Pa.)

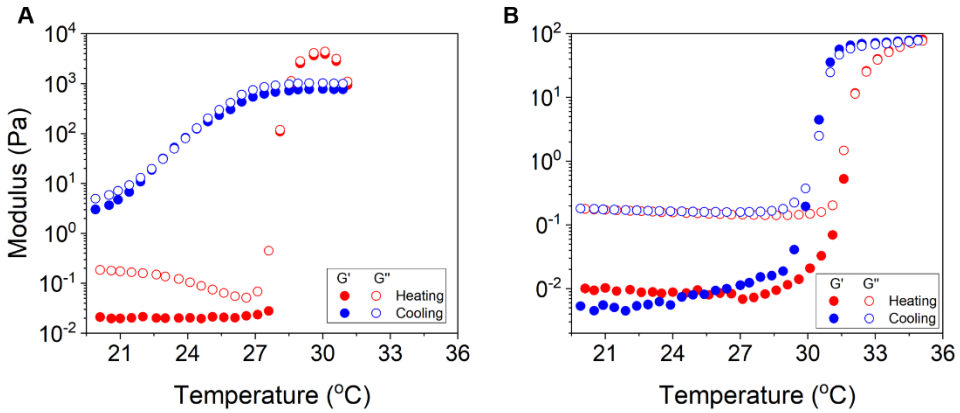

Figure III.36 Temperature-dependent storage and loss moduli for (A) PNIPAM$_{4k}$-*b*-PBA$_{2k}$-*b*-PNIPAM$_{4k}$ and (B) PBA$_{2k}$-*b*-PNIPAM$_{8k}$ solutions. (Copolymer concentrations were 20 wt.%, heating rate was 1 °C·min^{-1}, frequency was 1 Hz, stress was 1 Pa. Storage modulus G': filled marks, loss modulus G": empty marks.)

The sol-gel transition is observed at a temperature around 28 °C with a maximal modulus G' equal to 3000 Pa for PNIPAM$_{4k}$-*b*-PBA$_{2k}$-*b*-PNIPAM$_{4k}$ and 32.1 °C and 100 Pa for PBA$_{2k}$-

b-PNIPAM$_{8k}$. The measured temperatures are found slightly higher than cloud point temperatures measured by DSC measurements (25.1 and 27.6 °C for triblock and diblock structures, respectively). This might be ascribed to measurement conditions: for rheology measurements sample volume might induce inertia phenomenon and contrary to DSC measurements these values were not obtained by extrapolation of heating rate to 0 °C·min^{-1} (heating rate of 1 °C·min^{-1} used for rheology experiment). Moreover, a sufficient level of dehydration of the polymer is required in order to form the gels. Concerning the mechanical properties of obtained gels, the stiffness of the gel obtained from triblock structure is much higher than the one issued from diblock structure (G' equal to 3000 and 100 Pa respectively). These values are found significantly higher than the ones observed for homopolymer PNIPAM$_{10k}$ hydrogels at concentration of 20 wt.% (60 Pa) (see **Figure III.37**). [12]

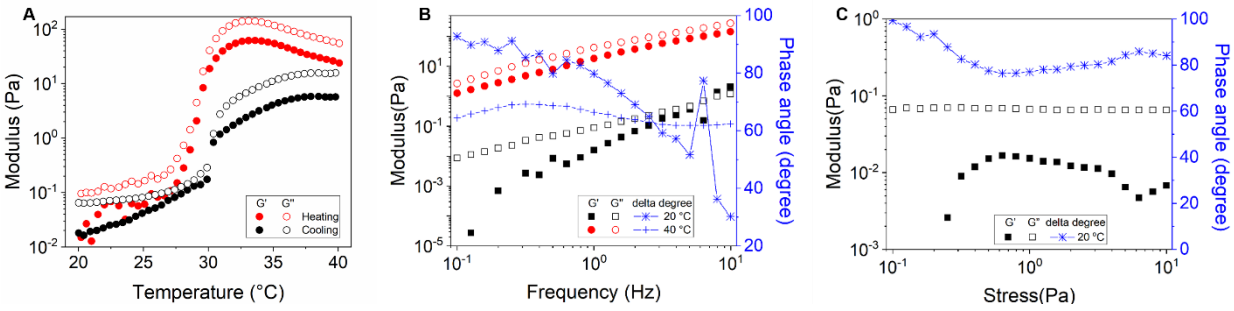

Figure III.37 (A) Temperature- (heating rate was 1 °C·min^{-1}, frequency was 1 Hz, stress was 1 Pa), (B) frequency- (stress amplitude was 1 Pa) and (C) stress-dependent (frequency was 1 Hz) storage and loss moduli of PNIPAM$_{10k}$ solution. ([PNIPAM$_{10k}$] = 20 wt.%, storage modulus G': filled marks, loss modulus G": empty marks, dephasing in blue marks.)

Before the transition, typically G" > G', while after the transition, G' becomes (slightly) higher than G" for both copolymers. In more details, the measurement of G' and G" with a frequency sweep for sol and gel phases has been performed to determine the viscoelastic nature of these phases (see **Figure III.38**). These measurements confirm the gel status for both triblock and diblock gels at 31 and 35 °C, G' and G" being nearly independent of the frequency from 10 to 0.1 Hz. Conversely, at 20 °C, when both copolymers preparations are liquid, G' and G" display a typical behavior of viscoelastic fluids that follow a Maxwell model: at low frequencies G' is proportional to $(f)^2$ and G" is proportional to f. G' and G" curves cross at a quite high frequency around 10 Hz, which gives an indication of the relaxation time of both polymer solutions, t ≈ 0.018 s (triblock) and 0.015 s (diblock). A small hysteresis effect is observed for diblock copolymer when cooling the solution to room temperature. For the triblock copolymer, a more pronounced hysteresis effect was observed that could be related to the higher viscosity and relaxation time than with the diblock copolymer that could affect the mobility of polymer

chains. Because of this large hysteresis, cycling the triblock polymer solution from 20 to 31 °C gives a good reproducibility of the sol-gel transition temperature, but G' and G" values and cooling curves (gel-sol) are more variable (see **Figure III.39**). The variability may also be related to the synaeresis effect observed with triblock structure.

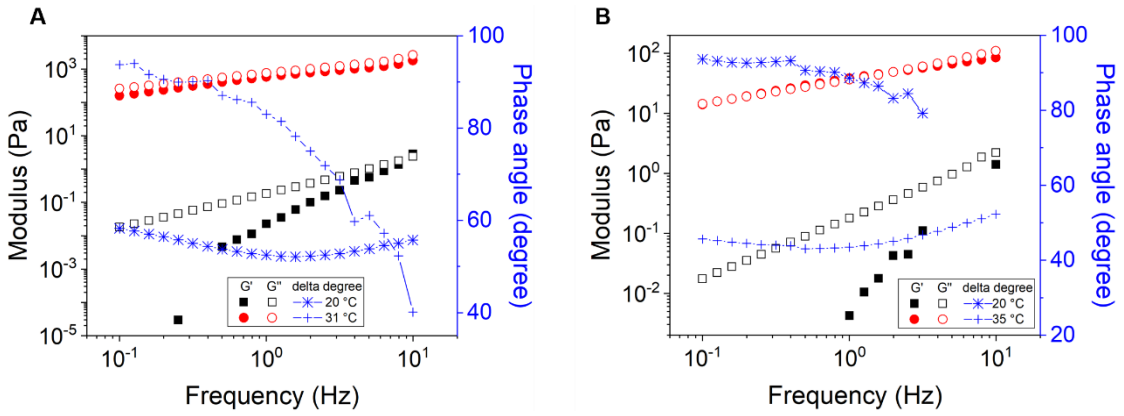

Figure III.38 Frequency-dependent storage and loss moduli of (A) $PNIPAM_{4k}$-*b*-PBA_{2k}-*b*-$PNIPAM_{4k}$ and (B) PBA_{2k}-*b*-$PNIPAM_{8k}$ solutions. (Copolymer concentrations were 20 wt.%, heating rate was 1 °C·min^{-1}, stress amplitude was 1 Pa. Storage modulus G': filled marks, loss modulus G": empty marks, dephasing in blue marks.)

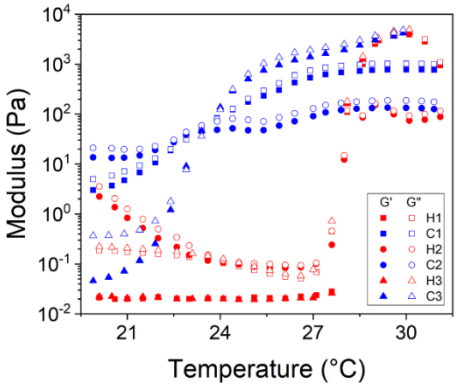

Figure III.39 Temperature cycles for $PNIPAM_{4k}$-*b*-PBA_{2k}-*b*-$PNIPAM_{4k}$ solution. (Copolymer concentration was 20 wt.%. Heating rate was 1 °C·min^{-1}, stress was 1 Pa, frequency was 1 Hz. Storage modulus G': filled marks, loss modulus G": empty marks. Heating: H1, H2, H3, cooling: C1, C2, C3.)

The properties of these hydrogels are likely to be strongly related to their internal structures. Thus, to gain insight into the network structure of hydrogels, freeze-dried samples were analyzed with scanning electron microscopy at cryogenic temperature (see **Figure III.40**).

Thus, the study of concentrated polymer solutions makes it possible to highlight the crucial effect of microstructure on macroscopic properties. For the same composition, the triblock structure leads to denser networks more likely to be the seat of important synaeresis and presents slower rehydration kinetic. The freeze-dried hydrogels show honeycomb-like microstructures with dense cell walls. Nevertheless, the cell/pore average size differs strongly, decreasing from diblock to triblock structures. Therefore, a clear relationship between molecular architecture and microstructure is evidenced: for a similar chemical composition,

triblock structure promotes denser network structure with smaller pore size. A good correlation is observed between the increase of G' modulus and the apparent density of the gels. This difference of microstructure could also explain the differences observed on synaeresis effect between diblock and triblock structures, since less dense networks might accommodate easily a large volume of solvent.

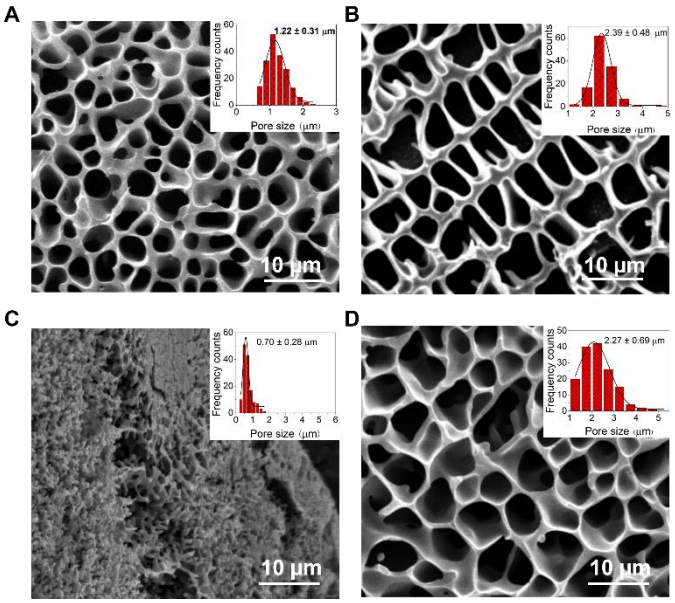

Figure III.40 Cryo-SEM images of gel structures formed at 40 °C for (A) $PNIPAM_{4k}$-*b*-PBA_{2k}-*b*-$PNIPAM_{4k}$, (B) PBA_{2k}-*b*-$PNIPAM_{8k}$, (C) $PNIPAM_{2.5k}$-*b*-PBA_{5k}-*b*-$PNIPAM_{2.5k}$ and (D) PBA_{5k}-*b*-$PNIPAM_{5k}$ (Pore size distributions are given as insets).

III.6 Thermoresponsiveness of copolymers at different conditions

Numerous studies in the past have already compared the properties of polymers with different microstructures but similar compositions in solution. For instance, solutions of statistical and block copolymers present different rheological properties. [32, 33] In the particular case of thermoresponsive polymers, branched and hyperbranched structures have been demonstrated to strongly affect the properties of PNIPAM-based polymers either in dilute conditions or in gel phase, [11, 12] and block copolymers with statistical structure present cloud point temperature more sensitive to their composition than block counterparts. [15, 34] Through this study we compared in a systematic way the effect of composition and microstructure (statistical, diblock and triblock) on properties in solution of amphiphilic thermoresponsive copolymers at different concentrations and temperatures. The transition temperature of these copolymers in solution depends, as expected, on their composition: an increase of the fraction of hydrophobic part leads to a decrease of transition temperature. This temperature also depends on the microstructure at a given composition: in comparison with block structures, the statistical

structure is detrimental, as expected, to the good hydration of hydrophilic monomers due to their microenvironment, thereby leading to a significant decrease in transition temperatures.

Below the transition temperature, block copolymers have an amphiphilic character, which leads spontaneously to the formation of colloidal structures above a critical aggregation concentration (cac) as illustrated in **Scheme III.1**. Their existence promotes the dispersibility of these copolymers in aqueous solution even at high concentration. The structure of objects formed depends in particular on the composition of block copolymer and on the preparation method used. [35] Moreover the rate of exchange of polymer chains within these objects primarily depends on the interfacial tension between hydrophobic block and water as well as the length of hydrophobic block and (co)polymer architecture. Due to a too large interfacial tension, exchanges are absent for large hydrophobic blocks as observed in the case of BA-based copolymers which lead to kinetically frozen aggregates. [36] Hence, different groups have reported that PBA-based amphiphilic block copolymers do not reorganize, or only very slowly, in spite of liquid like behavior of their hydrophobic blocks. [37-39] To induce faster exchange of polymer chains within these aggregates, copolymerization of hydrophilic units like acrylic acid in the PBA block can be used, it reduces the interfacial tension between the moderately hydrophobic block and the hydrophilic block and water. [40] Moreover, in the case of PBA-*b*-PNIPAM copolymers, the incorporation of hydrophilic units of dimethyl acrylamide within PBA block showed that decreasing degree of hysteresis is associated with the thermal transition. [20] All these results from literature suggests that, below T_c, PBA-*b*-PNIPAM diblock and PNIPAM-*b*-PBA-*b*-PNIPAM triblock structures act as frozen micelles above a critical aggregation concentration. Also as demonstrated by DLS and SANS measurements and as discussed above in **Section III.4**, compared to diblock copolymers, triblock counterparts lead to smaller and less dense frozen micellar structures with significantly lower aggregation number.

Above the transition temperature and at low concentrations, for a chosen polymer structure, the formation of colloidal aggregates (i.e. mesoglobules) is observed. These nanoobjects are issued from the dehydration of PNIPAM corona of previously described micelles. The frozen PBA core prevents further reorganization of the polymer within and between the aggregates. Thus, by decreasing temperature below T_c, a fast hydration process of PNIPAM corona is possible. This mechanism enables a fast and reversible formation of so-called mesoglobules from diblock and triblock structures. These aggregates have similar size whatever the nature of microstructure (diblock or triblock). At higher concentrations the formation of gels is observed (see **Scheme III.1**). Their formation might be related to the interconnection of dehydrated micelles in the whole solution when a sufficient concentration of nanoobjects is reached.

Diblock structures, compared to triblock structures, allows the formation of gels that are softer than triblock gels but that do not demix with time (no synaeresis). This might be ascribed to the ability of diblock structures to favor the formation of more efficiently interconnected network of dehydrated frozen micelles that have less tendency to aggregate as demonstrated in the case of dilute solutions. Triblock structures compared to their diblock counterparts form stiffer and more viscous gels, with high synaeresis and slower rehydration kinetics. These properties can be related to the nature of hydrogen-bonded network, which is denser and therefore with smaller pores due to the reception of a smaller quantity of solvent.

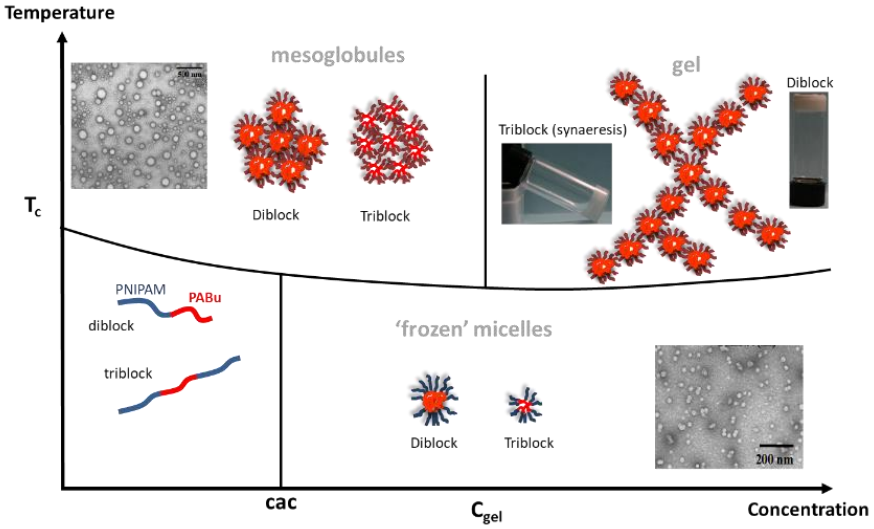

Scheme III.1 Schematic illustration of behaviour of diblock and triblock copolymers in solution as a function of concentration and temperature. For statistical copolymers, no micelle or gel were observed, only a transition towards a turbid solution above T_c.

III.7 Conclusions

The microstructural engineering of amphiphilic thermoresponsive copolymers of *n*-butyl acrylate and *N*-isopropylacrylamide allows significant modulations of self-assembly, morphological and mechanical properties of these materials in aqueous media. With similar composition, the hydrophobic acrylate monomer in block copolymers contributes to a decrease of cloud point temperatures compared to pure PNIPAM and to a much lesser extent compared to statistical structures, and enhances their solubility in aqueous solutions via self-assembly. In addition, below the cloud point temperature, block structures of appropriate composition lead to the formation of colloidal aggregates. Above this temperature, the formation of colloidal aggregates is observed at low concentration, and gels are formed at higher concentration. For a given composition, scattering experiments demonstrate that diblock structures lead to smaller colloids and mesoglobules than their triblock counterparts. Moreover, diblock copolymers lead

to larger and denser structures compared to triblock analogues and allow the formation of gels that do not demix with time (no synaeresis) but they are softer than triblock gels. While results in the literature have already demonstrated the important effect of architecture [11, 12] or microstructure [32, 33] on the properties of polymer solutions, the effect of microstructure on properties of amphiphilic polymer assemblies has been more rarely reported. [40] Our study based on a thermosensitive polymer family also shows the striking effect of microstructure related to temperature on solution-generated organizations. Further studies will concern amphiphilic gradient copolymers [41] whose intermediate microstructures between block and statistical should enable to further modulate thermoresponsiveness of polymers and to obtain micellar aggregates with improved dynamics of assembly.

III.8 References

[1] M.I. Gibson, R.K. O'Reilly, Chem. Soc. Rev. 42 (2013) 7204-7213.

[2] M. Beija, J.-D. Marty, M. Destarac, Chem. Commun. 47 (2011) 2826-2828.

[3] J. Liu, A. Debuigne, C. Detrembleur, C. Jérôme, Adv. Healthc. Mater. 3 (2014) 1941-1968.

[4] J.-F. Lutz, Ö. Akdemir, A. Hoth, J. Am. Chem. Soc. 128 (2006) 13046-13047.

[5] B. Verdonck, E.J. Goethals, F.E. Du Prez, Macromol. Chem. Phys. 204 (2003) 2090-2098.

[6] L. H. Gan, Y. Y. Gan, G.R. Deen, Macromolecules 33 (2000) 7893-7897.

[7] A.K.A.S. Brun-Graeppi, C. Richard, M. Bessodes, D. Scherman, O.-W. Merten, Prog. Polym. Sci. 35 (2010) 1311-1324.

[8] Z.M.O. Rzaev, S. Dinçer, E. Pişkin, Prog. Polym. Sci. 32 (2007) 534-595.

[9] M. Beija, J.-D. Marty, M. Destarac, Prog. Polym. Sci. 36 (2011) 845-886.

[10] R. Plummer, D.J.T. Hill, A.K. Whittaker, Macromolecules 39 (2006) 8379-8388.

[11] H.H. Nguyen, A. Brûlet, D. Goudounèche, P. Saint-Aguet, N. Lauth-de Viguerie, J.-D. Marty, Polym. Chem. 6 (2015) 5838-5850.

[12] H.H. Nguyen, B. Payré, J. Fitremann, N. Lauth-de Viguerie, J.-D. Marty, Langmuir 31 (2015) 4761-4768.

[13] S. Sistach, M. Beija, V. Rahal, A. Brûlet, J.-D. Marty, M. Destarac, C. Mingotaud, Chem. Mater., 22 (2010) 3712-3724.

[14] Z.-P. Xiao, K.-M. Yang, H. Liang, J. Lu, J. Polym. Sci. A Polym. Chem. 48 (2010) 542-550.

[15] X. Zhao, O. Coutelier, H.H. Nguyen, C. Delmas, M. Destarac, J.-D. Marty, Polym. Chem. 6 (2015) 5233-5243.

[16] A. Kermagoret, K. Mathieu, J.-M. Thomassin, C.-A. Fustin, R. Duchêne, C. Jérôme, C. Detrembleur, A. Debuigne, Polym. Chem. 5 (2014) 6534-6544.

[17] M. Destarac, A. Papon, E. Van Gramberen, K. Karagianni, Aust. J. Chem. 62 (2009) 1488-1491.

[18] A. Baranowska-Korczyc, E. Stelmach, B. Paterczyk, K. Maksymiuk, A. Michalska, J. Colloid Interface Sci. 542 (2019) 317-324.

[19] J. Škvarla, J. Zedník, M. Šlouf, S. Pispas, M. Štěpánek, Eur. Polym. J. 61 (2014) 124-132.

[20] L.D. Blackman, D.B. Wright, M.P. Robin, M.I. Gibson, R.K. O'Reilly, ACS Macro Lett. 4 (2015) 1210-1214.

[21] J.-H. Park, J.-W. Jang, J.-H. Sim, I.-J. Kim, D.-J. Lee, Y.-H. Lee, S.-H. Park, H.-D. Kim, Int. J. Polym. Sci. (2019) 3824207.

[22] M. Jacquin, P. Muller, G. Lizarraga, C. Bauer, H. Cottet, O. Théodoly, Macromolecules 40 (2007) 2672-2682.

[23] P. Lindner, T. Zemb, Neutron, North-Holland, Amsterdam. 1991, p19.

[24] A.H.E. Müller, R. Zhuang, D. Yan, G. Litvinenko, Macromolecules 28 (1995) 4326-4333.

[25] X. Wang, X. Qiu, C. Wu, Macromolecules 31 (1998) 2972-2976.

[26] S. Förster, M. Zisenis, E. Wenz, M. Antonietti, J. Chem. Phys. 104 (1996) 9956-9970.

[27] P. Kujawa, V. Aseyev, H. Tenhu, F.M. Winnik, Macromolecules 39 (2006) 7686-7693.

[28] J. Ye, J. Xu, J. Hu, X. Wang, G. Zhang, S. Liu, C. Wu, Macromolecules 41 (2008) 4416-4422.

[29] K. Van Durme, S. Verbrugghe, F.E. Du Prez, B. Van Mele, Macromolecules 37 (2004) 1054-1061.

[30] B. Li, M.E. Thompson, Phys. Chem. Chem. Phys. 20 (2018) 13623-13631.

[31] M. Füllbrandt, R. von Klitzing, A. Schönhals, Soft Matter 8 (2012) 12116-12123.

[32] W. Jakubowski, A. Juhari, A. Best, K. Koynov, T. Pakula, K. Matyjaszewski, Polymer 49 (2008) 1567-1578.

[33] M.W.M. Fijten, J.M. Kranenburg, H.M.L. Thijs, R.M. Paulus, B.M. van Lankvelt, J. de Hullu, M. Springintveld, D.J.G. Thielen, C.A. Tweedie, R. Hoogenboom, K.J. Van Vliet, U.S. Schubert, Macromolecules 40 (2007) 5879-5886.

[34] L. Hou, P. Wu, Soft Matter 11 (2015) 2771-2781.

[35] M. Dionzou, A. Morère, C. Roux, B. Lonetti, J.-D. Marty, C. Mingotaud, P. Joseph, D. Goudounèche, B. Payré, M. Léonetti, A.-F. Mingotaud, Soft Matter 12 (2016) 2166-2176.

[36] T. Nicolai, O. Colombani, C. Chassenieux, Soft Matter 6 (2010) 3111-3118.

[37] M. Jacquin, P. Muller, R. Talingting-Pabalan, H. Cottet, J.F. Berret, T. Futterer, O. Théodoly, J. Colloid Interface Sci. 316 (2007) 897-911.

[38] O. Colombani, M. Ruppel, M. Burkhardt, M. Drechsler, M. Schumacher, M. Gradzielski, R. Schweins, A.H.E. Müller, Macromolecules 40 (2007) 4351-4362.

[39] S. Garnier, A. Laschewsky, Langmuir 22 (2006) 4044-4053.

[40] E. Lejeune, M. Drechsler, J. Jestin, A.H.E. Müller, C. Chassenieux, O. Colombani, Macromolecules 43 (2010) 2667-2671.

[41] X. Liu, M. Wang, S. Harrisson, A. Debuigne, J.-D. Marty, M. Destarac, ACS Sustainable Chem. Eng. 5 (2017) 9645-9650.

Chapter IV

Synthesis, characterization and phase behavior of dual thermo- and pH-responsive block copolymer of poly(*N*-isopropylacrylamide)-*block*-poly(*N*-,*N*-diethylamino ethyl acrylamide) in aqueous solution

Contents

IV.1 Introduction

Stimuli-responsive (co)polymers [1-3] have attracted a great interest in recent years due to their ability to respond macroscopically, rapidly and reversibly to changes in their local environment, opening the way to multiple promising applications in areas from material science to biology. External stimuli can act as triggers that can be applied as chemical or physical or biological signals. Physical signals such as temperature, electric or magnetic fields, light and pressure modify the energies of chain dynamics and alter molecular interactions near critical points. Chemical signals, such as pH, [4] ionic species or biochemicals modify the conformations of polymer chains and the interactions between (co)polymer chains and solvents. Biochemical stimuli such as enzymes, [5, 6] antigens and biochemical agents contribute to promising biomedical applications such as controlled drug release.

One of the most significant class of stimuli-responsive (co)polymers are thermo-sensitive (co)polymers, [7-9] which are widely investigated due to the easy control of temperature change and the ease of their applications. This family of (co)polymers exhibits a soluble-to-insoluble phase transition at a lower critical temperature (LCST) or an insoluble-to-soluble phase transition at upper critical solution temperature (UCST). Various LCST-type thermoresponsive (co)polymers based on hydrogen bonding have been reported such as *N*-alkyl substituted polyacrylamides which represent the largest group of LCST-type thermoresponsive polymers. Typical LCST typed (co)polymers are based on the monomers of *N*-isopropylacrylamide (NIPAM), [10] *N*,*N*-diethylacrylamide (DEAM), *N*-vinylcaprolactam (VCL), [11] di(ethylene glycol) methyl ether methacrylate (DEGMA) and methyl vinyl ether (MVE) (**Scheme IV.1**).

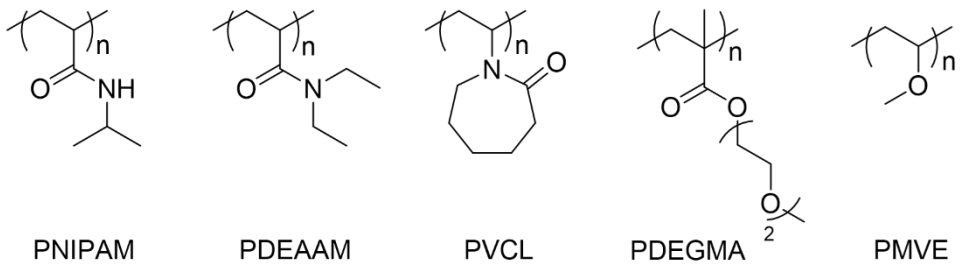

Scheme IV.1 LCST-type thermoresponsive polymers.

Among them, the most well-known and extensively studied thermoresponsive homopolymers are PNIPAM which exhibits a reversible phase transition from a hydrophilic coil state to a hydrophobic globule state as temperature increases above LCST. [12] The *N*-alkyl group in *N*-alkyl-substituted polyacrylamides is an important parameter to determine the thermo-response and phase behavior of polymer solution. For example, poly(*N*,*N*-

dimethylacrylamide) (PDMAm) is soluble in water and no LCST is detected, PNIPAM and poly(*N*,*N*-diethylacrylamide) (PDEAM) have similar LCST values of 32-33 °C, while poly(*N*-*n*-butylacrylamide) (PNNBAM) is insoluble in water (**Scheme IV.2**).

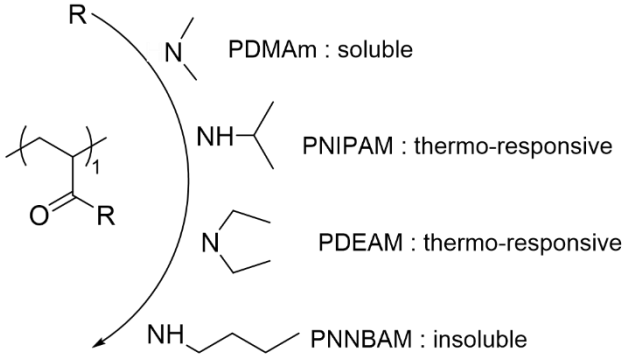

Scheme IV.2 Effect of *N*-alkyl group in *N*-alkyl-substituted polyacrylamides on thermoresponsive properties in aqueous solution.

Recently different families of homopolymers bearing a tertiary amine function grafted on poly((meth)acrylate)s and poly((meth)acrylamide)s main chains have been studied [13] as illustrated in **Scheme IV.3**. The presence of tertiary amine moieties exhibits pH-responsive characteristics due to their reversible protonation/deprotonation processes, and enables these polymers to combine thermo- and pH-responsive (soluble in acidic solution and insoluble in alkaline media) properties. [14] Depending on the nature of alkyl chains, these families of polymers present either pH or dual pH- and thermo-responsive properties. [15] Among them, poly(2-(dimethylamino) ethyl methacrylate) (PDMAEMA) is the most commonly studied due to its commercially available monomer. Additionally, PDMAEMA is a weak polybase partially protonated in a physiological solution owing to the p*K*a of around 7.4. Thanks to the inherent cationic charge, the polymer has potential to be a gene transfer agent. [16]

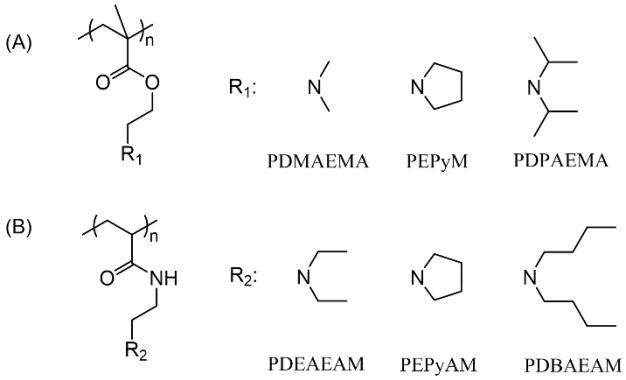

Scheme IV.3 Dual thermo- and pH-responsive homopolymers bearing tertiary amine moieties based on (A) poly((meth)acrylate)s and (B) poly((meth)acrylamide)s structure. (PDMAEMA: poly(2-(dimethylamino) ethyl methacrylate), [17] PEPyM: poly(*N*-ethylpyrrolidine methacrylate), [18] PDPAEMA: poly(2-(diisopropylamino) ethyl methacrylate), [15] PDEAEAM: poly(*N*,*N*-diethylamino

ethyl acrylamide), [14] PEPyAM: poly(*N*-(ethylpyrrolidine) acrylamide), [14] PDBEAM: poly(*N*-(2-(dibutylamino) ethyl) acrylamide). [14])

To prepare multi-responsive (co)polymers, one strategy is to develop multi-responsive homopolymers. However, very rare examples have been reported certainly due to the laborious synthesis of the monomers containing at least two differently functional moieties. For example, Huang et al. have described the synthesis of a homopolymer by polymerization of a dual responsive monomer containing both isopropylacrylamide and *N*,*N*-diethylaminoethyl moieties in the side chain. [19] The LCST of this homopolymer can be tuned by changing pH value of aqueous solution, and it increases with the degree of protonation of the tertiary amine groups. Another strategy widely documented is to combine several stimuli-responsive moieties within random, block, gradient or graft copolymers containing two or more than two stimuli-responsive segments or blocks. Diblock copolymers consisting of one thermoresponsive block (PNIPAM) and one pH-responsive block bearing tertiary amine moieties (i.e. poly(2-dimethylamino) ethyl acrylate) (PDMAEA), [20] PDEAEMA… [21, 22]) have been reported with tunable self-assemblies in aqueous media upon variation of solution pH and temperature.

In this chapter, we aimed at studying a family of block copolymers comprising of a thermo-responsive PNIPAM block and a doubly thermo- and pH-responsive PDEAEAM block (**Scheme IV.4**). These (co)polymers were synthesized by RAFT polymerization and characterized by different techniques (such as Nuclear Magnetic Resonance (NMR), Size Exclusion Chromatography (SEC), Differential Scanning Calorimetry (DSC) and Fourier Transform Infrared Spectroscopy (FTIR)). The effect of macromolecular parameters (i.e. composition) and pH on the thermoresponsive properties of these polymers in aqueous solution was studied, the self-organization behaviors upon variations of pH and temperature were also investigated. Within the frame of this study, we also highlighted the critical effect of functional end-groups coming from chain transfer agent on these properties.

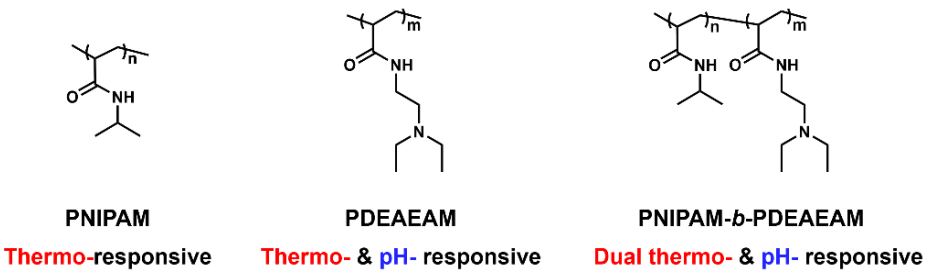

Scheme IV.4 PNIPAM, PDEAEAM and PNIPAM-*b*-PDEAEAM studied in this chapter.

IV.2 Synthesis and characterization of homo- and copolymers

DEAEAM monomer was synthesized according to a previously described synthetic pathway. [24] Well-defined thermo- and pH-responsive diblock copolymers comprising of PNIPAM and PDEAEAM blocks were further successfully synthesized by reversible addition-fragmentation chain transfer radical (RAFT) polymerization using 2,2'-azobisisobutyronitrile (AIBN) as free-radical initiator and 4-cyano-4-[(dodecylsulfanylthiocarbony) sulfanyl] pentanoic acid (CDTPA) as RAFT agent. This chain transfer agent (CTA) was chosen due to its known reactivity for both monomers leading to a well control of polymerization. [23, 24] It is noteworthy that the CTA used introduces a dodecyl and a carboxyl terminal groups which affect the properties of polymers (*vide infra*). The synthetic routes are illustrated in **Scheme IV.5**. Through tuning the feed ratio of monomer and CDTPA, a series of PNIPAM-*b*-PDEAEAM with different compositions were obtained: $PNIPAM_{2k}$-*b*-$PDEAEAM_{8k}$, $PNIPAM_{5k}$-*b*-$PDEAEAM_{5k}$ and $PNIPAM_{8k}$-*b*-$PDEAEAM_{2k}$. Corresponding homopolymers of PNIPAM and PDEAEAM with different molecular weights (2k, 5k, 8k and 10k) were also synthesized by using the same CTA. All PNIPAM, PDEAEAM and PNIPAM-*b*-PDEAEAM are abbreviated as PN, PD and PN-*b*-PD, respectively.

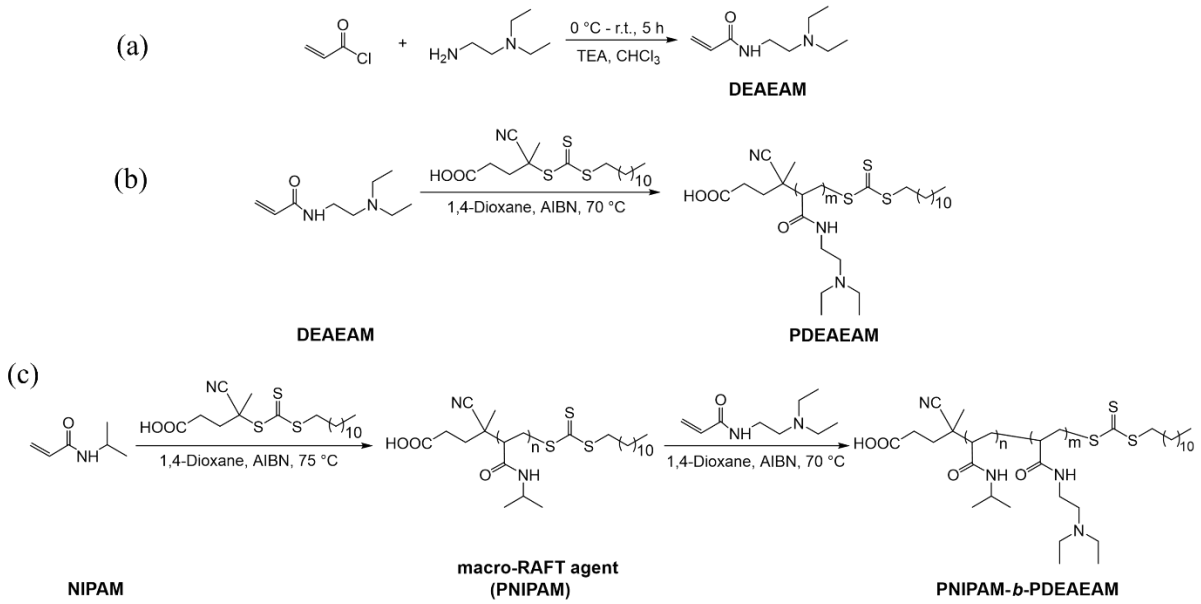

Scheme IV.5 Synthetic routes of (a) monomer of DEAEAM, (b) PDEAEAM homopolymer and (c) $PNIPAM_n$-*b*-$PDEAEAM_m$ (n/m values for block copolymers studied in this chapter are 2k/8k, 5k/5k and 8k/2k).

The successful preparation of DEAEAM was confirmed by ^{1}H and ^{13}C NMR spectra (see **Figure IV.1**), which are in good agreement with the results reported in the literature. [23]

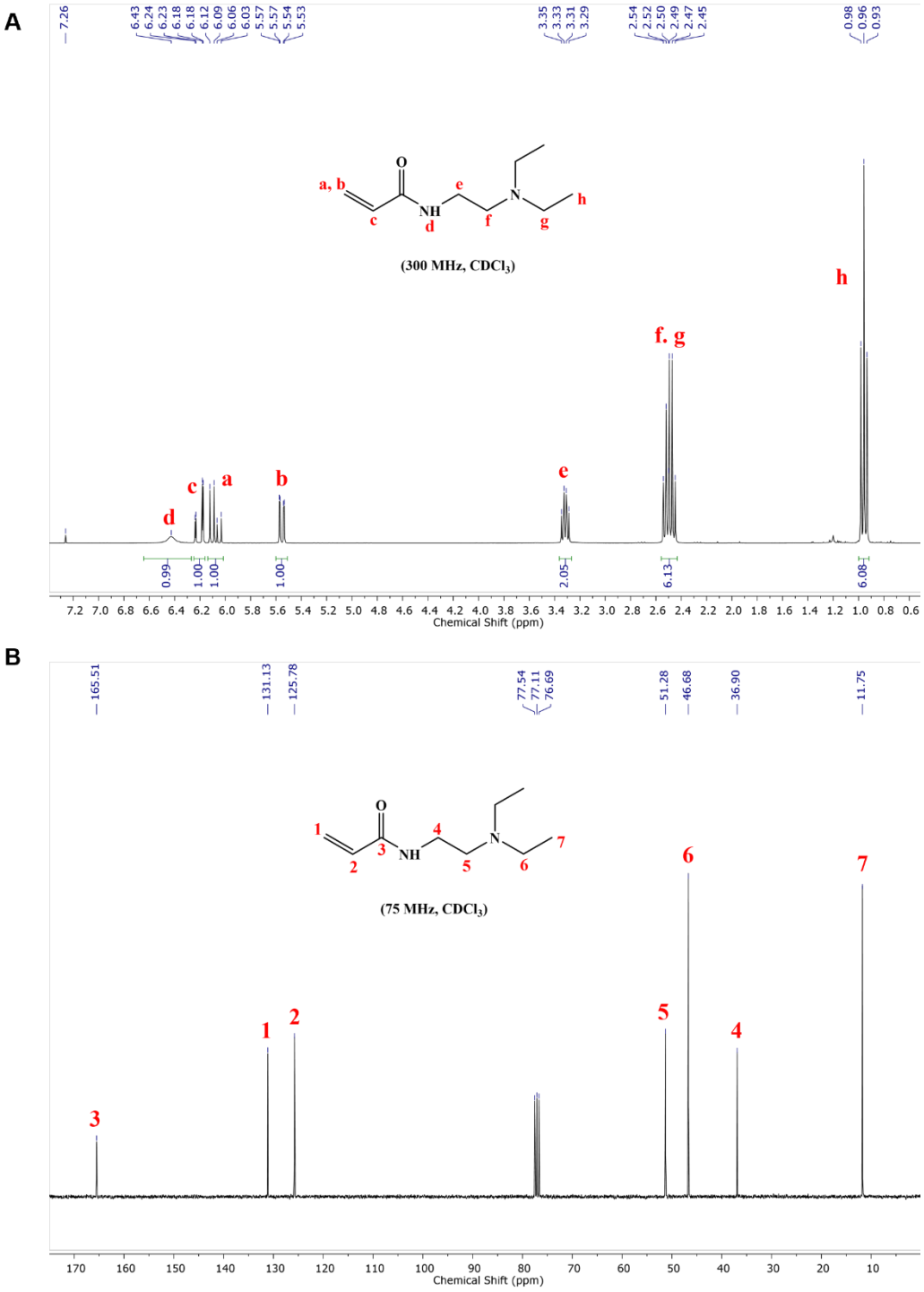

Figure IV.1 ^{1}H and ^{13}C NMR spectra of DEAEAM in $CDCl_3$.

The successful polymerization of DEAEAM from PN_{5k} macro-RAFT agent (synthetic route described in **Experimental Section**) is assessed from ^{1}H NMR experiments, in which the spectrum of PN_{5k}-*b*-PD_{5k} shows both characteristic peaks of PN_{5k} and PD_{5k} (**Figure IV.2**).

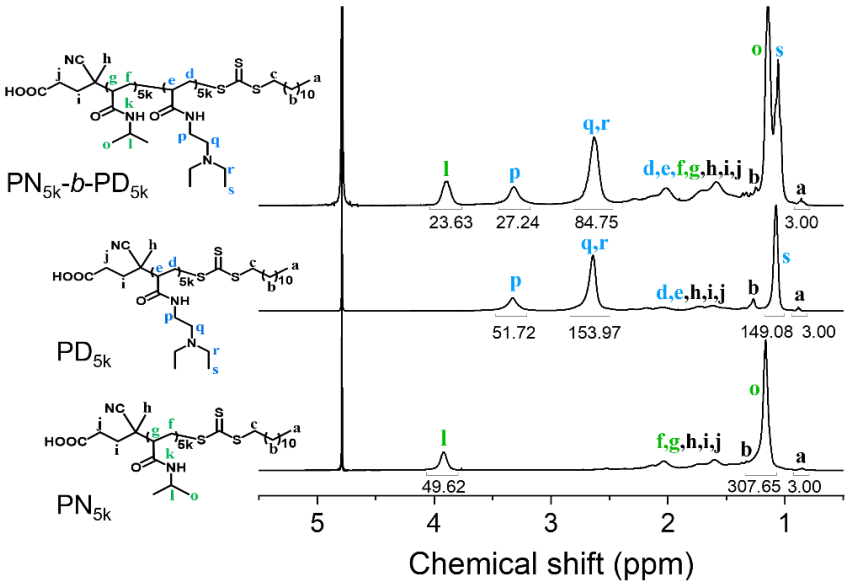

Figure IV.2 ^{1}H NMR spectra of PN_{5k} (bottom), PD_{5k} (middle) and PN_{5k}-*b*-PD_{5k} (top) in D_2O.

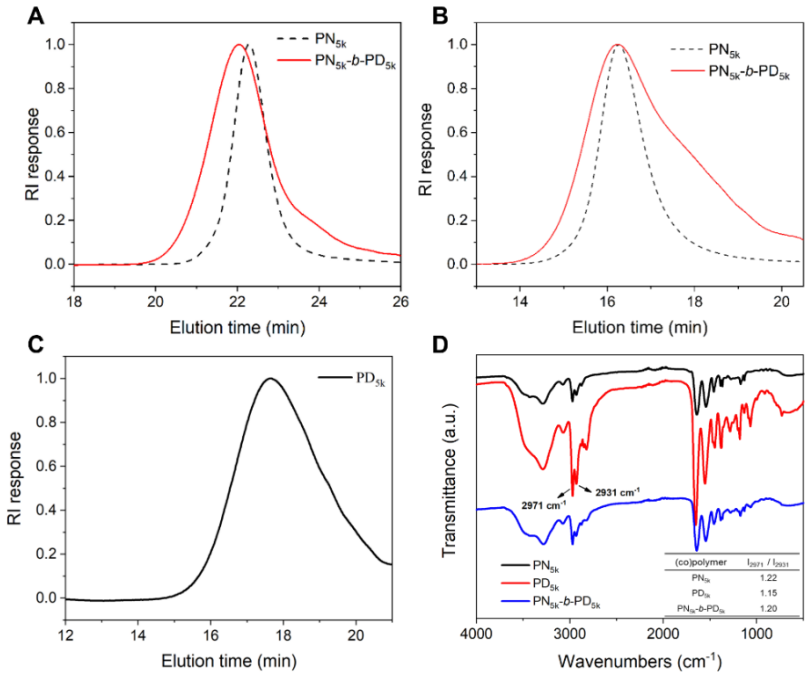

Figure IV.3 SEC chromatograms of PN_{5k}, PN_{5k}-*b*-PD_{5k} (A) in DMF (containing 10 mM LiBr) and (B) in THF (containing 2 v% TEA) and (C) PD_{5k} in THF (containing 2 v% TEA). (D) FTIR spectra of PN_{5k}, PD_{5k} and PN_{5k}-*b*-PD_{5k}. (Values in the Table corresponding to the ratio of the intensity of asymmetric C-H stretch band for CH_3 (around ν=2971 cm^{-1}) and the intensity of asymmetric C-H stretch band for CH_2 (around ν=2931 cm^{-1}), eluent flow rate for SEC measurements was 1 mL·min^{-1})

The molecular weight of PN_{5k}-*b*-PD_{5k} is calculated from ^{1}H NMR spectrum by comparing integration areas of peak **a** corresponding to methyl protons of dodecyl end group at 0.88 ppm to signals of **l** and **p** protons at 3.92 and 3.33 ppm, corresponding to PN (peak **l**) and PD (peak **p**), respectively. The molecular weight is also determined by SEC chromatograms, both THF (containing 2 v%) and DMF (containing 10 mM LiBr) eluents were used. Compared to the

macro-RAFT agent PN_{5k}, a clear shift of elution peak of PN_{5k}-*b*-PD_{5k} towards high molecular weight is evidenced in DMF solution (**Figure IV.3A**) but not in THF solution (**Figure IV.3B**). Additionally, SEC traces of PD homopolymers in THF show a broad elution peak (**Figure IV.3C**), which is ascribed to the interaction between the nitrogen-containing polymer and SEC columns as discussed elsewhere. [25] This hampers the precise determination of molecular weights of both PD_{5k} homopolymers and PN_{5k}-*b*-PD_{5k}. Consequently, a clear shift of elution peak in the latter case is not always detected when compared to macro-RAFT agent of PN homopolymers. Lastly FTIR spectra (**Figure IV.3D**) also presents characteristics peaks of PN_{5k}, PD_{5k} and PN_{5k}-*b*-PD_{5k}.

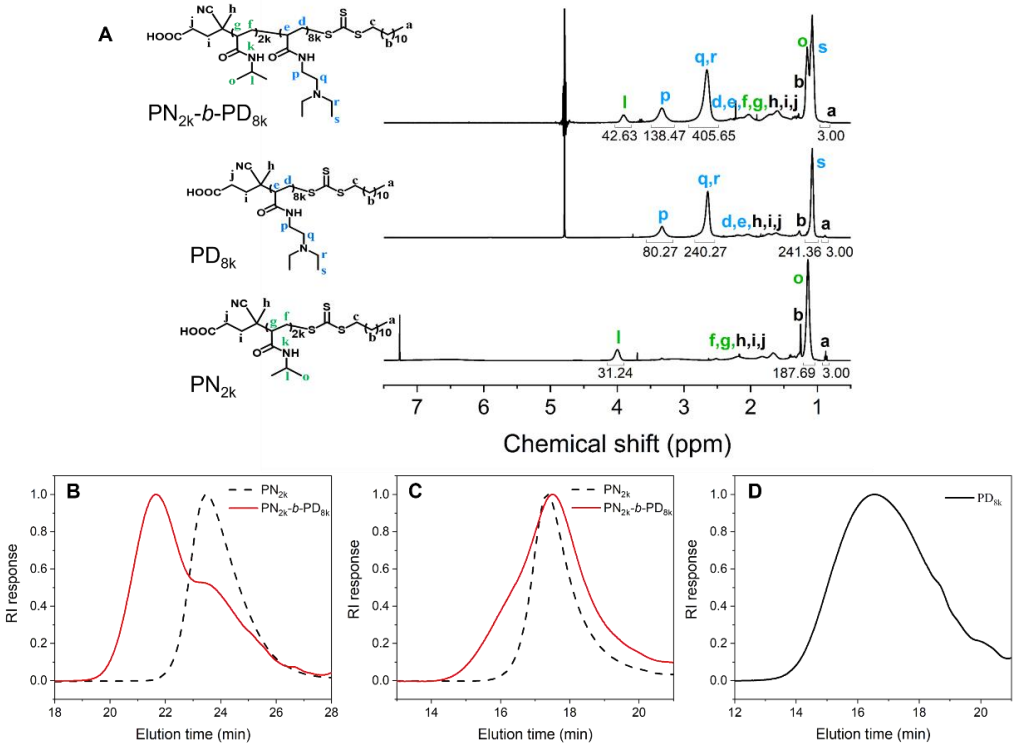

Figure IV.4 (A) ^{1}H NMR spectra of PN_{2k} (bottom), PD_{8k} (middle) and PN_{2k}-*b*-PD_{8k} (top) in D_2O. SEC curves of PN_{2k}, PN_{2k}-*b*-PD_{8k} (B) in DMF (containing 10 mM LiBr) and (C) in THF (containing 2 v% TEA) and (D) PD_{8k} in THF (containing 2 v% TEA). (Eluent flow rate for all SEC measurements was 1 mL·min^{-1})

By using the same synthetic methods, diblock copolymers of PN_{2k}-*b*-PD_{8k} and PN_{8k}-*b*-PD_{2k} were successfully prepared and characterized by ^{1}H NMR and SEC techniques as shown in **Figures IV.4 and IV.5**.

Detailed information on synthesized diblock copolymers and their corresponding reference homopolymers are summarized in **Table IV.1**.

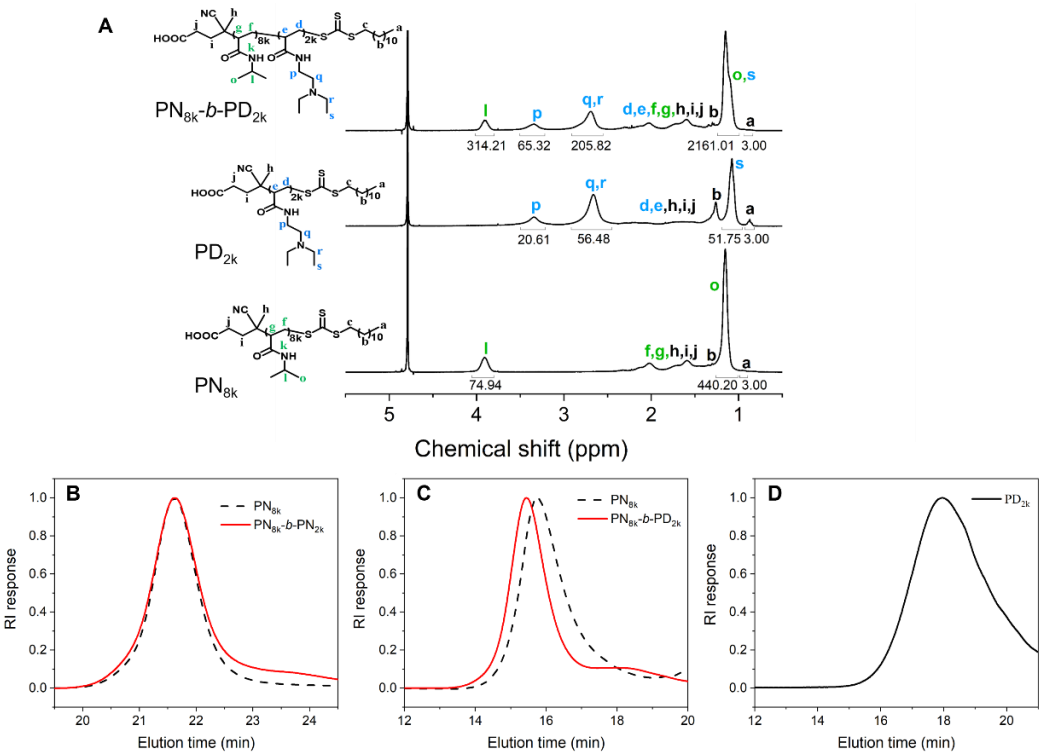

Figure IV.5 (A) ^{1}H NMR spectra of PN_{8k} (bottom), PD_{2k} (middle) and PN_{8k}-*b*-PD_{2k} (top) in D_2O. SEC curves of PN_{8k}, PN_{8k}-*b*-PD_{2k} (B) in DMF (containing 10 mM LiBr) and (C) in THF (containing 2 v% TEA) and (D) PD_{2k} in THF (containing 2 v% TEA). (Eluent flow rate for all SEC measurements was 1 mL·min^{-1})

Table IV.1 Main characteristics of synthesized (co)polymers.

(Co)polymer	DP_{PN}/DP_{PD} (theo.)	Conv. [a] (%)	T_g [b] (°C)	M_n			Đ[d]
				$M_{n,theo}$[c] (g·mol^{-1})	$M_{n,NMR}$ (g·mol^{-1})	$M_{n,SEC}$[d] (g·mol^{-1})	
PN_{2k}	14/0	97.0	85.9	1950	3940	2840 (1880)	1.02(1.09)
PN_{5k}	41/0	99.9	104.3	5000	6130	6080 (4720)	1.06 (1.03)
PN_{8k}	67/0	99.6	116.2	7970	8880	9090 (7210)	1.07 (1.04)
PN_{10k}	84/0	98.9	129.4	9890	12280	12230(10010)	1.09 (1.04)
PN_{2k}-*b*-PD_{8k}	14/43	90.8	51.9	9290	12580	9860 (8940)	1.32 (1.14)
PN_{5k}-*b*-PD_{5k}	41/28	96.6	54.6	9840	11090	8340 (6860)	1.09 (1.16)
PN_{8k}-*b*-PD_{2k}	67/9	78.5	72.3	9480	10220	10720 (9120)	1.08 (1.01)
PD_{2k}	0/10	99.8	31.5	2000	2160	(2500)	(1.06)
PD_{5k}	0/26	95.4	30.2	4790	4810	6900 (4210)	1.21 (1.09)
PD_{8k}	0/40	96.0	35.1	7290	8830	7820 (7210)	1.63 (1.41)
PD_{10k}	0/52	93.5	24.5	9350	9080	10740 (7730)	1.37 (1.19)

[a] Conversion determined by ^{1}H NMR spectra; [b] T_g measured by DSC with a heating rate of 10 °C·min^{-1}; [c] $M_{n,theo}$ = ([Monomer]$_0$/[RAFT]$_0$) × M_n(Monomer) × (Conv./%) + M_n(RAFT); [d]$M_{n,SEC}$ and Đ determined by SEC analysis in DMF with 10 mM LiBr (in THF containing 2 v% TEA).

IV.3 Thermoresponsive behavior of homopolymer solutions

To understand the thermoresponsive properties (phase transition temperature and self-organization behavior) of PN-*b*-PD under different conditions, the thermosensitive behaviors of PN and PD homopolymer solutions were investigated firstly.

IV.3.1 PN homopolymer

PNIPAM is by far the most commonly described thermoresponsive homopolymer. Incorporation of hydrophilic or hydrophobic comonomers enables to finely tune cloud point temperature (T_c) as stated in **Chapter I**. [26, 27] For example, when NIPAM is statistically copolymerized with hydrophilic monomers such as acrylamide, T_c increases up to about 45 °C when the polymer chain comprises 18 mol% acrylamide, whereas T_c decreases to around 26 °C when 20 mol% hydrophobic acrolein is incorporated into the polymer chain. [26] To a lesser degree, similar effects are observed in the cases of (co)polymers with various architectures (block, branched…). [27-29] Interestingly terminal groups also have a strong influence: hydrophobic terminal groups decrease T_c, whereas hydrophilic ones tend to have a reverse effect. [30] In the case of ionizable end groups, their hydrophilicity varies with the proportion of ionized form related to pH range. The more the ionized form is present and the more the hydrophilicity of the end of chain is marked, T_c of (co)polymer will be increased.

Here, synthesized PN_{xk} homopolymer chains contain, at pH 4, one hydrophilic carboxylic acid function on one side and a hydrophobic -$C_{12}H_{25}$ group on the other side (**Scheme IV.6**). These two groups play a key role in thermoresponsive property of PN_{xk} homopolymers in aqueous solution.

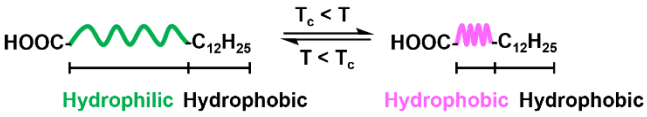

Scheme IV.6 Structure and effect of temperature on the conformation of PN chains at pH 4.

At pH 4, the measurement of T_c for 1 wt.% aqueous solutions of PN_{xk} by DLS, turbidity and DSC measurements shows a non-linear increase of T_c from 16 to 29 °C when molecular weight increases from 2000 to 10000 g·mol^{-1} (**Figure IV.6A**). The observed tendency is mainly ascribed to the nature of terminal group. For PN_{2k}, the hydrophobic -$C_{12}H_{25}$ tail group affects the solubility behavior and weakens the solvation of PN homopolymer in water, causing T_c of PN_{2k} shifts toward lower temperature. This effect is highly pronounced for polymers with low molecular weight, however, it is much less remarkable when polymer chains are lengthened or

become longer. [31] Polymer concentration has a drastic effect on T_c, for PN_{5k} with a concentration of 1 wt.%, T_c is measured at 28 °C and this value increases to 32 °C as concentration decreases to 0.1 wt.% (values obtained by DLS and transmittance measurements, see **Figures IV.6B and IV.6C**). Indeed, polymer chains entanglement promotes the formation of large aggregates at higher concentration. PN_{2k} has T_c value below 10 °C at concentration of 1 wt.%, its T_c determination by DLS and turbidity measurements could not be properly measured (**Figure IV.6A**). For DSC measurement, PN homopolymers with a concentration of 1 wt.% were tried, it turns out that signals of endothermic curves are too weak to be evaluated with precision. Therefore, PN concentration was raised to 20 wt.% for accurate analysis. Meanwhile, one point should be noted that increasing concentration tends to lower T_c.

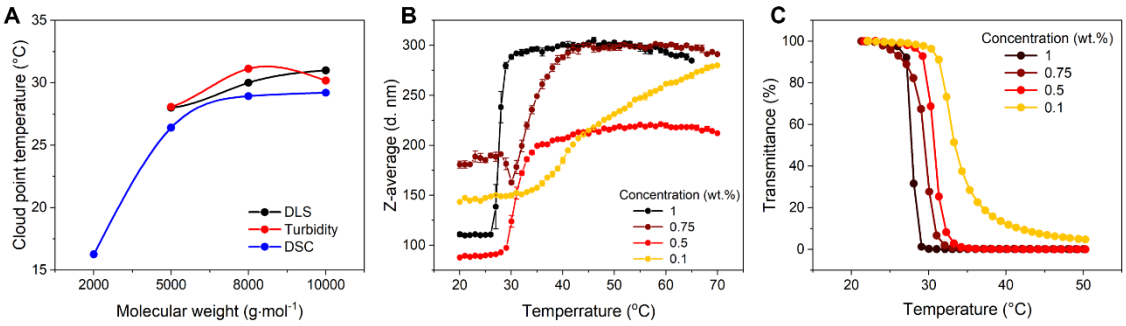

Figure IV.6 (A) T_c values of PN homopolymers in aqueous solutions determined by DLS, turbidimetry and DSC measurements upon heating (pH values of PN_{5k}, PN_{8k} and PN_{10k} at concentration of 1 wt.% were 4.6, 4.3 and 4.3, respectively. PN concentration used for DLS, turbidity and DSC measurements were 1, 1 and 20 wt.%, respectively). (B) Aggregates size change and (C) transmittance change of PN_{5k} as a function of temperature at different concentrations (pH ≈ 4, heating rate for turbidimetry measurement was 1 °C·min^{-1}).

As stated above, one extremity of the polymer bears a carboxylic function. It possesses a p*K*a value around 4.5 and therefore a modification of pH will induce a change of ionization/hydration state of this function and of the studied polymers. Consequently, a change in T_c of synthesized PN is expected. Thus, the thermoresponsive character of PN_{5k} at different pH was studied by turbidimetry measurement (see **Figure IV.7B**). In pH range from 3 to 6, PN_{5k} displays a clear LCST behavior, and its corresponding T_c value increases from 25.1 to 40.1 °C. Further increasing pH value, the transmittance at 70 °C no longer declines to 0 but approaches 44, 52 and 86% at pH 7, 8 and 9, respectively. When pH raises to 10, there is no detectable decrease in transmittance curve. In order to confirm the critical role of end group in the observed behavior, a PN homopolymer was synthesized from a different RAFT agent, namely 2-mercaptopropionic acid methyl ester *O*-ethyl dithiocarbonate (xanthate **X1**). No pH-dependance of thermoresponsive behavior is observed for this homopolymer (**Figure IV.7C**), which confirms the critical role of end groups.

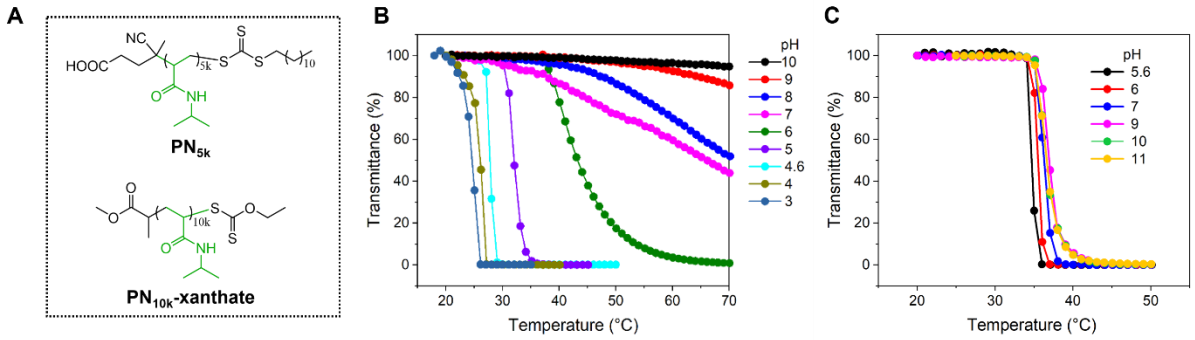

Figure IV.7 (A) Chemical structures of PN homopolymers synthesized by using different RAFT agents. Transmittance change of (B) PN_{5k} and (C) PN_{10k}-xanthate *versus* temperature at different pH values ([PN] = 1 wt.%, heating rate: 1 °C·min^{-1}).

The pH-dependence of T_c can be attributed to the degree of ionization of -COOH end group. Compared to -COOH group, -COO^- has a better solvation and helps to improve PN_{5k} solubility in water. With rising pH, the amount of -COO^- groups in solution becomes larger and results in an increase of T_c value. Such trend was previously reported in the cases of linear and star-type PN homopolymers terminated with -COOH or ionizable groups ($pKa_{COOH} = 4.5 \pm 0.1$). [24, 30, 32] In addition, the absence of transition observed at high pH value is ascribed to the formation of micellar system which hinders phase separation. For instance, PN polymers synthesized by RAFT polymerization using S-1-dodecyl-S-(α,α'-dimethyl-α,α'-acetic acid) trithiocarbonate as a chain transfer agent form micelles in aqueous solution with a core of hydrophobic terminal dodecyl groups and a corona of PN chains with carboxylic groups at the periphery, the ionization of which prevents phase separation of PN at temperature above T_c. Instead, a sphere-to-rod transition of micelles was observed by SANS. [30] In order to confirm the formation of micellar system and the critical role of end group, DLS measurements were performed as a function of temperature at two different pH values (4 and 10) and the behavior of PN_{5k} was compared to that of PN_{10k}-xanthate (without carboxylic acid end-group and long alkyl chain).

At pH 10, PN_{10k}-xanthate presents a transition at 35 °C that induces the formation of large aggregates (size around 500 nm) starting from aggregates around 70 nm. PN_{5k} displays a completely different behavior. Indeed, it forms poorly defined nanoobjects in low temperature range (20 - 32 °C) and forms small defined objects with an average diameter around 10 nm as temperature rises to 33 °C. (**Figure IV.8A**). Moreover, whatever the temperature (below or above T_c), a highly negative zeta potential is measured around -45 mV (**Figure IV.8B**), which is in agreement with nanoobjects bearing carboxylate function as an outer shell.

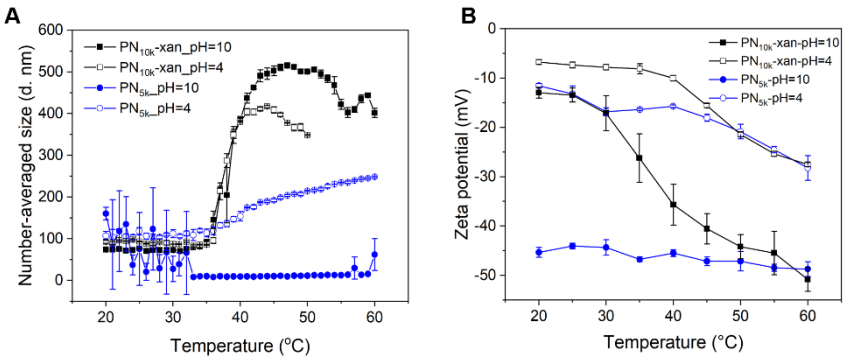

Figure IV.8 (A) Number-averaged size and (B) Zeta potential as a function of temperature for PN_{10k}-xanthate and PN_{5k} at pH 4 and 10, respectively ([PN] = 0.1 wt.%).

These measurements suggest the formation of micellar system stabilized by negatively charged carboxylate functions since increasing temperature results in contraction of PN chains as illustrated in **Scheme IV.7**.

At pH 4, both PN_{10k}-xanthate and PN_{5k} present clear phase transitions, which can be judged by the aggregates size change as a function of temperature, large aggregates (size of 400 and 250 nm for PN_{10k}-xanthate and PN_{5k}, respectively) are formed when temperature increases to 60 °C (**Figure IV.8A**). As expected from partial protonation of carboxylate functions, zeta potential values around -10 mV is found for PN_{5k}: this lower zeta potential does not enable to obtain stable colloidal structures and favored aggregation process upon heating.

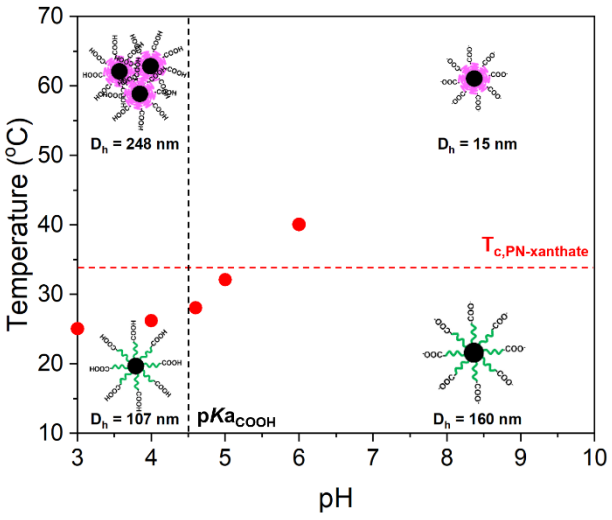

Scheme IV.7 Schematic illustration of T_c and self-assemblies of PN_{5k} at different pH values (T_c: red solid circle. 1 and 0.1 wt.% of PN_{5k} used for T_c and hydrodynamic diameter determinations, respectively).

IV.3.2 PD homopolymer

PD homopolymer is a weak polyelectrolyte, fully soluble in water whatever the pH at low temperature. The p*K*a value of pendant tertiary amine groups is calculated from pH titration

curve (**Figure IV.9**) and a value of 7.25 is found. This value is significantly lower than the one measured for the corresponding monomer (DEAEAM) at 9.17 and is close to the p*K*a values measured for PDEAEMA and PDMAEMA at 7.5 and 7.4 respectively. [33] At pH below pKa_{PD}, PD is fully protonated, increasing pH induces a decrease of degree of charging of the polymer. Moreover, it is noted that the carboxylic end group is in its deionized form at pH below pKa_{COOH}.

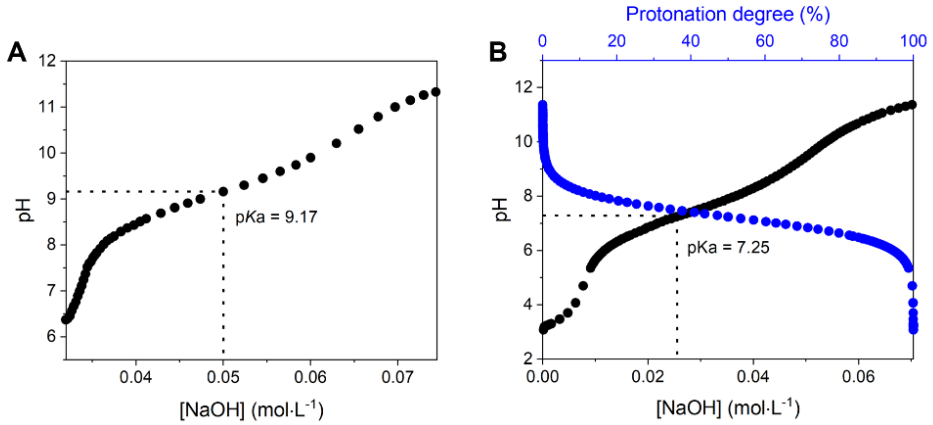

Figure IV.9 Titration curve of (A) DEAEAM monomer and (B) PDEAEAM homopolymer (along with protonation degree).

Transmittance change of aqueous solution of PD_{5k} was then measured as a function of temperature (20 - 70 °C) as pH increased from 3 to 10. No thermoresponsiveness is detected in the studied temperature range when pH is lower than 9. Interestingly for higher pH, deprotonation of tertiary amine promotes thermoresponsive properties of PD_{5k} in water (see **Figure IV.10A** and top of **Scheme IV.8**). PD_{5k} solution has a T_c equal to 60 °C at pH 9 then drops sharply to reach a value of 32 °C at pH 10.

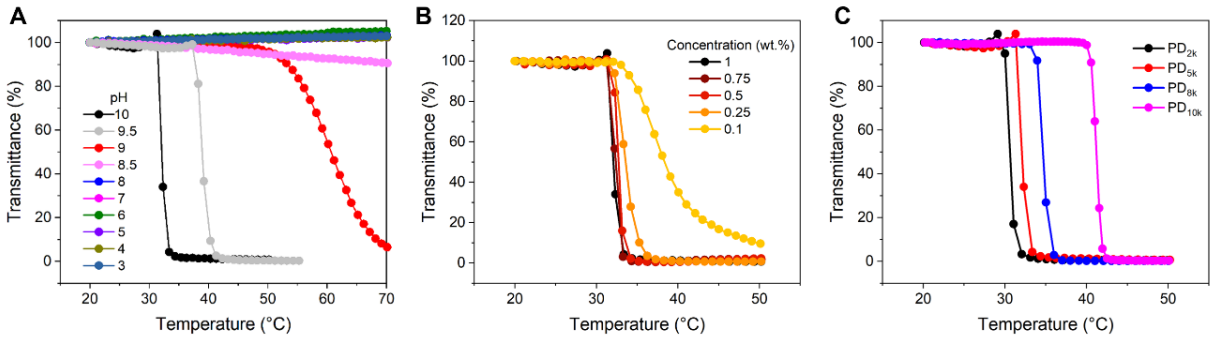

Figure IV.10 Transmittance change of PD_{5k} as a function of temperature (A) at different pH values and (B) at different concentrations (pH = 10). (C) Transmittance of PD homopolymers with different molecular weights at pH 10 versus temperature (PD concentration for all turbidimetry measurements was 1 wt.%).

The effects of polymer concentration and molecular weight on thermoresponsive properties were then studied at pH 10 (above p*K*a). It is observed that an increase of concentration from 0.1 to 0.5 wt.% leads to a decrease of T_c from 37 to 32 °C with no further

variation when concentration increases up to 1 wt.% (**Figure IV.10B**). This trend is similar to the one observed in the case of PN_{5k} described in previous section and is related to polymer chains entanglement, which promotes the formation of large aggregates at higher concentration. Moreover, an increase of molecular weight from 2000 to 10000 $g \cdot mol^{-1}$ induces an increase of measured T_c from 31 to 41 °C (**Figure IV.10C**).

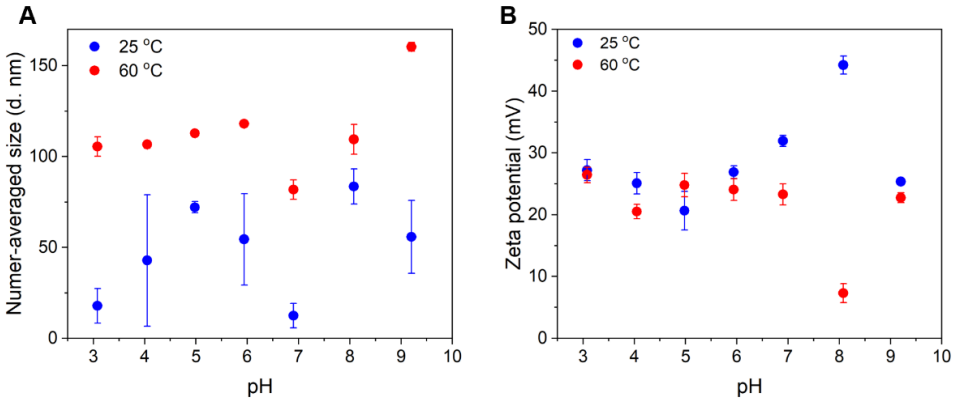

Figure IV.11 (A) Number-averaged size and (B) zeta potential of PD_{5k} as a function of pH at 25 and 60 °C ([PD_{5k}] = 0.1 wt.%).

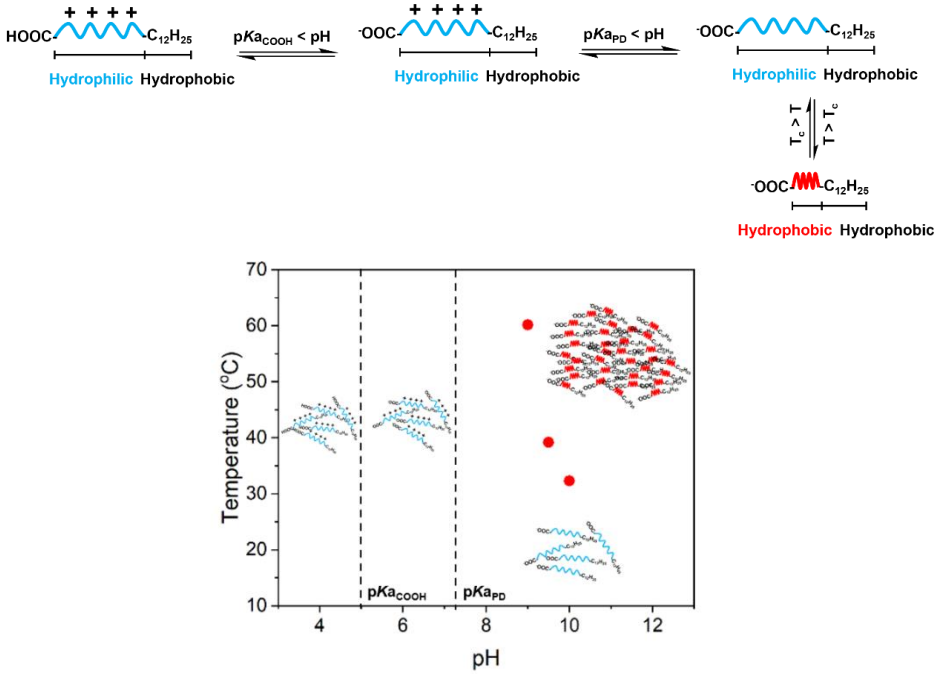

Scheme IV.8 (top) Structure and effects of pH and temperature on the conformation of PD chains, (bottom) schematic illustration of thermoresponsiveness and self-assembly behavior for PD_{5k} solution at different pH values. (T_c: red solid circle)

It has to be noted that contrary to what observed for PN_{5k} the formation of micellar system is not detected in the case of PD_{5k} (**Figure IV.11**). At pH below p*Ka*$_{PD}$, aggregates of polymer with hydrodynamic diameter below 75 nm measured from DLS experiments. These aggregates have a positive zeta potential (around 25 mV) as expected from the positively charged

protonated form of tertiary amine. Increasing temperature to 60 °C tends to slightly increase the size of these aggregates (around 100 nm) that remains positively charged but does not lead to the appearance of cloudy phase for bare eyes. At pH above p*Ka*$_{PD}$, PD becomes thermoresponsive (**Scheme IV.8**) and an increase of temperature leads to the formation of large aggregates (around 150 nm with positive zeta potential) that results in cloudy solution.

IV.4 Thermoresponsive properties of PN-*b*-PD in water

PN-*b*-PD block copolymers comprise of two blocks: a PN thermoresponsive block with a characteristic transition temperature at 30 °C (at 1 wt.%) and a PD block which is, at pH higher than p*K*a (7.25), deprotonated and thermoresponsive. In addition, the two end groups (carboxylic acid function and an -$C_{12}H_{25}$ group) are prone to promote the formation of micellar system above p*Ka*$_{COOH}$ as demonstrated in the case of PN$_{5k}$. The behavior of this block copolymer in aqueous solution was then studied as at different pH by means of scattering, microscopy and NMR measurements. The colloidal properties are illustrated in the following sections in the case of PN$_{5k}$-*b*-PD$_{5k}$.

IV.4.1 Thermoresponsive behavior of PN$_{5k}$-*b*-PD$_{5k}$ solution at pH 10

At pH 10, PN$_{5k}$-*b*-PD$_{5k}$ comprises of two thermoresponsive blocks (PN$_{5k}$ and PD$_{5k}$), a carboxylic acid end group in its carboxylate anionic form (-COO^-) and a hydrophobic -$C_{12}H_{25}$ end group (**Scheme IV.9**).

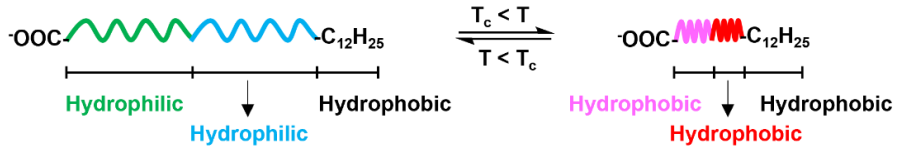

Scheme IV.9 Structure and effect of temperature on the conformation of PN-*b*-PD chains at pH 10.

The ability of this block copolymer to self-assemble in solution was evaluated by surface tension measurements at 20 °C. Surface tension of PN$_{5k}$-*b*-PD$_{5k}$ as a function of concentration is shown in **Figure IV.12**. In the concentration range from 10^{-6} to 2×10^{-4} wt.%, the surface tension changes slightly and is close to the value of pure water (73 mN/m at 20 °C), which is followed by a sharp reduction with an increase of concentration. This trend results from the adsorption of polymer to water-air interface which leads to an abrupt decrease of surface tension along with polymer concentration from 2×10^{-4} wt.% to a critical concentration of 3×10^{-3} wt.%, this point is known as critical aggregation concentration (cac), at which self-assembly of PN$_{5k}$-

b-PD_{5k} occurs in water phase. Consequently, in concentration range of 3×10^{-3} - 5 wt.%, a slower decrease of surface tension is observed relative to a slow reorganization of the copolymer at the interface, this surface tension becomes independent of concentration as PN_{5k}-*b*-PD_{5k} concentration is above 5×10^{-1} wt.%.

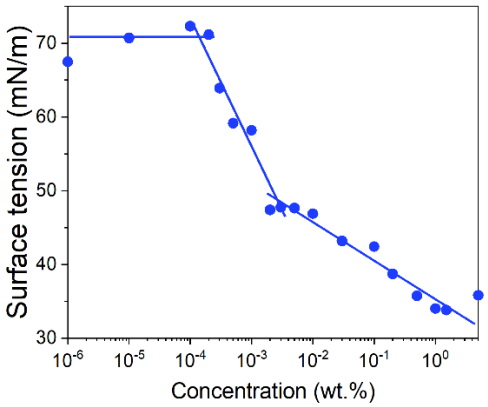

Figure IV.12 Evolution of surface tension as a function of concentration for PN_{5k}-*b*-PD_{5k} solution (20 °C, pH ≈ 9).

(i) Thermoresponsive behavior of PN_{5k}-*b*-PD_{5k} aqueous solution

The effect of temperature on self-assembly behavior of PN_{5k}-*b*-PD_{5k} at pH 10 was assessed by DLS, turbidimetry and ^{1}H NMR experiments above measured cac (3×10^{-3} wt.%) with a concentration of 0.1 or 1 wt.%. The detailed results are summarized in **Table IV.2**.

Table IV.2 T_c of PN_{5k}-*b*-PD_{5k} determined by different techniques at pH 10.

pH	Turbidimetry (°C)	DLS (°C)[a]	^{1}H NMR (°C)	DSC (°C)
10	38.0	40.0	40.0	42.0[b]

[a]Performed at concentration of 0.1 wt.%, T_c determined from inflection point of number-averaged size distribution curve upon heating. [b]Obtained by extrapolation to 0 °C·min^{-1} at the maximum of observed peaks upon cooling process (1 wt.% of PN_{5k}-*b*-PD_{5k} solution used for turbidimetry, ^{1}H NMR and DSC measurements).

Visually, colloidal solutions undergo a transition from transparent to cloudy phase around 40 °C. The formation of large aggregates is evidenced from DLS measurement as shown in **Figure IV.13A**. At 37 °C, an increase of size (inflection point at 40 °C) is evidenced and at 60 °C objects with an average hydrodynamic diameter of 520 nm are formed.

This behavior is different from the ones of pristine homopolymers as illustrated by turbidimetry experiments (**Figure IV.13B**). Whereas PN_{5k} does not lead to any significant change of transmittance due to the formation of micellar system and PD_{5k} has a T_c equal to 34 °C, PN_{5k}-*b*-PD_{5k} exhibits a thermoresponsive behavior with a T_c equal to 38 °C, which is

different from the one of both homopolymers. Considering that PNIPAM-xanthate displays a transition temperature around 36 °C at the same concentration, the observed behavior of PN_{5k}-*b*-PD_{5k} can be ascribed to the specific structure of block copolymer.

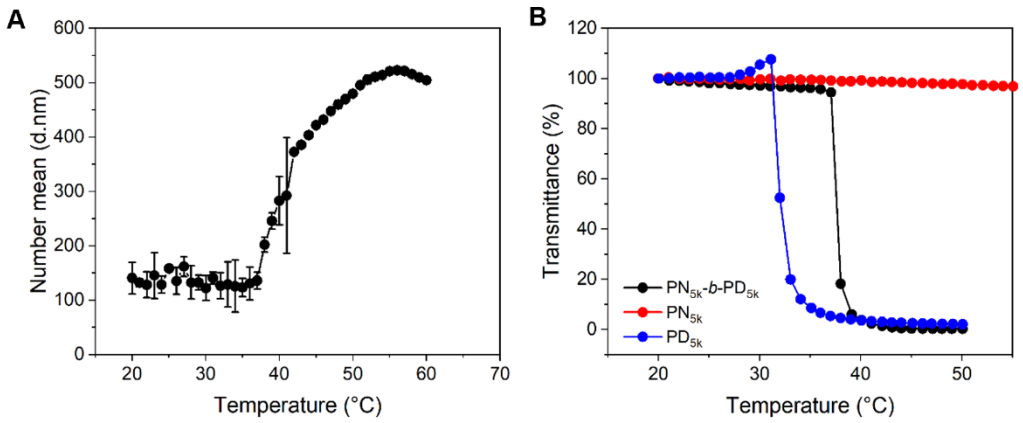

Figure IV.13 At pH 10, (A) number-averaged size distribution of PN_{5k}-*b*-PD_{5k} as a function of temperature ([PN_{5k}-*b*-PD_{5k}] = 0.1 wt.%). (B) Transmittance change of PN_{5k}-*b*-PD_{5k}, PN_{5k} and PD_{5k} versus temperature ([(co)polymer] = 1 wt.%, heating rate: 1 $^{o}C \cdot min^{-1}$).

(ii) Mechanism of aggregation upon heating

In order to have a further understanding of the mechanism behind this phase transition, ^{1}H NMR analysis was performed in a temperature range of 20 - 50 °C (**Figure IV.14A**). As stated above, with rising temperature, both PN and PD blocks undergo soluble-to-insoluble transitions in this temperature range and large aggregates are formed at higher temperature. Thus, this transition induces both an increase of longitudinal relaxation time (T_1) of the proton that can be associated with the decrease of the mobility of molecular chains, and a progressive decrease of integration value of corresponding peak is accompanied when compared to the integration of a peak relative to a soluble reference compound.

Figure IV.14B illustrates the evolution of T_1 as a function of temperature. At 20 °C, all measured T_1 values are above 750 ms, indicating the formation of large objects. When the temperature increases up to 40 °C, it is observed that T_1 of protons in α position of amide function of PN block rapidly increases to reach 1600 ms. Restricted motion of polymer chains consecutive to a dehydration phenomenon might be responsible for this observation. Meanwhile, T_1 of protons corresponding to PD block does not increase significantly. It seems that the dehydration mainly affects the mobility of PN block. Above 38 °C, all protons undergo a significant increase of T_1 due to the formation of larger aggregates. The decrease of T_1 observed for the proton in α position of amide function of PN block might be ascribed to the

poor resolution of corresponding peak that hinders the accurate determination of T_1 for this specific proton.

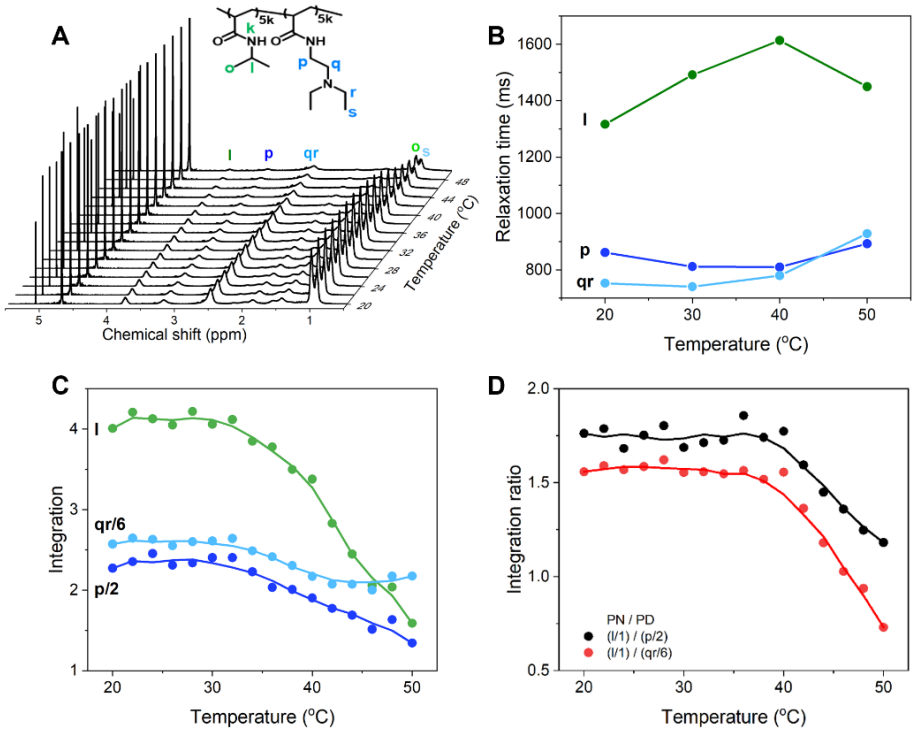

Figure IV.14 (A) ^{1}H NMR spectra of PN_{5k}-*b*-PD_{5k} as a function of temperature at pH 10 (trioxane as internal standard with a chemical shift at 5.1 ppm and integral of 1 at whatever temperature studied). (B) Evolution of relaxation time (T_1) as a function of temperature. (C) Evolution of integration of characteristic peaks in PN_{5k}-*b*-PD_{5k} relatively to the reference peak of trioxane. (D) Evolution of integration ratio between PN and PD block as a function of temperature. (T_1 was measured by Y. Coppel in LCC, Toulouse, France)

These T_1 values were further considered to obtain ^{1}H NMR spectra in quantitative conditions and to determine the evolution of integrals of characteristic protons associated to PD (2.5 and 3.2 ppm) and PN (3.8 ppm) units relatively to the integral of trioxane chosen as a reference. As depicted in **Figure IV.14C**, the integral corresponding to PN units at 3.8 ppm remains roughly constant up to 32 °C, it then decreases slowly and a more pronounced decrease is observed above 38 °C. For PD block, a decrease is also evidenced above 32 °C but with no change of slope at 38 °C. The relative evolution of the integral ratio of PN and PD peak is represented in **Figure IV.14D**, a constant value is kept until 38 °C, after which a decrease is detected due to a more pronounced decrease of PN peaks than the one observed for PD. It is noteworthy that no change of chemical shifts is measured for the characteristic peaks of these two blocks in PN_{5k}-*b*-PD_{5k}.

These results suggest that above 32 °C both PD and PN undergo progressive changes in their surroundings probably related to the progressive dehydration phenomenon. At 38 °C, an aggregation phenomenon occurs and promotes the formation of large aggregates in solution.

As peaks relative to PD are less modified than the ones corresponding to PN, this indicates that PD polymer chains present a higher mobility in aqueous solution. This might be ascribed to the formation of aggregates with core-shell structure, where PN is in the core and PD is mainly in the shell, causing PD has lower T_1 and less pronounced modification of integration than PN.

Therefore, aggregation induces the formation of large aggregates from preexisting self-assemblies. To gain a further understanding of the underlying mechanism and of their kinetics, turbidimetry experiments were performed with different heating rates (**Figure IV.15**). It is found that T_c is measured at 35 °C at 0.2 °C·min^{-1}, and this value rises to 40 °C when heating rate increases to 5 °C·min^{-1}.

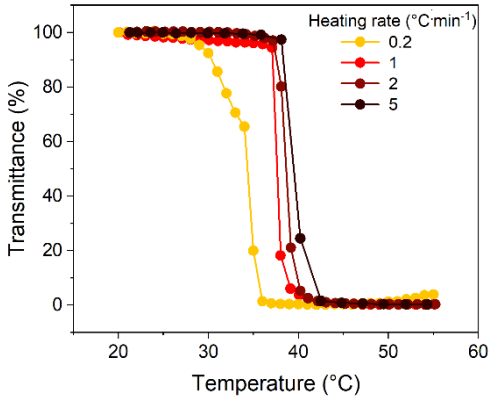

Figure IV.15 Transmittance change of PN_{5k}-*b*-PD_{5k} versus temperature at pH 10 at different heating rates ([PN_{5k}-*b*-PD_{5k}] = 1 wt.%, T_c determined by inflection point of transmittance curve).

Moreover, at 60 °C, the hydrodynamic diameter of obtained aggregates goes on increasing as shown in **Figure IV.16A** over a period of 2 hours, starting from 130 to 180 nm. This implies that objects size depends strongly on kinetic consideration for aggregates formed above T_c and therefore on the way how experiments are performed (heating rate, equilibrating time…). This also suggests a possible reorganization of polymer/colloidal structure within the aggregates. This is confirmed by performing an additional scattering measurement in which the sample was heated directly at a chosen temperature starting from a solution at 20 °C. In this case, a hydrodynamic diameter of 188.5 ± 3.1 nm is found at 60 °C. Furthermore, **Figure IV.16B** illustrates the number-averaged hydrodynamic diameter and derived count rate by using a different heating way, in which a copolymer solution was heated and kept for 10 min at a chosen temperature then it was cooled down at 20 °C before performing heating process at another temperature. Measured hydrodynamic diameters are found around 250 nm above T_c and around 23 nm below T_c. Interestingly, at 20 °C this size increases slightly depending on the history of measurements illustrating the key role of reorganization of polymer/colloidal structure within the aggregates that occurs with characteristic timescale within minutes to hours. Noteworthy,

polymer concentration is another parameter to be taken into account to have a precise control over the size of formed aggregates.

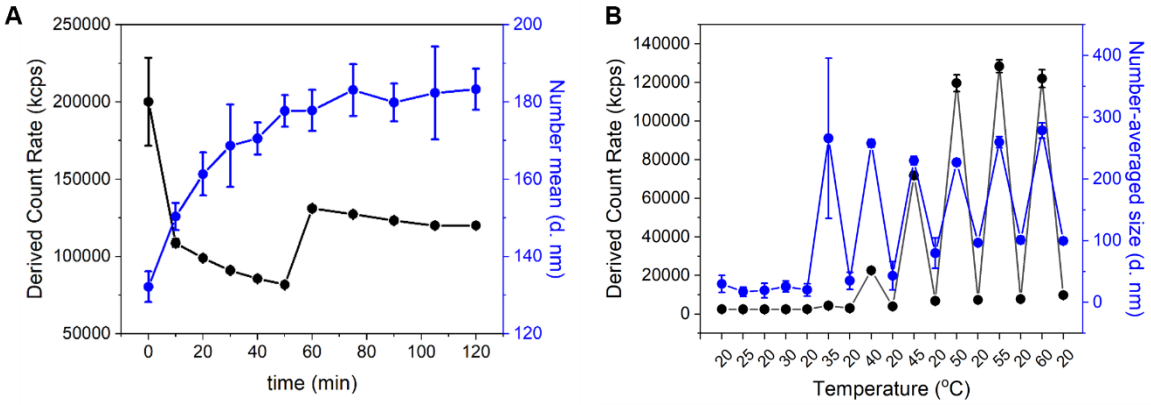

Figure IV.16 (A) Derived count rate and size change of PN_{5k}-*b*-PD_{5k} aggregates versus time at 60 °C. (B) Evolution of derived count rate and number-averaged size at different temperatures (PN_{5k}-*b*-PD_{5k} solution was heated and kept for 10 min at a chosen temperature, then it was cooled down to 20 °C before performing heating process at higher temperature). (pH = 10, [PN_{5k}-*b*-PD_{5k}] = 0.1 wt.%)

(iii) Characterization of obtained aggregates below and above T_c

The colloidal structures obtained from aqueous solution of PN_{5k}-*b*-PD_{5k} below and above T_c were characterized by TEM, cryo-TEM and DLS techniques. To avoid aggregation phenomenon at 1 wt.%, solution with a concentration of 0.1 wt.% was studied. **Table IV.3** summarizes obtained results from different techniques.

Table IV.3 PN_{5k}-*b*-PD_{5k} aggregates size at different temperatures determined by TEM, cryo-TEM and DLS measurements.

pH	Temperature (°C)	TEM (d. nm)	Cryo-TEM (d. nm)	DLS (d. nm)[b]
10	25	23.2 ± 5.7	34.3 ± 14.2	27.0 ± 8.8
	60	92.8 ± 34.6	173.8 ± 76.1[a]	188.5 ± 3.1

[a] Measurements performed at 50 °C; [b] Obtained from number-averaged size distribution (PN_{5k}-*b*-PD_{5k} concentrations of 0.1, 0.1 and 0.5 wt.% for TEM, DLS, and cryo-TEM measurements, respectively).

At 25 °C below T_c, both PN and PD segments are soluble in aqueous solutions and PN-*b*-PD comprises one hydrophobic terminal group (-$C_{12}H_{25}$) and a carboxylate function. TEM and cryo-TEM analysis (**Figure IV.17**) present spherical aggregates with an average diameter equal to 23.2 ± 5.7 and 34.3 ± 14.2 nm, respectively.

DLS experiments enable to evaluate an average hydrodynamic diameter of 27.0 ± 8.8 nm. Therefore, as observed in the case of PN_{5k}, PN_{5k}-*b*-PD_{5k} in aqueous solution is prone to self-assemble into micellar structure with a core of -$C_{12}H_{25}$ group and a corona of PN and PD blocks.

The presence of carboxylate function enables to limit the aggregation to the formation of quite small spherical colloidal system.

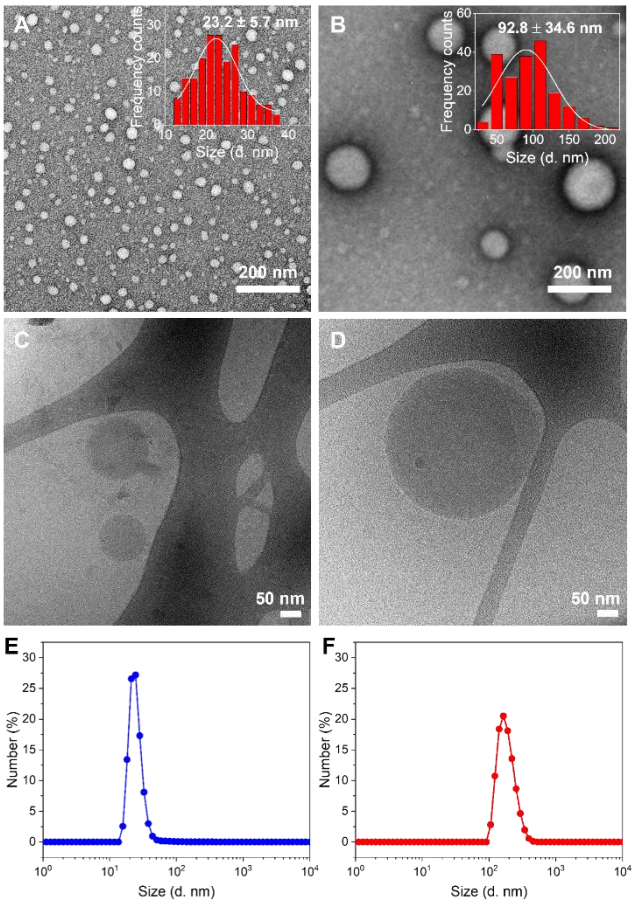

Figure IV.17 TEM, cryo-TEM images and Number-averaged size distribution of PN_{5k}-*b*-PD_{5k} (A) (C) (E) at 25 °C, (B) (F) at 60 °C and (D) at 50 °C. (pH = 10, 0.1, 0.5 and 0.1 wt.% of PN_{5k}-*b*-PD_{5k} solution for TEM, cryo-TEM and DLS measurements, respectively. TEM samples stained with 2 wt.% uranyl acetate solution, cryo-TEM measurements were done by S. Balor in CBI, Toulouse, France)

At temperature above T_c, both PN and PD moieties shrink and become hydrophobic. Spherical objects are evidenced by TEM and cryo-TEM analysis with measured diameter equal to 92.8 ± 34.6 and 173.8 ± 76.1 nm, respectively. As stated above, the extent of aggregation depends strongly on kinetic consideration and on the history of colloid preparation. This suggests that micellar structures observed at 25 °C tends to aggregate. An estimation of hydrodynamic diameter of PN_{5k}-*b*-PD_{5k} objects detected by DLS measurement is around 190 nm, which is in good agreement with TEM results. Once again, the presence of carboxylate function can explain the observed limitation of aggregation process. Moreover, NMR results demonstrate that PN chains upon dehydration are present in more constrained environment than PD chains. Based on these analyses, the morphologies of PN_{5k}-*b*-PD_{5k} aggregates below and above T_c at pH 10 are proposed in **Scheme IV.10**.

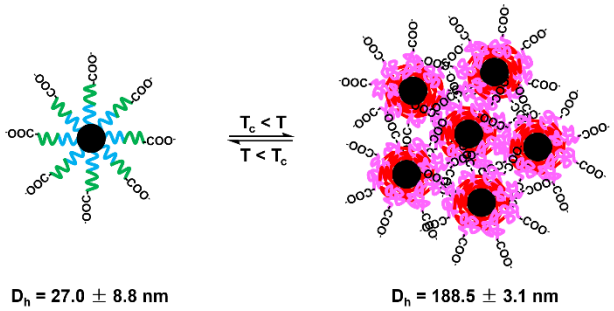

Scheme IV.10 Schematic illustration of self-assembly structure of PN_{5k}-*b*-PD_{5k} solution below and above T_c at pH 10.

IV.4.2 Thermoresponsive behavior of PN_{5k}-*b*-PD_{5k} solution at pH 4

At pH 4, PN_{5k}-*b*-PD_{5k} comprises of one thermoresponsive groups (PN_{5k}), one cationic block (PD_{5k}), a carboxylic acid end group and a hydrophobic -$C_{12}H_{25}$ end group.

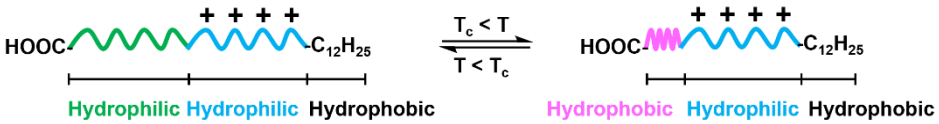

Scheme IV.11 Structure and effect of temperature on the conformation of PN-*b*-PD chains at pH 4.

Surface tension measurements performed at pH 4 show the same trend to the one measured at pH 10 (**Figure IV.18**) and a cac equal to 2×10^{-3} wt.% is evaluated. Therefore PN_{5k}-*b*-PD_{5k} forms aggregates at pH 4 probably induced by the presence of hydrophobic tail -$C_{12}H_{25}$.

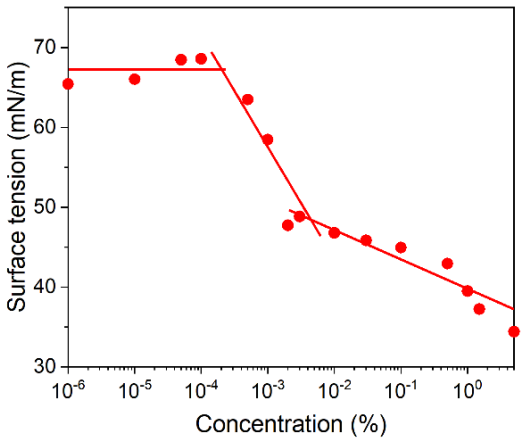

Figure IV.18 Evolution of surface tension as a function of concentration of PN_{5k}-*b*-PD_{5k} solution (20 °C, pH = 4).

(i) Thermoresponsive behavior of PN_{5k}-*b*-PD_{5k} aqueous solution

The effect of temperature on the self-assembly behavior at pH 4 was assessed by DLS, turbidimetry and ^{1}H NMR experiments above measured cac (2×10^{-3} wt.%) with a concentration of 0.1 or 1 wt.%. Visually, colloidal solutions undergo a transition from transparent to cloudy phase around 28 °C. The formation of large aggregates was evidenced by DLS measurements

as shown in **Figure IV.19**, at 26 °C, an increase of derived count rate relative to the formation of large objects is evidenced. A second transition seems to occur at 36 °C after which the measured diameter still increases, whereas derived count rate strongly decreases due to a partial decantation of the formed aggregates.

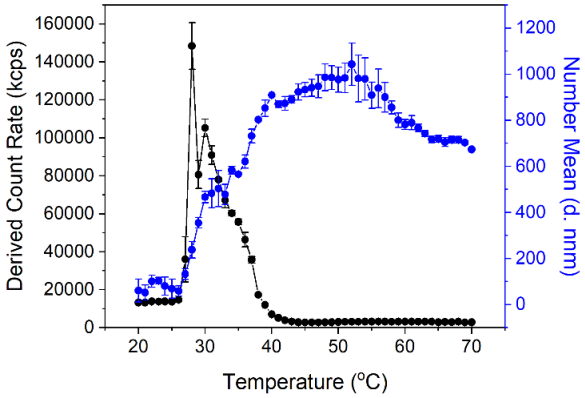

Figure IV.19 Evolutions of derived count rate and number-averaged size distribution of PN_{5k}-*b*-PD_{5k} as a function of temperature ([PN_{5k}-*b*-PD_{5k}] = 1 wt.%, pH = 4).

The evolution of transmittance as a function of temperature for PN_{5k}-*b*-PD_{5k}, PN_{5k} and PD_{5k} at pH 4 is shown in **Figure IV.20**. Whereas PN_{5k} homopolymer has a T_c at 26 °C, no transmittance change of reference PD_{5k} takes place in the studied temperature range. Indeed, PD_{5k} is protonated and no more thermoresponsive. In the case of PN_{5k}-*b*-PD_{5k}, a two-step transmittance decrease occurs starting at 23 °C with the first inflection point of 29 °C ($T_{c,1}$) and the second one at 39 °C ($T_{c,2}$).

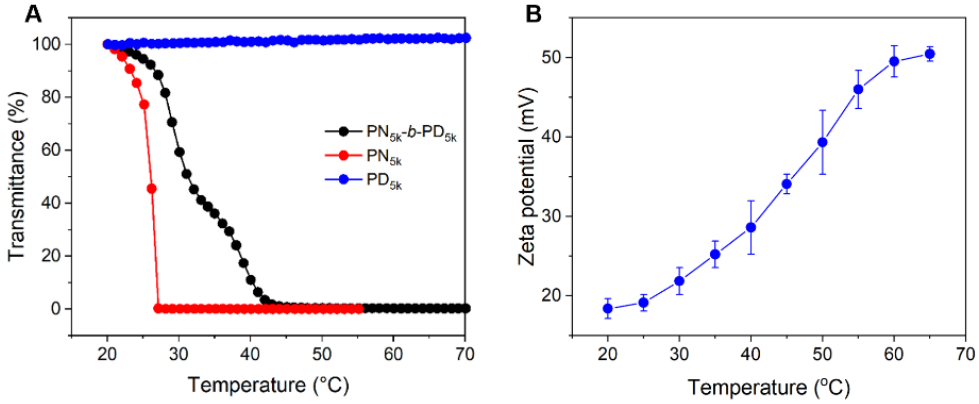

Figure IV.20 (A) Transmittance change of PN_{5k}-*b*-PD_{5k}, PN_{5k} and PD_{5k} at pH 4 as a function of temperature ([(co)polymer] = 1 wt.%, heating rate:1 °C·min^{-1}). (B) Evolution of zeta potential as a function of temperature for PN_{5k}-*b*-PD_{5k} at pH 4 ([PN_{5k}-*b*-PD_{5k}] = 0.1 wt.%).

The first transition at 29 °C might come from the thermoresponsive character of PN segment. Above $T_{c,1}$, PN chains in PN_{5k}-*b*-PD_{5k} collapse, inducing a reorganization of the colloidal structures formed at room temperature. With an increase of temperature, zeta potential is measured with an increasing tendency, which is in good agreement with a reorganization to

form objects with a PN dehydrated core and a shell of PD block in positively charged form. When temperature raises up to $T_{c,2}$, colloids undergo the second transition with the formation of very large objects with a poor colloidal stability.

(ii) Mechanism of aggregation upon heating

In order to have a further understanding of the mechanism behind these transitions, ^{1}H NMR analyses were performed with a temperature increasing from 20 to 50 °C using trioxane as a reference compound (**Figure IV.21**). As stated above, with rising temperature, only PN block undergoes a soluble-to-insoluble transition. This induces the formation of large aggregates in a two-step process and consequently an increase of longitudinal relaxation time (T_1) of protons and a progressive decrease of relative integration value of corresponding peaks.

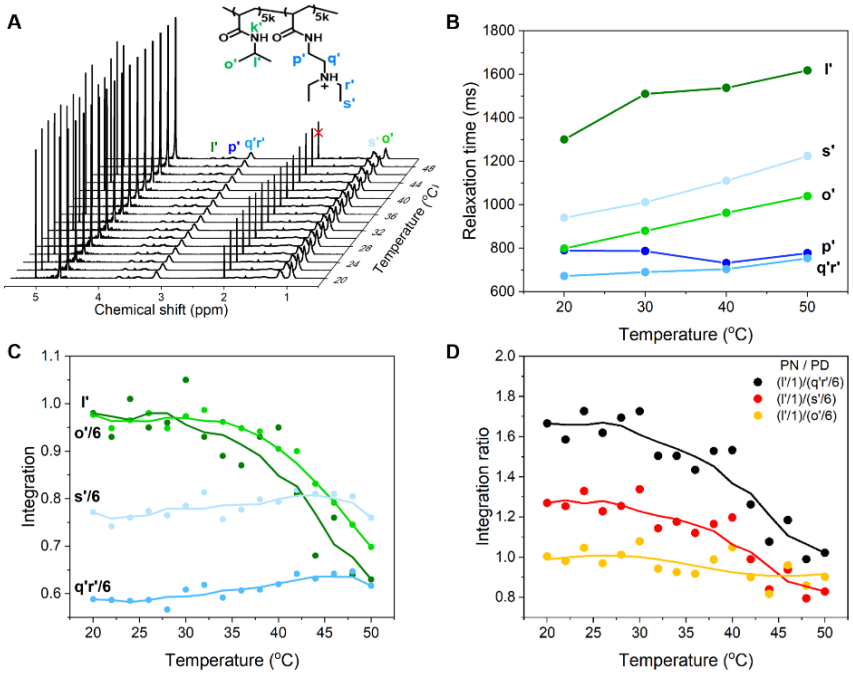

Figure IV.21 (A) ^{1}H NMR spectra of PN_{5k}-*b*-PD_{5k} as a function of temperature at pH 4 (trioxane as internal standard with a chemical shift at 5.1 ppm and an integral of 1 at whatever temperature studied). (B) Evolution of relaxation time (T_1) of characteristic peaks in PN_{5k}-*b*-PD_{5k} as a function of temperature. (C) Evolution of integration of characteristic peaks in PN_{5k}-*b*-PD_{5k} relatively to the reference peak of trioxane. (D) Evolution of integration ratio between PN and PD block as a function of temperature. ([PN_{5k}-*b*-PD_{5k}] = 1 wt.%, T_1 was measured by Y. Coppel in LCC, Toulouse, France)

Figure IV.21B illustrates the evolution of T_1 as a function of temperature. At 20 °C, all measured T_1 values are above 600 ms, indicating the formation of large objects. When the temperature increases up to 50 °C, T_1 of protons corresponding to PN increases. Restricted motion of polymer chains consecutive to a dehydration phenomenon and formation of larger objects might be responsible for this observation. At the same time, T_1 of protons corresponding to PD block does not increase to such an extent. The increase of temperature seems to affect

mainly PN block. These T_1 values were further taken into account to acquire ^{1}H NMR spectra in quantitative conditions and to determine the evolution of integration of the protons associated to PD and PN units relatively to the integral of trioxane. As depicted in **Figure IV.21C**, there is no significant change of integrals corresponding to PD units in studied temperature range from 20 to 50 °C, whereas integration area of PN signals remains roughly constant up to 32 °C, after which a further decreasing tendency along with temperature is observed. It is noteworthy that no change of chemical shifts is measured for the characteristic peaks of the polymer. These results confirm that upon heating PD and PN undergo a progressive change in their surroundings that occurs in two different steps. Therefore, as observed at pH 10, an increase of temperature induces the formation of large aggregates from preexisting self-assemblies. Turbidimetry experiments were performed by using different heating rates to highlight the formation kinetics (**Figure IV.22A**). Decreasing the heating rate induces a shift of measured T_c at pH 4 and a two-step process is observed whatever the heating rate.

The size of PN_{5k}-*b*-PD_{5k} fluctuates slightly within 2 h at a specific pH value (see **Figure IV.22B**), this phenomenon is attributed to the fact that electrostatic repulsion among positive charged PD chains inhibits particle aggregation. Moreover, with an increase of temperature, the PN chains collapse and become insoluble, the hydrophobic association among PN chains exceeds the electrostatic repulsion, which causes the particles aggregate to form larger size.

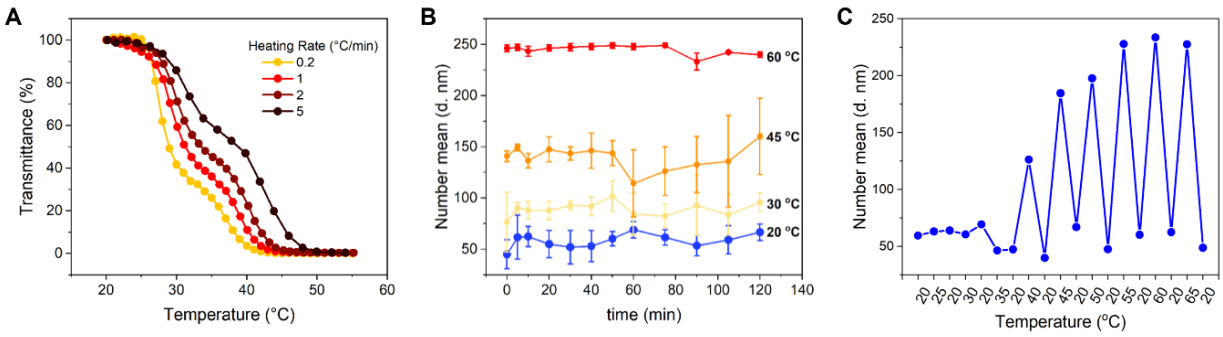

Figure IV.22 (A) Transmittance change as a function of temperature with different heating rates, (B) number-averaged size change as a function of time at 20, 30, 45 and 60 °C for PN_{5k}-*b*-PD_{5k} and (C) evolution of number-averaged size at different temperatures (PN_{5k}-*b*-PD_{5k} solution was heated and kept for 10 min at a chosen temperature, then it was cooled down to 20 °C before performing heating process at higher temperature). (pH = 4, 1 and 0.1 wt.% of PN_{5k}-*b*-PD_{5k} solution for turbidimetry and DLS measurements, respectively)

As already shown at pH 10, the size of obtained aggregate upon heating depends strongly on kinetic phenomenon due to reorganization of polymer/colloidal structure within the aggregates that occurs with characteristic timescale within minutes to hours (**Figure IV.22C**).

(iii) Characterization of obtained aggregates below and above $T_{c,1}$ and $T_{c,2}$

The colloidal structure obtained from aqueous solution of PN_{5k}-*b*-PD_{5k} were studied by TEM and DLS at 25 (below $T_{c,1}$), 30 (between $T_{c,1}$ and $T_{c,2}$) and 60 °C (above $T_{c,2}$). All results are summarized in **Table IV.4**. To avoid aggregation phenomenon at 1 wt.%, solution with a dilute concentration equal to 0.1 wt.% was studied. It is noteworthy that aggregates size measured above T_c is demonstrated in previous section that it highly depends on the method of preparation and equilibrating time. Measured number-averaged hydrodynamic diameters are 25.8 ± 9.4, 77.4 ± 8.5 and 200.3 ± 4.5 nm at 25 °C ($T < T_{c,1}$), 30 °C ($T_{c,1} < T < T_{c,2}$) and 60 °C ($T > T_{c,2}$) (**Table IV.4** and **Figure IV.23F**)

Table IV.4 PN_{5k}-*b*-PD_{5k} aggregates size at different temperatures determined by TEM, cryo-TEM and DLS measurements.

pH	T (°C)	TEM (d. nm)	cryo-TEM (d. nm)	DLS (d. nm)[b]
	25	23.1 ± 5.2	31.4 ± 12.4	25.8 ± 9.4
4	30	30.4 ± 8.9	/[c]	77.4 ± 8.5
	60	125.6 ± 38.9	159.5 ± 73.6[a]	200.3 ± 4.5

[a]Measured at 50 °C. [b]Obtained from number-averaged size distribution. [c]Not determined. (0.1, 0.5 and 0.1 wt.% of PN_{5k}-*b*-PD_{5k} solution for TEM, cryo-TEM and DLS measurements, respectively).

At 25 °C, as evidenced by TEM analysis (or cryo-TEM image, see **Figures IV.23A** and **IV.23D**), PN_{5k}-*b*-PD_{5k} polymer chains self-organize into uniform spherical aggregates with diameter of 23.1 ± 5.2 nm (or 31.4 ± 12.4 nm). This diameter is almost equal to the one of aggregates formed at pH 10. Whereas a carboxylic form is present on one hand, protonation of PD chains enables to ensure a good colloidal stability in solution.

At 30 °C above $T_{c,1}$, PN chains start to collapse due to the dehydration phenomenon. However, PD block still maintains hydrophilic property and cationic character. As shown in TEM images (**Figure IV.23B**), PN_{5k}-*b*-PD_{5k} assembles into flower-like micelles with a diameter equal to 30.4 ± 8.9 nm. These structures can be issued either from a partial aggregation of previous ones formed at 25 °C or from a rearrangement of polymer chains in a core-shell structure with a core of hydrophobic -$C_{12}H_{25}$ end group and a shell of partially dehydrated PN block and hydrated cationic PD segment.

When temperature goes up to temperature higher than $T_{c,2}$, larger spherical aggregates are formed (**Figures IV.23C** and **IV.23E**, diameter equal to 125.6 ± 38.9 nm and 159.5 ± 73.6 nm determined by TEM and cryo-TEM, respectively). These structures result from aggregation of previous ones and/or a more pronounced phase separation between PN and PD blocks.

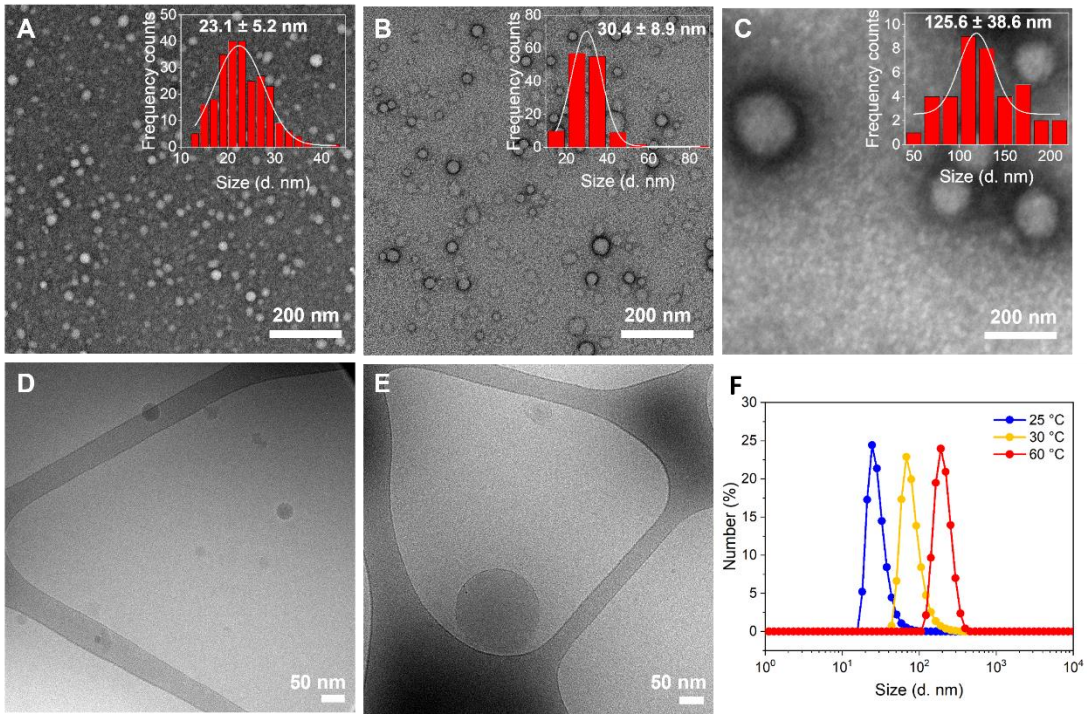

Figure IV.23 At pH 4, TEM, cryo-TEM images (A) (D) at 25 °C, (B) at 30 °C, (C) at 60 °C and (E) at 50 °C. (F) Number-averaged size distribution of PN_{5k}-*b*-PD_{5k} aggregates at different temperatures. (0.1, 0.5 and 0.1 wt.% of PN_{5k}-*b*-PD_{5k} solution for TEM, cryo-TEM and DLS measurements, respectively. TEM samples stained with 2 wt.% uranyl acetate solution, cryo-TEM measurements were done by S. Balor in CBI, Toulouse, France)

From the results obtained in this section, a schematic illustration of morphologies of PN_{5k}-*b*-PD_{5k} formed at pH 4 under different temperatures is proposed as shown in **Scheme IV.12**.

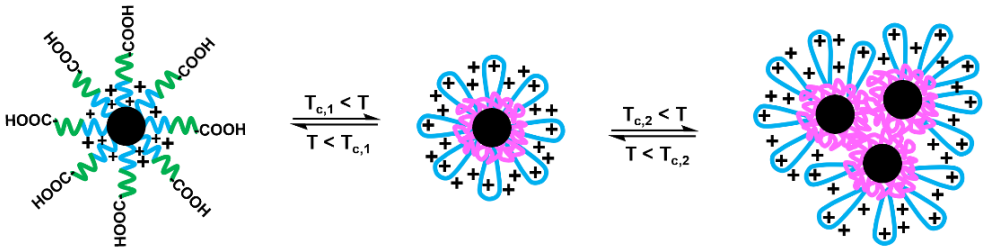

Scheme IV.12 Schematic illustration of morphological structures of PN_{5k}-*b*-PD_{5k} formed at pH 4 at different temperatures.

IV.4.3 Effect of pH on thermoresponsive property of PN_{5k}-*b*-PD_{5k} solution

The behaviors of PN_{5k}-*b*-PD_{5k} at pH 10 and 4 were studied in the two previous sections (**IV.4.1** and **IV.4.2**), respectively. A process with one single T_c is evidenced at pH 10, whereas a two-step process seems to occur at pH 4. To gain a further understanding of these phenomena, the thermoresponsive behavior of PN_{5k}-*b*-PD_{5k} at intermediate pH range were measured (**Figure IV.24**). As pH declines from 9 to 6, a single T_c is observed that decreases from 39 to 35 °C. Below pH 6, a two-steps process occurs. This might suggest the critical role of the

carboxylic function: in its carboxylate form a single step process is favored, whereas a two-step process is promoted by the carboxylic form. Further experiments are under way to assess this specific point, in particular complementary zeta potential measurements.

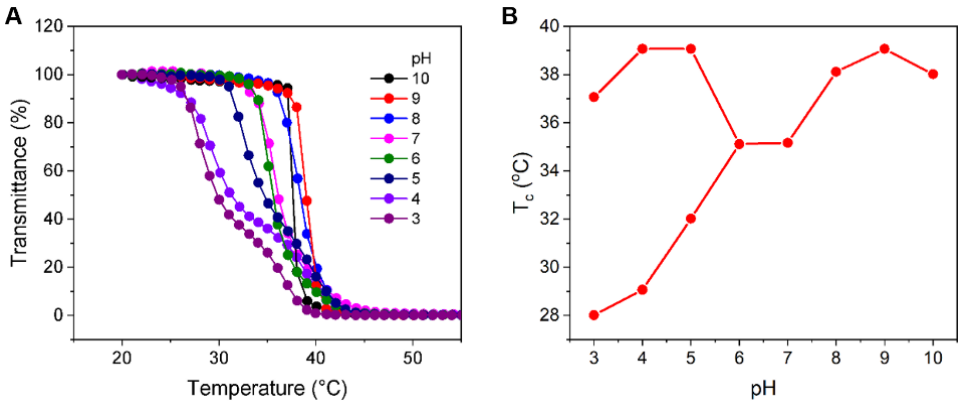

Figure IV.24 (A) Temperature-dependent transmittance change of PN_{5k}-*b*-PD_{5k} under different pH values and (B) evolution of T_c along with pH ([PN_{5k}-*b*-PD_{5k}] = 1 wt.%, heating rate: 1 °C·min^{-1}).

IV.4.4 Effect of copolymer composition on thermoresponsive properties

To evaluate the effect of copolymer composition on the thermoresponsive properties, two additional block polymers of PN_{2k}-*b*-PD_{8k} and PN_{8k}-*b*-PD_{2k} were studied.

(i) Effect of copolymer composition on T_c

The effect of copolymer composition on T_c was investigated via turbidimetry analysis (**Figures IV.25A** and **IV.25B**), the obtained T_c values at different pH are compared and shown in **Figure IV.25C**.

Whatever the pH value, PN_{8k}-*b*-PD_{2k} presents one single T_c which can be mainly ascribed to the large PN part. The observed transition temperature increases with an increase of pH value. Both PN_{2k}-*b*-PD_{8k} and PN_{5k}-*b*-PD_{5k} exhibit two T_c values in pH range 3 - 5 where PD block is totally protonated. As described in the case of PN_{5k}-*b*-PD_{5k}, the smaller $T_{c,1}$ results from aggregation of PN chains limited by the presence of charged PD block and the higher $T_{c,2}$ relates to the further aggregation of these nanostructures promoted by temperature increase. The deviation between $T_{c,1}$ and $T_{c,2}$ of PN_{2k}-*b*-PD_{8k} is larger than that of PN_{5k}-*b*-PD_{5k} at identical pH value.

In higher pH range of 6 - 8, protonation degree of PD decreases with increasing pH, therefore PD block is divided into uncharged thermoresponsive and charged non-thermoresponsive blocks. Upon heating the hydrophobic PN and partially uncharged PD blocks aggregate with only one T_c detected in such pH range. Whereas PN_{8k}-*b*-PD_{2k} and PN_{5k}-*b*-PD_{5k}

have similar transition temperature in higher pH window, the transition point of PN_{2k}-*b*-PD_{8k} is found to be significantly higher, which may relate to the high amount of PD block.

At pH above 9 PD is fully deprotonated and thermoresponsive. All block copolymers present a single T_c which is roughly at the same value. This single T_c might result as in the case of PN_{5k}-*b*-PD_{5k} from a cooperative behavior between PN and PD blocks.

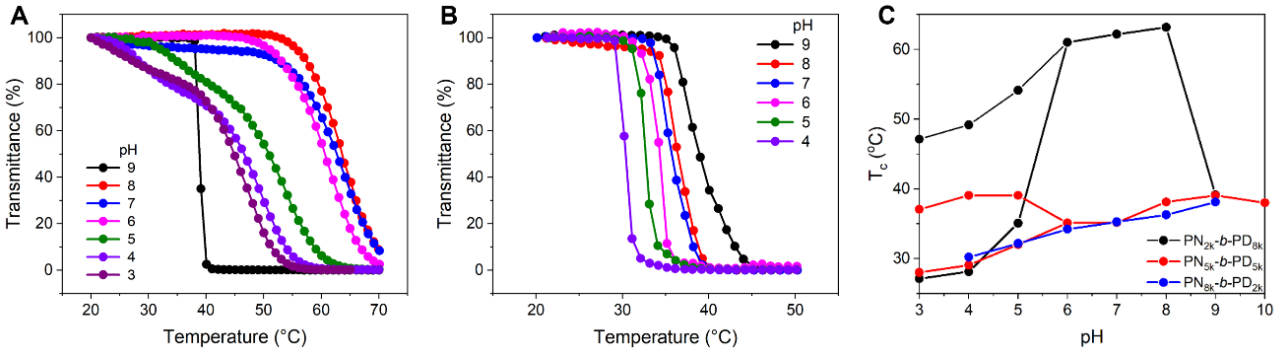

Figure IV.25 Transmittance curve of (A) PN_{2k}-*b*-PD_{8k} and (B) PN_{8k}-*b*-PD_{2k} as a function of temperature at different pH. (C) Cloud points of PN-*b*-PD with various compositions at different pH values. (T_c determined by inflection point of transmittance curve, [PN-*b*-PD] = 1 wt.%, heating rate: 1 $^oC \cdot min^{-1}$)

(ii) Effect of copolymer composition on aggregates size

To understand the effect of copolymer composition on aggregates morphology and size, we also performed TEM and DLS analysis on PN_{2k}-*b*-PD_{8k} and PN_{8k}-*b*-PD_{2k} at different pH values and at temperatures below and above T_c (**Figures IV.26** and **IV.27**), the detailed information on size is summarized in **Table IV.5**. As evidenced in TEM images, spherical aggregates are observed in all the studied cases. Whatever the pH value, spheres aggregates are formed with larger size at temperature above T_c as compared to that below T_c.

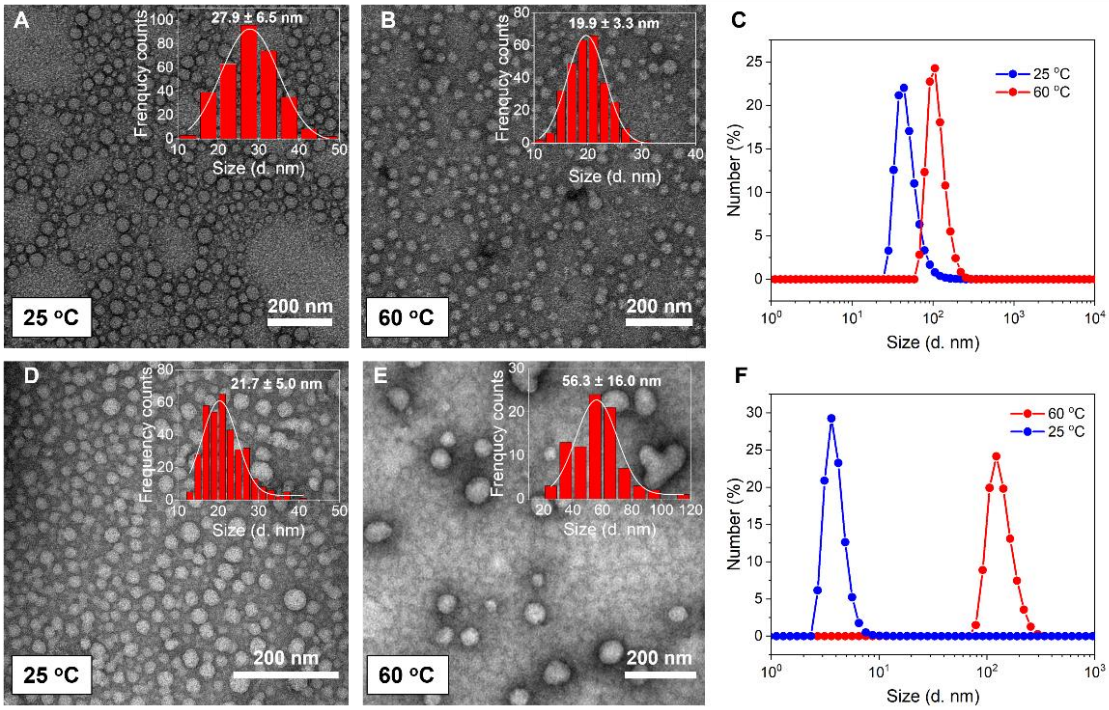

Figure IV.26 TEM images and number-averaged size distribution of PN_{2k}-*b*-PD_{8k} and PN_{8k}-*b*-PD_{2k} at 25 and 60 °C. PN_{2k}-*b*-PD_{8k}: (A) 25 °C, (B) 60 °C, (C) number-averaged size distribution. PN_{8k}-*b*-PD_{2k}: (D) 25 °C, (E) 60 °C, (F) number-averaged size distribution. (pH = 10, [PN-*b*-PD] = 0.1 wt.%, TEM samples stained with 2 wt.% uranyl acetate solution)

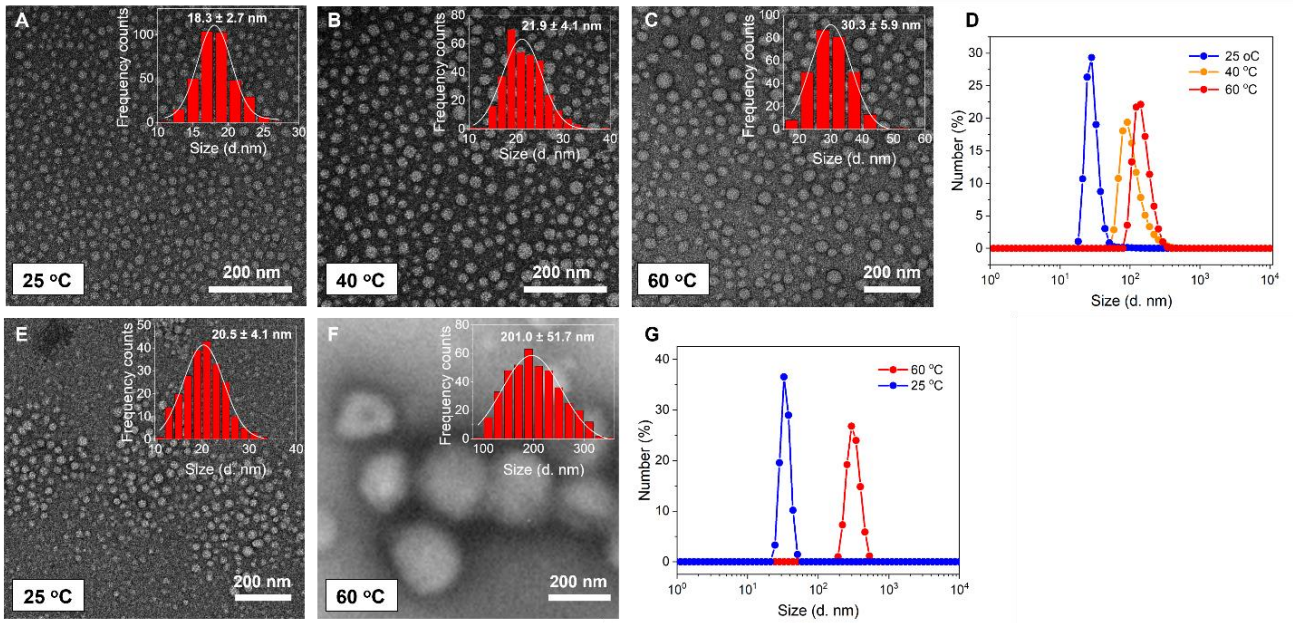

Figure IV.27 TEM images and number-averaged size distribution of PN_{2k}-*b*-PD_{8k} and PN_{8k}-*b*-PD_{2k} at different temperatures. PN_{2k}-*b*-PD_{8k}: (A) 25 °C, (B) 40 °C, (C) 60 °C, (D) number-averaged size distribution. PN_{8k}-*b*-PD_{2k}: (E) 25 °C, (F) 60 °C, (G) number-averaged size distribution. (pH = 4, [PN-*b*-PD] = 0.1 wt.%, TEM samples stained with 2 wt.% uranyl acetate solution)

Table IV.5 PN-*b*-PD aggregates size at different temperatures and pH values determined by TEM and DLS measurements.

Technique	Condition		Aggregate size (d. nm)		
	pH	Temperature (°C)	PN_{2k}-*b*-PD_{8k}	PN_{5k}-*b*-PD_{5k}	PN_{8k}-*b*-PD_{2k}
TEM	10	25	27.9 ± 6.5	23.2 ± 5.7	21.7 ± 5.0
		60	19.9 ± 3.3	92.8 ± 34.6	56.3 ± 16.0
	4	25	18.3 ± 2.7	23.1 ± 5.2	20.5 ± 4.1
		30	/[a]	30.4 ± 8.9	/[a]
		40	21.9 ± 4.1	/[a]	/[a]
		60	30.3 ± 5.9	125.6 ± 38.8	201.0 ± 51.7
DLS	10	25	45.9 ± 3.4	27.0 ± 8.8	4.1 ± 1.3
		60	109.4 ± 1.9	188.5 ± 3.1	137.8 ± 3.9
	4	25	30.7 ± 22.5	25.8 ± 9.4	31.1 ± 4.2
		30	/[a]	77.4 ± 8.5	/[a]
		40	64.4 ± 55.0	/[a]	/[a]
		60	154.0 ± 3.2	200.3 ± 4.5	321.8 ± 2.7

[a]Not detected. ([PN-*b*-PD] = 0.1 wt.%, TEM samples stained with 2 wt.% uranyl acetate solution)

Further experiments using multi-angle dynamic light scattering and static light scattering are still in progress to determine the hydrodynamic radii (R_h), aggregation numbers (N_{agg}) and average molecular weights of the assemblies formed above and below T_c whatever the pH. These data could provide complementary information on the morphology of the aggregates formed at different conditions, which could gain a deeper understanding of the observed differences induced by the modification of composition.

IV.5 Conclusions

Thanks to the RAFT polymerization process a series PN-*b*-PD copolymers and corresponding homopolymers have been successfully synthesized with controlled molecular weight and composition. The behavior of these (co)polymers in aqueous solutions was studied as a function of temperature and pH. We demonstrate in the case of PN homopolymer the key role of functional end-groups on its aggregation properties in water. Aggregation properties (size, phase transition temperature) of block copolymer depends strongly on pH value, composition and the history of formation. At pH 4, solely PN block is thermoresponsive. Solutions of PN_{2k}-*b*-PD_{8k} and PN_{5k}-*b*-PD_{5k} present two transition temperatures, which induce the formation of larger aggregates with a PD positively charged outer shell. At pH 10, PN and PD block are both thermoresponsive. PN-*b*-PD solutions have only one single transition point

upon which larger and stable spherical nanoobjects are formed. The presence of carboxylate function on the surface of these aggregates at least partially affects the colloidal stability of obtained nanoobjects.

IV.6 References

[1] A.E. Smith, X. Xu, C.L. McCormick, Prog. Polym. Sci. 35 (2010) 45-93.

[2] P. Schattling, F.D. Jochum, P. Theato, Polym. Chem. 5 (2014) 25-36.

[3] E.S. Gil, S.M. Hudson, Prog. Polym. Sci. 29 (2004) 1173-1222.

[4] G. Kocak, C. Tuncer, V. Bütün, Polym. Chem. 8 (2017) 144-176.

[5] R.V. Ulijn, J. Mater. Chem. 16 (2006) 2217-2225.

[6] J. Hu, G. Zhang, S. Liu, Chem. Soc. Rev. 41 (2012) 5933-5949.

[7] D. Roy, W.L.A. Brooks, B.S. Sumerlin, Chem. Soc. Rev. 42 (2013) 7214-7243.

[8] R. Liu, M. Fraylich, B.R. Saunders, Colloid Polym Sci 287 (2009) 627-643.

[9] I. Dimitrov, B. Trzebicka, A.H.E. Müller, A. Dworak, C.B. Tsvetanov, Prog. Polym. Sci. 32 (2007) 1275-1343.

[10] H.G. Schild, Prog. Polym. Sci. 17 (1992) 163-249.

[11] A. Laukkanen, L. Valtola, F.M. Winnik, H. Tenhu, Macromolecules 37 (2004) 2268-2274.

[12] J.S. Scarpa, D.D. Mueller, I.M. Klotz, J. Am. Chem. Soc. 89 (1967) 6024-6030.

[13] B. Pang, Y. Yu, W. Zhang, Macromol Rapid Commun (2021) 2100504.

[14] K. Wang, Z. Song, C. Liu, W. Zhang, Polym. Chem. 7 (2016) 3423-3433.

[15] T. Thavanesan, C. Herbert, F.A. Plamper, Langmuir 30 (2014) 5609-5619.

[16] P. Dubruel, E. Schacht, Macromol. Biosci. 6 (2006) 789-810.

[17] F.A. Plamper, M. Ruppel, A. Schmalz, O. Borisov, M. Ballauff, A.H.E. Müller, Macromolecules 40 (2007) 8361-8366.

[18] N. González, C. Elvira, J.S. Román, Macromolecules 38 (2005) 9298-9303.

[19] X. Jiang, C. Feng, G. Lu, X. Huang, ACS Macro Lett. 3 (2014) 1121-1125.

[20] D. Giaouzi, S. Pispas, Eur. Polym. J. 135 (2020) 109867.

[21] Y. Zhang, T. Wu, S. Liu, Macromol. Chem. Phys. 208 (2007) 2492-2501.

[22] A.E. Smith, X. Xu, S.E. Kirkland-York, D.A. Savin, C.L. McCormick, Macromolecules 43 (2010) 1210-1217.

[23] Z. Song, K. Wang, C. Gao, S. Wang, W. Zhang, Macromolecules 49 (2016) 162-171.

[24] K.K. Sharker, S. Takeshima, Y. Toyama, S. Ida, S. Kanaoka, S.-I. Yusa, Polymer 203 (2020) 122735.

[25] A.P. Narrainen, S. Pascual, D.M. Haddleton, J Polym Sci A Polym Chem 40 (2002) 439-450.

[26] S. Sistach, M. Beija, V. Rahal, A. Brûlet, J.-D. Marty, M. Destarac, C. Mingotaud, Chem. Mater. 22 (2010) 3712-3724.

[27] Z.-P. Xiao, K.-M. Yang, H. Liang, J. Lu, J Polym Sci A Polym Chem 48 (2010) 542-550.

[28] H.H. Nguyen, A. Brûlet, D. Goudounèche, P. Saint-Aguet, N. Lauth-de Viguerie, J.-D. Marty, Polym. Chem. 6 (2015) 5838-5850.

[29] R. Plummer, D.J.T. Hill, A.K. Whittaker, Macromolecules 39 (2006) 8379-8388.

[30] P.A. FitzGerald, S. Gupta, K. Wood, S. Perrier, G.G. Warr, Langmuir 30 (2014) 7986-7992.

[31] Y. Xia, N.A.D. Burke, H.D.H. Stöver, Macromolecules 39 (2006) 2275-2283.

[32] J. Škvarla, R.K. Raya, M. Uchman, J. Zedník, K. Procházka, V.M. Garamus, A. Meristoudi, S. Pispas, M. Štěpánek, Colloid Polym Sci 295 (2017) 1343-1349.

[33] P. van de Wetering, E.E. Moret, N.M.E. Schuurmans-Nieuwenbroek, M.J. van Steenbergen, W.E. Hennink, Bioconjugate Chem. 10 (1999) 589-597.

Chapter V

Study on dual thermo- and CO_2-responsive properties of poly(*N*-isopropylacrylamide)-*block*-poly(*N*-,*N*-diethylamino ethyl acrylamide) in water

Contents

V.1 Introduction

Carbon dioxide (CO_2) has emerged as a new and innovative trigger for stimuli-responsive materials due to its abundant, inexpensive, nontoxic and environmentally benign properties. CO_2-switchable polymers are a class of stimuli-responsive polymers in which CO_2 is used to induce modification of polymer properties (such as solubility, dimension, chain conformation and morphology…).

The immediate origins of these changes result from a neutral to charged state (or vice versa) of functional groups within polymer structure (i.e. amidines, tertiary amines). Indeed, as depicted in **Scheme V.1**, the dissolution of CO_2 in water acidifies the solution due to the dissociation of both carbonic acid and hydrated dissolved CO_2.

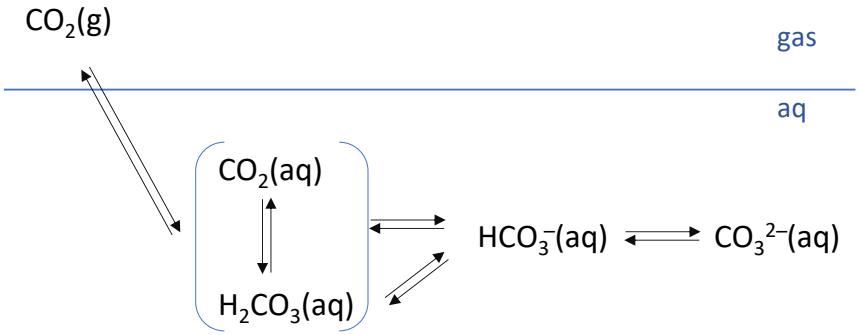

Scheme V.1 Equilibria involved in the dissolution of CO_2 in water

Further reversible reactions of CO_2 with various organic compounds are the basis for CO_2-triggered switchable substances. Neutral (uncharged) amines, amidines and guanidines can be converted to bicarbonate salts upon exposure to CO_2 in the presence of water (in eq. (1), B represents organic base). Amines, amidines and guanidines having N-H bonds can be converted to carbamate salts upon exposure to CO_2 illustrated in eq. (2) in the case of a secondary amine.

$$B + CO_2 + H_2O \rightleftharpoons [BH^+][HCO_3^-] \qquad \text{(eq. 1)}$$

$$2\,R_2NH + CO_2 + H_2O \rightleftharpoons [R_2NH_2^+][R_2NCO_2^-] \qquad \text{(eq. 2)}$$

By applying air or any nonacidic gas (such as N_2 or Argon) along with heating, CO_2 can be removed and active stabilizer is switched to a neutral form. The most important feature of these systems is that, during these transitions, CO_2 will not be accumulated in a system upon repeated cycles.

The basicity is required for facile switching depends greatly on the temperature and on the concentration at which the species can be switched. Ideally, the protonation degree is very low

when the system is under air, and in the presence of CO_2 it should be as high as possible to maximize the property change in polymer solution (**Scheme V.2**). Thus, the addition and removal of CO_2 should take the mixture back and forth across the system midpoint, which is defined as pH at which half of the switchable groups are protonated. Under air, the pH should be significantly higher than system midpoint, while upon exposure to CO_2, pH should be significantly lower than system midpoint. If the switchable species is entirely dissolved in the aqueous phase under air and under CO_2, the system midpoint is equal to pK_a value.

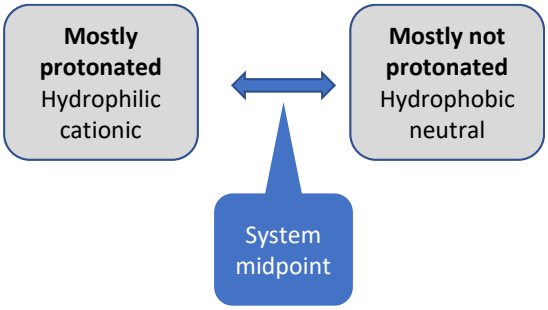

Scheme V.2 The principle of CO_2-switchable system in water. [1]

Among neutral switchable species, amines have appropriate basicity in water to be CO_2-responsive: they readily switch to bicarbonate salt upon CO_2 exposure and come back to neutral form after exposure to N_2 flow. The most studied CO_2-responsive moieties are PDEAEMA (p*K*a = 7.4) and PDMAEMA (p*K*a = 7.4) based (co)polymers. It is noteworthy that some of these amine-based CO_2-responsive homopolymers are also thermoresponsive (mostly in their uncharged from). Typical dual thermo- and CO_2-responsive homopolymers reported in the literature are listed in **Scheme V.3**, their corresponding cloud point temperature (T_c) can be tuned by CO_2 addition/removal.

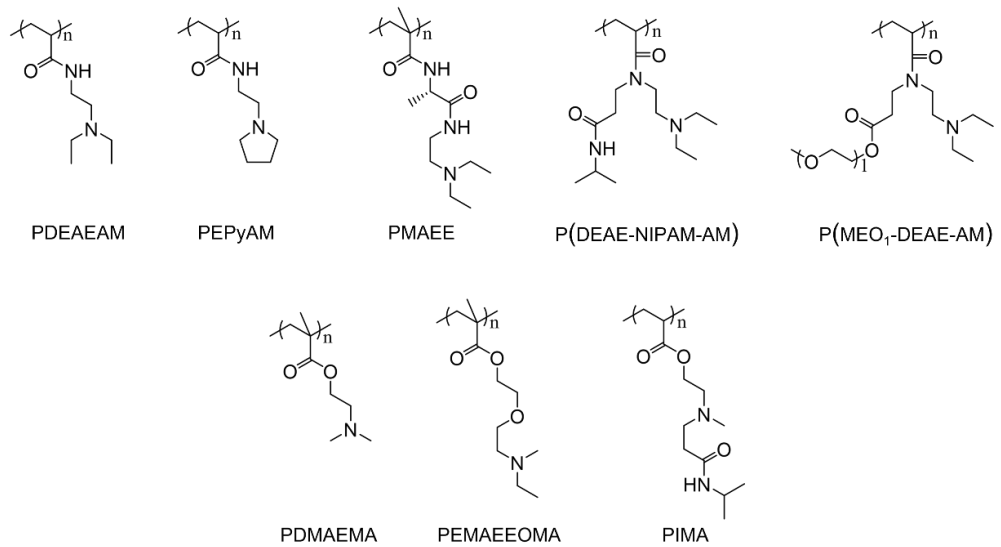

Scheme V.3 Summary of dual thermo- and CO_2-responsive homopolymers. (PDEAEAM: poly(*N*,*N*-diethylamino ethyl acrylamide, [2] PEPyAM: poly(*N*-ethylpyrrolidine acrylamide), [3] PMAEE:

poly(*N*-methacryloyl-$_L$-alanine 2-(diethylamino) ethylamide, [4] P(DEAE-NIPAM-AM): poly(*N*-(2-(diethylamino)ethyl)-*N*-(3-(isopropylamino)-3-oxopropyl)acrylamide), [5] P(MEO_1-DEAE-AM): poly(2-methoxyethyl 3-(*N*-(2-diethylamino ethyl) acrylamido) propanoate), [6] PDMAEMA: poly(*N*,*N*-dimethylaminoethyl methacrylate), [7] PEMAEEOMA: poly(2-(2-(ethyl (methyl) amino) ethoxy) ethyl methacrylate), [8] PIMA: poly(2-((3-(isopropylamino)-3-oxopropyl)(methyl) amino) ethyl acrylate) [9])

Such dual CO_2- and thermo-responsive (co)polymers have attracted huge interest in the last decade. Nevertheless, considering the difficulty in synthesis and subsequent purification of corresponding monomers and polymers (except commercial monomer DMAEMA), most multi-stimuli responsive copolymers are primarily prepared by combination of two or more blocks with different stimuli responsive behaviors. Taking advantage of controlled radical polymerization, such as nitro-mediated polymerization (NMP), atom-transfer radical polymerization (ATRP) and reversible addition-fragmentation chain-transfer (RAFT) polymerization, a considerable number of dual temperature- and CO_2- responsive copolymers with controlled compositions and well-defined microstructures have been synthesized, For instance, poly(*N*,*N*-diethylamino ethyl methacrylate)-*block*-poly(*N*-isopropylacrylamide) (PDEAEMA$_{60}$-*b*-PNIPAM$_{40}$) was synthesized via RAFT polymerization, it exhibited vesicles-to-unimers and unimers-to-micelles transition as CO_2 and temperature were applied. [10] *N*′-propargyl-*N*,*N*-dimethylacetamidine modified poly(*p*-azidomethylstyrene)-*block*-poly(*N*,*N*-dimethylamino ethyl methacrylate) (PAMS-*b*-PDMAEMA) self-assembled into vesicles with "breathing" character upon alternate bubbling CO_2/Ar and underwent a vesicles-to-(micelles cluster) transition in response to temperature change. [11] Amphiphilic poly(ε-caprolactone)-*block*-poly(*N*-isopropylacrylamide-*co*-*N*,*N*-dimethylamino ethyl methacrylate) terminated with a pyrene group, (Py-PCL-*b*-P(NIPAM-*co*-DMAEMA)), combining CO_2- and thermoresponsive properties was synthesized by a combination of ring open polymerization, dicyclohexylcarbodiimide (DCC) reaction and RAFT polymerization. [12] Triblock copolymer of PNIPAM-*b*-PCL-*b*-PDMAEMA was prepared by thiol-ene michael addition and host-guest interaction and displayed vesicle-to-micelle and vesicle-to-(swelled vesicle) transitions under stimulation of heating and CO_2. [13]

In this chapter, we aim at studying the CO_2-induced thermoresponsiveness of homopolymer, poly(*N*-,*N*-diethylamino ethyl acrylamide) (PDEAEAM), which bears thermo- and pH-/CO_2-responsive groups (acrylamide and tertiary amine group within one chain) and is one of multi-stimuli responsive homopolymers. Its corresponding cloud point temperature (T_c) can be tuned ranging from 50.2 to 33.1 ^oC with a pH change from 8.5 to 11.0. Moreover, its LCST behavior disappears upon CO_2 treatment and can be reversibly recovered by bubbling inert gas. [2] However, literature involving PDEAEAM-based copolymers is relatively scarce.

For instance, Guan and co-workers designed a multi-stimuli responsive star polymer of tetraphenylethene-*graf*-tetra-poly(*N*-(2-(diethylamino) ethyl acrylamide) with an aggregation-induced effect, the obtained star polymer displays a good performance in long-term cell tracing. [14] Kim and co-workers employed P(DEAEAM-*r*-NIPAM) as responsive surfactant to modulate particles shape of polystyrene-*b*-poly(4-vinylpyridine) between football and lens by subtly changing temperature and pH. [15]

Then we studied the responsiveness of PDEAEAM-based block copolymers. As described in **Chapters I** and **IV**, poly(*N*-isopropylacrylamide) (PNIPAM) is a typical thermoresponsive homopolymer with LCST behavior around 32 °C, which can be shifted by adjusting polymer concentration, polymer architecture, additives, end groups or by incorporating hydrophilic or hydrophobic blocks. A combination of thermoresponsive PNIPAM and thermo-, CO_2-responsive PDEAEAM creates a complex system that we studied in this chapter. By alternate bubbling CO_2/N_2, their responsive properties and self-assembly behaviors are investigated by nuclear magnetic resonance (NMR) spectra, turbidimetry, dynamic light scattering (DLS) and electronic microscopy techniques. This work will provide more information on CO_2-responsiveness of such family of PDEAEAM and help to broaden their potential applications.

Chemical structures of PDEAEAM homopolymer and block copolymer of PNIPAM-*b*-PDEAEAM are shown in **Scheme V.4**, their corresponding synthetic procedures can be referred to **Experimental Section** and **Chapter IV**. All $PDEAEAM_{mk}$ and $PNIPAM_{nk}$-*b*-$PDEAEAM_{mk}$ are abbreviated as PD_{mk} and PN_{nk}-*b*-PD_{mk} (mk and nk are molecular weights of PD and PN blocks, respectively).

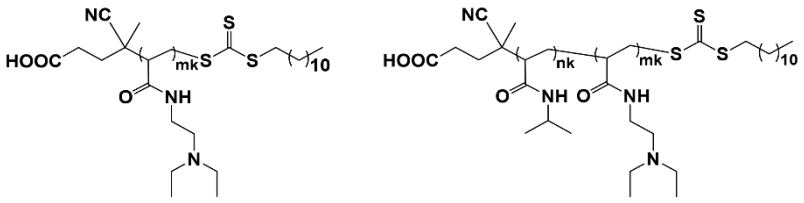

PDEAEAM **PNIPAM-*b*-PDEAEAM**

Scheme V.4 Chemical structures of PDEAEAM and PNIPAM-*b*-PDEAEAM used in this chapter.

V.2 Dual CO_2- and thermo-responsiveness of PD homopolymer

For polyamines, depending on the structure of amine groups and on the conditions of experiments, the reaction of amine function with CO_2 leads to the formation of ammonium bicarbonates or carbamates. Most of (co)polymers with tertiary amine groups are prone to

generate bicarbonate salts when a small quantity of CO_2 is added, [7, 16] while those bearing primary amines (such as poly(allylamine)) generally form into carbamates. [17]

In order to clarify the CO_2/N_2 switchability of PD, we first studied pH changes of PD_{5k} solution when CO_2 and N_2 were introduced alternatively. Protonation degree is calculated by the following eq. (3):

$$\% \text{ protonation} = \frac{1}{1+10^{\text{pH-p}Ka}} \qquad (3)$$

As depicted in **Figure V.1A**, before bubbling CO_2, system pH is 9.28 while corresponding protonation degree is 0.92%, thus PD_{5k} is regarded in deprotonated state. With introduction of CO_2 for 2.5 min, pH decreases sharply to 5.5, while a dramatic increase of protonation degree changes from 0.92 to 98.3%. After, both pH and protonation degree do not alter along with CO_2 concentration in system. As N_2 is alternatively bubbled, pH rises to 8 whereas protonation degree falls down to 15% after 5 min N_2 bubbling, which is followed by a slow increasing and decreasing tendency for changes of pH and protonation degree along with N_2 quantity, respectively. After 20 min bubbling N_2, pH returns to 8.53 and protonation degree comes to 5%.

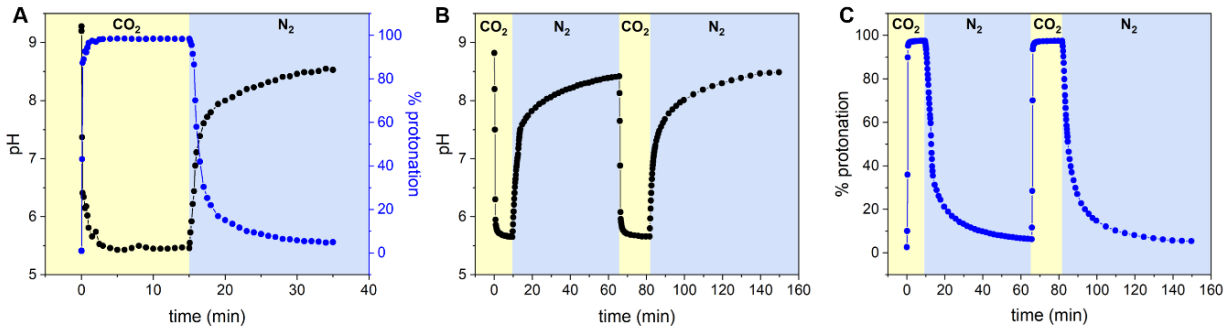

Figure V.1 (A) Changes in system pH and protonation degree of PD_{5k} solution in one cycle and (B, C) in two cycles upon alternate bubbling CO_2/N_2 ([PD_{5k}] = 0.1 wt.%, gas flow rate was 2 mL·min^{-1}).

The reversibility of pH and protonation degree upon bubbling CO_2/N_2 were traced (see **Figures V.1B** and **V.1C**), it is shown that PD_{5k} over alternate treatment with CO_2/N_2 exhibit good reversibility with at least two cycles.

The products of reaction of PD homopolymer with CO_2 at 25 °C was studied by ^{1}H NMR spectra. As shown in **Figure V.2B**, before addition of CO_2, PD_{5k} polymer presents three peaks at 3.32, 2.64 and 1.07 ppm corresponding to -C**H**$_2$CH$_2$N(CH$_2$CH$_3$)$_2$, -CH$_2$C**H**$_2$N(C**H**$_2$CH$_3$)$_2$ and -CH$_2$CH$_2$N(CH$_2$C**H**$_3$)$_2$, respectively. After 10 min of bubbling CO_2 (to make sure all PD units are protonated), these signals shift to 3.56, 3.27 and 1.32 ppm, respectively, and changes in system pH (from 9.9 to 6.1) and protonation degree (from 0.2 to 94%, calculated by eq. (3)) are accompanied with this process. Meanwhile signal at 160 ppm in ^{13}C NMR spectrum reveals the formation of ammonium bicarbonate (see **Figure V.2C**). After 30 min N_2 treatment, proton

peaks do not return to their original positions but shift to 3.39, 2.80 and 1.14 ppm, respectively. Additionally, pH of PD_{5k} goes up to 8.8, these results suggest that there is still a small quantity of PD_{5k} in protonated state (protonation degree is around 3%), more time of N_2 bubbling or heating PD_{5k} solution is needed for the complete recovery.

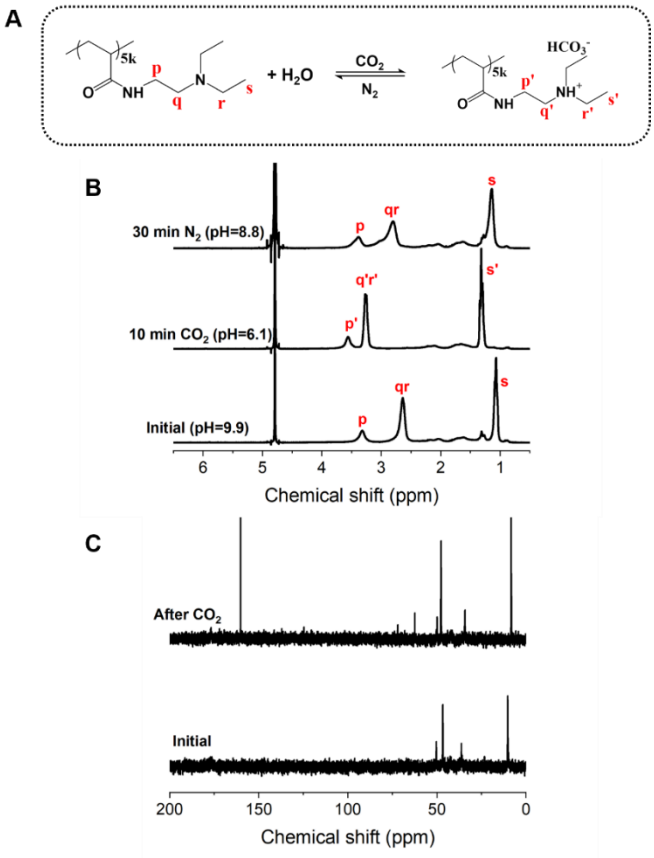

Figure V.2 (A) Chemical reaction of PD_{5k} with CO_2 in water. (B) ^1H and (C) ^{13}C NMR spectra of PD_{5k} in D_2O recorded at 25 °C upon alternate exposure to CO_2/N_2 (PD_{5k} concentration for NMR experiments was 1 wt.%, gas flow rate was 10 mL·min^{-1}, 10 and 30 min for bubbling CO_2 and N_2 respectively.).

Simultaneous coexistence of acrylamide and tertiary amine groups endows PD homopolymers with thermo- and CO_2-responsive properties. As shown in the previous chapter, their thermo-sensitivity is influenced by pH adjustment due to the protonation/deprotonation of tertiary amine groups. Here, CO_2 addition/removal can also modulate thermoresponsive properties of PD. Additionally, after removal of CO_2 by exposure to N_2, residual bicarbonate salts are prone to slightly modify the thermoresponsive behavior of PD in aqueous solutions.

To study the effect of CO_2 on thermoresponsiveness of PD_{5k}, turbidimetry measurements of PD_{5k} as a function of temperature upon alternative bubbling CO_2/N_2 were performed (**Figure V.3A**). Before exposure to CO_2, PD_{5k} displays a LCST behavior with a measured T_c at 31.5 °C. After treatment with CO_2, tertiary amine groups are protonated, which makes PD_{5k} hydrophilic. The transmittance value remains constant around 100% from 20 °C to 80 °C, suggesting that

PD_{5k} loses its thermoresponsiveness in the studied temperature range. Upon exposure to N_2, the LCST behavior of PD_{5k} is recovered with a higher T_c (64.9 °C). This phenomenon can be ascribed to the presence of residual CO_2 species in interactions with tertiary amine, being in good agreement with Zhang's work. [2]

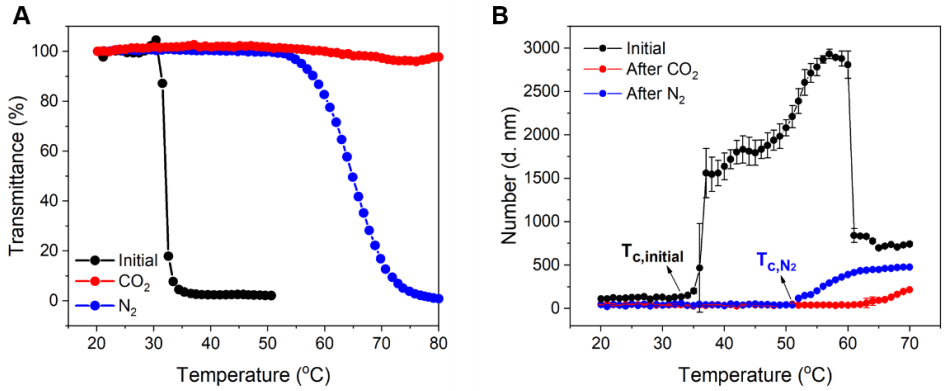

Figure V.3 Plots of (A) transmittance and (B) aggregates size *versus* temperature for PD_{5k} aqueous solution before, after bubbling CO_2 and after bubbling N_2. ([PD_{5k}] = 1 wt.%, heating rate for turbidimetry measurements was 1 °C·min^{-1}, gas flow rate was 10 mL·min^{-1}, 10 and 30 min for bubbling CO_2 and N_2 respectively.)

CO_2-switchable thermoresponsiveness of PD_{5k} was further analyzed by DLS measurements as shown in **Figure V.3B**. In the initial PD_{5k} solution, a change of measured hydrodynamic diameter is observed at 33 °C (T_c), which is related to the shrinkage of PD_{5k} units and hydrophobic association among intermolecular chains. Measured size goes on increasing upon heating up to 60 °C, then a precipitation takes place when larger aggregates are formed. In CO_2-rich environment, due to the protonation of PD_{5k} chains, T_c is shifted to higher temperature. As temperature is raised above 60 °C (apparent T_c), a slight increase of size is observed. This unexpected trend can be ascribed to a partial decarbonation phenomenon. Indeed, heating polymer solution at higher temperature for a long period of time is also a useful method to remove CO_2. When 30 min N_2 was bubbled to drive CO_2 out of the system, the responsiveness of PD_{5k} is recovered with a higher T_c at 52 °C, which is identical to the value (53 °C) obtained from turbidimetry measurements.

V.3 Thermo- and CO_2-responsiveness of PN_{5k}-*b*-PD_{5k} block copolymer

Block copolymers generally combine all properties of each block within structure. Thus, synthesized PN_{5k}-*b*-PD_{5k} block copolymers are expected to have both thermo- and CO_2-responsive properties.

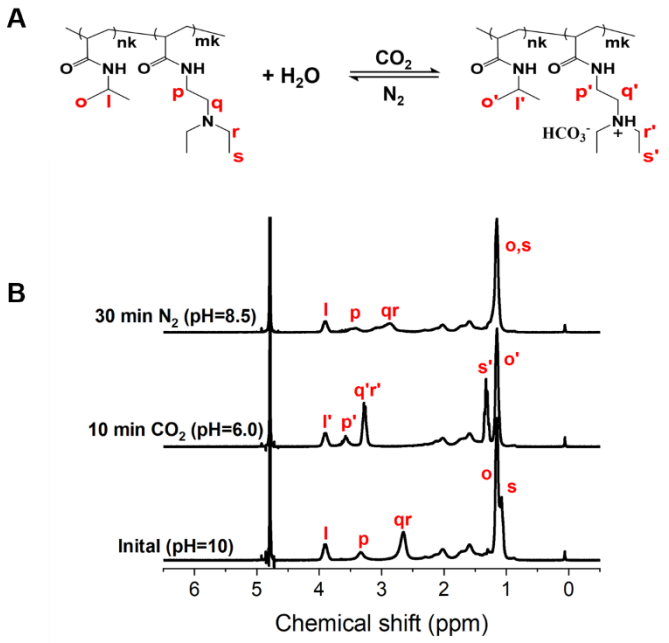

Figure V.4 (A) Chemical reaction of PN_{5k}-*b*-PD_{5k} with CO_2 in water, (B) ^1H NMR spectra of PN_{5k}-*b*-PD_{5k} in D_2O recorded at 25 °C upon alternate bubbling CO_2/N_2. (PN_{5k}-*b*-PD_{5k} concentration for NMR experiments was 1 wt.%, gas flow rate was 10 $mL \cdot min^{-1}$, 10 and 30 min for bubbling CO_2 and N_2 respectively.)

To confirm this, CO_2-responsiveness of PN_{5k}-*b*-PD_{5k} was analyzed by ^1H NMR spectra at room temperature **(Figure V.4)**. The site of interaction between CO_2 and PN_{5k}-*b*-PD_{5k} are evidenced in **Figure V.4B.** Chemical shifts of -C**H**$_2$CH$_2$N(CH$_2$CH$_3$)$_2$, -CH$_2$C**H**$_2$N(C**H**$_2$CH$_3$)$_2$ and -CH$_2$CH$_2$N(CH$_2$C**H**$_3$)$_2$ in PD_{5k} block move from 3.33, 2.65 and 1.08 ppm to 3.58, 3.28 and 1.33 ppm, respectively upon 10 min CO_2 bubbling, and subsequently return to 3.43, 2.87 and 1.15 ppm, respectively after bubbling N_2 for 30 min. Moreover, no chemical shift of signals at 3.89 and 1.15 ppm corresponding to -C**H**(CH$_3$)$_2$ and -CH(C**H**$_3$)$_2$ in PN_{5k} is observed, which means CO_2 only reacts with PD block to generate ammonium bicarbonate and has no effect on property of PN block. It has to be noted that upon alternate exposure to CO_2/N_2, PN_{5k}-*b*-PD_{5k} solution undergo a pH change: in the absence of CO_2, system pH of PN_{5k}-*b*-PD_{5k} solution is around 10, then decreases to 6 upon CO_2 aeration and comes to 8.5 after bubbling N_2.

V.3.1 CO_2-tunable thermoresponsiveness of PN_{5k}-*b*-PD_{5k}

The effect of CO_2 addition/removal on thermoresponsive behavior of PN_{5k}-*b*-PD_{5k} was studied by turbidimetry and DLS measurement (**Figure V.5**). After exposure to CO_2, PN_{5k}-*b*-PD_{5k} still displays a LCST behavior with a higher T_c (40 °C, determined from inflect point of transmittance curve) compared to the initial value (38 °C) since protonated PD_{5k} block increases the solubility of overall copolymer in water. Upon exposure to N_2, T_c is expected to return to initial value, however, due to the partial protonated PD_{5k} block, T_c of PN_{5k}-*b*-PD_{5k} is detected

at higher temperature (41 °C). This result is also confirmed by DLS analysis, in which the aggregates size before, after exposure to CO_2 and after bubbling N_2 starts to increase at 32, 40 and 37 °C, respectively.

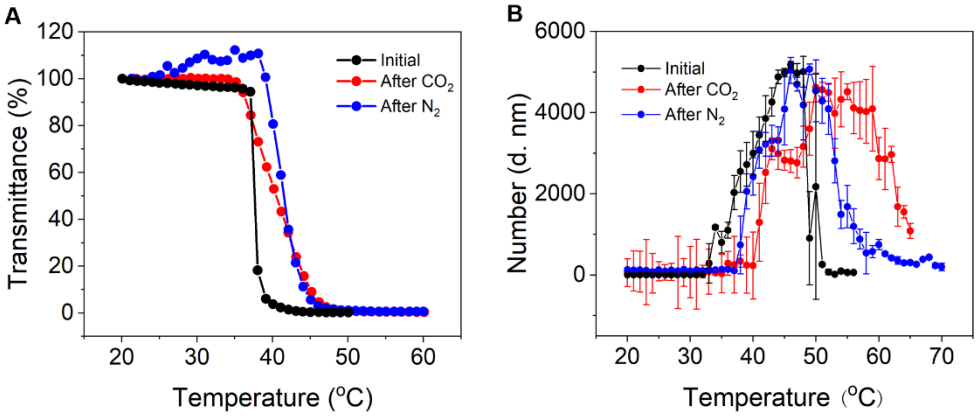

Figure V.5 Plots of (A) transmittance and (B) aggregates size *versus* temperature for PN_{5k}-*b*-PD_{5k} aqueous solution before, after bubbling CO_2 and after bubbling N_2. ([PN_{5k}-*b*-PD_{5k}] = 1 wt.%, gas flow rate was 10 mL·min^{-1}, 10 and 30 min for bubbling CO_2 and N_2 respectively, heating rate for turbidimetry measurements was 1 °C·min^{-1}.)

V.3.2 Self-assembly behavior of PN_{5k}-*b*-PD_{5k}

Solubility of PN and PD blocks in water can be tuned by temperature change and CO_2 treatment/removal, this causes a modification of polymer conformation in solution and induces a change in self-organization of aggregates. The conformation change of one chain of PN_{5k}-*b*-PD_{5k} in response to temperature and CO_2 is depicted in **Scheme V.5**. To study the self-organization of overall PN_{5k}-*b*-PD_{5k} under stimuli of temperature and CO_2, TEM and DLS measurements were carried out at different conditions.

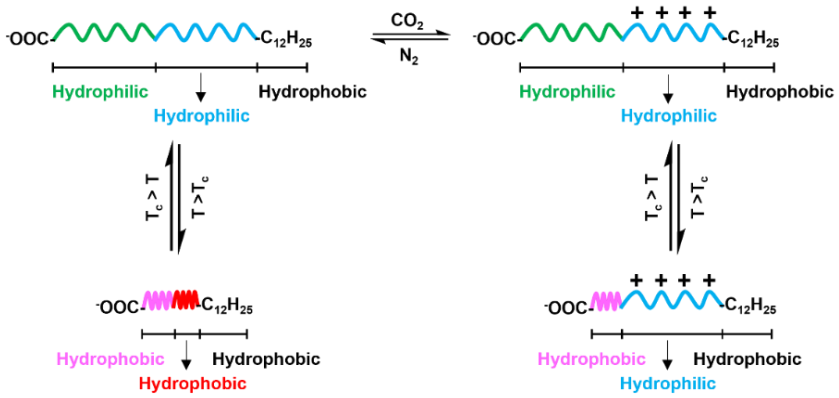

Scheme V.5 Conformation of PN_{5k}-*b*-PD_{5k} chains under heating/cooling and CO_2 treatment/removal.

(i) Self-assembly at low temperature ($T < T_c$)

In absence of CO_2, due to the hydrophobic -$C_{12}H_{25}$ end group and hydrated PN and PD chains, PN_{5k}-*b*-PD_{5k} assembles into spherical micelles (23.2 ± 5.7 nm) with a core of -$C_{12}H_{25}$

group and a corona of PN_{5k} and PD_{5k} blocks, as shown in **Figure V.6A**. Exposure to CO_2 improves the solvation of PD chains in water, but it does not trigger any effect on PN chains and $-C_{12}H_{25}$ terminal. Therefore, spherical structures (28.7 ± 7.8 nm) are still observed in **Figure V.6B**, whereas theses spheres present a different corona, which composes of hydrated PN_{5k} and charged PD_{5k}. As CO_2 is removed by bubbling N_2, PD_{5k} block recovers deprotonated state, and it still maintains good solubility in water. Consequently, micelle structures with an average diameter of 23.0 ± 5.0 nm are observed (**Figure V.6C**).

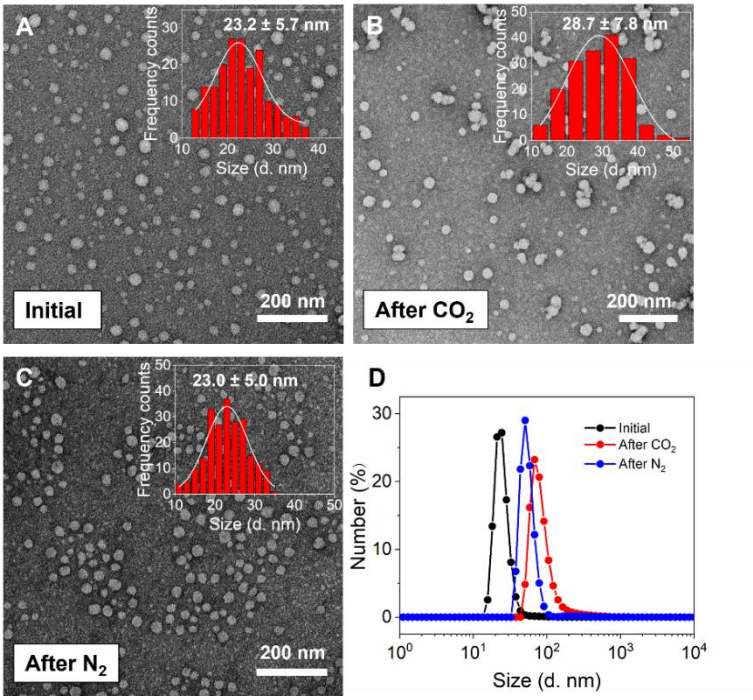

Figure V.6 (A-C) TEM images and (D) number-averaged hydrodynamic size distribution of PN_{5k}-*b*-PD_{5k} before, after CO_2 treatment and after exposure to N_2 at 25 °C. ([PN_{5k}-*b*-PD_{5k}] = 0.1 wt.%, gas flow rate was 10 mL·min^{-1}, 10 and 30 min for bubbling CO_2 and N_2 respectively. TEM samples stained with 2 wt.% uranyl acetate solution.)

Compared to the aggregates size analyzed by TEM images, DLS measurements (**Figure V.6D**) show larger hydrodynamic size of micelles under the same condition, which is expected since DLS data are obtained in hydrated state whereas TEM samples are tested in dried state. It has to be noted that after bubbling CO_2 and N_2, the micelles have larger size (68.9 ± 23.9 and 51.3 ± 7.6 nm obtained after bubbling CO_2 and N_2, respectively) than the value obtained before CO_2 treatment (27.0 ± 8.8 nm).

(ii) Self-assembly at high temperature ($T > T_c$)

Before exposure to CO_2, at 60 °C (above T_c), both PN and PD chains collapse. Poorly soluble PN_{5k}-*b*-PD_{5k} chains aggregate into spherical micelles cluster with an average diameter equal to 92.8 ± 34.6 nm (**Figure V.7A**).

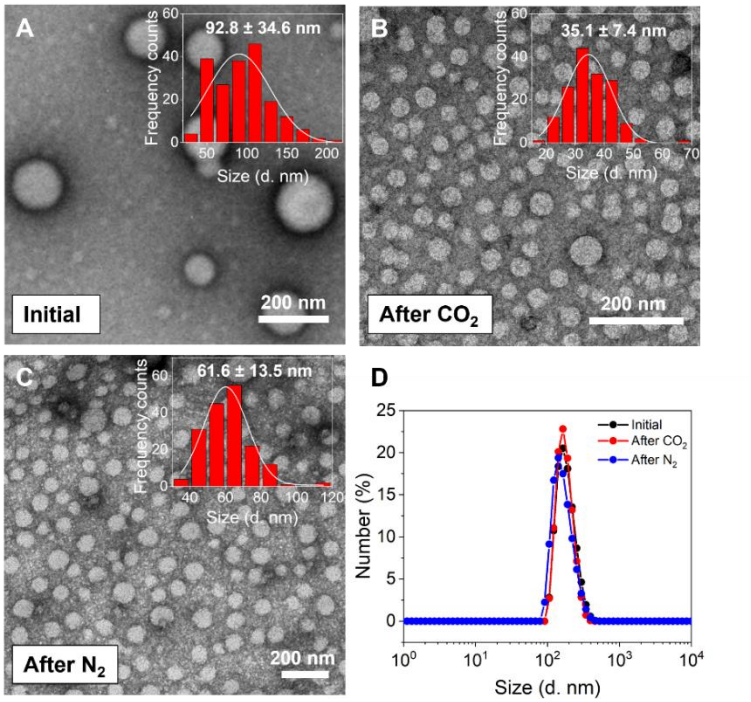

Figure V.7 (A-C) TEM images and (D) number-averaged hydrodynamic size distribution of PN_{5k}-*b*-PD_{5k} before, after CO_2 treatment and after exposure to N_2 at 60 °C. ([PN_{5k}-*b*-PD_{5k}] = 0.1 wt.%, gas flow rate was 10 mL·min^{-1}, 10 and 30 min for bubbling CO_2 and N_2 respectively. TEM samples stained with 2 wt.% uranyl acetate solution.)

In presence of CO_2, PN block is not affected and keeps its thermoresponsive property, whereas PD chains are protonated, which makes PD block no longer thermoresponsive in the studied temperature range. As temperature rises to 60 °C (above T_c), PN chains collapse and become hydrophobic, while PD chains remain good solubility. Therefore, flower-like micelles are formed with -$C_{12}H_{25}$ core, PN shell and PD corona. Moreover, the size of such aggregates (35.1 ± 7.4 nm) is smaller than that formed before CO_2 treatment at the same temperature (**Figure V.7B**). This result is also confirmed by DLS analysis, in which hydrodynamic diameters of aggregates before and after exposure to CO_2 are 188.5 ± 3.1 and 174.6 ± 4.5 nm, respectively. Upon bubbling N_2, PD block regains thermoresponsiveness, as temperature increases above T_c, both PN and PD chains shrink. Spherical micelles cluster with large diameter (61.6 ± 13.5 nm) are formed (**Figure V.7C**). This value is smaller compared to the initial size (92.8 ± 34.6 nm) and it is confirmed by DLS results (hydrodynamic diameter of 188.5 ± 3.1 and 166.3 ± 4.9 nm obtained before bubbling CO_2 and after treatment with N_2, respectively) (see **Figure V.7D**).

(iii) Self-assembly mechanism of PN_{5k}-*b*-PD_{5k} at different conditions

As revealed in TEM and DLS analysis, PN_{5k}-*b*-PD_{5k} self-assemble into spherical structures with different sizes in all studied conditions.

In absence of CO_2, both PN and PD block are soluble at 25 °C and form into core-corona micelles, in which core is hydrophobic -$C_{12}H_{25}$ group and corona is composed of PN and PD blocks. With an increase of temperature, PN and PD chains collapse to form core-shell micelles (hydrophobic core might be formed by $C_{12}H_{25}$ groups while PN and PD formed shell). Due to the strong hydrophobic association among shells, these micelles aggregate to form micelles cluster (see **Scheme V.6**). Upon exposure to CO_2, at 25 °C, PD chains are protonated, which has a slight or no effect on morphology and size of PN_{5k}-*b*-PD_{5k}, core-corona micelles with similar size are still detected, a main difference is corona composing of PN and charged PD or PN and uncharged PD. As temperature increases over T_c, PN block shrinks while protonated PD block maintains good solvation, therefore flower-like micelles are formed. The existed electrostatic repulsion prevents hydrophobic association of PN chains to some extent, which leads to appearance of spherical structure with an intermediate size (larger than the size at low temperature but smaller than that at 60 °C in absence of CO_2).

Further experiments (SAXS, Zeta potential…) are under way and are still required to assess proposed structures shown in **Scheme V.6** and the corresponding mechanism of formation under different conditions.

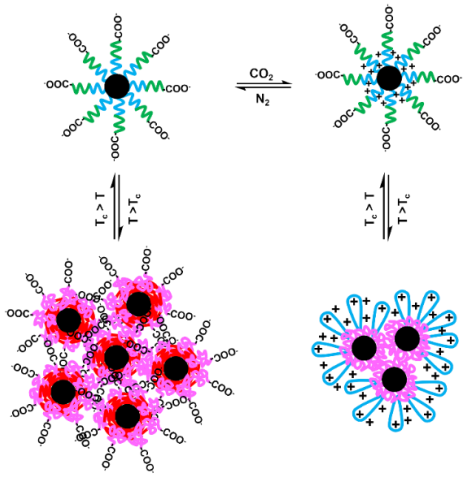

Scheme V.6 Schematic illustration of self-organization of PN_{5k}-*b*-PD_{5k} under dual stimuli of temperature and CO_2.

V.4 Effect of copolymer composition on thermoresponsiveness and self-assembly

As observed in the case of PN_{5k}-*b*-PD_{5k}, PD block interacts solely with CO_2 upon exposure to CO_2 and it, after treatment with N_2, is incompletely recovered to initial state. A similar phenomenon is also observed in the cases of PN_{2k}-*b*-PD_{8k} and PN_{8k}-*b*-PD_{2k} (see **Figure V.8**).

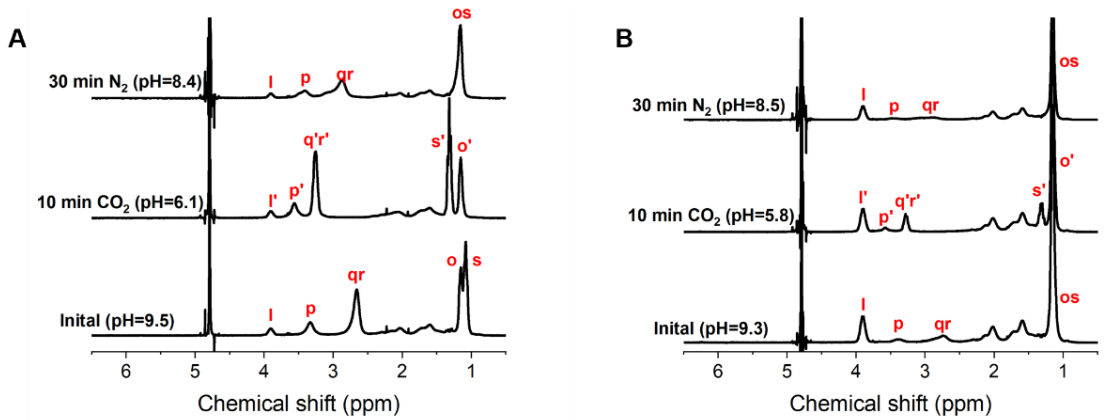

Figure V.8 ^{1}H NMR spectra of (A) PN_{2k}-*b*-PD_{8k} and (B) PN_{8k}-*b*-PD_{2k} in D_2O recorded at 25 °C upon alternate bubbling CO_2/N_2. ([PN-*b*-PD] = 1 wt.%, gas flow rate was 10 mL·min^{-1}, 10 and 30 min for bubbling CO_2 and N_2 respectively.)

As shown in **Figure V.8**, upon alternate bubbling CO_2/N_2, chemical shifts of -C**H**$(CH_3)_2$ and -CH(C**H**$_3)_2$ in PN block remain around 3.9 and 1.15 ppm and are not influenced by CO_2 treatment/removal. Whereas proton peaks of -C**H**$_2$CH$_2$N(CH$_2$CH$_3)_2$, -CH$_2$C**H**$_2$N(C**H**$_2$CH$_3)_2$ and -CH$_2$CH$_2$N(CH$_2$C**H**$_3)_2$ in the case of PN_{2k}-*b*-PD_{8k} shift from 3.33, 2.66 and 1.08 ppm to 3.56, 3.26 and 1.32 ppm after 10 min exposure to CO_2 and return to 3.41, 2.87 and 1.16 ppm as N_2 is bubbled for 30 min. These signals in ^{1}H NMR spectra of PN_{8k}-*b*-PD_{2k} at 3.38, 2.73 and 1.15 ppm undergo a similar change under the same conditions, CO_2 treatment causes a downfield shift (3.57, 3.27 and 1.3 ppm) and N_2 aeration leads PD signals almost recover to initial positions (3.42, 2.9 and 1.15 ppm).

V.4.1 Effect of copolymer composition on T_c

The effect of CO_2 addition/removal on the thermoresponsive behavior of PN_{2k}-*b*-PD_{8k} and PN_{8k}-*b*-PD_{2k} was studied by turbidimetry measurements (**Figure V.9**). Measured T_c are summarized in **Table V.1**.

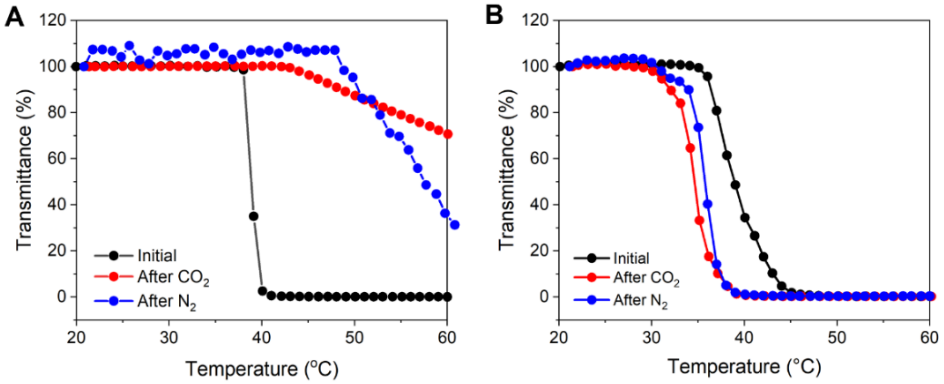

Figure V.9 Plots of transmittance for (A) PN_{2k}-*b*-PD_{8k} and (B) PN_{8k}-*b*-PD_{2k} aqueous solution before, after bubbling CO_2 and after bubbling N_2. ([PN-*b*-PD] = 1 wt.%, gas flow rate was 10 mL·min^{-1}, 10 and 30 min for bubbling CO_2 and N_2 respectively.)

Table V.1 Measurements of T_c for PN-*b*-PD from turbidimetry measurements.

Copolymer	Initial		After exposure to CO_2		After exposure to N_2	
	$T_{c,\ oneset}$ (^oC)[a]	$T_{c,\ ip}$ (^oC)[b]	$T_{c,\ oneset}$ (^oC)	$T_{c,\ ip}$ (^oC)	$T_{c,\ oneset}$ (^oC)	$T_{c,\ ip}$ (^oC)
PN_{2k}-*b*-PD_{8k}	38	39	43	/[c]	48	/[c]
PN_{5k}-*b*-PD_{5k}	37	38	35	40	38	41
PN_{8k}-*b*-PD_{2k}	35	37	30	34	30	36

[a]$T_{c,onset}$ determined from temperature where transmittance of copolymer solution starts to decrease. [b]$T_{c,ip}$ determined from inflection point of transmittance curve. [c]Not determined. (Gas flow rate was 10 $mL \cdot min^{-1}$, 10 and 30 min for bubbling CO_2 and N_2 respectively.)

As demonstrated in **Figure V.9**, upon bubbling CO_2, the transmittance of PN_{2k}-*b*-PD_{8k} solution starts to decrease at 43 ^oC, which is higher than the value obtained (38 ^oC) before bubbling CO_2. Then it goes up to 48 ^oC after 30 min treatment with N_2. The similar phenomenon also takes place in PN_{8k}-*b*-PD_{2k}, the transmittance starts to decrease at 35 ^oC, which shifts to 30 ^oC upon exposure to CO_2, and it remains at 30 ^oC after N_2 treatment. While $T_{c,ip}$ of PN_{8k}-*b*-PD_{2k} changes from 37 to 34 to 36 ^oC under the same conditions.

In all cases the addition of CO_2 deeply modifies the value of T_c of studied copolymers. After bubbling N_2, none of the systems returns to initial state due probably to the presence of residual ammonium bicarbonate. Nevertheless, the magnitude of thermoresponsiveness shift relates to the length of PD chain. Due to the presence of longer PD block, the effect seems to be more pronounced in the case of PN_{2k}-*b*-PD_{8k} block copolymer than that in PN_{8k}-*b*-PD_{2k}.

V.4.2 Effect of copolymer composition on self-assembly behavior

Figures V.10 and V.**11** present TEM and DLS analyses of PN_{2k}-*b*-PD_{8k} and PN_{8k}-*b*-PD_{2k} at 25 and 60 °C of the aggregates present in solution before, after exposure to CO_2 and after bubbling N_2. Detailed aggregates sizes of PN-*b*-PD under different conditions are summarized in **Table V.2**.

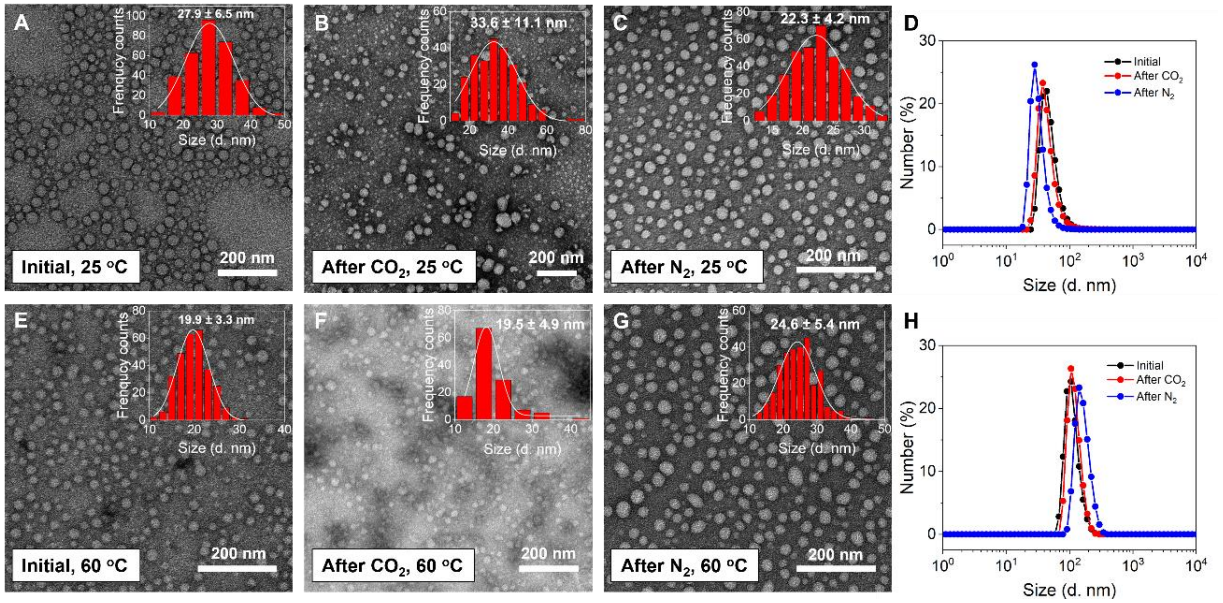

Figure V.10 (A-C, E-F) TEM images and (D, H) number-averaged hydrodynamic size distribution of PN_{2k}-*b*-PD_{8k} before, after bubbling CO_2 and after bubbling N_2 at different temperatures. (A): before bubbling CO_2, 25 °C, (B): after bubbling CO_2, 25 °C, (C): bubbling N_2, 25 °C, (E): before bubbling CO_2, 60 °C, (F): before bubbling CO_2, 60 °C, (G) before bubbling N_2, 60 °C. ([PN_{2k}-*b*-PD_{8k}] = 0.1 wt.%, gas flow rate was 10 mL·min^{-1}, 10 and 30 min for bubbling CO_2 and N_2 respectively. TEM samples stained with 2 wt.% uranyl acetate solution.)

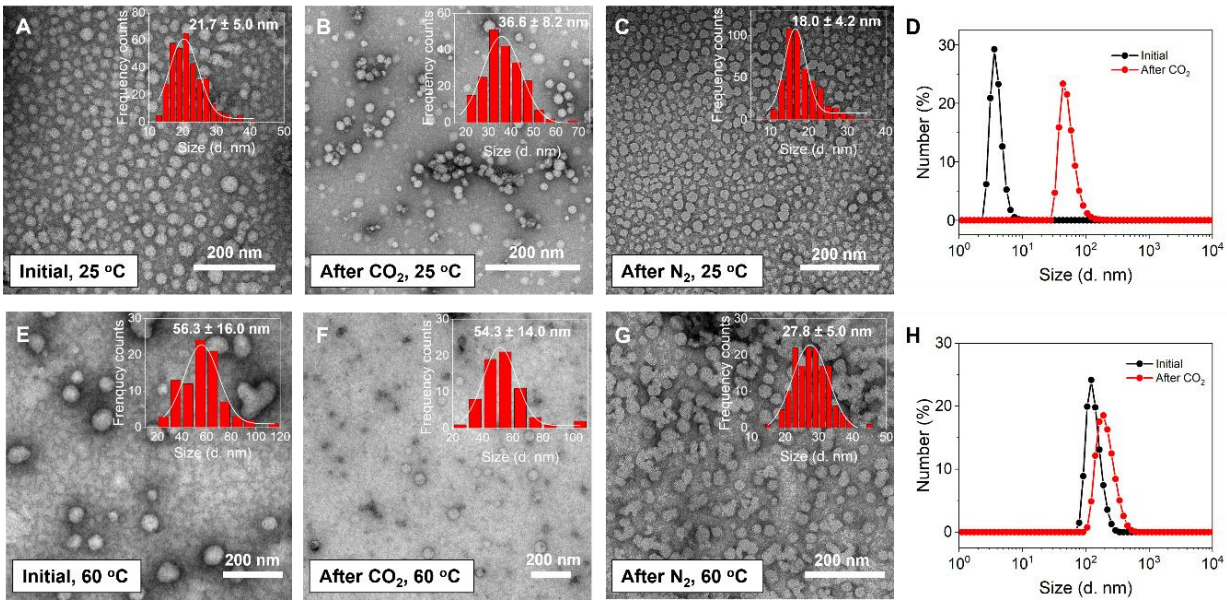

Figure V.11 (A-C, E-F) TEM images and (D, H) number-averaged hydrodynamic size distribution of PN_{8k}-*b*-PD_{2k} before, after bubbling CO_2 and after bubbling N_2 at different temperatures. (A): before bubbling CO_2, 25 °C, (B): after bubbling CO_2, 25 °C, (C): bubbling N_2, 25 °C, (E): before bubbling CO_2, 60 °C, (F): before bubbling CO_2, 60 °C, (G) before bubbling N_2, 60 °C. ([PN_{8k}-*b*-PD_{2k}] = 0.1 wt.%, gas flow rate was 10 mL·min^{-1}, 10 and 30 min for bubbling CO_2 and N_2 respectively. TEM samples stained with 2 wt.% uranyl acetate solution.)

Table V.2 PN-*b*-PD aggregates size upon CO_2 treatment/removal at 25 and 60 °C determined by TEM and DLS measurements.

Technique		Condition	Aggregates size (d. nm)		
			PN_{2k}-*b*-PD_{8k}	PN_{5k}-*b*-PD_{5k}	PN_{8k}-*b*-PD_{2k}
TEM	25 °C	Initial	27.9 ± 6.5	23.2 ± 5.7	21.7 ± 5.0
		After bubbling CO_2	33.6 ± 11.1	28.7 ± 7.8	36.6 ± 8.2
		After bubbling N_2	22.3 ± 4.2	23.0 ± 5.0	18.0 ± 4.2
	60 °C	Initial	19.9 ± 3.3	92.8 ± 34.6	56.3 ± 16.0
		After bubbling CO_2	19.5 ± 4.9	35.1 ± 7.4	54.3 ± 14.0
		After bubbling N_2	24.6 ± 5.4	61.6 ± 13.5	27.8 ± 5.0
DLS	25 °C	Initial	45.9 ± 3.4	27.0 ± 8.8	4.1 ± 1.3
		After bubbling CO_2	46.3 ± 26.9	68.9 ± 23.9	45.0 ± 13.0
		After bubbling N_2	34.3 ± 8.2	51.3 ± 7.6	/[a]
	60 °C	Initial	109.4 ± 1.9	188.5 ± 3.1	137.8 ± 3.9
		After bubbling CO_2	119.3 ± 3.6	174.6 ± 4.5	209.0 ± 5.4
		After N_2	160.5 ± 5.6	166.3 ± 4.9	/[a]

[a]Not determined. (Gas flow rate was 10 mL·min^{-1}, 10 and 30 min for bubbling CO_2 and N_2 respectively.)

Obtained results are in good agreement with the ones observed in the case of PN_{5k}-*b*-PD_{5k} copolymers, leading to the similar conclusions. Further experiments (SAXS, Zeta potential…) are under way concerning the characterization of observed structures.

V.5 Reversibility of PN-*b*-PD upon alternate bubbling CO_2/N_2

As demonstrated above, exposure to CO_2 enables to protonate tertiary amine groups in PD block. Deprotonation state can be almost recovered upon bubbling N_2. To test the reversibility of CO_2/N_2 responsiveness, PN-*b*-PD solutions were repeatedly treated with alternate bubbling CO_2/N_2. The change of chemical shift of characteristic proton peaks in PD block was recorded by NMR experiments. As shown in **Figure V.12A**, only chemical shifts of **p**, **qr** and **s** signals in PN_{5k}-*b*-PD_{5k} shift toward downfield after CO_2 treatment, then shift toward upfield and almost return to initial positions as CO_2 is removed by bubbling N_2. Meanwhile, pH of PN_{5k}-*b*-PD_{5k} solution decreases and increases after CO_2 and N_2 treatment, respectively. This suggests that

PN_{5k}-*b*-PD_{5k} exhibits a good reversibility with a minimum of 7 cycles. The same phenomenon is also observed in other two PN-*b*-PD block copolymers whatever PN content (see **Figures V.12C - V.12F**).

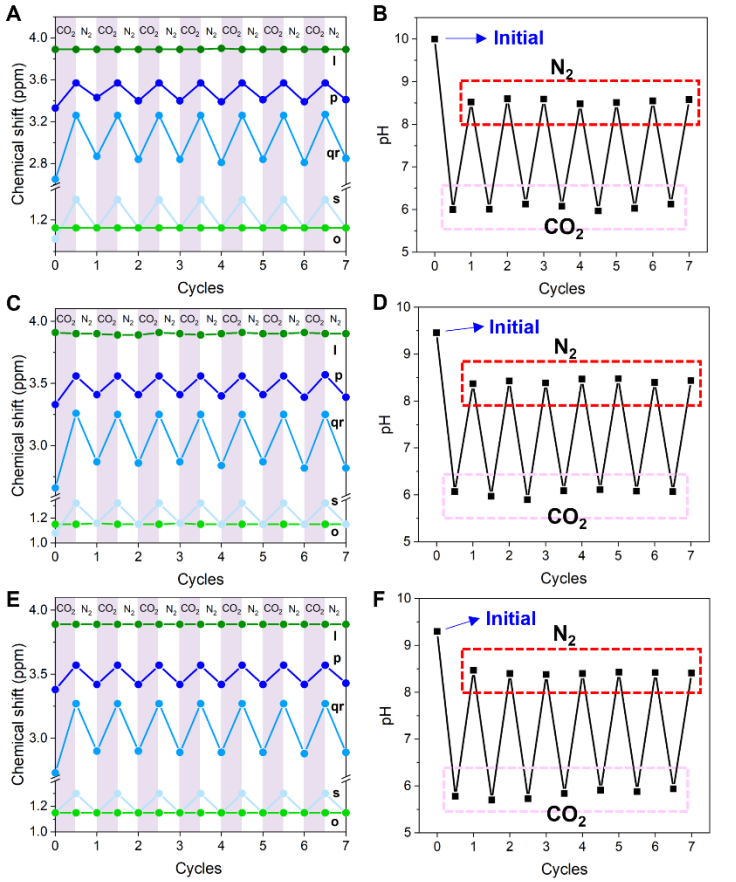

Figure V.12 Changes of chemical shifts and system pH of (A, B) PN_{5k}-*b*-PD_{5k}, (C, D) PN_{2k}-*b*-PD_{8k} and (E, F) PN_{8k}-*b*-PD_{2k} at 25 °C upon alternate bubbling CO_2/N_2 for 7 cycles. ([PN-*b*-PD] = 1 wt.%, gas flow rate was 10 mL·min^{-1}, 10 and 30 min for bubbling CO_2 and N_2, respectively.)

V.6 Conclusions

In summary, CO_2-switchable thermoresponsive properties (including cloud point temperature and self-assembly behavior) of $PDEAEAM_{5k}$ homopolymer and block copolymers of PNIPAM-*b*-PDEAEAM with variable compositions were investigated. It is found that CO_2 addition leads to the protonation of tertiary amine groups in PD chains, which improves solvation of PD in water and results in a partial loss of thermoresponsiveness of PN-*b*-PD aqueous solution. After CO_2 is removed by bubbling N_2, the LCST behavior is recovered but with a higher T_c value. Additionally, for self-assembly of PN-*b*-PD, at 25 °C (below T_c), CO_2 treatment has no or slight effect on morphology and size of PN-*b*-PD, whereas a more pronounced effect is measured at temperature above T_c. All PN-*b*-PD block copolymers exhibit a good reversibility at least 7 cycles upon alternate bubbling CO_2/N_2.

V.7 References

[1] A.K. Alshamrani, J.R. Vanderveen, P.G. Jessop, Phys. Chem. Chem. Phys. 18 (2016) 19276-19288.

[2] Z. Song, K. Wang, C. Gao, S. Wang, W. Zhang, Macromolecules 49 (2016) 162-171.

[3] K. Wang, Z. Song, C. Liu, W. Zhang, Polym. Chem. 7 (2016) 3423-3433.

[4] C. Luo, W. Fu, Z. Li, B. Zhao, Polymer 101 (2016) 319-327.

[5] X. Jiang, C. Feng, G. Lu, X. Huang, ACS Macro Lett. 3 (2014) 1121-1125.

[6] X. Jiang, C. Feng, G. Lu, X. Huang, Polymer 64 (2015) 268-276.

[7] D. Han, X. Tong, O. Boissière, Y. Zhao, ACS Macro Lett. 1 (2012) 57-61.

[8] K. Wang, S. Chen, W. Zhang, Macromolecules 50 (2017) 4686-4698.

[9] J. Huang, H. Qin, B. Wang, Q. Tan, J. Lu, Polym. Chem. 10 (2019) 6379-6384.

[10] A. Feng, C. Zhan, Q. Yan, B. Liu, J. Yuan, Chem. Commun. 50 (2014) 8958-8961.

[11] H. Zou, W. Yuan, Polym. Chem. 6 (2015) 2457-2465.

[12] W. Yuan, J. Shen, H. Zou, RSC Adv. 5 (2015) 13145-13152.

[13] B.-W. Liu, H. Zhou, S.-T. Zhou, H.-J. Zhang, A.-C. Feng, C.-M. Jian, J. Hu, W.-P. Gao, J.-Y. Yuan, Macromolecules 47 (2014) 2938-2946.

[14] X. Guan, L. Meng, Q. Jin, B. Lu, Y. Chen, Z. Li, L. Wang, S. Lai, Z. Lei, Macromol Mater Eng 303 (2018) 1700553.

[15] J. Lee, K.H. Ku, C.H. Park, Y.J. Lee, H. Yun, B.J. Kim, ACS Nano 13 (2019) 4230-4237.

[16] Y. Zhang, Z. Chu, C.A. Dreiss, Y. Wang, C. Fei, Y. Feng, Soft Matter 9 (2013) 6217-6221.

[17] D. Nagai, A. Suzuki, Y. Maki, H. Takeno, Chem. Commun. 47 (2011) 8856-8858.

Conclusions

The objective of this thesis is to study the effect of composition, molar mass, architecture, concentration of (co)polymers on their behaviors in aqueous solution induced by a change of temperature and/or pH (modified by addition of base/acid or bubbling CO_2/N_2).

We synthesized three different families of block or statistical copolymers bearing thermo-, and/or pH-, and/or CO_2-responsive groups: (1) thermoresponsive statistical copolymers of P(VCL-*stat*-VP) with different compositions; (2) thermosensitive copolymers of P(BA-*co*-NIPAM) with different compositions and architectures (diblock, triblock and statistical); (3) multi-stimuli (thermo-, pH- and CO_2-responsive) block copolymers of PNIPAM-*b*-PDEAEAM with variable compositions and their corresponding homopolymers of PNIPAM and PDEAEAM. These studied (co)polymers with well-defined structures and low polydispersities were prepared via RAFT/MADIX (employed in synthesis of P(VCL-*stat*-VP) and P(BA-*co*-NIPAM)) or RAFT polymerization (employed in synthesis of PNIPAM-*b*-PDEAEAM).

Hybrid nanoparticles were prepared by *in-situ* formation and by coating P(VCL-*stat*-VP) on preformed AuNPs, which confers obtained nanohybrids with thermoresponsive properties of P(VCL-*stat*-VP) as well as optical and catalytic properties of AuNPs. The effects of copolymer composition, concentration, pH values and ionic strength on colloidal stabilization of Au@P(VCL-*stat*-VP) were investigated. The results show that increasing copolymer concentration shift stability of nanohybrids toward modification of pH or addition of salt due to the higher steric hindrance. Moreover, at a specific concentration, increasing VP content weakens the colloidal stability and thermosensitivity of nanohybrids. Additionally, the catalytic activity of Au@P(VCL-*stat*-VP) in reduction of *p*-nitrophenol to *p*-aminophenol increases along with temperature until T_c reaches, at which copolymer chains collapse in response to temperature, this hinders the reactant from diffusing onto AuNPs surface, and results in a decreasing or no catalytic efficiency. The influence of VP content on catalytic activity is attributed to a compromise between more hydrophobicity of two additional methylene group in VCL units (favoring access of reactants towards AuNPs) and stronger adsorption of VCL (inhibiting catalytic efficiency) compared to VP moieties.

The introduction of hydrophobic BA segments can lower T_c of PNIPAM segments, and the shift intensity increases with an increase of BA content in whatever architecture. It is found that the effect of microstructure on T_c in dilute solution follows such an order: $T_{c,statistical} < T_{c,triblock} < T_{c,diblock}$ at the same (co)polymer concentration and composition. Moreover, spherical

structures are detected with larger diameter at temperature above T_c than ones formed at lower temperature. In concentrated solution, gelation temperature and network density between diblock and triblock copolymers are compared, it is evidenced that gels in triblock analogues are formed at lower temperature with denser microstructure.

The study of multi-stimuli thermo-, pH-responsive block copolymer PNIPAM-*b*-PDEAEAM with variable compositions and corresponding homopolymers of PNIPAM and PDEAEAM was then performed. Firstly, we demonstrated the critical role of the remaining chemical functions issued from RAFT agent present at the end of polymer. Both -COOH and hydrophobic $-C_{12}H_{25}$ end groups exert a strong effect on the colloidal properties at different pH values. T_c of PNIPAM homopolymers increases along with pH due to the ionization of -COOH end group, whereas PDEAEAM displays an opposite behavior caused by sequential deprotonation of tertiary amine groups within PDEAEAM chains. The effect of the different stimuli on the corresponding block copolymers were then studied. At pH 10 (above p*K*a of PDEAEAM block), both PNIPAM and PDEAEAM exhibit thermoresponsiveness, and one T_c is detected in case of $PNIPAM_{5k}$-*b*-$PDEAEAM_{5k}$. Stable spherical nanoobjects with different sizes are formed at lower and higher temperature. At pH 4 (below p*K*a of PDEAEAM block), PDEAEAM loses its thermosensitive property. Two T_c values are measured, and a gradual growth of aggregates size is detected upon heating.

Lastly, we investigated CO_2-responsiveness of PDEAEAM upon CO_2 treatment/removal. The effect of addition of CO_2 on the behavior of PNIPAM-*b*-PDEAEAM block copolymer is studied and illustrated how colloidal properties (phase transition temperature and colloid formation) of this copolymer solution can be tuned by using different stimuli: temperature and CO_2. Additionally, all these block copolymers of PNIPAM-*b*-PDEAEAM exhibit a good reversibility with at least 7 cycles upon alternate bubbling CO_2/N_2.

Experimental Section

Contents

ES.1 Materials

Chapter II: Sodium tetrachloroaurate dihydrate ($NaAuCl_4 \cdot 2H_2O$) and sodium borohydride ($NaBH_4$) were purchased from Aldrich and were used without further purification. 1,4-dioxane (Aldrich, 99%) was passed through basic alumina to remove BHT inhibitor prior to polymerization, *N*-vinylcaprolactam (VCL, Aldrich, 98%) and *N*-vinylpyrrolidone (VP, Aldrich, > 99%) were both distilled over CaH_2 and stored under argon prior to use. 2,2'-azobisisobutyronitrile (AIBN, Fluka, 98%) was recrystallized twice from methanol. *O*-ethyl-*S*-(1-methoxycarbonyl) ethyl dithiocarbonate (xanthate **X1**) was synthesized as previously described. [1] Ultrapure water (ρ = 18 MΩ·cm) was obtained from Purite device.

Chapter III: Ethyl xanthic acid potassium salt (97+%), *N*-isopropylacrylamide (99%, NIPAM) and *n*-butyl acrylate (99%, BA) were supplied from Acros Organics. BA was filtrated over alumina to remove inhibitor prior to polymerization. NIPAM was purified by recrystallization (twice) using a toluene : hexane (1:10 weight ratio) mixed solvent. The reversible addition-fragmentation chain transfer (RAFT) agent *O*-ethyl-*S*-(1-methoxycarbonyl) ethyl dithiocarbonate (xanthate **X1**) was synthesized according to an earlier procedure from our group. Diethyl 2,5-dibromoadipate and ethyl xanthic acid potassium salt were purchased from Sigma-Aldrich (98%) and use as received. The 2,2'-azobis(2-methylproprionitrile) (98%, AIBN) was purchased from Janssen Chimica and recrystallized from methanol before use. Absolute ethanol (AnalaRnormapur VWR) was used as received. Water was purified through a filter and ion exchange resin using a Purite device (resistivity ≈ 18 MΩ·cm).

Chapter IV: *N*-isopropylacrylamide (NIPAM, Sigma-Aldrich), *N*, *N*-diethylethylenediamine (≥ 99%, Sigma-Aldrich), acryloyl chloride (≥ 97%, Sigma-Aldrich), 4-cyano-4-[(dodecylsulfanylthiocarbonyl) sulfanyl] pentanoic acid (CDTPA, 97%, Sigma-Aldrich), triethylamine (TEA, 99%, Lancaster) were used as received. 2, 2'-Azobis(isobutyronitrile) (AIBN) was crystallized twice from methanol. 1, 4-dioxane and chloroform were purified through alumina columns prior to use. All other reagents were used as received without further purification. Deionized water used in all experiments was purified through a filter and ion exchange resin using a Purite device with a resistivity of 18 MΩ·cm.

ES.2 Synthesis

ES.2.1 Methods of synthesis used in **Chapter II**

(i) Synthesis of P(VCL-*stat*-VP)$_{20k}$

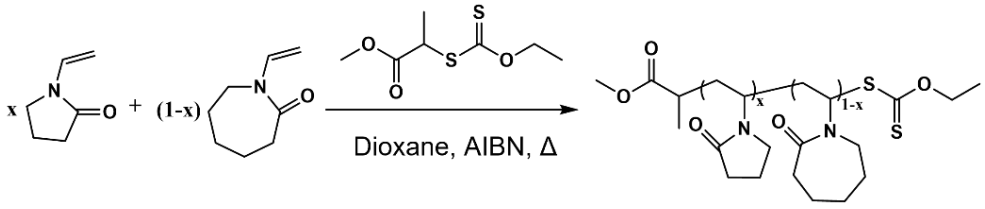

Scheme ES.1 Synthesis of P(VCL-*stat*-VP)$_{20k}$ by RAFT/MADIX polymerization (synthesis was performed by X. Zhao in IMRCP, Toulouse, France).

A general synthetic procedure for synthesis of P(VCL$_{75}$-*stat*-VP$_{25}$) was (see **Scheme ES.1**): A Schlenk tube containing VP (1.54 g, 1.4 mmol), AIBN (6.8 mg, 0.041 mmol), **X1** (21 mg, 0.1 mmol), VCL (0.51 g, 3.7 mmol) and dioxane (4.12 g) was degassed by three freeze-pump-thaw cycles, put under argon and heated at 65 °C for 20 h in an oil bath. After cooling down to room temperature, the polymerization was stopped and the solution was precipitated in diethyl ether. The precipitated polymer was dried under vacuum and analyzed by SEC-RI-MALS in THF and in DMF (containing LiBr) to determine molecular weight (M_n) and dispersity (Đ).

(ii) Preparation of Au@P(VCL-*stat*-VP)$_{20k}$ nanohybrids

(a) *In situ* formation of Au@P(VCL-*stat*-VP)$_{20k}$ nanohybrids

The *in situ* formation of nanohybrids was performed by addition of $NaBH_4$ solution (final concentration equal to 5×10^{-4} mol·L^{-1}) to a mixture of $NaAuCl_4{\cdot}2H_2O$ solution (final concentration equal to 5×10^{-4} mol·L^{-1}) and (co)polymer at different concentrations (10^{-3}, 10^{-2}, 0.1 and 0.5 wt.%) under vigorous stirring. The color of the solution turned immediately from pale yellow to red or pale yellow depending on the nature of the (co)polymer and its concentration. The nanohybrids were purified by dialysis (membrane with molecular weight cutoff of 3500 Da) before further analysis (*In situ* formation of nanohybrids was done by H.H. Nguyen in IMRCP, Toulouse, France).

(b) Coating of preformed gold nanoparticles with P(VCL-*stat*-VP)$_{20k}$

AuNPs were prepared by adding 50 µL fresh $NaBH_4$ solution (0.1 mol·L^{-1}) to a mixture of 0.5 mL $NaAuCl_4{\cdot}2H_2O$ solution (0.01 mol·L^{-1}), 9.4 mL of MilliQ water and 25 µL of an

aqueous solution of sodium hydroxide (NaOH, 1 mol·L^{-1}) under vigorous stirring. The solution turned immediately dark red, indicating the formation of AuNPs (final concentration equal to 5×10^{-4} mol·L^{-1}). These colloidal solutions were stable but rapidly aggregated when salt was added. Then, a series of stock aqueous solutions of copolymer solutions at 2×10^{-3}, 2×10^{-2}, 0.1, 0.2 wt.% and a stock solution of preformed AuNPs at 5×10^{-4} mol·L^{-1} were prepared separately. Experiments were performed using a 96-well plate (Costar 96) with a well final volume equal to 200 µL. Typically, 100 µL aliquots of a AuNPs solution were introduced in each well then completed with an appropriate volume of (co)polymer aqueous solution to reach the chosen final concentration. This experiment was repeated for other (co)polymers with different compositions. After a brief shaking of the plate, UV-vis spectra were recorded ($[(co)polymer]_{final}$ = 10^{-4}, 10^{-3}, 5×10^{-3} or 10^{-2} wt.% and $[Au]_{final}$ = 2.5×10^{-4} mol·L^{-1}).

In order to test the colloidal stability of obtained nanohybrids, the same experiments were performed with a complementary addition of NaOH (stability in basic condition) or by adding 40 µL of a 5 mol·L^{-1} NaCl aqueous solution (effect of ionic strength) in complement to the other reactants.

(iii) Catalytic efficiency of Au@P(VCL-*stat*-VP)$_{20k}$

The kinetics of reduction of *p*-nitrophenol to *p*-aminophenol in presence of $NaBH_4$ was monitored by *in situ* UV-vis spectroscopy. In a standard quartz cuvette, 1730 µL deionized water and 200 µL AuNPs (0.5 mol·L^{-1}) were mixed with 10 µL (co)polymer solution (1 wt.%) under continuous stirring, the catalyst of Au@P(VCL-*stat*-VP)$_{20k}$ was therefore obtained. Then 20 µL *p*-nitrophenol (0.01 mol·L^{-1}) was injected into the mixture solution. After 10 min of equilibrium at a given temperature (20, 30, 40, 50, 60 and 70 °C), 60 µL fresh $NaBH_4$ solution (0.1 mol·L^{-1}) was added quickly to start the catalytic reaction. Meanwhile, the UV-vis spectra were recorded in the wavelength range of 200-700 nm at an interval of 30 s. The kinetic constant of reduction was determined by absorbance change of band at 400 nm where the phenolate form of *p*-nitrophenol were (the $NaBH_4$ also provided basic environment). The final concentration of Au, *p*-nitrophenol, $NaBH_4$ and (co)polymer were 5×10^{-5} mol·L^{-1}, 10^{-4} mol·L^{-1}, 3×10^{-3} mol·L^{-1} and 5×10^{-3} wt.%, respectively.

ES.2.2 Methods of synthesis used in **Chapter III**

(i) Synthesis of meso-2,5-di(O-ethyl xanthate) diethyladipate (bis-xanthate **X2**)

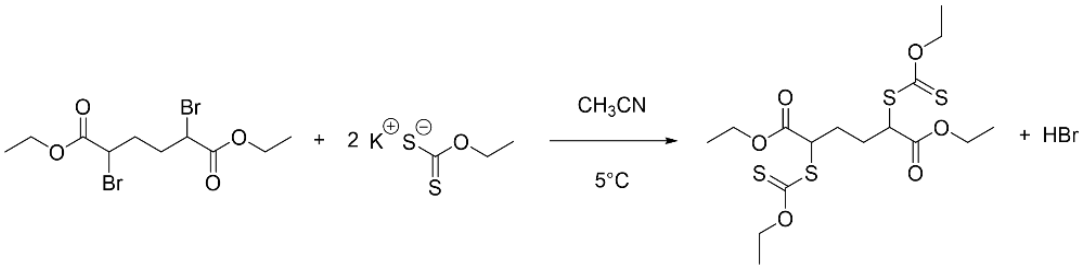

Scheme ES.2 Synthesis of bis-xanthate **X2.**

As shown in **Scheme ES.2**, 1.7246 g potassium *O*-ethylxanthate was added by fractions to a solution of diethyl 2,5-dibromoadipate (1.937 g, 5.38 mmol) in 20 mL anhydrous acetonitrile at 5 °C during 30 min. Then the mixture was stirred 2 h at 5 °C, at which reaction was complete (monitored by TLC). After evaporation of acetonitrile, the residue was dissolved in diethyl ether and washed with water. The organic phase was dried over anhydrous $MgSO_4$, filtered and evaporated under vacuum to afford desired bis-xanthate **X2** (2.25 g, yield: 94%) as a crystallized solid. R_f = 0.80 (CH_2Cl_2). ^{1}H NMR (300 MHz, $CDCl_3$, 25 °C): δ_H 4.66 (q, J = 7 Hz, 4H, -SCS-OC**H**$_2$CH$_3$); 4.42-4.38 (m, 2H, -CH$_2$C**H**COO-); 4.23 (q, J= 7 Hz, 4H, -OCOC**H**$_2$CH$_3$); 2.17-1.97 (m, 4H, -CHC**H**$_2$-); 1.44 (t, J = 7 Hz, 6H, -SCS-OCH$_2$C**H**$_3$); 1.29 (t, J = 7 Hz, 6H, -COOCH$_2$C**H**$_3$). ^{13}C NMR (75 MHz, $CDCl_3$, 25 °C): δ 211.6 (-S**C**S-); 170.3 (-O**C**O-); 70.5 (-SCS-O**C**H$_2$CH$_3$); 61.9 (-COO**C**H$_2$); 51.9 (-**C**HCOO-); 28.8 (-**C**H$_2$CH-); 14.2 (-COOCH$_2$**C**H$_3$); 13.7 (-SCS-OCH$_2$**C**H$_3$).

(ii) Synthesis of P(BA-*co*-NIPAM) with statistical, diblock and triblock architectures

Statistical, diblock and triblock copolymers were synthesized by RAFT/MADIX polymerization with a target M_n of 10000 g·mol^{-1}.

(a) Synthesis of PBA-*b*-PNIPAM diblock copolymer

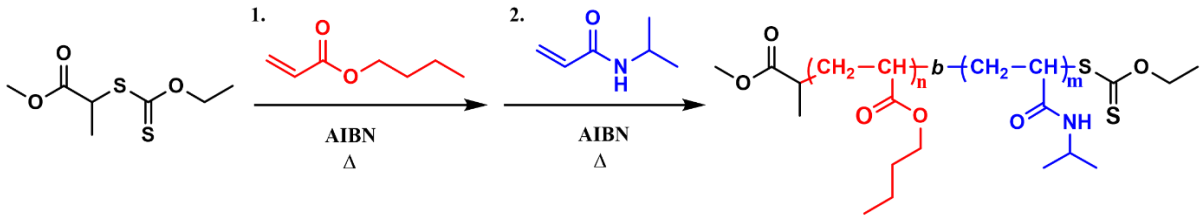

Scheme ES.3 Synthesis of PBA-*b*-PNIPAM by RAFT/MADIX polymerization (Synthesis was performed by V. Rahal in IMRCP, Toulouse, France).

Diblock copolymers of PBA-*b*-PNIPAM were synthesized as previously described (**Scheme ES.3**). [2] A typical procedure for synthesizing block copolymers of BA and NIPAM was as follows: 51 mg AIBN, 0.521 g xanthate **X1**, 4.994 g BA and 3.39 g ethanol were placed into a two-neck round-bottomed flask equipped with a magnetic stirrer and a reflux condenser. The solution was then degassed for 15 min by bubbling argon. It was then heated at 75 °C for three hours, keeping a slow stream of argon in the reactor. After a given time, the mixture solution was cooled down to ambient temperature and solvent was removed to analyze the obtained polymer. BA conversion > 99% (^{1}H NMR); M_n = 2250 g·mol^{-1}, Đ = 1.55 (given by SEC in THF). 3.873 g obtained PBA was mixed with 187 mg AIBN, 15.556 g NIPAM and 16.446 g ethanol. The mixture solution was then degassed for 15 min by bubbling argon. It was then heated at 75 °C for nine hours, keeping a slow stream of argon in the reactor. The reaction mixture was then cooled down to ambient temperature and the solvent was removed to analyze the block copolymer. NIPAM conversion > 99% (^{1}H NMR); M_n = 7350 g·mol^{-1}, Đ = 1.29 (given by SEC analysis in THF).

(b) Synthesis of PNIPAM-*b*-PBA-*b*-PNIPAM triblock copolymer

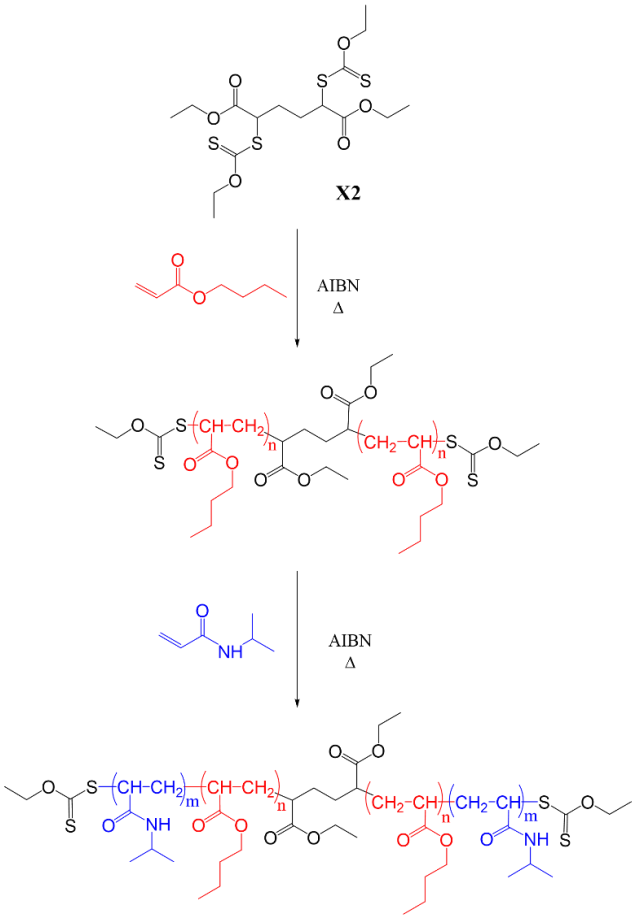

Scheme ES.4 Synthesis of PNIPAM-*b*-PBA-*b*-PNIPAM by RAFT/MADIX polymerization (synthesis was performed by J.S. Behra and N. Lauth-de Viguerie in IMRCP, Toulouse, France).

PNIPAM-*b*-PBA-*b*-PNIPAM triblock copolymers were synthesized as follows: appropriate amounts (**Table ES.1**) of AIBN, bis-xanthate **X2**, BA and ethanol were placed in a two-neck round-bottomed flask equipped with a magnetic stirrer and a reflux condenser. The solution was then degassed by four freeze-pump-thaw cycles and set under argon atmosphere. It was then heated at 75 °C for one to four hours, keeping a slow stream of argon in the reactor. Samples were periodically withdrawn from the polymerization medium for determination of BA conversion by ^{1}H NMR. After cooling down the solution to room temperature, the polymer was analyzed. BA conversions (> 98%) were determined via ^{1}H NMR spectra, comparing the signal area of vinyl protons (δ ~ 5.8-6.5 ppm, 3H/molecule for BA) to the signal area of methylene in α OCO (δ ~ 4.1 ppm, 2H/molecule).

Table ES.1 Step 1: Synthesis of PBA_{xk} block.

Homopolymer	AIBN (g/mmol)	Bis-xanthate **X2** (g/mmol)	Ethanol (g/mmol)	BA (g/mmol)	Conv./%
PBA_{2k}	0.01037 (0.0632)	0.22493 (0.4998)	0.6982 (15.16)	1.06 (8.263)	99
PBA_{5k}	0.00922 (0.0561)	0.19974 (0.452)	0.61994 (13.46)	2.2590 (17.625)	98
PBA_{8k}	0.01024 (0.0624)	0.22115 (0.4996)	0.68294 (14.82)	4.019 (31.24)	98

The obtained PBA macro-chain transfer agent was mixed with appropriate amounts of AIBN, NIPAM and ethanol (**Table ES.2**). The solution was then degassed for 20 min by bubbling Ar. It was then heated at 62 °C for three hours, keeping a slow stream of Ar in the reactor. The reaction mixture was then cooled down to room temperature and the polymer was analyzed. NIPAM conversions (> 97%) were determined via ^{1}H NMR spectra, comparing the signal area of vinyl protons (δ ~ 5.5-6.4 ppm, 3H/molecule for NIPAM) to signal area of isopropyl methylene (δ ~ 3.9-4.2 ppm, 1H/molecule).

Table ES.2 Step 2: Synthesis of triblock copolymers.

Triblock copolymer	AIBN (g/mmol)	Synthesized PBA (g/mmol)	Ethanol (g/mmol)	NIPAM (g/mmol)	Conv. /%	[NIPAM] : [BA]
$PNIPAM_{4k}$-*b*-PBA_{2k}-*b*-$PNIPAM_{4k}$	0.0399 (0.243)	0.8428 (0.4214)	2.907 (64.66)	2.800 (24.74)	98	4.37
$PNIPAM_{2.5k}$-*b*-PBA_{5k}-*b*-$PNIPAM_{2.5k}$	0.03209 (0.1954)	2.40907 (0.482)	2.2184 (48.123)	2.2192 (19.609)	100	1.21

(c) Synthesis of P(BA-*stat*-NIPAM) copolymers

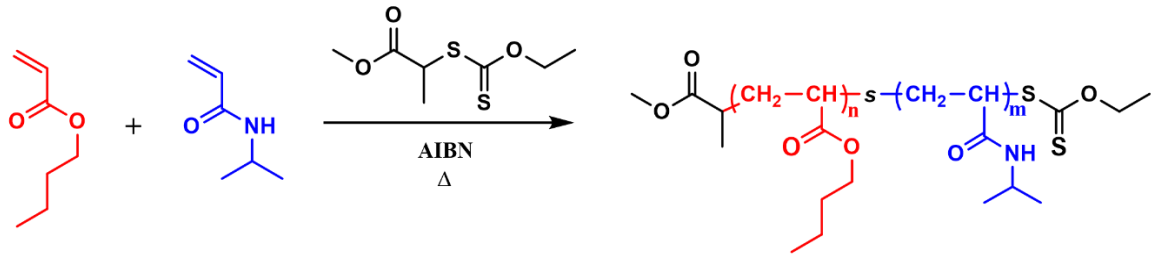

Scheme ES.5 Synthesis of P(BA-*stat*-NIPAM) by RAFT/MADIX polymerization.

P(BA-*stat*-NIPAM) copolymers were synthesized using xanthate **X1** as RAFT agent (see **Scheme ES.5**). P(BA-*stat*-NIPAM) was prepared as follows (**Table ES.3**): Into an argon-filled Schlenk flask with a magnetic bar, a mixture of xanthate **X1**, AIBN, BA and NIPAM dissolved in 1,4-dioxane was added under argon. The flask was degassed *via* four cycles of freeze-pump-thaw and then placed in an oil bath at 75 °C. After 9 h, the reaction was terminated upon exposure to air and the flask was cooled rapidly with liquid nitrogen. Solvent was removed by evaporation under vacuum to obtain the white powder.

Table ES.3 Synthesis of statistical copolymers (see **Scheme ES.5**).

Statistical copolymer	AIBN (g/mmol)	xanthate **X1** (g/mmol)	BA (g/mmol)	1,4-dioxane (g)	NIPAM (g/mmol)	Con. /%	[NIPAM] : [BA]
P(BA_{2k}-*stat*-$NIPAM_{8k}$)	0.055 (0.338)	0.106 (0.511)	1.00 (7.802)	5.162	4.00 (35.348)	99	4.20
P(BA_{1k}-*stat*-$NIPAM_{9k}$)	0.028 (0.169)	0.0532 (0.0255)	0.25 (1.951)	2.581	2.25 (19.883)	99	8.65
P($BA_{0.5k}$-*stat*-$NIPAM_{9.5k}$)	0.0277 (0.169)	0.0532 (0.0255)	0.125 (0.975)	2.581	2.375 (20.988)	99	11.33

ES.2.3 Methods of synthesis used in **Chapter IV**

(i) Synthesis of monomer of *N*,*N*-(diethylamino) ethyl acrylamide (DEAEAM)

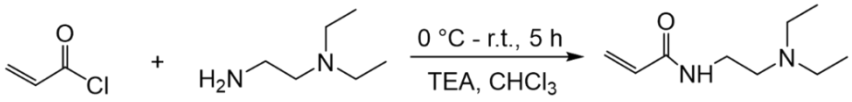

Scheme ES.6 Synthesis of DEAEAM.

DEAEAM was prepared according to the literature procedure (**Scheme ES.6**). [3] Briefly, *N*,*N*-diethylethylenediamine (60 mmol, 6.972 g), triethylamine (TEA, 72 mmol, 7.286 g) and $CHCl_3$ (100 mL) were added in a Schlenk flask under argon atmosphere in an ice-water bath. Acryloyl chloride (72 mmol, 6 mL) dissolved in $CHCl_3$ was added dropwise into flask within 1 h, after complete addition, the reaction was warmed up to room temperature for 4 h. Then the reaction mixture was washed with dilute NaOH solution and with deionized water three times, respectively. The organic phase was collected and concentrated under reduced pressure, the resulting residue was purified by aluminum oxide column chromatography (petroleum ether/ethyl acetate gradient 3 : 1 to 0 : 1, v/v) to give DEAEAM (5.39 g, yield: 53%). ^{1}H NMR (300 MHz, $CDCl_3$, 25 °C) δ_H (ppm): 6.43 (s, 1H, -N**H**-), 6.21 (dd, 1H, C**H**$_2$=CH-), 6.08 (dd, 1H, C**H**$_2$=CH-), 5.55 (dd, 1H, CH_2=C**H**-), 3.32 (q, 2H, -NHC**H**$_2$-), 2.55-2.44 (m, 6H, -N(C**H**$_2$)$_3$), 0.96 (t, 6H, -CH_3) ; ^{13}C NMR (75 MHz, $CDCl_3$, 25 °C) δ_C (ppm): 165.51, 131.13, 125.78, 51.28, 46.68, 36.90 and 11.75.

(ii) Synthesis of poly(*N*-isopropylacrylamide) macro-RAFT agent (PN)

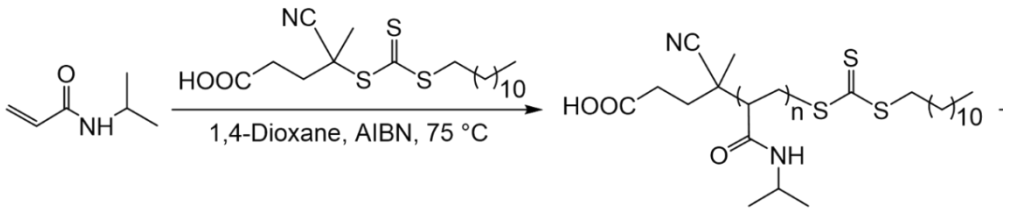

Scheme ES.7 Synthesis of PN homopolymers by RAFT polymerization.

In the case of PN_{5k}, into a Schlenk flask, a mixture of NIPAM (2 g, 17.674 mmol), AIBN (0.036 g, 0.218 mmol) and CDTPA (0.176 g, 0.436 mmol) dissolved in 1,4-dioxane (4.741 g) was added with an argon flow, the flask was degassed through three freeze-pump-thaw cycles and placed in a preheated oil bath (75 °C). After 9 h, the reaction was quenched by rapid immersion of flask in liquid nitrogen, the obtained mixture was concentrated and precipitated in cold diethyl ether twice to remove unreacted monomer, followed by drying under vacuum to afford pure PN_{5k} (conversion: 99.9%). NIPAM conversion was calculated by comparing integrals at 5.44 ppm corresponding to vinyl protons in monomer to that at 3.92 ppm corresponding to methylene in -$CH_2(CH_3)_2$ group. $M_{n,NMR}$ was determined by signal areas at 0.85 ppm (RAFT terminal, -CH_3) and at 4.00 ppm (NIPAM, -CH- adjacent to CH_3 group) in ^{1}H NMR spectrum. $M_{n,theo}$ = 5000 g·mol^{-1}, $M_{n,NMR}$ = 6130 g·mol^{-1}. In DMF (containing 10 mM LiBr): $M_{n,SEC}$ = 6080 g·mol^{-1}, Đ= 1.06 ; In THF (containing 2 v% TEA): $M_{n,SEC}$= 4720 g·mol^{-1}, Đ =1.03. ^{1}H NMR (500 MHz, D_2O, 25 °C) δ_H (ppm): 3.92 (s, 1H, -C**H**$(CH_3)_2$), 2.52-1.60 (m,

-C**H**$_2$CH-CONH-, -CH$_2$C**H**-CONH-, -C(CN)-C**H**$_3$)-, -C**H**$_2$CH$_2$COOH, -CH$_2$C**H**$_2$COOH), 1.33 (s, 20H, -(C**H**$_2$)$_{10}$-CH$_3$), 1.16 (s, 6H, -CH(C**H**$_3$)$_2$), 0.85 (s, 3H, -(CH$_2$)$_{10}$-C**H**$_3$).

(iii) Synthesis of poly(*N*-isopropylacrylamide)-*block*-poly(*N*,*N*-(diethylamino) ethyl acrylamide) (PN-*b*-PD)

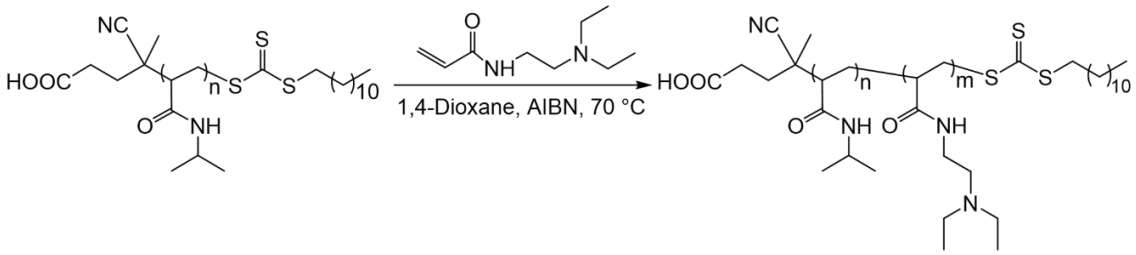

Scheme ES.8 Synthesis of PN-*b*-PD by RAFT polymerization.

In the case of PN$_{5k}$-*b*-PD$_{5k}$, DEAEAM (2 g, 11.747 mmol), PN$_{5k}$ (2 g, 0.4 mmol, as macro-RAFT agent), AIBN (0.059 g, 0.36 mmol) and 1,3,5-trioxane (0.106 g, 1.175 mmol, as internal standard) dissolving in 1,4-dioxane (3.43 g) were placed into a Schlenk flask with a magnetic stirrer. After three freeze-pump-thaw cycles, the flask was immersed in a preheated oil bath at 70 °C. The conversion of DEAEAM was determined by ^{1}H NMR spectrum. Once the desired conversion was obtained, the polymerization reaction was stopped by rapidly cooling in liquid nitrogen. The resulting mixture was precipitated in the cold diethyl ether twice and dried under vacuum (conversion: 96.6%). $M_{n,theo}$ = 9840 g·mol^{-1}. $M_{n,NMR}$ = 11090 g·mol^{-1}, which is calculated on the basis of $M_{n,NMR}$ of PN$_{5k}$ as well as integrals ratio of characteristic signal of PN at 3.91 ppm and that of PD at 3.39 ppm. In DMF (containing 10 mM LiBr): $M_{n,SEC}$ = 8340 g·mol^{-1}, Đ = 1.09; in THF (containing 2 v% TEA): $M_{n,SEC}$ = 6860 g·mol^{-1}, Đ = 1.16. ^{1}H NMR (500 MHz, D$_2$O, 25 ^{o}C) δ_H (ppm): 3.90 (s, 1H, -C**H**(CH$_3$)$_2$), 3.32 (s, 2H, -CONH-C**H**$_2$-), 2.63 (s, 6H, -N(C**H**$_2$)$_3$), 2.02-1.33 (m, -C**H**$_2$CH-CONH-, -CH$_2$C**H**-CONH-, -C(CN)-C**H**$_3$)-, -C**H**$_2$CH$_2$COOH, -CH$_2$C**H**$_2$COOH), 1.25 (s, 20H, -(C**H**$_2$)$_{10}$-CH$_3$), 1.14 (s, 6H, -NHCH(C**H**$_3$)$_2$), 1.06 (s, 6H, -N(CH$_2$C**H**$_3$)$_2$), 0.86 (s, 3H, -(CH$_2$)$_{10}$-C**H**$_3$).

(iv) Synthesis of poly(*N*,*N*-(diethylamino) ethyl acrylamide) homopolymer (PD)

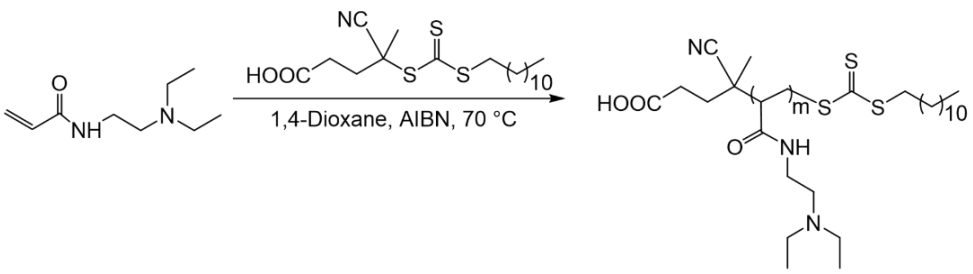

Scheme ES.9 Synthesis of PD homopolymer by RAFT polymerization.

In the case of PD_{5k} (see **Scheme ES.9**), a mixture of DEAEAM (2 g, 11.747 mmol), AIBN (0.050 g, 0.305 mmol), CDTPA (0.176 g, 0.435 mmol), 1,3,5-trioxane (0.106 g, 1.175 mmol, as internal standard) and 1,4-dioxane (3.497 g) was placed into a Schlenk flask with a magnetic stir, the flask was degassed by three freeze-pump-thaw cycles and placed in a preheated oil bath at 70 °C. After a given time, the polymerization was quenched by rapid immersion of flask in liquid nitrogen. PD_{5k} was purified by dialysis against deionized water for three days and dried by lyophilization (conversion: 95.4%). $M_{n,theo}$ = 4790 g·mol^{-1}. $M_{n,NMR}$ = 4810 g·mol^{-1}, which is calculated by comparing integrals of signal at 0.88 ppm (RAFT terminal, -CH_3) to signal at 3.33 ppm (DEAEAM, -CH_2- adjacent to -CONH- group) in ^{1}H NMR spectrum. In DMF (containing 10 mM LiBr): $M_{n,SEC}$ = 6900 g·mol^{-1}, Đ = 1.21; in THF (containing 2 v% TEA): $M_{n,SEC}$ = 4210 g·mol^{-1}, Đ = 1.09. ^{1}H NMR (500 MHz, D_2O, 25 °C) δ_H (ppm): 3.33 (s, 2H, -CONH-C**H$_2$**-), 2.64 (s, 6H, -N(C**H$_2$**)$_3$), 2.31-1.62 (m, -C**H$_2$**CH-CONH-, -CH_2C**H**-CONH-, -C(CN)-C**H$_3$**)-, -C**H$_2$**CH_2COOH, -CH_2C**H$_2$**COOH), 1.26 (s, 20H, -(C**H$_2$**)$_{10}$-CH_3), 1.08 (s, 6H, -N(CH_2C**H$_3$**)$_2$), 0.88 (t, 3H, -$(CH_2)_{10}$-C**H$_3$**).

Other PN, PD homopolymers and block copolymers of PN-*b*-PD with variable compositions were synthesized with the similar procedure. The detailed information is summarized in **Table ES.4**.

Table ES.4 Synthesis of PN, PD homopolymers and block copolymers of PN-*b*-PD.

(Co)polymer	NIPAM (g/mmol)	DEAEAM (g/mmol)	CTA (g/mmol)	AIBN (g/mmol)	$[M]_0$:$[CTA]_0$:$[AIBN]_0$	1,4-Dioxane (g)	Temperature (°C)	Trioxane (g/mmol)
PN_{2k}	2 (17.674)	0	0.506 (1.253)	0.103 (0.626)	14 : 1 : 0.5	5.217	75	0
PN_{8k}	2 (17.674)	0	0.106 (0.263)	0.022 (0.132)	67 : 1 : 0.5	4.256	75	0
PN_{10k}	2 (17.674)	0	0.084 (0.208)	0.017 (0.104)	85 : 1 : 0.5	4.202	75	0
PN_{2k}-*b*-PD_{8k}	0	2 (11.747)	0.484 (0.248)	0.037 (0.224)	47 : 1 : 0.9	5.254	70	0.106 (1.175)
PN_{8k}-*b*-PD_{2k}	0	0.2 (1.175)	1.592 (0.179)	0.026 (0.161)	6.6 : 1 : 0.9	3.658	70	0.011 (0.117)
PD_{2k}	0	2 (11.747)	0.506 (1.253)	0.144 (0.877)	9 : 1 : 0.7	4.133	70	0.106 (1.175)
PD_{8k}	0	2 (11.747)	0.106 (0.263)	0.030 (0.184)	45 : 1 : 0.7	3.363	70	0.106 (1.175)
PD_{10k}	0	2 (11.747)	0.084 (0.208)	0.024 (0.146)	56 : 1 : 0.7	3.321	70	0.106 (1.175)

ES.3 Characterization

ES.3.1 NMR spectroscopy

^{1}H and ^{13}C NMR spectra were recorded on Bruker ARX 400 at 400.13 MHz (or Bruker ARX 500 at 500.13 MHz) and at 100.61 MHz, respectively. All spectra were referenced to the solvent residual peak.

ES.3.2 Size Exclusion Chromatography (SEC)

Number-average molecular weights (M_n) and dispersities (Đ) of all synthesized homopolymers and copolymers in **Chapters II**, **III** and **IV** were determined by SEC on an apparatus equipped with a Varian ProStar 325 UV detector (dual wavelength analysis) and a Waters 410 refractive index detector as well as two Shodex K-805L columns (8 mm×300 mm, 13 µm). Molecular weights were calculated based on RI-MALS detection. [4] The value of dn/dc for block or statistical copolymers were calculated by using the measured values of homopolymer weighted by the composition of measured copolymer. Typically, (co)polymer samples were prepared with a concentration of 10 $mg \cdot mL^{-1}$ and filtered through 0.45 µm PTFE filter. The eluents used in **chapter II** was DMF containing 10 mM LiBr, in **Chapter III** was THF, and in **Chapter IV** were DMF containing 10 mM LiBr and THF containing 2 v% TEA, the flow rate was set at 1 $mL \cdot min^{-1}$.

ES.3.3 Differential Scanning Calorimetry (DSC)

The thermal properties of the (co)polymer (in bulk and in solution) were determined by using a Mettler Toledo DSC 1 STARe System Thermal Analysis calorimeter equipped with a Gas Controller GC200. Glass transition temperatures (T_g) of bulk (co)polymers were determined at a heating rate of 10 $°C \cdot min^{-1}$.

For (co)polymers aqueous solution, cloud point temperatures (T_c) of 1, 5 and 20 wt.% sample solutions were determined by using DSC measurements. Solution samples were sealed in impermeable crucibles of 120 µL. T_c values were estimated at the top of observed peaks on DSC thermograms when temperature decreased/increased at different rates: 5, 4, 3, 2 and 1 $°C \cdot min^{-1}$, and finally extrapolated to 0 $°C \cdot min^{-1}$. The variation of enthalpy was measured at a heating rate of 1 $°C \cdot min^{-1}$.

ES.3.4 Turbidimetry measurement

Transmittance of (co)polymer aqueous solutions at 500 nm with increasing temperature was recorded by a Cary 100 Bio spectrophotometer with 4 cycles at different heating/cooling rates (0.5, 1, 2.5 and 5 °C·min^{-1}). Cloud points were calculated from the value obtained by extrapolation to 0 °C·min^{-1} of inflexion point on each transmittance curve at different rates. Three independent measurements were performed for each sample.

ES.3.5 Dynamic Light Scattering (DLS)

DLS measurements were carried out at different temperatures on a Malvern Instrument Nano-ZS equipped with a He-Ne laser (λ = 633 nm). Samples were introduced into cells (pathway: 10 mm). The reported apparent equivalent hydrodynamic diameter, D_h, is obtained by analysing measured correlation function via non-negative least square algorithm and using the Stokes-Einstein equation. T_c values were obtained by the inflection points (or onset temperature, where aggregates size start to change) of hydrodynamic size change curve as a function of temperature.

ES.3.6 Visual Assessment

In **Chapter III**, the phase state of polymer solutions as a function of temperature and concentration was visually assessed. This experiment was carried out in a dry box ranging from 20 to 40 °C with 2 °C intervals, the sample was equilibrated for 5 min at each temperature before visual observation. Then the same procedure was performed at higher temperature as sample recovered to transparent state.

ES.3.7 Rheological measurement

In **Chapter III**, the rheological measurements were performed on an AR1000 rheometer from TA instruments in cone plate configuration (diameter 2 cm, 2° angle) equipped with a Peltier plate. An oscillatory stress with an amplitude of 1 Pa and frequency of 1 Hz was applied to the sample for viscoelastic measurements. With these settings, the variations of the storage modulus G' and the loss modulus G" along with temperature were monitored by applying a continuous linear temperature ramp at 1 °C·min^{-1}. The inflection point was selected as phase transition temperature.

ES.3.8 Cryo-Scanning Electron Microscopy (cryo-SEM)

In **Chapter III**, cryo-SEM images were performed on FEG FEI Quanta 250 microscope (Japan). (Co)polymer solution was preheated and underwent sol-to-gel transition before being frozen in nitrogen slush at -220 °C. The frozen sample was transferred under vacuum in the cryo-fracture apparatus (Quorum PP3000T Cryo Transfer System) chamber where it was fractured at -145 °C. After a sublimation step at -95 °C during 30 min, the sample was introduced into the microscope chamber at -145 °C, operating at 5 kV accelerating voltage.

ES.3.9 Transmission Electron Microscopy (TEM)

A drop of (co)polymer aqueous solution was placed on a formvar carbon-coated copper TEM grid (200 mesh, Ted Pella Inc.) and left to dry under air at the chosen temperature. For samples needing negative staining, these samples were prepared by depositing a 6 µL drop of (co)polymer solution preheated at a given temperature for 20 min, onto TEM grid and dried at the same temperature, followed by a negative stain with uranyl acetate (2 wt.%) aqueous solution for 2 min, the excess solution was removed with a filter paper, sample was dried again at the same temperature. TEM observation was performed on a HITACHI HU12 operating at 70 kV, The size distribution of the particles was determined by measuring at least 100 particles in each sample, WCIF ImageJ software was used to give average diameter ± standard deviation.

ES.3.10 Cryogenic Transmission Electron Microscopy (cryo-TEM)

In **Chapter IV**, cryo-TEM images were acquired on a JEOL 2010F TEM instrument [200 kV field-emission gun (FEG)] equipped with a Gatan UltraScan 4000 camera and cryogenic sample holder using lacey carbon film grids (300 mesh Cu, Agar Sc. S166-3H) The solutions were preheated at the chosen temperature, then a small droplet of each solution was placed on an ionized grid, and the excess solution was blotted with a piece of filter paper. The thus-obtained thin film of solution spanning the grid was quickly plunged into liquid ethane (~90 K) that was cooled by liquid nitrogen. The samples were then kept in liquid nitrogen before transfer by a cryogenic sample holder to the microscope and imaged at -178 °C. Adequate phase contrast was obtained at a nominal underfocus of 3-15 µm. (cryo-TEM measurements were performed by S. Balor in CBI, Toulouse, France)

ES.3.11 Small Angle Neutron Scattering (SANS)

In **Chapter III**, SANS experiments were performed with PACE spectrometer on Orphée reactor. Polymer solutions in D_2O solvent were put inside quartz cells of 2 mm gap and measured at 20 °C and 40 °C. Different spectrometer configurations were used: a neutron wavelength (λ) of 7Å with a sample to detector distance of 3 m to obtain intermediate q value range, a wavelength of 7Å with a distance of 1m to reach high q values and a wavelength of 17Å and 4.8 m to reach low q values required to observe large objects. The neutron wavelength distribution Δλ/λ was 0.11. The incident collimation was obtained from two circular holes, one close to the sample with a 7 mm diameter and the second one of either 16 mm diameter, 2.5 m apart from the sample diaphragm for the two highest q domains, or of 12 mm diameter, 5 m apart from the sample diaphragm for the smallest q range. The scattering vector range thus reached was $0.0025 < q\ (Å^{-1}) < 0.35$. Scattering intensities have also been normalized by the incoherent signal delivered by a 1 mm gap water sample in order to account for efficiency of detector cells. Absolute values of the scattering intensity, I(q) in cm^{-1}, were obtained from the direct determination of the number of neutrons in the incident beam and the detector cell solid angle. [5] No background was subtracted to the copolymer sample scattering, thus a flat incoherent signal is observed at high q values. The scattering curves of diluted copolymer solutions have been fitted using SASView software (http://sasview.org) to the model of polydisperse sphere (radius R) using a Gaussian distribution of radius (σ_R) and taking into account for each spectrometer configuration the corresponding resolution function. For triblock at 20 °C, the best fit radii were very small (3 nm) and the distribution very large ($\sigma_R \sim 2$-3). The curves of triblock at 20 °C were also fitted to the model of polydisperse sphere but with a log-normal distribution (an asymmetric distribution compared to the Gaussian one) in order to obtain more reasonable values of fit parameters. (SANS experiments were performed by A. Brûlet and N. Lauth-de Viguerie in LLB, Gif sur Yvette Cedex, France)

ES.3.12 Determination of p*K*a

In **Chapter IV**, prior to measurement, the pH of (co)polymer solution (0.01 M) was calibrated by HCl solution (0.1 M), then the solution was titrated with NaOH solution (0.1 M) and its pH was monitored continuously by pH meter until pH did not change. The p*K*a value was determined by the inflection point of pH curve as a function of NaOH concentration.

ES.3.13 CO_2/N_2 bubbling

In **Chapter V**, a gas regulator was used to quantitatively control gas amount, CO_2/N_2 was introduced at room temperature by inserting a needle in (co)polymer solution with an appropriate flow rate at a given period of time.

ES.4 References

[1] X. Liu, O. Coutelier, S. Harrisson, T. Tassaing, J.-D. Marty and M. Destarac, ACS Macro Lett. 4 (2015) 89-93.
[2] S. Sistach, M. Beija, V. Rahal, A. Brûlet, J.-D. Marty, M. Destarac and C. Mingotaud, Chem. Mater. 22 (2010) 3712-3724.
[3] Z. Song, K. Wang, C. Gao, S. Wang and W. Zhang, Macromolecules 49 (2015) 162-171.
[4] H.H. Nguyen, M. El Ezzi, C. Mingotaud, M. Destarac, J.-D. Marty and N. Lauth-de Viguerie, Soft Matter 12 (2016) 3246-3251.
[5] P. Lindner, T. Zemb, Noth-Holland, Amsterdam. 1991, p19.

Résumé de thèse

Introduction

Les (co)polymères sensibles aux stimuli ou dits « intelligents » ont séduit ces dernières années en raison de l'altération de leurs propriétés physico-chimiques (solubilité, conformation de la chaîne, propriétés d'agrégation, etc.) pour s'adapter aux changements de l'environnement extérieur. Cette réactivité rapide et réversible confère à ces (co)polymères de multiples applications potentielles (telles que l'administration et la libération contrôlée de médicaments, les capteurs, les textiles intelligents et les membranes fonctionnalisées, etc.).

Le mécanisme de réponse est attribué à la modification des interactions inter- ou intramoléculaires induites par une réponse au stimulus. De plus, le niveau de réponse dépend fortement des conditions externes (telles que la nature du stimulus et son intensité, les solvants choisis, la présence d'additifs, etc.) et des paramètres structuraux du (co)polymère (tels que l'architecture (bloc, statistique), composition, concentration en (co)polymères, poids moléculaire et dispersité).

Chapitre I

Dans le **Chapitre I**, les principales familles de (co)polymères sensibles aux stimuli (thermo, pH et CO_2) sont passées en revue, leurs propriétés de réponse correspondantes (comportement de transition de phase et comportement d'auto-organisation) lors de l'application/suppression des stimuli, impacts pour affectant la réactivité, les principales stratégies de polymérisation et leurs applications sont présentées avec une description détaillée.

I.1 (co)polymères thermosensibles

Les (co)polymères thermosensibles subissent généralement un changement de solubilité dans l'eau en réponse à une modification de température. Un bel équilibre hydrophobe-hydrophile dans leur structure est responsable de ce phénomène. De petits changements de température autour d'une valeur critique induisent l'effondrement ou l'expansion des chaînes polymères en réponse aux nouveaux ajustements des interactions hydrophobes et hydrophiles entre le polymère et l'eau. La température à laquelle se produit la séparation des phases est appelée température de point de trouble (T_c).

Selon le comportement de transition de phase, il existe principalement deux catégories de (co)polymères thermosensibles, leurs diagrammes de phases sont présentés dans le **Schéma I.1**. La première famille est constituée de (co)polymères avec une température de solution critique inférieure (LCST), cette famille subit une transition de phase d'une région monophasique à une

région biphasique lors du chauffage. La deuxième famille est celle des (co)polymères à température critique supérieure de solution (UCST), ce type de (co)polymères présente un comportement opposé: une transition d'une région biphasique à une région monophasique est généralement observée lors du processus de chauffage.

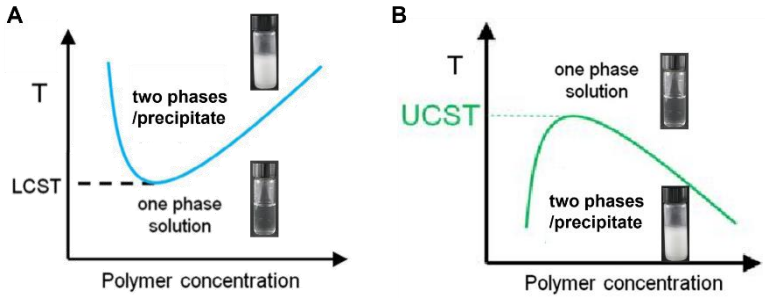

Schéma I.1. Diagrammes de phases de (co)polymères thermosensibles avec un comportement (A) LCST et un comportement (B) UCST.

T_c fait référence à la température à laquelle une transition de phase de (co)polymères thermosensibles à une concentration fixe a lieu. Sa détermination est un préalable aux applications potentielles. Différentes techniques, notamment la turbidimétrie, la diffusion dynamique de la lumière (DLS), la calorimétrie différentielle à balayage (DSC), la spectroscopie par résonance magnétique nucléaire (RMN) et la spectroscopie infrarouge à transformée de Fourier (FTIR) ont été adoptées dans la littérature. Le réglage fin de Tc est un point clé pour élargir les applications potentielles des polymères thermosensibles, ce qui peut être réalisé en modifiant le poids moléculaire, la concentration en (co)polymères, la structure topologique, la polarité des comonomères incorporés, les groupes terminaux, les additifs, etc.

Concernant la difficulté de synthétiser des copolymères thermosensibles multiples bien définis, la combinaison de deux blocs thermosensibles ou plus est une stratégie courante pour obtenir des matériaux avec une transition de phase par étapes ou un comportement d'auto-assemblage. Sur la base du type thermosensible et de la température de transition de phase, les copolymères thermosensibles doubles sont classés en types LCST-LCST, LCST-UCST et UCST-UCST.

Changement de solubilité induit par la température des fractions thermosensibles, qui influence davantage la formation/modification des agrégats en solution. Les morphologies de ces agrégats et l'effet de la température sur la structure des agrégats peuvent être étudiés par diffusion (lumière, neutrons et rayons X) ou par des mesures de microscopie. Les (co)polymères thermosensibles dans différentes régions de concentration affichent divers états d'agrégation, tels que des unimères, des nanoparticules à géométrie micellaire sphérique, vermiforme et vésiculaire en solution diluée ainsi que sol et hydrogel en solution concentrée.

I.2 (co)polymères sensibles au pH

L'élément clé des polymères sensibles au pH est la présence de fragments acides ou basiques faibles ionisables attachés à un squelette hydrophobe. Lors de l'ionisation, les chaînes enroulées s'étendent de façon spectaculaire en réponse aux répulsions électrostatiques des anions ou des cations générés. Cependant, l'ionisation complète sur les polyélectrolytes est plus difficile en raison des effets électrostatiques exercés par d'autres groupes ionisés adjacents. Cette transition entre l'état étroitement enroulé et expansé est influencée par toute condition qui modifie la répulsion électrostatique, telle que la force ionique et le type de contre-ions. Par conséquent, il faut garder à l'esprit qu'après plusieurs cycles de protonation/déprotonation par addition d'acides ou de bases, l'accumulation de sel peut avoir un effet néfaste sur l'organisation des (co)polymères en solution.

Selon les groupes fonctionnels, les polymères sensibles au pH sont divisés en deux catégories : les polymères avec des groupes acides et les polymères avec des groupes basiques. Les polyacides faibles sont non protonés avec des charges négatives à pH neutre et élevé. Les polybases faibles avaient un comportement opposé, étant protonées à de faibles valeurs de pH. Pour ces (co)polymères sensibles au pH, il est donc crucial de déterminer la constante de dissociation acide, *K*a (ou son log négatif : p*K*a) pour savoir à quel pH se produit la transition ionique/non ionique.

L'ajustement du pH modifie le degré de protonation/déprotonation des fractions sensibles au pH et la répulsion électrostatique parmi les chaînes chargées, ce qui influence le réseau de liaison hydrogène, les interactions ioniques/hydrophobes dans le système, et provoque en outre un changement de solubilité des (co)polymères en solution aqueuse . Bien comprendre et contrôler le comportement d'auto-assemblage des (co)polymères sensibles au pH, en dehors du rapport hydrophile/hydrophobe à un pH spécifique, les impacts de différents paramètres tels que le pH, la longueur de chaîne sensible au pH, la concentration en sel, (l'architecture des copolymères sur la forme et la taille des agrégats doit être prise en compte.

La transition morphologique induite par le pH des (co)polymères linéaires (tels que bloc, statistique, gradient, etc.) est l'objet le plus étudié. À l'exception des transitions des unimères vers les micelles déclenchées par le pH, des micelles vers les micelles inverses et des vésicules vers les vésicules inverses, les vésicules vers les cylindres vers les sphères, les unimères vers le mélange de micelles et les amas de micelles, les sphères vers -un mélange de micelles et de vésicules ressemblant à des vers, et des transitions sphères-vésicules sont également observées dans la littérature.

L'auto-assemblage de doubles (co)polymères thermosensibles et sensibles au pH est relativement complexe. Généralement, l'ajustement du pH modifie l'état d'ionisation/déionisation (ou de protonation/déprotonation) des segments sensibles au pH, tandis que le changement de température modifie l'équilibre hydrophilie/hydrophobie des fragments thermosensibles. Les deux changements influencent la morphologie des copolymères.

I.3 (co)polymères sensibles au CO_2

Les (co)polymères sensibles au CO_2 sont des (co)polymères susceptibles de réagir avec le CO_2 en solution aqueuse, cette réaction peut être inversée lors d'une aération alternée CO_2/gaz inerte. En tant que stimulus, le CO_2 a des perspectives prometteuses en raison de son abondance, de son ininflammabilité, de sa faible toxicité et de sa biocompatibilité. De plus, le CO_2 est facile à éliminer sans aucune accumulation ni contamination dans le système lors de cycles répétés. La réactivité au CO_2 des (co)polymères est obtenue par l'incorporation de groupes fonctionnels sensibles au CO_2 le long des chaînes polymères. Les groupes fonctionnels sensibles au CO_2 les plus rapportés sont les organobases telles que : amine, amidine, guanidine et imidazole.

La solubilité en solution aqueuse de (co)polymères est fortement influencée par la protonation/déprotonation provoquée par le traitement/l'élimination du CO_2. En raison de la modification de l'équilibre hydrophile/hydrophobe dans le système, les (co)polymères peuvent s'assembler en différents agrégats avec des géométries, tailles variables... De plus, les impacts de l'architecture (co)polymère, séquence de blocs et (co)polymère la composition doit également être prise en compte lors de l'analyse de l'agrégation des particules.

I.4 Méthode synthétique de (co)polymères stimuli-sensibles

La synthèse précise de (co)polymères bien définis est une condition préalable pour obtenir les propriétés souhaitées, telles que le réglage précis des valeurs de Tc sur une large plage de températures ou le contrôle de l'auto-assemblage déclenché par des stimuli externes. Pour atteindre un tel objectif, les méthodes de polymérisation radicalaire contrôlées telles que la polymérisation radicalaire induite par le nitroxyde (NMP), la polymérisation radicalaire par transfert d'atomes (ATRP), la polymérisation par transfert de chaîne par addition-fragmentation réversible (RAFT) sont les outils de choix. En effet, le développement rapide de la polymérisation radicalaire contrôlée fournit des informations pour concevoir et synthétiser des (co)polymères avec un poids moléculaire contrôlé, une polydispersité étroite et une

microstructure avancée. Grâce à ces techniques sophistiquées et à la modification post-polymérisation, un grand nombre de (co)polymères réactifs multi-stimuli ont été synthétisés.

I.5 Applications des (co)polymères sensibles aux stimuli

Les (co)polymères réactifs aux stimuli multiples sont un type de matériaux intelligents et ont suscité un grand intérêt ces dernières années. En raison de leur changement de propriétés physicochimiques (telles que la solubilité, la conformation de la chaîne, la dimension, la configuration…) domaines de la biotechnologie, de la nanotechnologie, des membranes fonctionnelles et des revêtements intelligents.

Chapitre II

Les nanoparticules métalliques, en particulier les nanoparticules d'or (AuNPs), ont attiré beaucoup d'attention en raison de leurs propriétés électroniques, optiques et catalytiques uniques résultant de leur large application allant de l'optoélectronique à la biologie. Ces propriétés dépendent fortement de la taille et de la forme des particules, de la nature de l'enveloppe organique protectrice et de la distance interparticulaire. Les AuNP sont instables du point de vue colloïdal et sont susceptibles d'agrégation irréversible, mais elles peuvent être stabilisées par greffage ou adsorption de petites molécules organiques telles que des citrates, des tensioactifs, des ligands ou des polymères. Ces molécules organiques constituent un outil supplémentaire pour moduler les propriétés physico-chimiques. À cette fin, les polymères se sont avérés être un matériau de choix en raison de leur flexibilité pour des utilisations spécifiques sur mesure et également pour leurs propriétés de stabilisation à long terme supérieures à celles des petites molécules. Des exemples notables incluent les polymères réactifs. En effet, le revêtement des AuNPs avec des stimuli sensibles est un moyen pratique de modifier de manière réversible les propriétés des AuNPs. Des polymères thermosensibles au comportement de type LCST ont été greffés sur des AuNPs sans perdre leur thermoréactivité.

II.1 Synthèse de P(VCL-*stat*-VP)$_{20k}$

La synthèse d'homopolymères (PVCL et PVP) et de copolymères de VCL et VP a été précédemment réalisée par X. Zhao dans notre laboratoire. Il s'agit d'une série de copolymères statistiques de VCL et VP de M_n prédéterminé (20000 g·mol^{-1}) et de compositions diverses qui ont été synthétisés par polymérisation RAFT/MADIX (**Schéma II.1**), leurs propriétés en solution aqueuse ont été déterminées par nucléaire spectroscopie par résonance magnétique

(RMN), chromatographie d'exclusion stérique (SEC) et calorimétrie différentielle à balayage (DSC).

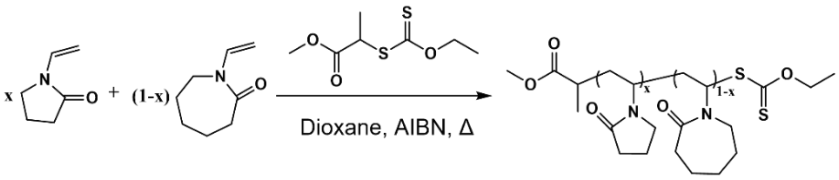

Schéma II.1. Synthèse de P(VCL-*stat*-VP) par polymérisation RAFT/MADIX.

II.2 Croissance et stabilité des AuNPs

Pour étudier la stabilisation, les propriétés optiques et catalytiques des nanohybrides formés, deux méthodes, comme indiqué dans le **Schéma II.2**, ont été adoptées pour obtenir des nanohybrides: (1) la formation in situ et (2) le revêtement d'AuNPs préformés.

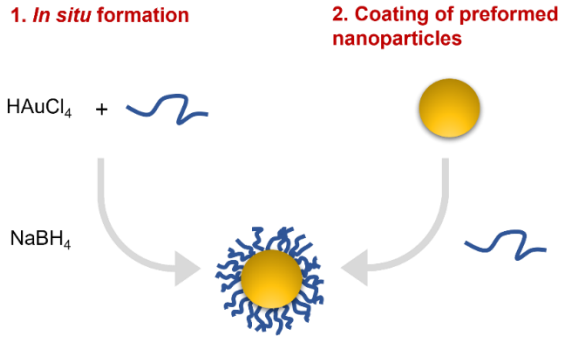

Schéma II.2. Deux voies de synthèse utilisées pour la formation de nanohybrides (formation *in situ* et revêtement de nanoparticules préformées).

Les effets de la concentration et de la composition du polymère sur la croissance in situ des AuNPs ont été mis en évidence par la couleur de la solution colloïdale, le microscope électronique à transmission (MET) et les mesures de spectroscopie UV-visible. Il est montré que l'augmentation de la concentration en polymère a conduit à la couleur de la solution colloïdale passée du brun au jaune pâle, qui s'accompagnait d'une diminution progressive de l'intensité de la bande de plasmon de surface, suggérant que la concentration en polymère a considérablement modifié la croissance des AuNPs. De plus, une augmentation de l'intensité de la bande de plasmon mesurée avec une augmentation de la fraction VP dans le copolymère a été observée. L'analyse MET a confirmé que la tendance observée est liée à une augmentation progressive de la taille moyenne de Au@P(VCL-*stat*-VP)$_{20k}$ formé lorsque la teneur en VP augmente. Les différents copolymères ont les mêmes groupes terminaux, ainsi les différences observées ne peuvent être attribuées qu'à une différence de composition: une teneur en VCL plus élevée conduisant à un meilleur contrôle de la croissance des NPs.

L'effet de la composition de copolymère sur la stabilisation colloïdale d'une solution de particules (préparées en enrobant des AuNPs préformées avec une quantité choisie de chaque polymère) soumise à une augmentation du pH ou de la force ionique est ensuite évalué après addition de solution de NaOH ou de NaCl. Un changement de couleur progressif lié à la modification de la bande plasmonique des particules due à des phénomènes d'agrégation ou de sédimentation traduit une faible stabilité colloïdale. L'augmentation de la concentration en polymère permet d'augmenter la stabilité des AuNPs vis-à-vis de la modification du pH ou de l'ajout de sel en raison d'un encombrement stérique plus élevé. De plus, pour une concentration choisie, PVCL favorise les NPs avec une stabilité colloïdale légèrement supérieure.

II.3 Thermoréactivité des nanohybrides

L'effet de la température sur les matériaux hybrides obtenus est ensuite évalué en mesurant l'absorbance des solutions à 520 nm entre 20 et 70 °C en fonction de la composition du copolymère. Seuls les systèmes Au@PVCL et Au@P(VCL_{75}-*stat*-VP_{25}) présentent une augmentation significative de l'absorbance induite par l'augmentation de la température, indiquant que les nanohybrides revêtus de polymères avec une teneur en VP inférieure à 40 % présentent des propriétés thermosensibles en solution à une température choisie. concentration.

II.4 Efficacité catalytique des nanohybrides

Les performances catalytiques de tous les systèmes Au@P(VCL-*stat*-VP)$_{20k}$ ont été testées à différentes températures (20, 30, 40, 50, 60 et 70 °C) dans la réduction du p-nitrophénol en *p*-aminophénol dans l'eau en utilisant $NaBH_4$ comme le montre la **Figure II.1**. Les constantes de vitesse observées (k_{obs}) pour toutes les cinétiques ont été extraites de la relation linéaire entre ln (A_t/A_0) en fonction du temps t en supposant une cinétique de pseudo premier ordre.

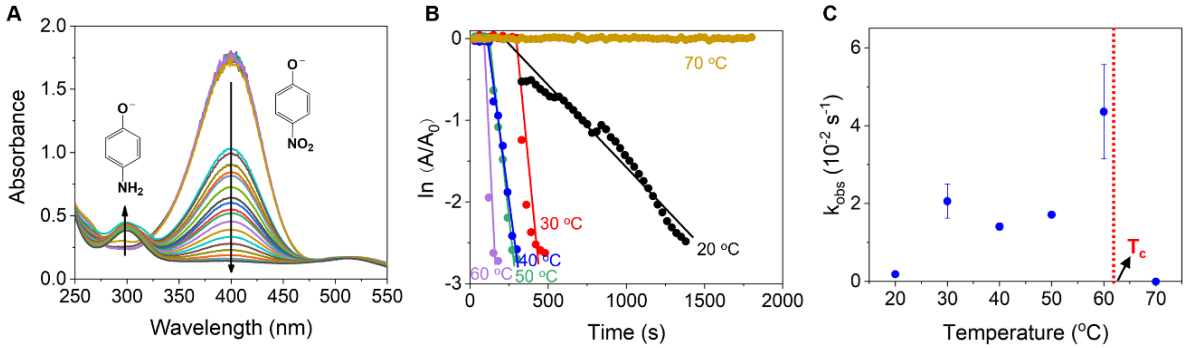

Figure II.1. (A) Spectres UV-vis à 20 °C, (B) Tracé de ln(A/A_0) en fonction du temps et (C) Constante cinétique de pseudo-premier ordre (k_{obs}) en fonction de la température dans la réduction du *p*-nitrophénol en *p*-aminophénol par $NaBH_4$ catalysé par Au@P(VCL_{75}-*stat*-VP_{25}) (la ligne rouge n'est qu'un guide pour les yeux) ([*p*-nitrophénol] = 10^{-4} mol·L^{-1}, [Au] = 5×10^{-5} mol·L^{-1}, [$NaBH_4$] = 3×10^{-3} mol·L^{-1}), [(co)polymère] = 5×10^{-3} % en poids.

Les **Figures II.1B** présentent les ajustements des données expérimentales obtenues à différentes températures pour Au@P(VCL$_{75}$-*stat*-VP$_{25}$). Dans un premier temps, il existe une période d'induction qui est liée à une restructuration de surface des nanoparticules avant le démarrage de la réaction catalytique. La réaction ne peut se produire qu'entre espèces adsorbées en surface. L'évolution de la constante cinétique de pseudo-premier ordre (k_{obs}) en fonction de la température pour Au@P(VCL$_{75}$-*stat*-VP$_{25}$) a été donnée sur la **Figure II.1C**. Les résultats suggèrent que l'activité catalytique augmente avec la température jusqu'à ce que le point de trouble soit atteint, après quoi aucune efficacité catalytique n'est observée.

Résultats supplémentaires obtenus à 20 °C pour les différents systèmes Au@polymère. Les nanoparticules hybrides basées sur des copolymères statistiques présentent des valeurs de kobs plus élevées que celles évaluées pour Au@PVCL et Au@PVP. De plus, un kobs optimal mesuré pour une teneur en VP est égal à 50 %. La tendance observée de l'efficacité catalytique en fonction de la composition du copolymère pourrait être rationalisée comme un compromis entre deux effets opposés. D'une part, une teneur plus élevée en VCL augmentait le caractère hydrophobe de l'enveloppe organique entourant les AuNPs et favorisait ainsi la diffusion des réactifs vers la surface des AuNPs. D'autre part, dans le même temps, la plus forte adsorption de VCL par rapport à VP limite l'efficacité catalytique des nanohybrides résultants.

En résumé, l'effet de la composition a été évalué à la fois sur la croissance des nanoparticules d'or synthétisées en présence des polymères (voie in situ) et sur les propriétés (stabilisation, optique, catalytique...) des nanoparticules préformées enrobées par ces polymères. Le caractère hydrophobe accru du PVCL lui permet d'agir comme un agent de stabilisation et de contrôle de la croissance plus efficace que le PVP pour la synthèse in situ d'AuNPs. De plus, la copolymérisation statistique de VCL et de VP permet de moduler dans une certaine mesure les propriétés du polymère, et donc des matériaux hybrides obtenus. A une fraction molaire de VP dans le copolymère inférieure à 40%, il a été possible d'augmenter la température de transition du matériau hybride et d'améliorer ses propriétés catalytiques par rapport à des homologues comprenant des homopolymères PVP et PVCL. De plus, l'incorporation d'une fraction plus élevée d'unités VCL dans les copolymères VCL/VP favorise une stabilité colloïdale accrue des nanohybrides d'or.

Chapitre III

Les systèmes thermosensibles, obtenus en dissolvant un polymère dans des solutions aqueuses, ont été largement étudiés. Ils présentent une température de transition caractéristique appelée température de point de trouble (T_c) à laquelle les interactions entre les chaînes

polymères et les milieux aqueux ont radicalement changé. Cela entraîne l'effondrement ou l'expansion des chaînes polymères. Il est intéressant de noter que les propriétés (telles que le T_c, l'auto-assemblage, etc.) des matériaux thermosensibles sont influencées non seulement par les paramètres macromoléculaires d'un polymère choisi (composition, masse molaire, architecture…), mais également par la polarité des composants hydrophiles ou hydrophobes incorporés. comonomères.

Dans ce chapitre, nous avons cherché à étudier plus avant les propriétés des copolymères de *N*-isopropylamide (NIPAM) et de monomère hydrophobe d'acrylate de *n*-butyle (BA) à différentes températures et concentrations de solution en relation avec leur composition et leur microstructure.

III.1 Synthèse de P(BA-*co*-NIPAM)

Trois familles de copolymères de P(BA-*stat*-NIPAM), PBA-*b*-PNIPAM et PNIPAM-*b*-PBA-*b*-PNIPAM ont été synthétisées par polymérisation par transfert de chaîne par addition-fragmentation réversible (RAFT)/conception macromoléculaire par échange de xanthates (MADIX) polymérisation. Pour chacun d'eux, une valeur M_n similaire de 10 000 g·mol^{-1} (en abrégé 10k) a été sélectionnée, les structures des copolymères dibloc, tribloc et statistiques sont données dans le **Schéma III.1**. Leurs propriétés ont été caractérisées par des mesures RMN, SEC et DSC.

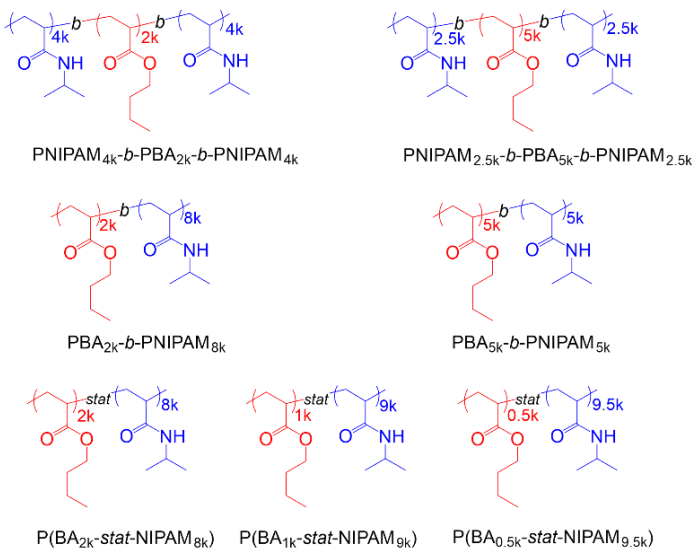

Schéma III.1. Structures de P(BA-*co*-NIPAM) utilisées dans ce chapitre.

III.2 Détermination de T_c en solution diluée

Pour évaluer l'influence de la composition et de la microstructure sur la T_c, le comportement des solutions de polymères a été étudié en fonction de la température par mesure

DSC (**Figure III.1**). Par rapport à l'homopolymère PNIPAM, l'incorporation d'un monomère hydrophobe dans la chaîne PNIPAM a conduit à une diminution significative de T_c quelle que soit la structure considérée. En plus de cet effet de composition, l'effet de la microstructure est très prononcé. Ainsi, pour une composition donnée (c'est-à-dire 80 % en poids de PNIPAM), la T_c mesurée pour un copolymère statistique est bien inférieure à celle mesurée pour les structures tribloc et dibloc. Dans le cas d'un copolymère statistique, sa microstructure spécifique semble désavantager fortement l'hydratation du polymère. Elle ne permet pas non plus d'étudier des copolymères contenant des fractions de PBA supérieures à 20 % en poids. Enfin, les valeurs légèrement inférieures de T_c pour les structures triblocs par rapport aux diblocs pourraient être liées à un phénomène similaire : en effet, pour une composition donnée, les structures triblocs présentent une transition supplémentaire entre les blocs PBA et PNIPAM.

En plus des effets sur la T_c, la microstructure impacte également fortement la solubilité des différents polymères étudiés. Ainsi, les copolymères à structure statistique présentent une faible solubilité dans les solutions aqueuses, tandis que les copolymères diblocs et triblocs grâce à leur structure amphiphile spécifique permettent d'obtenir des solutions limpides pour des rapports pondéraux allant jusqu'à 20 % en poids.

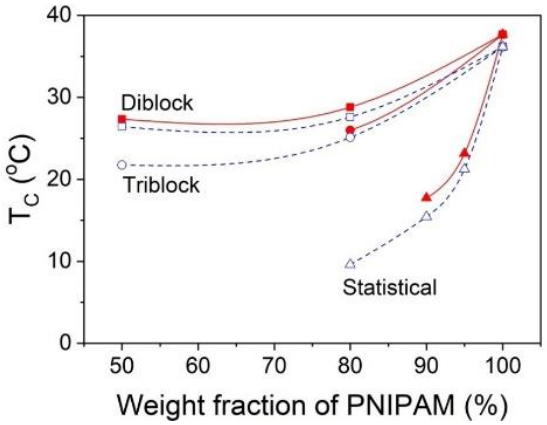

Figure III.1. Températures de point de trouble T_c obtenues par DSC par chauffage (traits rouges pleins) ou refroidissement (traits bleus ouverts) pour l'homopolymère PNIPAM et les copolymères statistiques, diblocs et triblocs à base de PNIPAM à une concentration de 1% en poids.

III.3 Comportement d'auto-assemblage du P(BA-*co*-NIPAM) en solution diluée

Des mesures MET et SANS ont été réalisées pour analyser la taille et la conformation en fonction de l'architecture du copolymère (voir **Figure III.2**). A 20 °C (en dessous de T_c), les images MET de solutions séchées de $PNIPAM_{4k}$-*b*-PBA_{2k}-*b*-$PNIPAM_{4k}$ montrent des structures sphériques monodisperses très régulières, suggérant la formation de structures micellaires sphériques pour le copolymère, ce qui est confirmé par les mesures SANS. Il est à noter que le rayon micellaire déduit du SANS est le rayon du noyau PBA hydrophobe seul.

À 40 °C (au-dessus de T_c), la formation d'agrégats sphériques avec une distribution de taille étroite a été confirmée par des expériences MET (coloration négative) et des mesures SANS. Étant donné que les agrégats semblent être sphériques, il était cohérent d'ajuster les données SANS au-dessus de T_c avec le modèle de sphère polydisperse, qui a donné un rayon moyen pour PNIPAM$_{4k}$-*b*-PBA$_{2k}$-*b*-PNIPAM$_{4k}$. À partir des mesures SANS, PNIPAM$_{2.5k}$-*b*-PBA$_{5k}$-*b*-PNIPAM$_{2.5k}$ forme des agrégats avec un rayon similaire dans les limites de l'erreur expérimentale. Ainsi, au dessus de T_c, ces agrégats ont une taille similaire quelle que soit la nature de la microstructure (dibloc ou tribloc). La formation d'agrégats sphériques également appelés mésoglobules, qui sont stables en solution et se transforment spontanément en micelles sphériques lorsque la solution est refroidie en dessous de T_c.

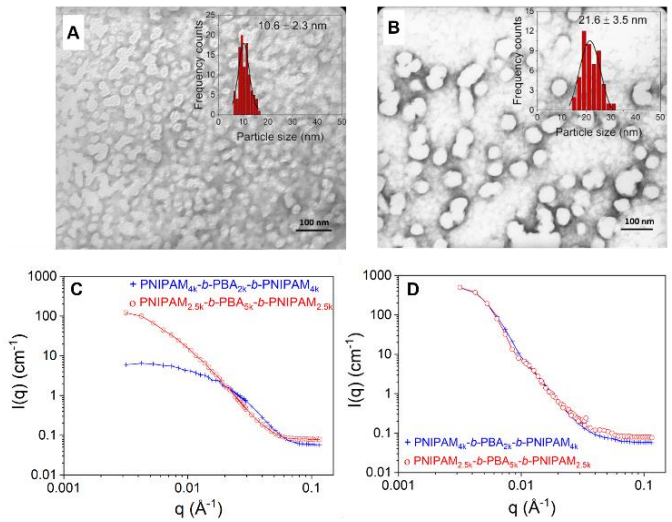

Figure III.2. Images MET de PNIPAM$_{4k}$-*b*-PBA$_{2k}$-*b*-PNIPAM$_{4k}$ (A) à 20 °C et (B) à 36 °C. Intensité de diffusion en unités absolues (cm^{-1}) de D_2O de PNIPAM$_{4k}$-*b*-PBA$_{2k}$-*b*-PNIPAM$_{4k}$ (+) et PNIPAM$_{2.5k}$-*b*-PBA$_{5k}$-*b*-PNIPAM$_{2.5k}$ (o) (C) à 20 °C et (D) à 36 °C.

III.4 Thermoréactivité du P(BA-*co*-NIPAM) en solution concentrée

Le comportement des solutions de polymères pour des concentrations allant de 0.1 à 20% en poids a ensuite été étudié. Une évaluation visuelle initiale de l'effet de la température pour différentes structures, compositions ou concentrations de polymère a été réalisée. La **Figure III.3** montre des photographies de la transition de phase observée pour la structure tribloc PNIPAM$_{4k}$-*b*-PBA$_{2k}$-*b*-PNIPAM$_{4k}$ à une concentration de 20% en poids. Des phases de solution transparente, de solution opaque, de gel opaque et de gel déshydraté apparaissent lors du chauffage. Cette transition de phase est attribuée au tassement et à l'enchevêtrement des micelles.

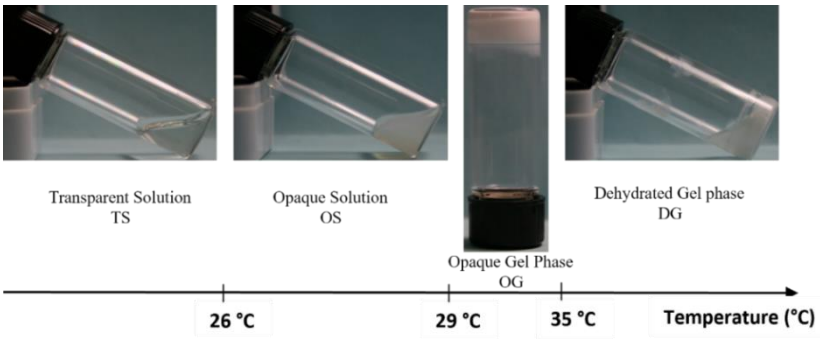

Figure III.3. Photographies de la transition de phase observée pour la structure tribloc PNIPAM$_{4k}$-*b*-PBA$_{2k}$-*b*-PNIPAM$_{4k}$ à une concentration de 20% en poids en fonction de la température: Solution transparente (phase TS), solution opaque (OS), phase de gel opaque (OG) et phase de gel déshydraté (DG).

Les propriétés de ces hydrogels sont susceptibles d'être fortement liées à leur structure interne. Ainsi, pour mieux comprendre la structure du réseau des hydrogels, des échantillons lyophilisés ont été analysés par microscopie électronique à balayage à température cryogénique (cryo-MEB). Comme le montre la **Figure III.4**, sous une même composition, la structure tribloc, formant des réseaux plus denses avec des pores de plus petite taille, est plus susceptible d'être le siège d'une synérèse importante et présentant une cinétique de réhydratation plus lente.

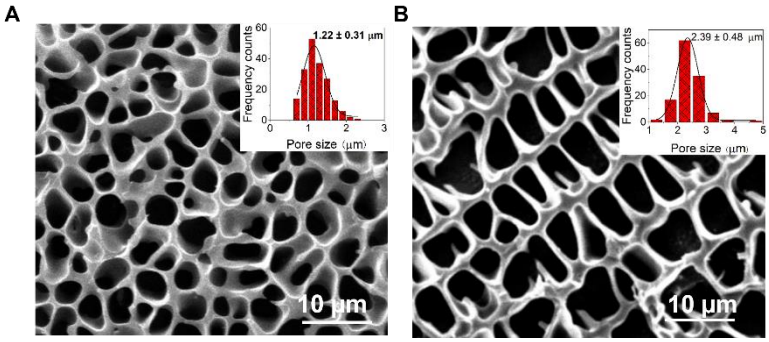

Figure III.4. Images cryo-SEM de structures de gel à 40 °C obtenues à partir de (A) PNIPAM$_{4k}$-*b*-PBA$_{2k}$-*b*-PNIPAM$_{4k}$ et (B) PBA$_{2k}$-*b*-PNIPAM$_{8k}$.

En résumé, la microstructure du P(BA-*co*-NIPAM) module significativement les propriétés d'auto-assemblage, morphologiques et mécaniques de ces matériaux en milieu aqueux. À composition similaire, le BA hydrophobe dans les copolymères à blocs contribue à une diminution de T_c par rapport au PNIPAM pur dans une bien moindre mesure par rapport aux structures statistiques. De plus, les structures à blocs inférieures à T_c de composition appropriée conduisent à la formation d'agrégats colloïdaux. Au-dessus de T_c, la formation d'agrégats colloïdaux est observée à de faibles concentrations et des gels se forment à des concentrations plus élevées. Pour une composition donnée, les copolymères diblocs conduisent à des structures plus grosses et plus denses par rapport aux analogues triblocs et permettent la

formation de gels qui ne se démixent pas avec le temps (pas de synérèse) mais qui sont plus mous que les gels triblocs.

Chapitre IV

Le polymère thermosensible le plus connu et le plus étudié est le PNIPAM qui présente une transition de phase réversible d'un état de bobine hydrophile à un état de globule hydrophobe en raison de sa LCST. Le groupe *N*-alkyle des polyacrylamides *N*-alkyl-substitués est un paramètre important pour déterminer la thermoréponse et le comportement en solution des polymères. Par exemple, le poly(*N*,*N*-diméthylacrylamide) (PDMA) est soluble dans l'eau et aucune LCST n'est détectée, le poly(*N*-isopropylacrylamide) (PNIPAM) et le poly(*N*,*N*-diéthylacrylamide) (PDEAAM) ont des LCST similaires de 32-33 °C, et le poly(*N*-*n*-butylacrylamide) (PNNBAM) est insoluble dans l'eau.

Récemment, différentes familles d'homopolymères portant une fonction amine tertiaire greffée sur des chaînes principales de poly((méth)acrylamide)s ont été étudiées. Dans le cas de chaînes alkyle *N*,*N*-diéthyle substituées avec un lieur éthylène. La présence de fragments amine tertiaire présente des caractéristiques de réponse au pH en raison de leurs processus de protonation/déprotonation réversibles et permet à ces polymères de combiner des propriétés de réponse aux stimuli thermo et pH. Par conséquent, le poly(*N*,*N'*-diéthylamino éthyl acrylamide) (PDEAEAM) sensible aux stimuli présente une caractéristique sensible au pH (soluble dans l'eau en solution acide et insoluble dans les milieux alcalins) et un comportement de phase LCST en solution aqueuse.

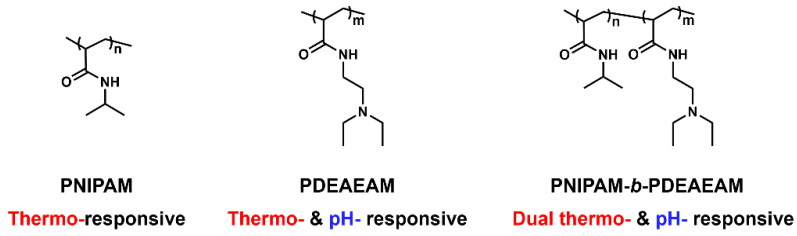

Schéma IV.1. Copolymère séquencé PNIPAM-*b*-PDEAEAM (noté PN-*b*-PD) étudié dans cet article présentant une double réactivité thermo/pH.

Pour préparer des (co)polymères multi-sensibles, une stratégie largement documentée consiste à combiner plusieurs fragments sensibles aux stimuli au sein de copolymères statistiques ou séquencés contenant deux ou plus de deux segments ou blocs sensibles aux stimuli. Dans ce chapitre, nous avons cherché à étudier une famille de copolymères à blocs comprenant un bloc thermo-réactif de *N*-isopropylacrylamide (NIPAM) et un bloc doublement thermo- et pH-réactif (PDEAEAM) (**Schéma IV.1**), ils sont synthétisés par Polymérisation

RAFT et caractérisée par des mesures RMN, SEC et DSC. Ensuite, l'effet des paramètres macromoléculaires et du pH sur les propriétés thermosensibles de ces polymères en solution aqueuse. Leurs propriétés d'auto-assemblage en milieu aqueux lors des variations de pH et de température ont également été étudiées.

IV.1 Comportement thermosensible des homopolymères

Les propriétés thermosensibles des homopolymères PNIPAM (noté PN) et PDEAEAM (noté PD) ont été étudiées. La T_c de PN pourrait être finement ajustée par incorporation de fragments hydrophiles ou hydrophobes. Dans le cas des groupes terminaux ionisables, leur hydrophilie varie avec la proportion de forme ionisée liée à la gamme de pH. Plus la forme ionisée est présente, plus l'hydrophilie du bout de chaîne sera marquée conduisant à une augmentation de T_c.

L'homopolymère PN synthétisé porte une fonction carboxylique. Il possède une valeur de p*K*a autour de 4.5 et donc une modification du pH va induire un changement d'état d'ionisation/hydratation de cette fonction et des polymères étudiés. Par conséquent, un changement de la valeur T_c du PN synthétisé est attendu. Pour confirmer le rôle critique du groupe terminal dans le comportement observé, un homopolymère PN a été synthétisé à partir d'un agent RAFT différent, à savoir l'ester méthylique de l'acide 2-mercaptopropionique O-éthyl dithiocarbonate (Rhodixan A1). Aucune autre dépendance au pH du comportement thermosensible n'est en outre observée pour ce dernier polymère, ce qui confirme le rôle critique des groupes terminaux.

L'homopolymère PD est un polyélectrolyte faible, totalement soluble dans l'eau quel que soit le pH à température ambiante. La valeur p*K*a des groupes amino tertiaires pendants a été déterminée par titrage du pH et une valeur de 7.25 est trouvée. La transmittance de la solution aqueuse de PD_{5k} est ensuite mesurée en fonction de la température à un pH passant de 3 à 10, le PD_{5k} affiche un comportement LCST dans une plage de pH de 10 à 9 et perd sa thermoréactivité lorsque le pH diminue à 8.

IV.2 Propriétés réactives du PNIPAM-*b*-PDEAEAM (noté PN-*b*-PD)

Les copolymères à blocs PN-*b*-PD comportent deux blocs: un bloc PN thermosensible avec une température de transition caractéristique à 30 °C et un bloc PD qui est, pour un pH supérieur à p*K*a, déprotoné (7.25) et thermosensible. De plus, les deux groupements terminaux (fonction acide carboxylique, un groupement $-C_{12}H_{25}$) sont susceptibles de favoriser la

formation de systèmes micellaires au dessus du p*K*a de la fonction acide carboxylique comme démontré dans le cas de PN.

(i) Réactivité à pH 10

A pH 10, PD-*b*-PN comprend deux groupes thermosensibles (PD et PN), un groupe terminal acide carboxylique dans sa forme déprotonée anionique carboxylate et un groupe terminal hydrophobe -$C_{12}H_{25}$ (**Schéma IV.2**).

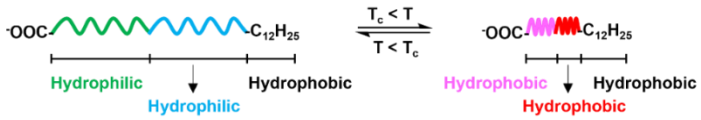

Schéma IV.2. Structure et effet de la température sur la conformation des chaînes PN-*b*-PD à pH 10. Comme dans ce qui suit, une seule température de transition est mise en évidence par les mesures de diffusion et de turbidimétrie à pH 10, une seule valeur T_c est notée dans ce schéma.

Le comportement thermosensible de PN_{5k}-*b*-PD_{5k} est différent de celui des homopolymères vierges, comme illustré par des expériences de turbidimétrie (voir **Figure IV.1**). Alors que PN_{5k} n'entraîne pas de changement significatif de transmittance en raison de la formation de systèmes micellaires et que PD_{5k} a une T_c, PN_{5k}-*b*-PD_{5k} présente un comportement thermosensible différent de celui des deux homopolymères. Considérant que le PNIPAM-xanthate présente une température de transition autour de 36 ° C à une concentration similaire, le comportement observé du copolymère séquencé peut être attribué à la structure spécifique du copolymère séquencé.

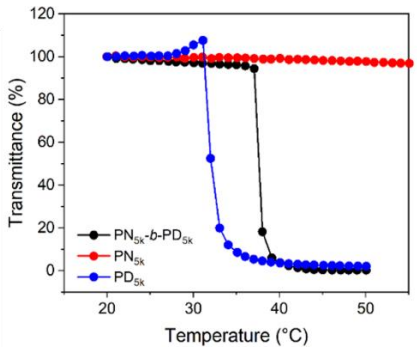

Figure IV.1. Changement de transmittance de PN_{5k}-*b*-PD_{5k}, PN_{5k} et PD_{5k} à pH 10 ([(co)polymère] = 1 % en poids).

Pour mieux comprendre le mécanisme à l'origine de cette transition, une analyse par RMN 1H a été réalisée avec une augmentation de température de 20 à 50 °C (**Figure IV.2A**). Les deux intégrales des unités PN et PD sont restées à peu près constantes jusqu'à 32 °C, ce qui est suivi d'une tendance à la baisse en fonction de la température, confirmant en outre le fait qu'avec l'augmentation de la température, les blocs PN et PD subissent des transitions de soluble à insoluble. dans cette gamme de température qui va induire la formation de gros agrégats.

La structure colloïdale obtenue à partir d'une solution aqueuse de PN_{5k}-*b*-PD_{5k} au-dessous et au-dessus de T_c a été caractérisée par les techniques MET, cryo-TEM, DLS (voir **Figure IV.2**).

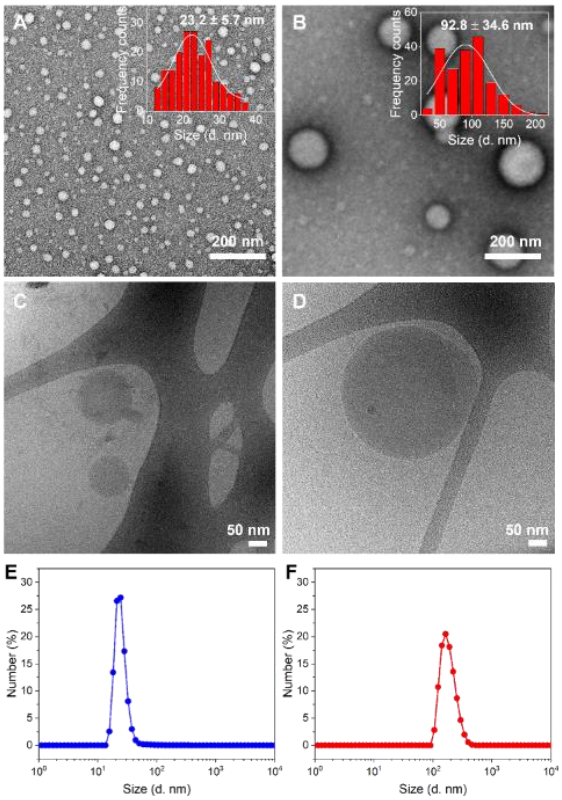

Figure IV.2. Images MET, cryo-TEM et distribution de taille moyenne en nombre de PN_{5k}-*b*-PD_{5k} (A) (C) (E) à 25 °C et (B) (D) (F) à 60 °C (pH = 10, échantillons TEM ont été colorées avec une solution d'acétate d'uranyle à 2 % en poids).

À 25 °C, en raison de la propriété amphiphile (groupe hydrophobe -$C_{12}H_{25}$ et chaînes hydrophiles PN, PD), des micelles sphériques avec noyau -$C_{12}H_{25}$ et couronne PN, PD sont observées. À 60 °C, les chaînes PN et PD s'effondrent sont déshydratées et deviennent hydrophobes, les structures micellaires observées à 25 °C ont tendance à s'agréger, ce qui a entraîné la formation d'objets sphériques plus gros. À travers les morphologies et la taille des agrégats de PN_{5k}-*b*-PD_{5k} formés à une température inférieure et supérieure à Tc à pH 10, la transition morphologique induite par la température est représentée dans le **Schéma IV.3**.

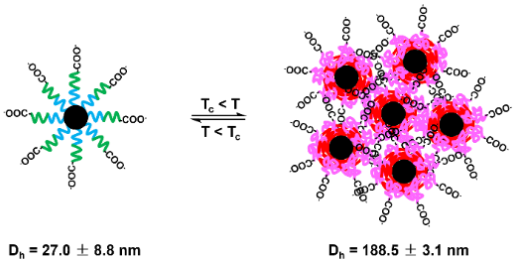

Schéma IV.3. Illustration schématique de la thermoréactivité et du comportement d'auto-assemblage pour la solution PN_{5k}-*b*-PD_{5k} à pH 10.

(ii) Réactivité à pH 4

A pH 4, PD-*b*-PN comprend un groupe thermosensible (PN), un bloc cationique (PD), un groupe terminal acide carboxylique et un groupe terminal hydrophobe -$C_{12}H_{25}$. La conformation de la chaîne de PD-*b*-PN en réponse à la température est représentée dans le **Schéma IV.4** sur la base des comportements des homopolymères PN et PD.

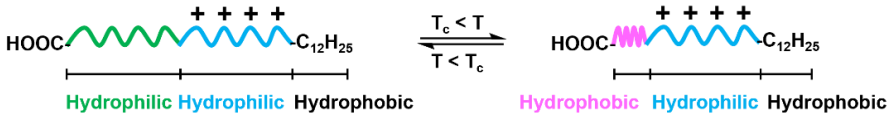

Schéma IV.4. Structure et effet de la température sur la conformation des chaînes PN-*b*-PD à pH 4.

La thermoréactivité de PN_{5k}-*b*-PD_{5k} à pH 4 est comparée à celles de PN_{5k} et PD_{5k} par mesure de turbidimétrie. Comme le montre la **Figure IV.3**, l'homopolymère PN_{5k} a une T_c à 26 °C, aucun changement de transmittance de la référence PD_{5k} n'a lieu dans la plage de température étudiée: en effet, PD_{5k} est désormais protoné et non plus thermosensible. Dans le cas de PN_{5k}-*b*-PD_{5k}, une diminution de la transmittance en deux étapes s'est produite à partir de 23 °C avec un premier point d'inflexion de 29 °C ($T_{c,1}$) et un second à 39 °C ($T_{c,2}$).

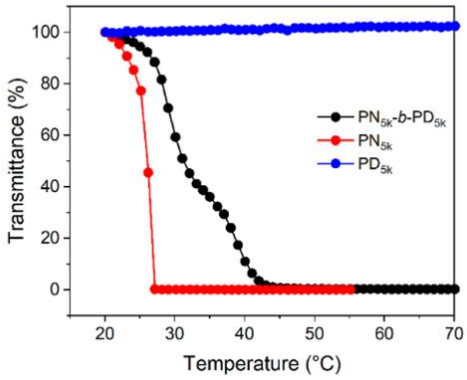

Figure IV.3. Changement de transmittance de PN_{5k}-*b*-PD_{5k}, PN_{5k} et PD_{5k} à pH 4 en fonction de la température ([(co)polymère] = 1 % en poids, vitesse de chauffage = 1 °C·min^{-1}).

Le mécanisme derrière ces transitions a été analysé par des spectres RMN ^{1}H avec une augmentation de température de 20 à 50 °C. Avec l'augmentation de la température, seul le bloc PN subit une transition de soluble à insoluble. Alors que les intégrales des unités PD n'ont pas de changement significatif dans la plage de température étudiée. La structure colloïdale obtenue à partir d'une solution aqueuse de PN_{5k}-*b*-PD_{5k} a été étudiée par MET, cryo-TEM et DLS à 25, 30 et 60 °C (voir **Figure IV.4**).

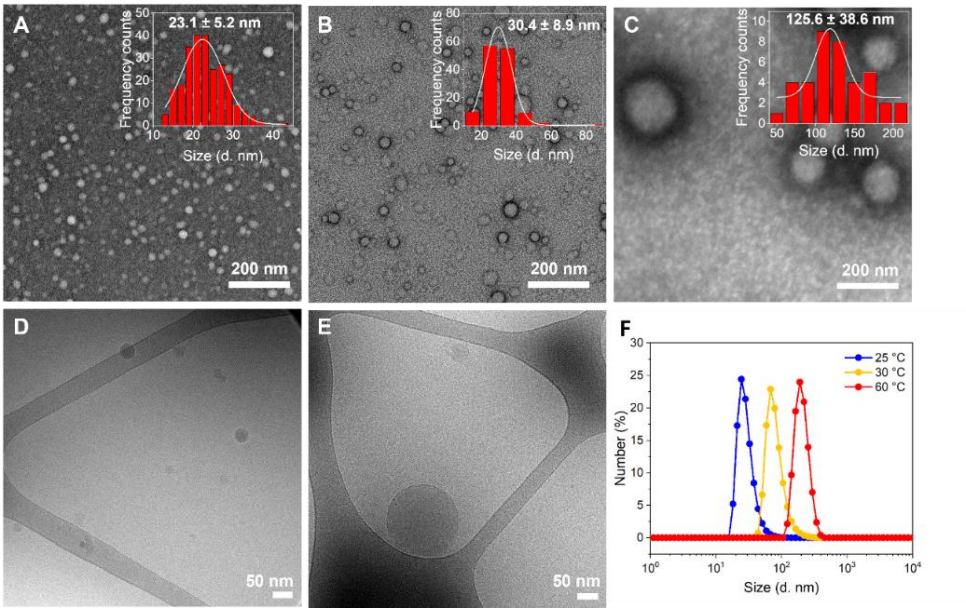

Figure IV.4. Images MET, cryo-TEM à (A) (D) 25, (B) 30, (C) 60 et (E) 50 °C et (F) Distribution granulométrique moyenne en nombre des agrégats pour PN_{5k}-*b*-PD_{5k} formés sous pH 4 (les échantillons TEM ont été colorés avec une solution d'acétate d'uranyle à 2 % en poids, la concentration de PN_{5k}-*b*-PD_{5k} pour les mesures TEM et DLS était de 0.1 % en poids, pour l'analyse Cryo-TEAM était de 0.5 % en poids).

À partir des résultats obtenus dans cette section, un diagramme de phase schématique peut être proposé comme indiqué dans le **Schéma IV.5**, en dessous de $T_{c,1}$, les chaînes polymères PN_{5k}-b-PD_{5k} s'auto-organisent en agrégats sphériques uniformes avec un noyau -$C_{12}H_{25}$ et une couronne de PN, blocs PD. Au-dessus de $T_{c,1}$, les chaînes PN commencent à s'effondrer. Cependant, PD conserve toujours la propriété hydrophile et le caractère cationique, ainsi PN_{5k}-*b*-PD_{5k} s'assemble en micelles ressemblant à des fleurs. Ces structures peuvent être issues soit d'une agrégation partielle de précédentes formées à 25 °C soit d'un réarrangement de chaînes polymères en une structure coeur-écorce avec un groupe terminal hydrophobe -$C_{12}H_{25}$ dans le coeur et un bloc PN partiellement déshydraté et un segment PD cationique hydraté en la coquille interagissant ensemble. Lorsque la température monte jusqu'à $T_{c,2}$, les colloïdes subissent une seconde transition avec la formation de très gros objets.

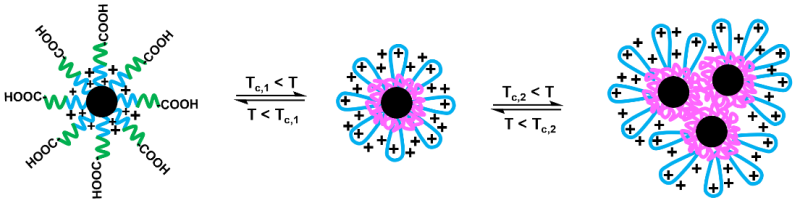

Schéma IV.5. Illustration schématique des morphologies de la solution PN_{5k}-*b*-PD_{5k} à pH 4 à différentes températures.

En résumé, une série de copolymères PN-*b*-PD et d'homopolymères correspondants ont été synthétisés avec succès avec un poids moléculaire et une composition contrôlés en utilisant

la polymérisation RAFT. Le comportement de ces polymères en solutions aqueuses a été étudié en fonction de la température et du pH. À pH 10, les blocs PN et PD sont tous deux thermosensibles. Les solutions de copolymères séquencés ont une seule transition sur laquelle des nano-objets sphériques plus grands et stables sont formés. A pH 4, seul le bloc PN est thermosensible, les solutions de polymère présentent deux températures de transition, chacune induisant la formation d'agrégats plus gros une fois atteinte avec une enveloppe externe PN chargée positivement.

Chapitre V

Grâce à ses propriétés abondantes, peu coûteuses, non toxiques et sans danger pour l'environnement, le dioxyde de carbone (CO_2) est devenu un déclencheur nouveau et innovant pour les matériaux sensibles aux stimuli. La faisabilité des propriétés commutables par le CO_2 des (co)polymères dépend de la température et de la concentration à laquelle l'espèce doit être commutée. Idéalement, le % de protonation est très faible lorsque le système est sous air et, en présence de CO_2, il doit être le plus élevé possible pour maximiser le changement de propriétés de la solution de polymère. Ainsi, l'ajout et l'élimination de CO_2 devraient faire aller et venir le mélange à travers le point médian du système, qui est défini comme le pH auquel la moitié des groupes commutables sont protonés. Sous l'air, le pH doit être significativement plus élevé que le point médian du système, tandis qu'en cas d'exposition au CO_2, le pH doit être significativement inférieur au point médian du système. Si l'espèce commutable est entièrement dissoute dans la phase aqueuse sous air et sous CO_2, alors le point médian du système est égal au p*K*a. Les fractions réactives au CO_2 les plus étudiées sont les (co)polymères à base de PDEAEMA (p*K*a 7.4) et de PDMAEMA (p*K*a 7.4). Il est également intéressant de noter que certains de ces homopolymères sensibles au CO_2 à base d'amine sont également thermosensibles (principalement dans leur version non chargée). Leur Tc correspondant varie en fonction du CO_2 appliqué/supprimé.

La plupart des copolymères doubles CO_2 et thermosensibles sont principalement préparés par combinaison de deux blocs ou plus avec différents comportements de réponse aux stimuli. Tirant parti de la polymérisation radicalaire contrôlée, telle que la polymérisation à médiation nitro (NMP), la polymérisation radicalaire par transfert d'atomes (ATRP) et la polymérisation par transfert de chaîne par addition-fragmentation réversible (RAFT), un nombre considérable de copolymères doubles réactifs à la température et au CO_2 avec des compositions contrôlées et des microstructures bien définies ont été synthétisés.

Dans ce chapitre, nous visons tout d'abord à étudier la thermoréactivité induite par le CO_2 de l'homopolymère PD. Ensuite, nous étudierons les copolymères à blocs à base de PD avec le PNIPAM comme second bloc thermoréactif.

V.1 Réactivité au CO_2 de l'homopolymère PD

Afin de clarifier la commutation CO_2/N_2 du PD, nous avons d'abord étudié les changements de pH et de degré de protonation de la solution de PD_{5k} lorsque le CO_2 et le N_2 étaient introduits alternativement.

Ensuite, les produits de réaction de l'homopolymère PD avec le CO_2 sont étudiés par analyse RMN à 25 °C dans D_2O. Les déplacements chimiques de trois types de protons dans PD_{5k} subissent un mouvement vers le bas et vers le haut après exposition au CO_2 et au N_2, respectivement. Pendant ce temps, le signal à 160 ppm dans le spectre RMN ^{13}C révèle la formation de bicarbonate d'ammonium après bullage de CO_2.

La thermoréactivité réglable au CO_2 du PD_{5k} a été détectée par turbidimétrie et mesures DLS (voir **Figure V.1**). Avant exposition au CO_2, le PD_{5k} affiche un comportement LCST avec une T_c mesurée à 31.5 °C. Après traitement au CO_2, les groupes amine tertiaire sont protonés, ce qui rend le PD_{5k} hydrophile. La valeur de transmittance reste constante autour de 100% de 20 °C à 80 °C, suggérant que le PD_{5k} perd sa thermoréactivité dans la plage de température étudiée. Lors de l'exposition à N_2, le comportement LCST de PD_{5k} est récupéré avec un T_c plus élevé (64.9 °C). Ce phénomène peut être attribué à la présence d'espèces résiduelles de CO_2 dans les interactions avec l'amine tertiaire et est en bon accord avec les travaux de Zhang.

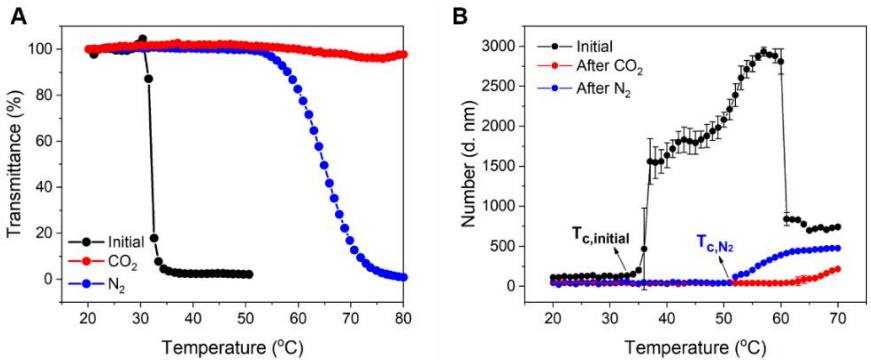

Figure V.1. Graphiques de (A) transmittance et (B) taille des agrégats en fonction de la température pour la solution aqueuse de PD_{5k} avant, après bullage de CO_2 et après bullage de N_2 ([PD_{5k}] = 1 % en poids).

V.2 Réactivité thermique et au CO_2 des copolymères séquencés PN_{5k}-*b*-PD_{5k}

les copolymères séquencés PN_{5k}-*b*-PD_{5k} synthétisés devraient avoir des propriétés thermo-sensibles et réactives au CO_2. La réactivité au CO_2 de PN_{5k}-*b*-PD_{5k} est d'abord analysée par

RMN ^{1}H à température ambiante. Les déplacements chimiques de -$CH_2CH_2N(CH_2CH_3)_2$, -$CH_2CH_2N(CH_2CH_3)_2$ et -$CH_2CH_2N(CH_2CH_3)_2$ dans le bloc PD_{5k} se déplacent vers le bas après 10 min de bullage de CO_2, puis reviennent à la position d'origine après avoir fait bouillonner N_2 pendant 30 min. De plus, aucun déplacement chimique des signaux dans PN_{5k} n'est observé en même temps. Par conséquent, le CO_2 ne réagit qu'avec le bloc PD pour générer du bicarbonate d'ammonium et aucun effet n'a été observé sur le bloc PN.

L'effet de l'ajout/suppression de CO_2 sur le comportement thermoréactif de PN_{5k}-*b*-PD_{5k} est étudié par mesure de turbidimétrie (**Figure V.2**). Après exposition au CO_2, PN_{5k}-*b*-PD_{5k} affiche toujours un comportement LCST avec un T_c plus élevé (40 °C) par rapport à la valeur initiale (38 °C). Lors de l'exposition à N_2, T_c devrait revenir à sa valeur initiale, cependant, en raison du bloc PD protoné partiel, la thermoréactivité de PN_{5k}-*b*-PD_{5k} est toujours conservée mais se produit à une température plus élevée (41 °C).

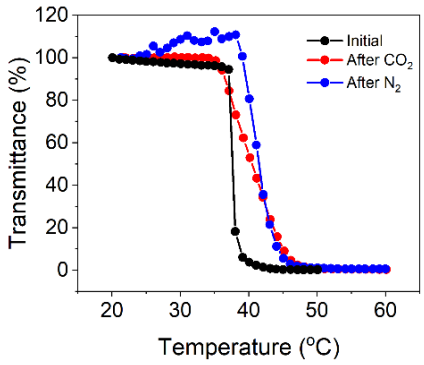

Figure V.2. Changement de transmittance de la solution PN_{5k}-*b*-PD_{5k} en fonction de la température avant, après bullage avec CO_2 et après bullage avec N_2. ([PN_{5k}-*b*-PD_{5k}] = 1 % en poids)

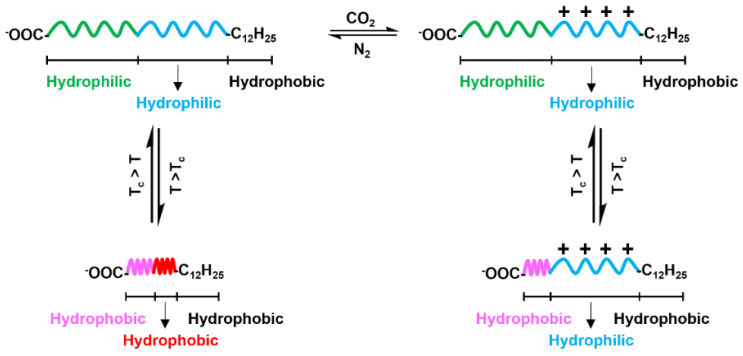

Schéma V.1. Conformation des chaînes PN_{5k}-*b*-PD_{5k} sous chauffage/refroidissement et traitement/élimination du CO_2.

La solubilité des blocs PN et PD dans l'eau peut être ajustée par changement de température et traitement/élimination du CO_2. Il en résulte une modification de la conformation du polymère en solution qui favorisera (ou non) la formation d'agrégats en fonction de la température et de la quantité de CO_2. Le changement de conformation d'une chaîne de PN_{5k}-*b*-PD_{5k} en réponse à la température et au CO_2 est représenté dans le **Schéma V.1**.

Le comportement d'auto-assemblage de PN_{5k}-*b*-PD_{5k} sous des stimuli de température et des mesures de CO_2, TEM et DLS ont été effectuées dans différentes conditions.

(i) À une température inférieure à T_c

En l'absence de CO_2, en raison du groupe terminal hydrophobe -$C_{12}H_{25}$ et des chaînes PN et PD hydratées, PN_{5k}-*b*-PD_{5k} peut s'auto-assembler en micelles sphériques avec un noyau de groupe -$C_{12}H_{25}$ et une couronne de blocs PN_{5k} et PD_{5k}. L'exposition au CO_2 améliore la solvatation des chaînes PD dans l'eau, mais elle ne déclenche aucun effet sur les chaînes PN et -$C_{12}H_{25}$ terminal, des structures sphériques sont toujours observées. Ces structures devraient présenter une couronne différente, composée de PN_{5k} et de PD_{5k} chargé. Au fur et à mesure que le CO_2 est éliminé par barbotage de N_2, le bloc PD_{5k} récupère l'état déprotoné et conserve toujours une bonne solubilité.

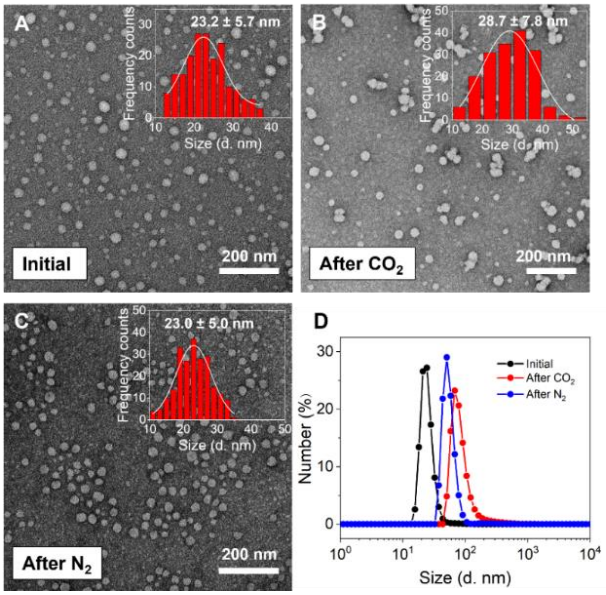

Figure V.3. Images MET (A) avant, (B) après traitement au CO_2, (C) après exposition à N_2 et (D) Taille hydrodynamique distribuée en nombre de PN_{5k}-*b*-PD_{5k} à 25 °C ([PN_{5k}-*b*-PD_{5k}] = 0,1 % en poids, échantillons colorés avec une solution d'acétate d'uranyle à 2 % en poids).

(ii) À une température supérieure à T_c

Avant l'exposition au CO_2, à 60 °C, les chaînes PN et PD s'effondrent. Les chaînes polymères peu solubles s'agrègent en un amas de micelles sphériques. En présence de CO_2, le bloc PN conserve sa thermoréactivité, alors que les chaînes PD sont protonées, ce qui rend le bloc PD non plus thermoréactif dans la plage de température étudiée. Lorsque la température s'élève à 60 °C (au-dessus de T_c), les chaînes PN s'effondrent et deviennent hydrophobes, tandis que les chaînes PD conservent une bonne solubilité. Par conséquent, des micelles ressemblant à des fleurs sont formées avec un noyau -$C_{12}H_{25}$, une coque PN et une couronne PD. Après

aération avec N_2, PD récupère déprotoné et retrouve sa thermoréactivité, par conséquent, à 60 °C, PN et PD s'effondrent et se forment dans la coquille.

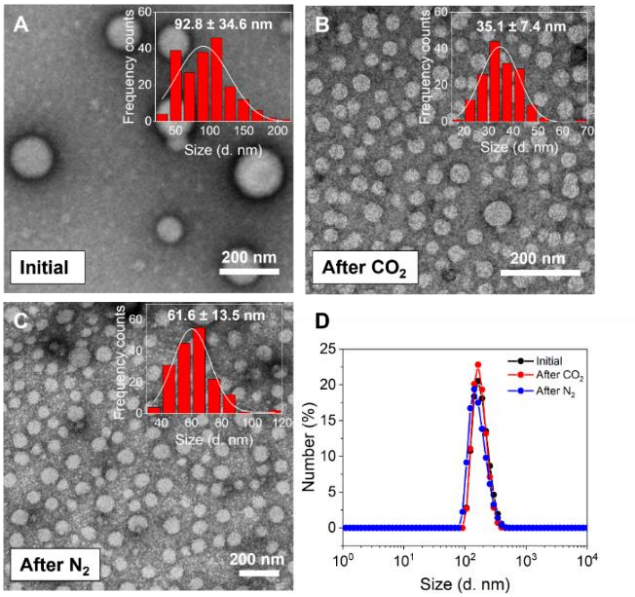

Figure V.4. Images MET des agrégats PN_{5k}-*b*-PD_{5k} (A) avant, (B) après exposition au CO_2 et (C) après exposition au N_2 à 60 °C ([PN_{5k}-*b*-PD_{5k}] = 0.1 % en poids, échantillons coloré avec une solution d'acétate d'uranyle à 2 % en poids).

Comme l'ont révélé les analyses MET et DLS, PN_{5k}-*b*-PD_{5k} s'est auto-assemblé en structures sphériques de différentes tailles dans toutes les conditions étudiées. Une illustration schématique de PN_{5k}-*b*-PD_{5k} sous des stimuli de température et de CO_2 est proposée dans le **Schéma V.2**.

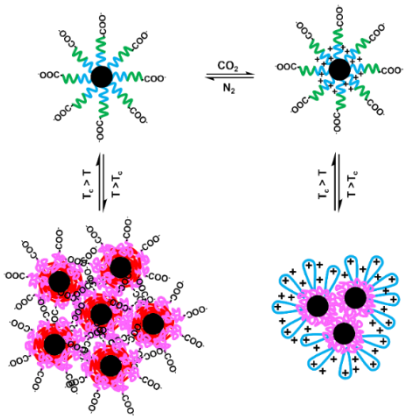

Schéma V.2. Illustration schématique de l'auto-organisation des réponses doubles PN_{5k}-*b*-PD_5k et température-CO_2.

La réversibilité de la solution de PN-*b*-PD a été détectée en termes de déplacements chimiques du bloc PD et de changement de pH lors d'un bouillonnement alterné de CO_2/N_2 à 25 °C. Seuls les signaux du bloc PD dans PN_{5k}-*b*-PD_{5k} se déplacent vers le bas après le traitement au CO_2, puis reviennent aux positions initiales lorsque le CO_2 est éliminé par barbotage de N_2. Pendant ce temps, le pH de la solution de PN_{5k}-*b*-PD_{5k} diminue et augmente

après le traitement au CO_2 et au N_2, respectivement. Cela suggère que PN_{5k}-*b*-PD_{5k} présente une bonne réversibilité avec un minimum de 7 cycles.

En résumé, les propriétés thermosensibles commutables par le CO_2 (y compris le T_c et le comportement d'auto-assemblage) de l'homopolymère PD_{5k} et des copolymères séquencés de PN_{5k}-*b*-PD_{5k} ont été étudiées. On constate que l'ajout de CO_2 conduit à la protonation des groupes amine tertiaire dans les chaînes PD_{5k}, ce qui améliore la solvatation de PD_{5k} dans l'eau et entraîne une perte partielle de la thermoréactivité. Une fois le CO_2 éliminé par barbotage de N_2, le comportement LCST est récupéré mais avec une valeur T_c plus élevée. Dans le cas du PN_{5k}-*b*-PD_{5k}, à 25 ^oC (inférieur à T_c), le traitement au CO_2 n'a pas ou peu d'effet sur la morphologie et la taille du PN-*b*-PD. Un effet plus prononcé est mesuré au-dessus de T_c.

Conclusion

Trois familles différentes de copolymères séquencés ou statistiques portant des groupes thermosensibles et/ou pH et/ou CO_2: (1) les copolymères statistiques thermosensibles de P(VCL-*stat*-VP) de compositions différentes; (2) des copolymères thermosensibles de P(BA-*co*-NIPAM) avec différentes compositions et architectures (dibloc, tribloc et statistique); (3) des copolymères séquencés multi-stimuli (thermo-, pH et CO_2-sensibles) de PNIPAM-*b*-PDEAEAM avec des compositions variables et des homopolymères correspondants de PNIPAM et PDEAEAM. Ces trois familles de (co)polymères ont été synthétisées par polymérisation RAFT.

Des nanoparticules hybrides ont été préparées par revêtement de P(VCL-*stat*-$VP)_{20k}$ sur des AuNPs, ce qui a conféré aux NPs obtenues les propriétés thermosensibles de P(VCL-*stat*-$VP)_{20k}$ ainsi que les propriétés optiques et catalytiques des AuNPs. Les effets de la composition du polymère, de la concentration, des valeurs de pH et de la force ionique sur la stabilisation colloïdale de Au@P(VCL-*stat*-$VP)_{20k}$ ont été étudiés. Les résultats ont montré que l'augmentation de la concentration en copolymère déplaçait la stabilité des AuNPs vers la modification du pH ou l'ajout de sel en raison d'un encombrement stérique plus élevé. De plus, à une concentration spécifique, l'augmentation de la teneur en VP a supprimé la stabilité des AuNP et affaibli la thermosensibilité. De plus, l'activité catalytique de Au@P(VCL-*stat*-$VP)_{20k}$ dans la réduction du *p*-nitrophénol en *p*-aminophénol a augmenté avec la température jusqu'à ce que T_c atteigne, auquel les chaînes polymères se sont effondrées en réponse à la température, ce qui a empêché le réactif de se diffuser sur les AuNPs surface, et a entraîné une diminution ou aucune efficacité catalytique. L'influence de la teneur en VP sur l'activité catalytique a été

attribuée à un compromis entre le caractère hydrophobe (favorisant l'accès des réactifs vers les AuNPs) et une forte adsorption de VCL (inhibant l'efficacité catalytique).

L'introduction de fragments PBA hydrophobes abaisse la T_c des segments PNIPAM et l'intensité du décalage augmente avec une augmentation de la teneur en BA quelle que soit l'architecture. On constate qu'en solution diluée, l'effet de la microstructure sur le T_c en solution diluée suit un tel ordre : $T_{c,\ statistique} < T_{c,\ tribloc} < T_{c,\ dibloc}$ à la même concentration de (co)polymère et composition. De plus, des structures sphériques ont été détectées avec un diamètre plus grand à une température supérieure à T_c que celles formées à des températures plus basses. En solution concentrée, la température de gélification et la densité du réseau entre les copolymères dibloc et tribloc ont été comparées, il est démontré que les gels dans les analogues triblocs se sont formés à des températures plus basses avec une microstructure plus dense.

L'étude du copolymère séquencé thermo-réactif multi-stimuli PNIPAM-*b*-PDEAEAM avec des compositions variables et des homopolymères correspondants de PNIPAM et PDEAEAM a été réalisée. Les groupes terminaux de -COOH et hydrophobe -$C_{12}H_{25}$ ont exercé un effet important sur les propriétés colloïdales à différentes valeurs de pH. La Tc des homopolymères PNIPAM a augmenté avec le pH en raison de l'ionisation du groupe terminal -COOH, tandis que le PDEAEAM a affiché un comportement opposé causé par la déprotonation séquentielle des groupes amine tertiaire au sein des chaînes PDEAEAM. L'effet des différents stimuli sur les copolymères blocs correspondants a ensuite été étudié, à pH 10 (au-dessus du p*K*a de PDEAEAM), à la fois PNIPAM et PDEAEAM ont présenté une thermoréactivité, et un T_c a été détecté dans le cas de $PNIPAM_{5k}$-*b*-$PDEAEAM_{5k}$. Des nano-objets sphériques stables de différentes tailles ont été formés à des températures plus basses et plus élevées. A pH 4 (inférieur au p*K*a du PDEAEAM), le PDEAEAM a perdu sa propriété thermosensible. Deux valeurs de T_c ont été mesurées et une croissance progressive de la taille des agrégats a été mesurée lors du chauffage.

Enfin, la réactivité au CO_2 du PDEAEAM lors du traitement/de l'élimination du CO_2 a été étudiée. L'effet de l'ajout de CO_2 sur le comportement thermosensible du copolymère séquencé PNIPAM-*b*-PDEAEAM a été étudié et illustré comment les propriétés colloïdales (température de transition et formation de colloïdes) de ce polymère en solution peuvent être ajustées en utilisant différents stimuli: température et CO_2. De plus, tous les copolymères PNIPAM-*b*-PDEAEAM présentaient une bonne réversibilité avec au moins 7 cycles de bulles alternées CO_2/N_2.